

# Assessment of Adelaide Plains Groundwater Resources: Appendices Part I – Field and Desktop Investigations



Goyder Institute for Water Research  
Technical Report Series No. 15/32



[www.goyderinstitute.org](http://www.goyderinstitute.org)

**Goyder Institute for Water Research Technical Report Series ISSN: 1839-2725**

The Goyder Institute for Water Research is a partnership between the South Australian Government through the Department of Environment, Water and Natural Resources, CSIRO, Flinders University, the University of Adelaide and the University of South Australia. The Institute will enhance the South Australian Government's capacity to develop and deliver science-based policy solutions in water management. It brings together the best scientists and researchers across Australia to provide expert and independent scientific advice to inform good government water policy and identify future threats and opportunities to water security.



The following associate organisation contributed to the report:



Enquires should be addressed to: Goyder Institute for Water Research  
Level 4, 33 King William Street  
Adelaide, SA, 5000  
tel: 08-8236 5200  
e-mail: [enquiries@goyderinstitute.org](mailto:enquiries@goyderinstitute.org)

**Citation**

Bresciani E, Batelaan O, Banks EW, Barnett SR, Batlle-Aguilar J, Cook PG, Costar A, Cranswick RH, Doherty J, Green G, Kozuskanich J, Partington D, Pool M, Post VEA, Simmons CT, Smerdon BD, Smith SD, Turnadge C, Villeneuve S, Werner AD, White N and Xie Y, 2015, *Assessment of Adelaide Plains Groundwater Resources: Appendices Part I – Field and Desktop Investigations*, Goyder Institute for Water Research Technical Report Series No. 15/32, Adelaide, South Australia

**Copyright**

© 2015 Flinders University. To the extent permitted by law, all rights are reserved and no part of this publication covered by copyright may be reproduced or copied in any form or by any means except with the written permission of Flinders University.

**Disclaimer**

The Participants advise that the information contained in this publication comprises general statements based on scientific research and does not warrant or represent the completeness of any information or material in this publication.





# Contents

Figures v

Tables xii

Appendix A	Drilling program	1
A.1	Executive summary	1
A.2	Introduction	1
A.3	Study Area	1
A.3.1	Regional Hydrogeology	1
A.4	Drilling, Well design and construction	2
A.4.1	Diamond coring of the aquitard	3
A.4.2	Downhole wireline logging	3
A.5	Site locations	3
A.5.1	Rostrevor- Site 1	6
A.5.2	Trinity Gardens- Site 3	9
A.5.3	North Adelaide- Site 5	12
A.5.4	Welland- Site 6	14
A.5.5	Woodville- Site 12	18
A.5.6	Gilman- Site 13	20
A.6	References	22
Appendix B	Review of the hydrogeological properties of aquifers and aquitards	23
B.1	Introduction	23
B.1.1	BACKGROUND AND OBJECTIVES	23
B.1.2	Location of Study Area and Geological Features	24
B.2	Methodology	26
B.3	Literature Review	26
B.3.1	Reports That Contain Relevant Hydrogeological Data	26
B.3.2	Reports That do not Contain new or Relevant Hydrogeological Data	28
B.4	Discussion	30
B.4.1	hydrogeological zones	30
B.4.2	aquifer sequence	32
B.4.3	confining beds	34
B.4.4	review of hydraulic parameters	34
B.5	Results and Conclusions	36
B.6	References	45
Appendix C	Groundwater recharge estimation – chloride mass balance approach	47
C.1	Executive Summary	47
C.2	Introduction	47

C.3	Methodology, Data Collection and Development .....	48
C.3.1	chloride mass balance.....	48
C.3.2	data collection.....	50
C.3.3	spatial analysis .....	51
C.4	Results and Discussion .....	51
C.4.1	EC derived chloride concentrations.....	51
C.4.2	CMB groundwater recharge rates .....	61
C.6	Conclusions .....	64
C.8	Additional Information.....	65
C.8.1	Measured chloride.....	65
C.8.1	chloride across the faults map series .....	65
C.8.1	EC derived chloride vs maximum drilled depth.....	71
C.9	References.....	72
Appendix D	Groundwater – surface water exchange .....	73
D.1	Executive Summary.....	73
D.2	Introduction .....	73
D.3	Methodology.....	76
D.3.1	Dilution Gauging .....	76
D.3.2	ENVIRONMENTAL TRACERS .....	77
D.3.3	Spatial Analysis.....	77
D.4	Results and Discussion .....	78
D.4.1	Creek Discharge rates .....	78
D.4.2	Creek and Groundwater electrical conductivity .....	81
D.4.3	Quantifying Groundwater – Surface water Exchange .....	83
(i)	spatial variability.....	83
(ii)	Temporal variability .....	86
D.4.4	HydraUlic state of groundwater – surface water interaction.....	88
D.4.5	Recharge via creek infiltration.....	88
D.5	Conceptual Model.....	89
D.6	Conclusions .....	90
D.8	Additional Information.....	91
D.9	References.....	103
Appendix E	Groundwater hydrochemistry.....	104
E.1	Introduction .....	104
E.2	Methods .....	105
E.3	Results .....	107
E.3.1	MAJOR IONS.....	107
E.3.2	stable isotopes of water .....	115
E.3.3	carbon isotopes.....	116
E.3.4	noble gases and n <sub>2</sub> .....	121
E.4	Discussion.....	126

E.5	Conclusions .....	129
E.6	References.....	129
Appendix F Leakage estimation across the Munno Para Clay.....		131
F.1	Executive Summary .....	131
F.2	Introduction .....	131
	F.2.1 Study Area.....	132
	F.2.2 Site description .....	132
	F.2.3 Hydrogeology.....	133
	F.2.4 Drill sites.....	133
	F.2.5 Previous Permeability and Leakage Estimates .....	133
F.3	Methods .....	135
	F.3.1 Field methods .....	135
	F.3.2 Analytical methods .....	136
	F.3.3 Modelling methods.....	137
F.4	Results .....	138
	F.4.1 Environmental tracer results .....	138
	F.4.2 Modelling results .....	148
	F.4.3 Leakage rate.....	152
F.5	Discussion.....	153
	F.5.1 Permeability Estimates .....	153
	F.5.2 Interpretation of Transient conditions .....	154
F.6	Conclusions .....	154
F.7	References.....	155
Appendix G Seawater intrusion and sources of groundwater salinity.....		157
G.1	Executive Summary .....	157
G.2	Introduction .....	157
G.3	Methods .....	159
G.4	Results .....	161
G.5	Discussion.....	170
G.6	Comparison with the Adelaide Plains .....	171
G.7	References.....	174
Appendix H Coastal aquifer hydraulic parameter estimation based on tidal responses.....		176
H.1	Executive summary .....	176
H.2	Introduction .....	176
H.3	Study Area.....	177
	H.3.1 Hydrogeology.....	177
	H.3.2 Tidal Forcing.....	178
H.4	Methods .....	178
	H.4.1 Tidal harmonic analysis.....	178
	H.4.2 Tidal Method.....	179

H.5	Results .....	182
	H.5.1 Data analysis .....	182
	H.5.2 Estimates of Transmissivity .....	184
H.6	Conclusions .....	189
H.7	References.....	190
Appendix I Vibrating wire piezometers – determination of other aquitard properties through pressure response .....		192
I.1	Executive summary .....	192
I.2	Introduction .....	192
I.3	Study area .....	193
	I.3.1 Site description .....	193
	I.3.2 Hydrogeology.....	193
I.4	Methods .....	193
	I.4.1 Installation .....	193
	I.4.2 Data reduction .....	194
I.5	Results .....	195
I.6	Discussion and Summary .....	200
I.7	References.....	201
Appendix J Groundwater flow processes across fault zones.....		202
J.1	Introduction .....	202
	J.1.1 Background .....	202
	J.1.2 Adelaide Plains and Willunga Embayment .....	202
J.2	Study Area .....	203
J.3	Methods .....	206
	J.3.1 Hydraulics.....	206
	J.3.2 Hydraulic Modelling.....	210
J.4	Results .....	211
	J.4.1 Hydraulics.....	211
	J.4.2 Hydraulic modelling .....	214
J.5	Discussion.....	216
J.6	Conclusion.....	217
J.7	References.....	219

# Figures

Apx Figure A.1 Location map of the new drill site locations, Adelaide Plains and Golden Grove Embayment. ....	2
Apx Figure A.2 Location map of drill site 1 at Rostrevor. ....	6
Apx Figure A.3 Geophysical logs of deepest well (ID: 1A, PN229338) at site 1, Rostrevor. ....	8
Apx Figure A.4 Location map of drill site 3 at Trinity Gardens. ....	9
Apx Figure A.5 Geophysical logs of deepest well (ID: 3A, PN230061) at site 3, Trinity Gardens. ....	11
Apx Figure A.6 Location map of drill site 5 at North Adelaide. ....	12
Apx Figure A.7 Location map of drill site 6 at Welland. ....	14
Apx Figure A.8 Geophysical logs of deepest well (ID: 6A, PN227513) at site 6, Welland. ....	16
Apx Figure A.9 Location map of drill site 12 at Woodville. ....	18
Apx Figure A.10 Location map of drill site 13 at Gilman. ....	20
Apx Figure A.11 Geophysical logs of deepest well (ID:13A, PN231758) at site 13, Gilman. ....	22
Apx Figure B.1 Location, topography and lateral extent of the previous model boundary (Georgiou, J. et al., 2011). ....	24
Apx Figure B.2 Generalised surface geology of the Adelaide Plains region. ....	25
Apx Figure B.3 Plan showing location and extent of hydrogeological zones (Martin and Hodgkin, 2006).....	31
Apx Figure B.4 An Overview of the Hydrogeological Setting of the Study Area (Georgiou, J. et al., 2011).....	33
Apx Figure C.1 The change in rainfall chloride concentration with approximate distance from the coast in the direction of the major weather systems. This includes both raw data and relationships that have been derived based on this and other data not displayed. Where data was not presented in table format, values were approximated from graphs and so may contain some error. This error is considered to be small and not relevant for the purposes of this study. ....	49
Apx Figure C.2 Latest EC derived chloride values from Fractured Rock and Quaternary Aquifers. Note that the bin ranges are increased for the right-most three categories. ....	53
Apx Figure C.3 Latest EC derived chloride values from T1 and T2 Aquifers. Note that the bin ranges are increased for the right-most three categories. ....	54
Apx Figure C.4 Interpolated EC derived chloride from the Fractured Rock Aquifers.....	55
Apx Figure C.5 Interpolated EC derived chloride from the Quaternary Aquifers. ....	56
Apx Figure C.6 Interpolated EC derived chloride from the T1 Aquifers. ....	57
Apx Figure C.7 Interpolated EC derived chloride from the T2 Aquifers. ....	58
Apx Figure C.8 Interpolated EC derived chloride difference between the QA and T1 Aquifers. ....	59
Apx Figure C.9 Interpolated EC derived chloride difference between the T1 and T2 Aquifers. ....	60
Apx Figure C.10 Histograms of the CMB groundwater recharge estimates for the Fractured Rock and Quaternary Aquifers. Note that the histogram of the FRA recharge rates has been truncated at 30 mm/year. The tail of this distribution for FRA includes 143 recharge estimates that are > 100 mm/year (i.e. from very fresh groundwater samples).....	62

Apx Figure C.11 Histograms of the CMB groundwater recharge estimates based on data from the T1 and T2 Aquifers, where we assume recharge originally occurred in the WMLR and entered the T1 and T2 via lateral flow.....	63
Apx Figure C.12 Latest measured chloride values from Fractured Rock and Quaternary Aquifers. Note that the bin ranges are increased for the right-most three categories. ....	66
Apx Figure C.13 Latest measured chloride values from T1 and T2 Aquifers. Note that the bin ranges are increased for the right-most three categories. ....	67
Apx Figure C.14 Interpolated chloride surface of the Quaternary and Fractured Rock Aquifers, separated by Faults.....	68
Apx Figure C.15 Interpolated chloride surface of the T1 and Fractured Rock Aquifers, separated by Faults. ....	69
Apx Figure C.16 Interpolated chloride surface of the T2 and Fractured Rock Aquifers, separated by Faults. ....	70
Apx Figure C.17 Scatter plots of depth vs EC derived chloride. Note the different y-axis on the QA scatter plot.....	71
Apx Figure D.1 Electrical conductivity interpolation for the AP Quaternary and shallow aquifers (<30 m).....	75
Apx Figure D.2 Longitudinal gauging for selected western draining creeks, October 2014. River flow is from right to left.....	79
Apx Figure D.3 Longitudinal gauging for the Torrens River, December 2014. River flow is from right to left and EC measurements are shown in red while flow measurements are shown in blue. ....	81
Apx Figure D.4 Quaternary and Fractured Rock aquifer EC, Quaternary aquifer RWL and inferred groundwater flow direction. ....	82
Apx Figure D.5 creek electrical conductivity relative to the Eden Burnside fault, October 2014. River flow is from right to left.....	83
Apx Figure D.6 Groundwater – surface water exchange rates (L/s/km) in October 2014 and January 2015. Numerals represent measured exchange rates (positive in gain and negative is loss), and their relative magnitudes are also indicated by colours of the creek reaches. ....	84
Apx Figure D.7 First Creek mass balance for October 2014 gauging (after Cook <i>et al.</i> , 2006). ....	85
Apx Figure D.8 Brownhill Creek mass balance for October 2014 gauging (after Cook <i>et al.</i> , 2006). ....	86
Apx Figure D.9 Groundwater – surface water exchange for Brownhill creek at four gauging times. Numerals represent measured exchange rates (positive in gain and negative is loss), and their relative magnitudes are also indicated by colours of the creek reaches. ....	87
Apx Figure D.10 Groundwater – surface water exchange rates for all creeks relative to the EB fault. River flow is from right to left.....	88
Apx Figure D.11 An alternative conceptual model of groundwater flow and groundwater – surface water exchange in the vicinity of Brownhill Creek. ....	90
Apx Figure D.12 creek electrical conductivity relative to the Eden Burnside fault, January 2015. River flow is from right to left.....	91
Apx Figure D.13 Reference map for Brownhill Creek hydrograph comparisons. Blue numerals indicate hydraulic heads (m AHD) in the shallow Quaternary aquifer while grey numerals are hydraulic heads in the fractured rock aquifer. ....	93
Apx Figure D.14 Hydrograph comparisons between Brownhill creek and the FRA. ....	94
Apx Figure D.15 Hydrograph comparisons between Brownhill creek and nearby aquifers. ....	94

Apx Figure D.16 Reference map for Torrens River, Fourth and Fifth Creek hydrograph comparisons. Blue numerals indicate hydraulic heads (m AHD) in the shallow Quaternary aquifer while grey numerals are hydraulic heads in the fractured rock aquifer. ....	95
Apx Figure D.17 Hydrograph comparisons between Fifth creek and underlying QA and FRA. ....	96
Apx Figure D.18 Hydrograph comparisons between Fifth creek and nearby aquifers. ....	96
Apx Figure D.19 Hydrograph comparison between the Torrens river and nearby aquifers. ....	97
Apx Figure D.20 Hydrograph comparison between the aquifers between Fourth and Fifth creeks. ....	97
Apx Figure D.21 Hydrograph comparison for the aquifers between Fourth and Fifth creeks near the Hope Valley fault. ....	98
Apx Figure D.22 Hydrograph comparison between the aquifers near First creek. ....	98
Apx Figure D.23 Hydrographs near the Gawler river, approximately 3.5 km upstream of the Alma fault. ....	99
Apx Figure D.24 Hydrographs near the Gawler river, approximately 2.5 km downstream of the Alma fault. ....	99
Apx Figure D.25 Hydrographs near the Gawler river, approximately 14 km downstream of the Alma fault. ....	100
Apx Figure D.26 Hydrographs near the Gawler river, approximately 18 km downstream of the Alma fault. ....	100
Apx Figure D.27 Hydrographs near the Little Para river, adjacent to the Para fault. ....	101
Apx Figure D.28 Hydrographs near the Little Para river, approximately 2.6 km downstream of the Para fault. ....	101
Apx Figure D.29 Hydrographs near the Little Para river, approximately 5.5 km downstream of the Para fault. ....	102
Apx Figure E.1 Map showing locations of transects and sampled wells. The symbol colours represent the different aquifers sampled, and shapes represent the source of the data. Locations of the three transects are indicated by broken lines. ....	106
Apx Figure E.2 Major ion concentrations versus chloride concentrations showing groundwater samples from the Quaternary, T1, T2 and FRA aquifer systems. Both data obtained during the present study and data of Baird (2010) and Green et al. (2010) are shown. ....	112
Apx Figure E.3 Piper plot showing groundwater samples from the Quaternary, T1, T2 and fractured rock (FRA) aquifer systems. Both data obtained during the present study and data of Baird (2010) and Green et al. (2010) are shown. ....	113
Apx Figure E.4 Distribution of chloride (mg/L) along the three transects: (a) North Transect, (b) Central Transect, and (c) South Transect. Screen intervals for piezometers are shown using vertical bars only when screen lengths exceed the size of the symbols. Vertical broken lines indicate the approximate locations of the major faults: Alma Fault (AF), Para Fault (PF), Para Fault West (PFW), and Eden-Burnside Fault (EBF). ....	114
Apx Figure E.5 Relationship between oxygen-18 and deuterium ( <sup>2</sup> H) values in groundwater. Both data obtained during the present study and data of Baird (2010) are shown. (Where piezometers were sampled in both studies, the most recent values are plotted.) The Local Meteoric Water Line (LMWL; Liu et al., 2010) is shown for comparison. ....	115
Apx Figure E.6 Relationship between deuterium values and chloride concentration for groundwater from different aquifer systems. Both data obtained during the present study and data previously obtained by Dighton et al. (1994) and Baird (2010) are shown. (Where piezometers were sampled more than once, the most recent values are plotted.) ....	116

Apx Figure E.7 Relationship between <sup>14</sup> C activity and <sup>13</sup> C value for groundwater samples. Both data obtained during the present study and data previously obtained by Dighton et al. (1994) and Baird (2010) are shown. (Where piezometers were sampled more than once, the most recent values are plotted.).....	117
Apx Figure E.8 Distribution of corrected <sup>14</sup> C activity (pmC) along the three transects: (a) North Transect, (b) Central Transect, and (c) South Transect. Screen intervals for piezometers are shown using vertical bars, only when screen lengths exceed the size of the symbols. Vertical broken lines indicate the approximate locations of the major faults: Alma Fault (AF), Para Fault (PF), Para Fault West (PFW), and Eden-Burnside Fault (EBF). .....	118
Apx Figure E.9 Relationship between corrected <sup>14</sup> C age and location within the T2 aquifer along the north transect. The corrected <sup>14</sup> C age is plotted versus the location of the piezometer screen below the top of the T2 aquifer at that location. (Vertical bars denote the length of the piezometer screen.) Piezometers are grouped according to their horizontal distance along the transect (0 – 6, 7 – 13, 14 – 19 and 20 – 25 km from the coast). Both data obtained during the present study and data previously obtained by Dighton et al. (1994) and Baird (2010) are shown. Where piezometers were sampled more than once, the most recent values are plotted. ....	119
Apx Figure E.10 Relationship between corrected <sup>14</sup> C activity and distance from the coast along the three transects. Scales are the same for all three transects to permit easy comparison. Both data obtained during the present study and data previously obtained by Dighton et al. (1994) and Baird (2010) are shown. Where piezometers were sampled more than once, the most recent values are plotted. ....	120
Apx Figure E.11 Relationship between corrected <sup>14</sup> C activity and <sup>2</sup> H values in groundwater. Both data obtained during the present study and data previously obtained by Dighton et al. (1994) and Baird (2010) are shown. Where piezometers were sampled more than once, the most recent values are plotted. ....	121
Apx Figure E.12 Comparison of measured concentrations of neon, argon, helium and nitrogen in groundwater, with expected concentrations based on equilibrium solubility of atmospheric gases in water at temperatures between 5 and 30°C, and excess air volumes up to 10 cm <sup>3</sup> kg <sup>-1</sup> . (The solid line indicates the relationship between gas concentrations based on water temperatures between 5 and 30°C, with lower concentrations at higher temperatures. Broken lines indicate the effect of 0 – 10 cm <sup>3</sup> kg <sup>-1</sup> excess air.) Note that helium is plotted on a logarithmic scale, whereas the scale for the other gases is linear. ....	122
Apx Figure E.13 Distribution of helium (10 <sup>-6</sup> cm <sup>3</sup> /g) along the three transects: (a) North Transect, (b) Central Transect, and (c) South Transect. Screen intervals for piezometers are shown using vertical bars, only when screen lengths exceed the size of the symbols. Vertical broken lines indicate the approximate locations of the major faults: Alma Fault (AF), Para Fault (PF), Para Fault West (PFW), and Eden-Burnside Fault (EBF)......	123
Apx Figure E.14 Relationship between corrected and uncorrected <sup>14</sup> C activity and dissolved helium concentration. ....	124
Apx Figure E.15 Helium concentrations versus estimated <sup>14</sup> C ages in groundwater. ....	125
Apx Figure E.16 Helium, corrected <sup>14</sup> C and deuterium versus chloride. ....	126
Apx Figure E.17 Comparison between measured apparent <sup>14</sup> C ages in the T2 aquifer along the North Transect and results of the advective model (Equation A.1) based on different values of aquifer thickness (H). ....	128
Apx Figure F.1 Coring locations and thickness and extent of the Munno Para Clay; thicknesses are from the WaterConnect database (DEWNR, 2015). ....	132
Apx Figure F.2 Noble gas results for Site 6: (a) F(He), (b) helium concentrations, and Site 13: (c) F(He), (d) helium concentrations.....	139
Apx Figure F.3 Depth profiles of chloride Site 6 and Site 13. ....	141

Apx Figure F.4 Depth profiles of stable isotopes at Site 6: (a) $\delta^2\text{H}$ and (b) $\delta^{18}\text{O}$ and Site 13: (c) $\delta^2\text{H}$ and (d) $\delta^{18}\text{O}$ ; data from contaminated samples are not shown.....	145
Apx Figure F.5 $\delta^{18}\text{O}$ vs. $\delta^2\text{H}$ for (a) Site 6 and (b) Site 13.....	146
Apx Figure F.6 Comparison of deuterium and chloride measurements in core samples; (a) Site 6 and (b) Site 13.....	146
Apx Figure F.7 Site 6 modelled helium profiles from (a) Scenario 1 and (b) Scenario 2.....	149
Apx Figure F.8 Site 6 modelled helium profiles for (a) Scenario 3 and (b) Scenario 4.....	150
Apx Figure F.9 Site 13 modelled helium concentrations for (a) Scenario 1 and (b) Scenario 2.....	151
Apx Figure F.10 Site 13 modelled helium concentrations for (a) Scenario 3 and (b) Scenario 4.....	152
Apx Figure F.11 2014 map of T2 – T1 (a) head difference and (b) hydraulic gradient.....	153
Apx Figure G.1 Map showing the locations of the wells along the seawater intrusion transect, and other wells in the vicinity.....	160
Apx Figure G.2 Cross-section along the seawater intrusion well transect in Aldinga Beach showing the geology, electrical conductivity distribution and the boundary between fresh, saline and hypersaline groundwater. Black and blue lines represent the measured bulk conductivity (mS/m) of the aquifer. Black dashed line shows the boundary between intruded seawater and fresh groundwater. Red dashed line shows the bounds of the hypersaline groundwater.....	161
Apx Figure G.3 Graphs showing (left) $\delta^{18}\text{O}$ versus Cl <sup>-</sup> concentration (right) $\delta^2\text{H}$ versus Cl concentration for the samples from the seawater intrusion well transect in Aldinga Beach. Sample labels show the mid-screen depth referenced to mAHD. Samples from nearby observation wells not part of the transect are also shown (star symbol). Green and blue lines represent line of best fit, which is included to emphasise the mixing behaviour between hypersaline groundwater and seawater. Black dashed lines represent mixing lines between fresh groundwater (sample WLG102) and seawater (based on Short, 2011, Corlis et al. 2001), as well as fresh groundwater and the selected hypersaline end member (WLG096). Blue stars represent data from the new wells drilled for this project in the Adelaide Plains.....	164
Apx Figure G.4 Graph showing $\delta^2\text{H}$ versus $\delta^{18}\text{O}$ published by Herczeg et al. (2001) with data points from this study overlain. The dashed blue line shows the line of best fit through the data points of the samples from the SWI transect and nearby wells that were found to have a contribution of the seawater end member less than 5%.....	164
Apx Figure G.5 Cross-section along the seawater intrusion well transect in Aldinga Beach showing $^{87}\text{Sr}/^{86}\text{Sr}$ ratios.....	165
Apx Figure G.6 Cross-section along the seawater intrusion well transect in Aldinga Beach showing the fractions of the end members in each of the samples and the inferred three end member mixing based on a ternary contour plot. Inset triangle shows colour scheme with green indicating hypersaline water, red indicating seawater and blue freshwater.....	167
Apx Figure G.7 Ternary diagrams showing measured $^{14}\text{C}$ activity (pmC) as a function of the fractions of the three end members in each sample.....	168
Apx Figure G.8 Graph showing $\delta^{13}\text{C}_{\text{corr}}$ versus $\delta^{13}\text{C}_{\text{sample}}$ for the wells of the seawater intrusion transect. The dashed black line represents a 1:1 relationship. Samples with a fraction of seawater $f_{\text{sea}} > 0.5$ have been encircled.....	169
Apx Figure G.9 Ternary diagram showing the corrected age (in ka BP) estimates as a function of the fractions of the three end members in each sample.....	169
Apx Figure G.10 Graphs showing (left) the ratio of Cl / (TIC + SO4) versus the chloride concentration and (right) the ratio of Na / (K + Ca + Mg) versus the chloride concentration. Ratios are based on concentrations expressed in meq/L. Numbered lines represent the relationships resulting from mixing between freshwater and seawater (1), freshwater and hypersaline water (2) and seawater and	

hypersaline water (3). Black lines are based on the most saline sample from the Wilunga area (WLG096), grey lines are based on the most saline sample from the Adelaide Plains area (YAT067). See Figure G.3 for legend of the coloured symbols, grey symbols are data points for the Adelaide Plains area from the WaterConnect database, blue stars represent data from the new wells drilled for this project. ....	172
Apx Figure G.11 Map showing location of selected wells with high groundwater salinity (circles) and/or that appear to have a brine signature (triangles). ....	173
Apx Figure H.1 Monitoring wells locations. Red and blue colours represent the wells screened in T1 and T2 aquifers, respectively. A separate logger was attached to the Henley Beach Jetty to record the tide in the Gulf St Vincent.....	178
Apx Figure H.2 Schematic of: (a) an idealized aquifer with an overlying confining layer crop out at or near coastline, (b) an infinite confined aquifer extending under the sea, and (c) a leaky confined aquifer with a finite semi-permeable layer under the sea. ....	181
Apx Figure H.3 Atmospheric pressure recorded for a period of one month at the top of the well YAT043.....	183
Apx Figure H.4 Periodogram of harmonic frequencies present in ocean-tide data collected (a) and the predicted ocean tide at the Henley beach (b), October 2014.....	183
Apx Figure H.5 Results from the harmonic analysis at four different wells: ADE005 and YAT037, screened in the T1 aquifer; YAT099 and YAT066, screened in the T2 aquifer. Black lines represent the head data, red lines the nontidal residual noise (right y-axis) and blue lines the tidal response (left y-axis). ....	184
Apx Figure H.6 Time series head data in the monitoring wells (left y-axis) and tidal signal (right y-axis) for the entire period of record (left) and detail over two tidal cycles. ....	185
Apx Figure H.7 Temporal variation of the tidal efficiency (a) and phase lag (b) calculated in the well ADE005. ....	185
Apx Figure H.8 Results for the tidal efficiency and with respect to the distance from the coast for measurements at the monitoring wells screened in the T1 aquifer. ....	186
Apx Figure H.9 Transmissivity estimates obtained from the methods of Jacob (1950) and Van der Kamp (1972) at the monitoring wells in the T1 (a) and T2 aquifer (b) as a function of the distance from the coast. ....	187
Apx Figure H.10 Transmissivity estimates obtained from the methods of Li and Jiao (2001a) as a function of the (a) vertical conductivity of the leaky semipermeable layer, and (b) length of the aquitard.....	189
Apx Figure I.1 Locations of vibrating wire piezometer installation and thickness and extent of the Munno Para Clay; thicknesses are from the WaterConnect database (DEWNR, 2015). ....	193
Apx Figure I.2 Site 3 – Trinity Gardens: (a) 23 m (b) 97 m and (c) RSWL with water levels from nested or adjacent wells and relative head differences between measurements. ....	196
Apx Figure I.3 Site 5 – North Adelaide: (a) 16 m (b) 53 m and (c) RSWL with water levels from nested or adjacent wells and relative head differences between measurements. ....	197
Apx Figure I.4 Site 6 – Welland: (a) 126.7 m and (b) RSWL with water levels from nested or adjacent wells and relative head differences between measurements. ....	198
Apx Figure I.5 Site 13 – Gillman: (a) 77 m (b) 168 m and (c) RSWL with water levels from nested or adjacent wells and relative head differences between measurements. ....	199
Apx Figure I.6 Specific storage versus piezometer depth. ....	200
Apx Figure J.1 Location map of the Willunga Embayment and the three field sites THR, MR and WHR	205
Apx Figure J.2 Geological cross section of the Willunga embayment along transect north to south near coastline (modified from Watkins, 1995).....	206

Apx Figure J.3 (a) 3D numerical model domain and (b) 2D conceptual model of the groundwater system showing the three different hydraulic conductivity zones across the fault as defined in the numerical model.....	210
Apx Figure J.4 Hydraulic heads corrected to mAHD (2013) at the study sites (top) THR, (middle) MR and (bottom) WHR. Also shown are the inferred groundwater flow directions.....	212
Apx Figure J.5 Waterlevel time series data from study site THR showing the seasonal aquifer responses in the wells completed above and below the fault. Labels for each time series are: Above fault (AF), below fault (BF). .....	213
Apx Figure J.6 Potentiometric surfaces generated from all available well data from the SAGeodata base within the Willunga Embayment for the four major aquifer systems; (top left) Quaternary, (top right) Port Willunga Formation, (bottom left) Maslin Sands and (bottom right) Fractured rock.....	214
Apx Figure J.7 Realisations of different hydraulic conductivity combinations to match observed hydraulic head (top) above and (bottom) below the fault at site MR. Blue dashed lines are the measured heads above and below the fault zone at the site. Selected data points (black) are within 5 metres of the measured head and show a very broad range of values for the fault. ....	215
Apx Figure J.8 Realisations of different hydraulic conductivity combinations showing (top) the RMSE of heads and (bottom) the observed head difference above and below the fault at site MR. Blue dashed line is the measured head difference across the fault zone at the site. Selected data points (black) are within 5 metres of the measured head difference. ....	216
Apx Figure J.9 Realisations of different hydraulic conductivity combinations showing the combined RMSE of heads at the three sites. Data points highlighted in black have a $K_2$ value of 0.5-10 m/d and an RMSE less than 20 m (below the fault).....	217

# Tables

Apx Table A.1 Well construction details for all drill sites. ....	4
Apx Table A.2 Drillhole strata log of deepest well (ID: 1A, permit number [PN]: PN229338) at site 1, Rostrevor. ....	7
Apx Table A.3 Drillhole strata log of deepest well (ID: 3A, PN230061) at site 3, Trinity Gardens. ....	10
Apx Table A.4 Drillhole strata log of deepest well (ID: 5A, PN227509) at site 5, Strangways Tce, North Adelaide. ....	13
Apx Table A.5 Drillhole strata log of deepest well (ID: 5B, PN236133) at site 5, War Memorial Drive, North Adelaide. ....	13
Apx Table A.6 Drillhole strata log of deepest well (ID: 6A, PN227513) at site 6, Welland. ....	15
Apx Table A.7 Drillhole strata log of well 12 (PN227519) at site 12, Woodville. ....	19
Apx Table A.8 Drillhole strata log of deepest well (ID: 13A, PN231758) at site 13, Gilman. ....	21
Apx Table B.1 Overview of Hydrogeological Zones (Gerges, 2006, Martin and Hodgkin, 2006). ....	30
Apx Table B.2 Overview of Hydrogeological Zones (Martin and Hodgkin, 2006, Gerges, 2006). ....	32
Apx Table B.3 Range of reported hydraulic parameter values for each of the aquifers. ....	36
Apx Table B.4 Summary of aquifer parameters for Quaternary aquifers and confining beds. ....	37
Apx Table B.5 Summary of aquifer parameters for Tertiary aquifers and confining beds. ....	39
Apx Table C.1 Details of CMB parameters used in previous studies in the Western Mount Lofty Ranges, Adelaide Plains and Willunga Basin. ....	50
Apx Table C.2 Summarised EC derived chloride values from selected wells with aquifer names. ....	52
Apx Table C.3 Summarised recharge rate estimations for all Aquifers. ....	61
Apx Table C.4 Summarised measured chloride values from selected wells. ....	65
Apx Table D.1 Details of trial dilution gauging on Brownhill Creek (13/08/2014) including potential errors. ....	76
Apx Table D.2 Dilution and other gauging details. ....	80
Apx Table D.3 Mean $Q_{ex}$ and creek Loss below or near the E-B Fault. ....	89
Apx Table D.4 Summary of flow direction and approximate head difference between from creeks/ rivers to aquifers, positive values indicates downward while negative values indicates upward difference. Note that the ranges of head difference values. ....	92
Apx Table E.1 Field parameters and major ion analyses on groundwater samples. ....	108
Apx Table E.2 Results of environmental isotope and dissolved gas analyses on groundwater samples. ....	110
Apx Table E.3 SI saturation indices for the Quaternary, T1, T2 and fractured rock (FRA) aquifer systems. ....	113
Apx Table E.4 Best fit values for the advective model. ....	128
Apx Table F.1 Summary of vertical hydraulic conductivities of Quaternary aquitards (Unit 1). ....	134
Apx Table F.2 Summary of vertical hydraulic conductivities of Tertiary aquitards including the Munno Para Clay (Unit 7). ....	134
Apx Table F.3 Summary of aquitard leakage coefficients for Quaternary and Tertiary confining beds. .	134
Apx Table F.4 Noble gas concentrations and ratios in core samples and adjacent wells. ....	140

Apx Table F.5 Chloride concentrations from core samples and adjacent wells – Site 6.....	142
Apx Table F.6 Chloride concentrations from core samples and adjacent wells – Site 13.....	143
Apx Table F.7 Chemistry of drilling mud.....	143
Apx Table F.8 Stable isotope ratios from core samples and adjacent wells – Site 6.....	147
Apx Table F.9 Stable isotope ratios from core samples and adjacent wells – Site 13.....	148
Apx Table G.1 Coordinates, well depths, pH, alkalinity and major ion concentrations of the wells along the seawater intrusion transect. ....	162
Apx Table G.2 Isotope values of the wells along the seawater intrusion transect. ....	163
Apx Table G.3 Chloride concentration, isotopic composition and ionic ratio of the end members used in the mixing calculations. ....	166
Apx Table H.1 Observation well number, unit number, aquifer, coordinates and screen depths of the monitoring wells used in this study.....	177
Apx Table H.2 Tidal harmonics at Port Adelaide. ....	178
Apx Table H.3 Tidal efficiency and phase lag measured in the monitoring wells. ....	186
Apx Table H.4 Summary of transmissivities computed for the monitoring wells using the amplitude attenuation calculation methods of Jacob (1950) and Van der Kamp (1972). ....	187
Apx Table H.5 Summary of the variables and transmissivities computed for the monitoring well YAT099 using the amplitude attenuation calculation method of Ji and Jiao (2001a). ....	188
Apx Table H.6 Summary of transmissivities computed for the T1 and T2 aquifers from the wells ADE005 and YAT 099, using the amplitude attenuation calculation methods of Jacob (1950), Van der Kamp (1972) and Li and Jiao (2001a).....	190
Apx Table I.1 Vibrating wire installation sites and depths; formations estimated from Appendix A. ....	194
Apx Table I.2 Formation parameters determined by vibrating wire data analysis. ....	195
Apx Table J.1 Construction details of the observation wells either side of the Willunga Fault at the three study sites.....	207
Apx Table J.2 Range of hydraulic conductivity values for each of the model zones. ....	211



# Appendix A Drilling program

Authors: *Banks EW and Costar A*

## A.1 Executive summary

As part of the Goyder Adelaide project, a drilling program was conducted to install new groundwater monitoring wells within the major aquifer systems along an east-west transect across the Adelaide Plains and Golden Grove Embayment. Additional drill sites were also chosen as part of the study to investigate inter-aquifer leakage across the Munno-Para Clay. Specifically designed and constructed groundwater monitoring wells, targeting each of the main aquifers at a number of sites across Adelaide Metropolitan area provides discrete sample intervals to analyse for a range of environmental and 'groundwater age' tracers and invaluable information for long term monitoring of the groundwater resource.

## A.2 Introduction

As part of the Goyder Adelaide project, a drilling program was conducted to install new groundwater monitoring wells within the major aquifer systems along an east-west transect across the Adelaide Plains and Golden Grove Embayment. Additional drill sites were also chosen as part of the study investigating inter-aquifer leakage across the Munno-Para Clay and other locations as requested by the Department of Water and Natural Resources (DEWNR) as part of the state's groundwater observation network. The location of these new drill sites is shown in Apx Figure A.1.

## A.3 Study Area

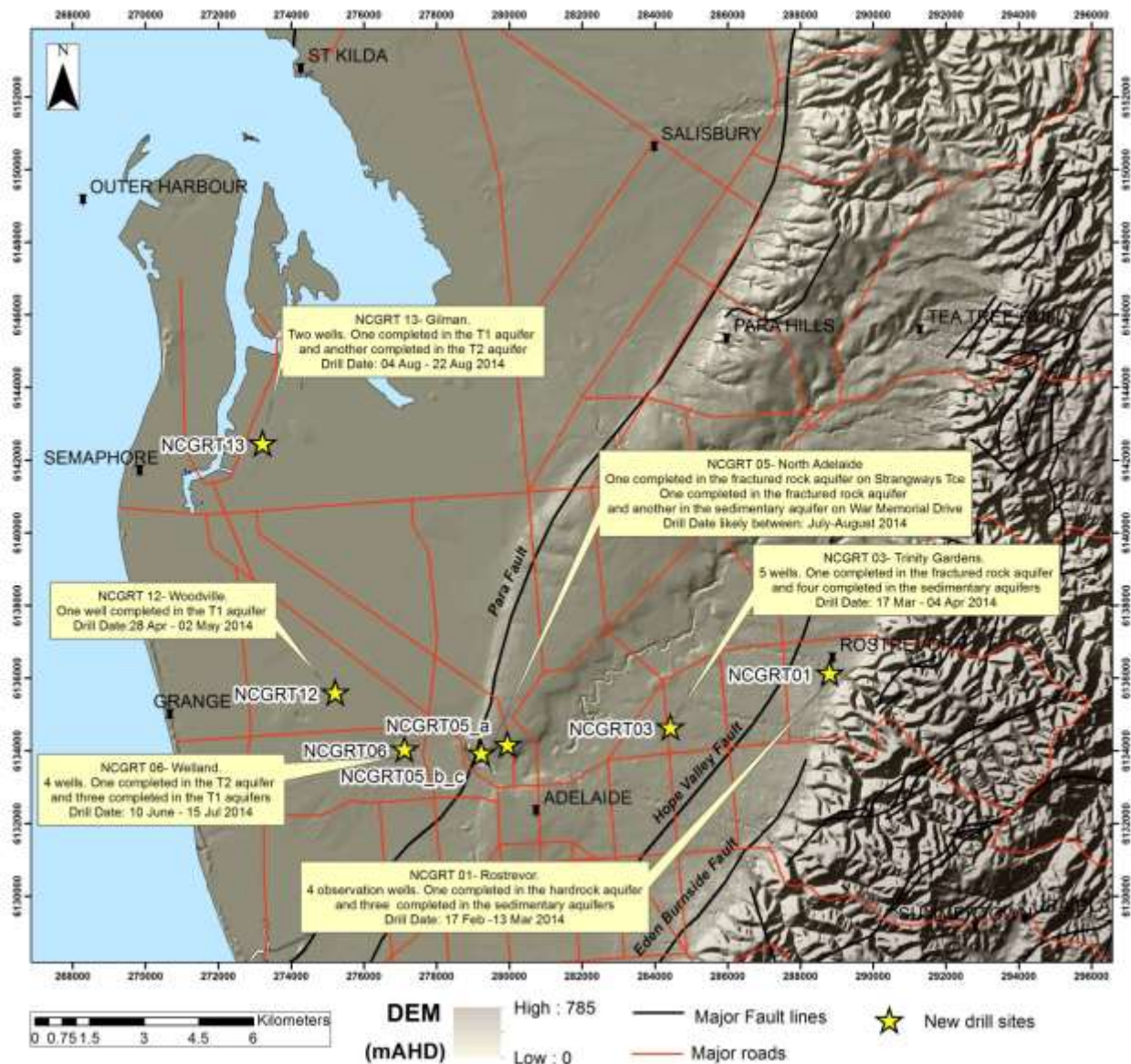
### A.3.1 REGIONAL HYDROGEOLOGY

The regional hydrogeology of the Adelaide Plains and Golden Grove Embayment has been extensively summarised by Gerges (1999; 2006) and a more recent review by Zulfic et al. (2008). The hydrogeological system of the Adelaide Plains includes three major fault systems (1) the Eden Burnside Fault, (2) The Para Fault, and (3) the Hope Valley Fault. The Eden-Burnside (E-B) Fault separates the Precambrian fractured rock aquifers to the east of the Golden Grove- Adelaide Embayment and the Tertiary and Quaternary sedimentary deposits on the plains. The Para Fault is a significant geological boundary that exists within the central part of the embayment and delineates the Quaternary and Tertiary sedimentary deposits into two main sub basins (Adelaide Plains sub-basin and the Golden Grove- Adelaide embayment) with much greater displacement and thickness of the sediments to the west of the fault (up to ~600m thickness) compared to ~150 metres east of fault. Groundwater extraction is far more prevalent from the Quaternary and Tertiary aquifers to the west of the Para Fault. The Hope Valley Fault is a less continuous fault and lies to the west of the Eden-Burnside Fault.

Groundwater is typically extracted from four major aquifers and there are subtle variations within each of these aquifers defined by unique stratigraphic formations separated by a series of aquitards or confining beds. There are two deeper tertiary aquifers (T3 and T4), however, due to the cost to drill to these deeper aquifers they are not heavily used. The four main aquifers are:

- Quaternary Aquifers (Q1- Q6)
- T1 Aquifers

- T2 Aquifer
- Fractured Rock Aquifer



Apx Figure A.1 Location map of the new drill site locations, Adelaide Plains and Golden Grove Embayment.

## A.4 Drilling, Well design and construction

The drilling program was contracted to Diverse Resources Group Pty Ltd and onsite drilling supervision (hydrogeologist) was provided by Flinders University and DEWNR. Both mud rotary and air hammer drilling techniques were undertaken using a Schramm T40WS and Atlas Copco T3W. Drilling specifications were conducted as per the minimum construction requirements for water bores in Australia manual (National Uniform Drillers Licensing Committee 2012).

The new groundwater monitoring wells were designed and constructed to target the major aquifer systems and completed with short screen intervals so that a representative sample could be collected from a discrete interval within the aquifer of interest. Additional sites were also chosen to investigate inter-aquifer leakage by completing monitoring wells above and below the Muno-Para Clay.

The completion details of the new wells at each of the sites are shown in the following section A.5: Site locations. All well elevations (top of casing- TOC) and natural ground elevations at each of the sites were

surveyed using a Trimble RTK differential survey system which typically has minimal error of +/- 10mm in the vertical direction and +/- 5 mm in the horizontal direction.

#### **A.4.1 DIAMOND CORING OF THE AQUITARD**

Diamond HQ coring was undertaken by Diverse Resources Group using an LF90 diamond drill rig with a 3 metre split tube at site 6 and site 13. The coring interval was based on the strata samples and geophysical logs to target the last few metres of the T1 aquifer through the Munno Para Clay aquitard and into the top few metres of the T2 aquifer. At site 6 HQ coring was done from 215 to 241 metres below ground and at site 13 HQ coring was done from 163 to 175 metres below ground

#### **A.4.2 DOWNHOLE WIRELINE LOGGING**

DEWNR Geophysical services completed down-hole geophysical surveys on the deepest drillhole at each site for the following parameters:

- *Natural Gamma Log (GAPI)* — Measures natural presence of gamma rays. Aids in defining lithology changes, bed boundaries and clay content.
- *Neutron Log (NEUT)*— Measures the amount of hydrogen around the probe. Can provide an indication of porosity and clay content (in combination with gamma).
- *Near/Far Density (NEAR,FAR) Log* — Gamma source and gamma receiver measures the electron density, which is a function of the bulk density of the formation.
- *Med/Deep Induction (ME, DEEP) Log* — The induction tool uses electromagnetics to sense the conductivity (inverse of resistivity) of the adjacent formation. Comparisons between deep and medium results can indicate porosity.
- *Single Point Resistance (SPR) Log* — Changes between a down-hole electrode and a reference surface electrode reflect changes in the formation resistivity. This can represent changes in porosity, water salinity, and fluid connectivity.
- *Calliper Log* — Spring-loaded arms that press against the side of the hole and can indicate well and casing integrity. It can also be used to identify fractures in the lithology intercepted by the well.

The results from these surveys coupled with the lithological and hydrostratigraphy descriptions obtained from drillhole sample cuttings informed the aquifer boundaries at each of the sites and the selected intervals for the screens of the monitoring wells.

### **A.5 Site locations**

Existing drillhole information, geological maps, hydrostratigraphy, surface geophysical surveys and site access planning were used to finalise the site locations for the new drillholes as part of the drilling program. Drillhole construction details for all the new sites are shown in Apx Table A.1.

The following sub-sections provide geological and geophysical logs from each of the drill sites.

Apx Table A.1 Well construction details for all drill sites.

UNIT NUMBER	PERMIT NO	WELL ID	SITE NO	LOCATION	AQUIFER	EASTINGS	NORTHINGS	NATURAL GROUND (MAHD)	TOP OF CASING (MAHD)	COMPLETION DEPTH (MBG)	TYPE OF COMPLETION
6628-27213	229338	1a			FRA	288808	6136159	117.15	117.10	142.00	single well, telescopic
6628-27218	229339	1b		Site 1 Rostrevor	T2	288811	6136157	117.23	117.17	98.50	multi, inline screen
6628-27217	229339	1c	T1		288811	6136157	117.23	117.17	56.00	multi, inline screen	
6628-27216	229339	1d	Q		288810	6136157	117.23	117.18	38.00	multi, inline screen	
6628-27212	230061	3a			FRA	284430	6134668	58.42	58.36	169.00	single well, telescopic
6628-27255	230062	3b		T2	284433	6134669	58.46	58.28	118.58	multi, inline screen	
6628-27256	230063	3c		Site 3 Trinity Gardens	T1(?)	284433	6134669	58.46	58.30	65.46	multi, inline screen
6628-27257	230064	3d	T1		284433	6134669	58.46	58.28	36.78	multi, inline screen	
6628-27258	230062	3e	Q		284433	6134669	58.46	58.31	18.90	multi, inline screen	
6628-27386	227509	5a	Site 5		Strangways Tce, North Adelaide	FRA	279946	6134189	19.442	19.323	102
6628-27504	236133	5b		War Memorial Dve, North Adelaide	FRA	279230	6133957	22.260	22.209	66	single well, open hole
6628-27435	236134	5c		War Memorial Dve, North Adelaide	Q	279229	6133956	22.274	22.223	12	single well, inline
		6a		Site 6 Welland	T2	277122	6134066	14.665	14.707	248	single well, telescopic
		6b			T1b	277120	6134072	14.665	14.811	218	single well, telescopic
		6c			T1a	277116	6134068	14.665	14.744	174	multi, inline screen
		6d			Q6	277116	6134068	14.665	14.739	117	multi, inline screen
6628-27253	227519	12	Site 12	Woodville	T1	275216	6135618	9.822	9.717	128	single well, telescopic
6628-27436	231758	13a		Site 13 Gilman	T2	273213	6142479	1.370	1.308	185	single well, telescopic
6628-27503	231759	13b			T1	273213	6142477	1.386	1.305	98	single well, telescopic

UNIT NUMBER	SCREEN INTERVAL (M)	CASING	SCREEN TYPE	GROUT METHOD	DEVELOPMENT	WELL HEAD	DATE SWL	SWL (MBOC)	RSWL (MAHD)
6628-27213	136-142	100mm class 18 PVC	100mm dia., 0.5mm apt. s/steel	pressure cement	air	Gatic cover	2/05/2014 13:13	61.15	55.95
6628-27218	95.5-98.5	50mm class 18 PVC	50mm class 18 PVC	tremie	air	Gatic cover	8/05/2014 11:14	61.13	56.04
6628-27217	53-56	50mm class 18 PVC	50mm class 18 PVC	tremie	air	Gatic cover		DRY	
6628-27216	35-38	50mm class 18 PVC	50mm class 18 PVC	tremie	air	Gatic cover		DRY	
6628-27212	163-169	100mm class 18 PVC	100mm dia., 0.5mm apt. s/steel	pressure cement	air	Gatic cover	5/05/2014 14:38	19.37	38.99
6628-27255	114-120	50mm class 18 PVC	50mm class 18 PVC	tremie	air	Gatic cover	9/05/2014 12:13	16.21	42.07
6628-27256	63-66	50mm class 18 PVC	50mm class 18 PVC	tremie	air	Gatic cover	May	16.76	41.54
6628-27257	33-36	50mm class 18 PVC	50mm class 18 PVC	tremie	air	Gatic cover	14/05/2014 13:53	19.48	38.80
6628-27258	16-19	50mm class 18 PVC	50mm class 18 PVC	tremie	air	Gatic cover	May	18.6	39.71
6628-27386	78-102	150mm class 12 PVC	open hole	pressure cement	air	Gatic cover	23/09/2014	16.43	2.89
6628-27504	62-66	200mm class 12 pvc	open hole	pressure cement	air	Gatic cover	24/09/2014	0	22.21
6628-27435	11.0-12.0	50mm class 18 PVC	50mm class 18 PVC	tremie	air	Gatic cover	24/09/2014	7.165	15.06
	245-251	150mm class 18 PVC	100mm dia., 0.5mm apt. s/steel	pressure cement	air	Gatic cover	17/09/2014	13.65	1.06
	212-218	150mm class 18 PVC	100mm dia., 0.5mm apt. s/steel	pressure cement	air	Gatic cover	16/09/2014	16.596	-1.79
	168-174	100mm class 18 PVC	100mm dia., 0.5mm apt. s/steel	tremie	air	Gatic cover	18/09/2014	16.9	-2.16
	111-117	50mm class 18 PVC	50mm class 18 PVC	tremie	air	Gatic cover	16/09/2014	30.96	-16.22
6628-27253	120-128	150mm class 12 PVC	100mm dia., 0.5mm apt. s/steel	pressure cement	air	Gatic cover	19/09/2014	12.07	-2.35
6628-27436	178-184	150mm class 18 PVC	100mm dia., 0.5mm apt. s/steel	pressure cement	air	Gatic cover	7/10/2014	3.635	-2.33
6628-27503	94-100	150mm class 18 PVC	100mm dia., 0.5mm apt. s/steel	pressure cement	air	Gatic cover	9/10/2014	9.3	-8.00

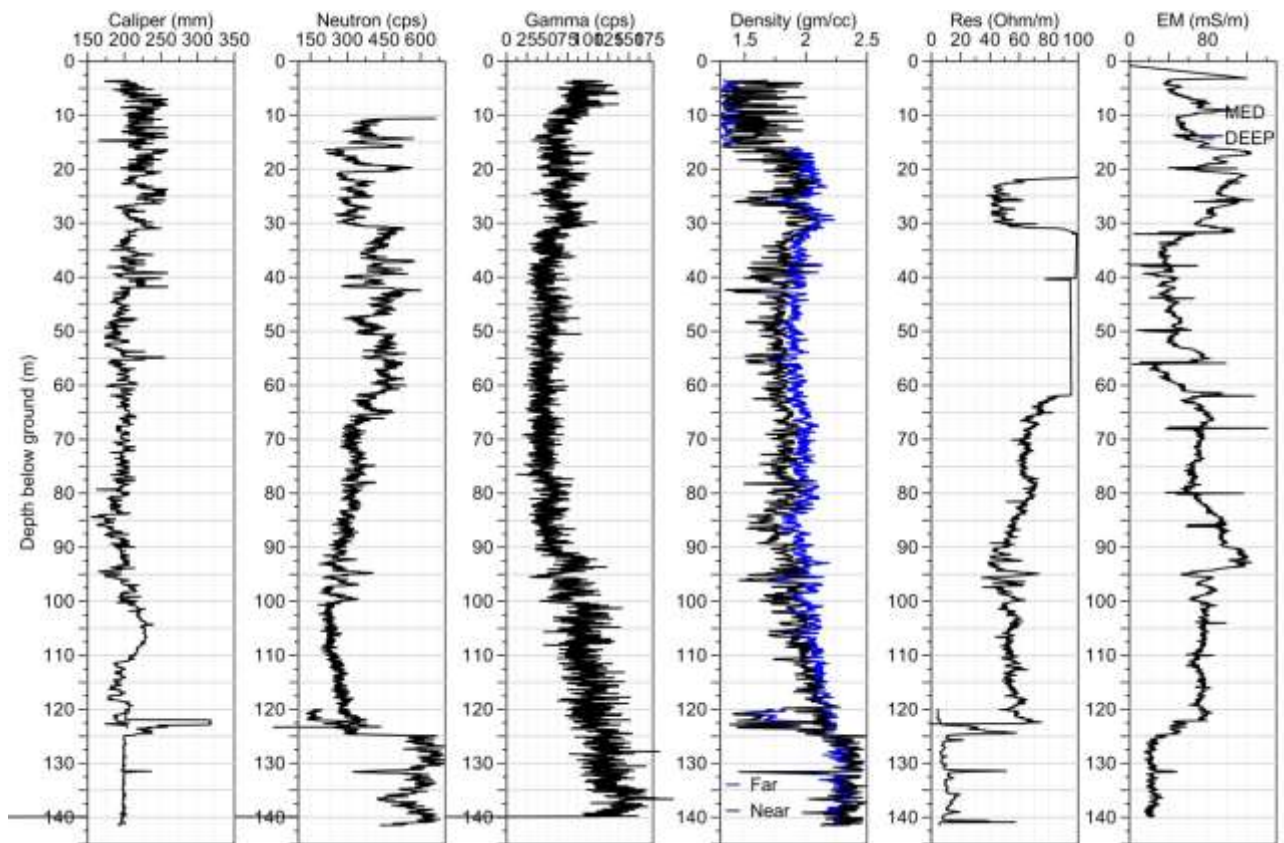
### A.5.1 ROSTREVOR- SITE 1



Apx Figure A.2 Location map of drill site 1 at Rostrevor.

Apx Table A.2 Drillhole strata log of deepest well (ID: 1A, permit number [PN]: PN229338) at site 1, Rostrevor.

SCREEN INTERVAL (MBG)	AQUIFER	DEPTH FROM (MBG)	DEPTH TO (MBG)	DESCRIPTION
		0	2.00	TOPSOIL.
		2.00	8.00	SILT. Medium brown.
		8.00	10.00	SAND. Red-brown medium grained sand with some clay.
		10.00	15.00	SILTY SAND. White silty fine grained sand with minor gravels.
		15.00	23.00	SANDY CLAY. Brown clay with fine-medium grained sand with some quartz; 15-17m red.
		23.00	30.00	CLAY. Mottled red-brown-red dense clay.
		30.00	33.00	SANDY CLAY. Red clay with fine grained sand.
Scr: 35-38	T1 (?)	33.00	56.00	SAND. Light brown fine grained sand.
Scr 53-56	T1 (?)	56.00	73.00	SAND. Yellow-white fine grained sand.
		73.00	85.00	SAND. Yellow-orange fine grained sand; 73-75m red.
		85.00	92.00	SAND. Orange fine grained sand with some quartz.
		92.00	99.00	SAND. Grey-brown medium grained sand.
Scr: 95.5-98.5	T2 (?)	99.00	111.00	SILTY SAND. Brown-grey silty medium grained sand with 15% gravels.
		111.00	128.00	SHALE. Grey shale with silt and fine grained sand; hard in places (weathered zone)
Scr: 136-142	FRA	128.00	142.00	SLATE. Dark grey-blue hard slate.

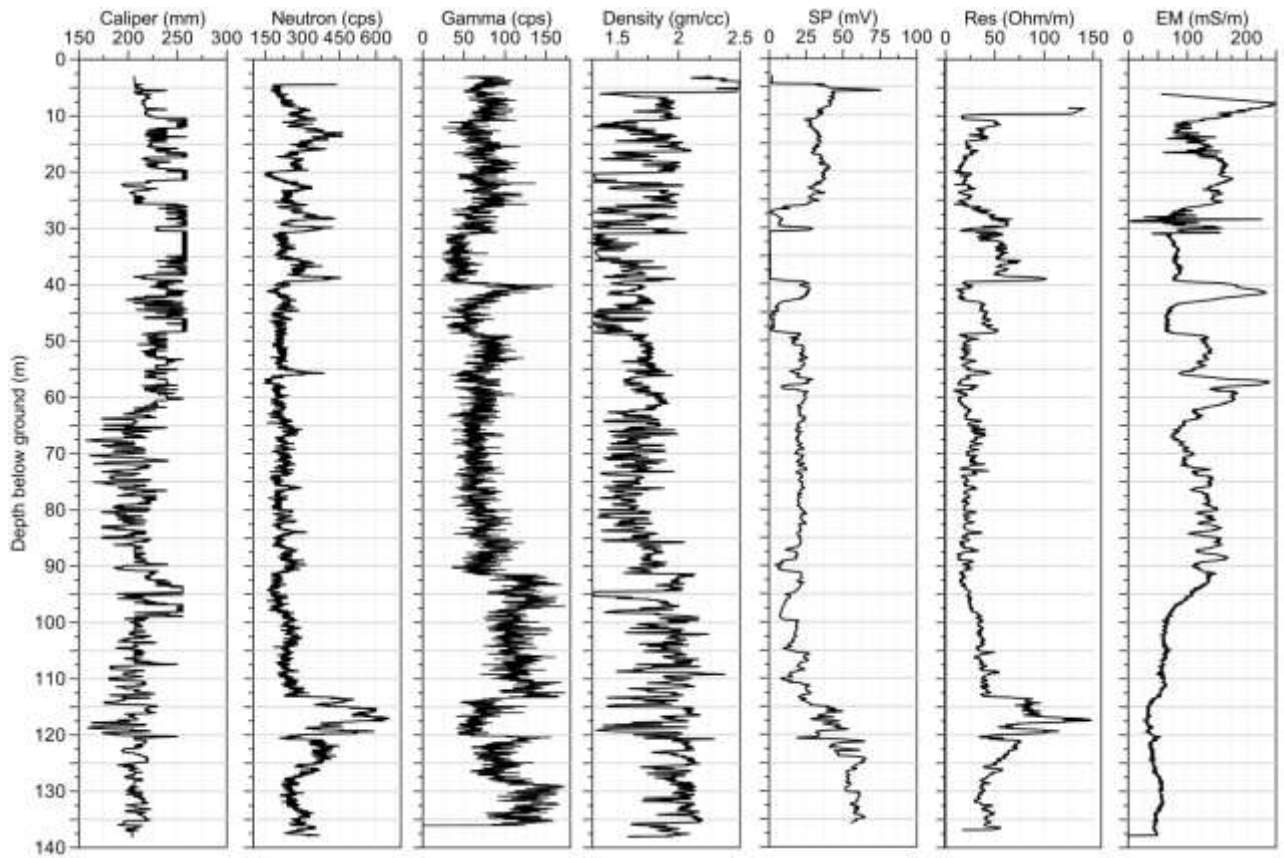


Apx Figure A.3 Geophysical logs of deepest well (ID: 1A, PN229338) at site 1, Rostrevor.



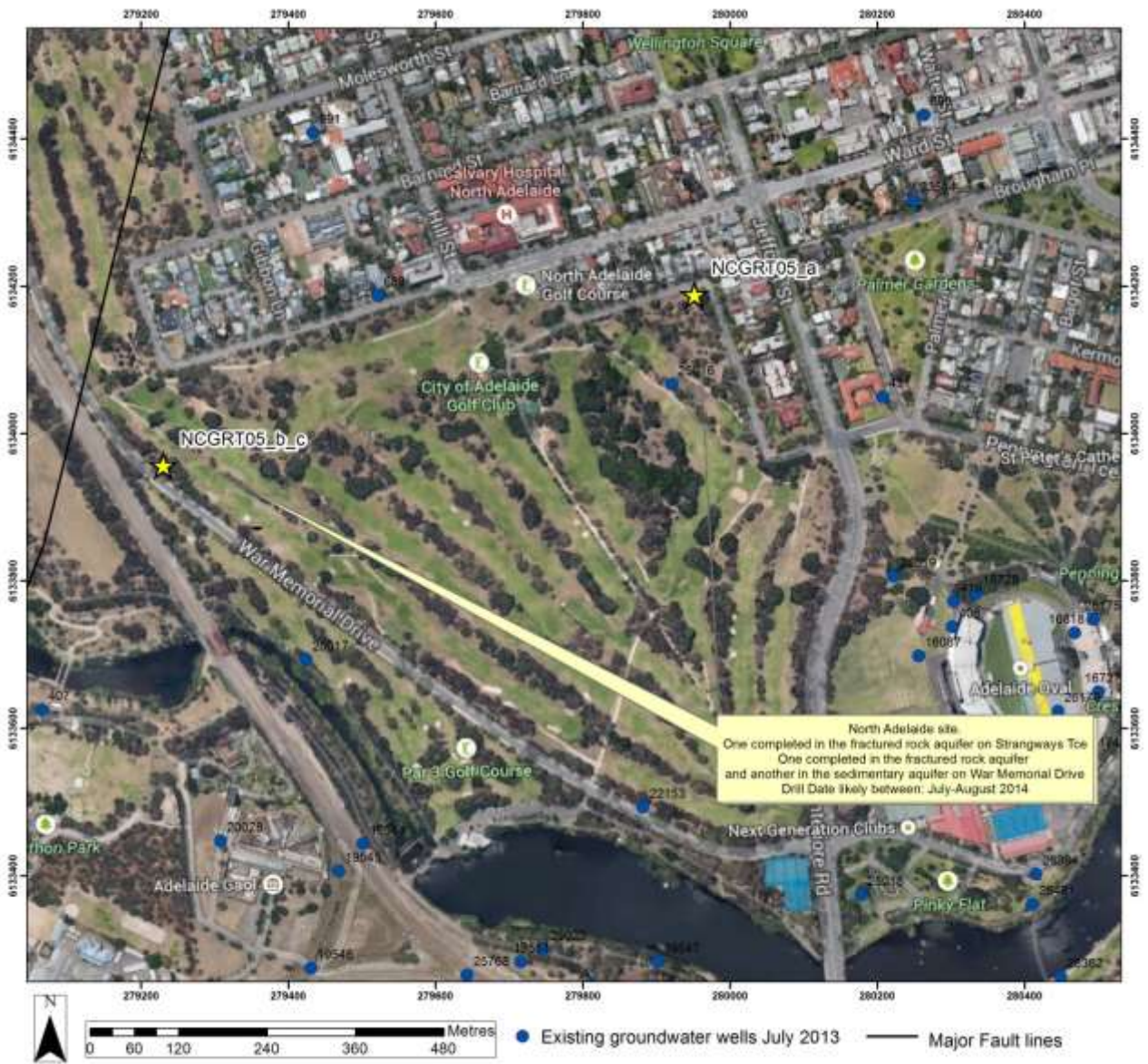
**Apx Table A.3 Drillhole strata log of deepest well (ID: 3A, PN230061) at site 3, Trinity Gardens.**

SCREEN INTERVAL (MBG)	AQUIFER	DEPTH FROM (MBG)	DEPTH TO (MBG)	DESCRIPTION
		0	1.00	TOPSOIL.
		1.00	6.00	SILT. Medium brown.
		6.00	9.00	CLAY. Light brown.
		9.00	10.00	COBBLES. Red fine-medium grained sand with 10% quartz cobbles.
		10.00	15.00	SAND. Light brown fine-medium grained sand with gravels increasing with depth to 15m.
		15.00	18.00	COBBLES. Red fine-medium grained sand with 95% quartz cobbles.
Scr: 16-19	Q	18.00	23.00	CLAY. Light grey/yellow dense clay. Becoming white with depth to 23m.
		23.00	27.00	CLAYEY SAND. Light brown/yellow clayey sand with yellow clay band 25-27m.
		27.00	33.00	SAND. Light brown medium grained sand. 30-32m coarse sand with 25% quartz.
Scr: 34-37	T1	33.00	41.00	SAND. Yellow fine grained sand.
		42.00	49.00	SILT. Dark grey sandy silt.
		49.00	63.00	CLAY. Black silty lignitic clay. 61-62m abundant quartz chips.
Scr: 63-66	T1 (?)	63.00	76.00	SILTY SAND. Light grey silty sand. 72-73m abundant shells.
		76.00	93.00	CLAY. Black boggy silty clay.
		93.00	102.00	CLAY. Light grey to white silty clay.
		102.00	109.00	SILTY SAND. Light brown to orange silty sand.
		109.00	110.00	SAND. Light brown to orange coarse grained sand.
		110.00	114.00	SANDY CLAY. Light brown sandy clay.
Scr: 113.5-119.5	T2	114.00	120.00	SAND. White medium grained sand. Very coarse 119-120m.
		120.00	130.00	SILTY SAND. Light brown to orange silty sand with 40% quartz.
		130.00	142.00	SILTY CLAY. Light brown to orange silty clay with minor sand.
		142.00	165.00	DOLOMITE. Grey hard dolomite.
		165.00	168.00	SAND. Light grey medium-coarse grained sand.
Scr: 162.5-168.5	FRA	168.00	168.50	SLATE. Dark grey-blue hard slate.



Apx Figure A.5 Geophysical logs of deepest well (ID: 3A, PN230061) at site 3, Trinity Gardens.

### A.5.3 NORTH ADELAIDE- SITE 5



Apx Figure A.6 Location map of drill site 5 at North Adelaide.

**Apx Table A.4 Drillhole strata log of deepest well (ID: 5A, PN227509) at site 5, Strangways Tce, North Adelaide.**

SCREEN INTERVAL (MBG)	AQUIFER	DEPTH FROM (MBG)	DEPTH TO (MBG)	DESCRIPTION
		0	1.00	TOPSOIL.
		0	2.00	TOPSOIL.
		2.00	5.00	CLAY. Red hard clay.
		5.00	8.00	SAND. Red-brown fine grained sand with some clay.
		8.00	11.00	SAND. Brown fine grained sand.
		11.00	12.00	GRAVELS. Mottled white-red-brown fine gravels with some medium grained sand and silt.
		12.00	15.00	GRAVELS. Red-brown fine-medium gravels with some medium grained sand and silt.
		15.00	16.00	As above with yellow clay.
		16.00	19.00	CLAY. Yellow soft clay.
		19.00	38.00	No sample.
		38.00	48.00	LIGNITE. Black lignite; 46-48 coal like.
		48.00	75.00	CLAY. 48-54 dark brown stiff clay; 54-59 white-grey stiff clay; 59-63 light grey-greenish stiff clay; 64-75 (refusal at 75m) dark grey stiff clay.
Scr: 76.7-102 (OH)	FRA	75.00	102.00	SHALE. Light grey-bluish hard consolidated shale.

**Apx Table A.5 Drillhole strata log of deepest well (ID: 5B, PN236133) at site 5, War Memorial Drive, North Adelaide.**

SCREEN INTERVAL (MBG)	AQUIFER	DEPTH FROM (MBG)	DEPTH TO (MBG)	DESCRIPTION
		0	1.00	TOPSOIL.
		1.00	8.00	CLAY. Red/brown hard clay.
		8.00	9.00	CLAY. Light brown moderate plasticity clay, mica present.
		9.00	10.00	CLAY. brown silty clay, grey/white colouring showing signs of oxidation.
		10.00	12.00	SAND. Fine to medium grained, micaceous, moderately sorted. Clear/opaque grains. Wet.
Scr: 11-12	Q	12.00	16.00	SAND. Fine sandy gravel. Subrounded/rounded. 1-10mm diameter. Appears to be associated with old riverbed (Torrens River adjacent). Lignite bed also encountered
		16.00	50.00	LIGNITE. Black/brown lignite. Dry and coal like biscuits
		50.00	56.00	CLAY. Brown/grey clay. Weathered bedrock material
		56.00	62.00	SHALE. Light grey-bluish weathered soft shale.
Scr: 62-66 (OH)	FRA	62.00	66.00	SHALE. Light grey-bluish hard consolidated shale.

No geophysical logs were undertaken at site 5b, War Memorial Drive, North Adelaide. Well completion was based on the strata log and other existing hydrogeological information in the nearby area.

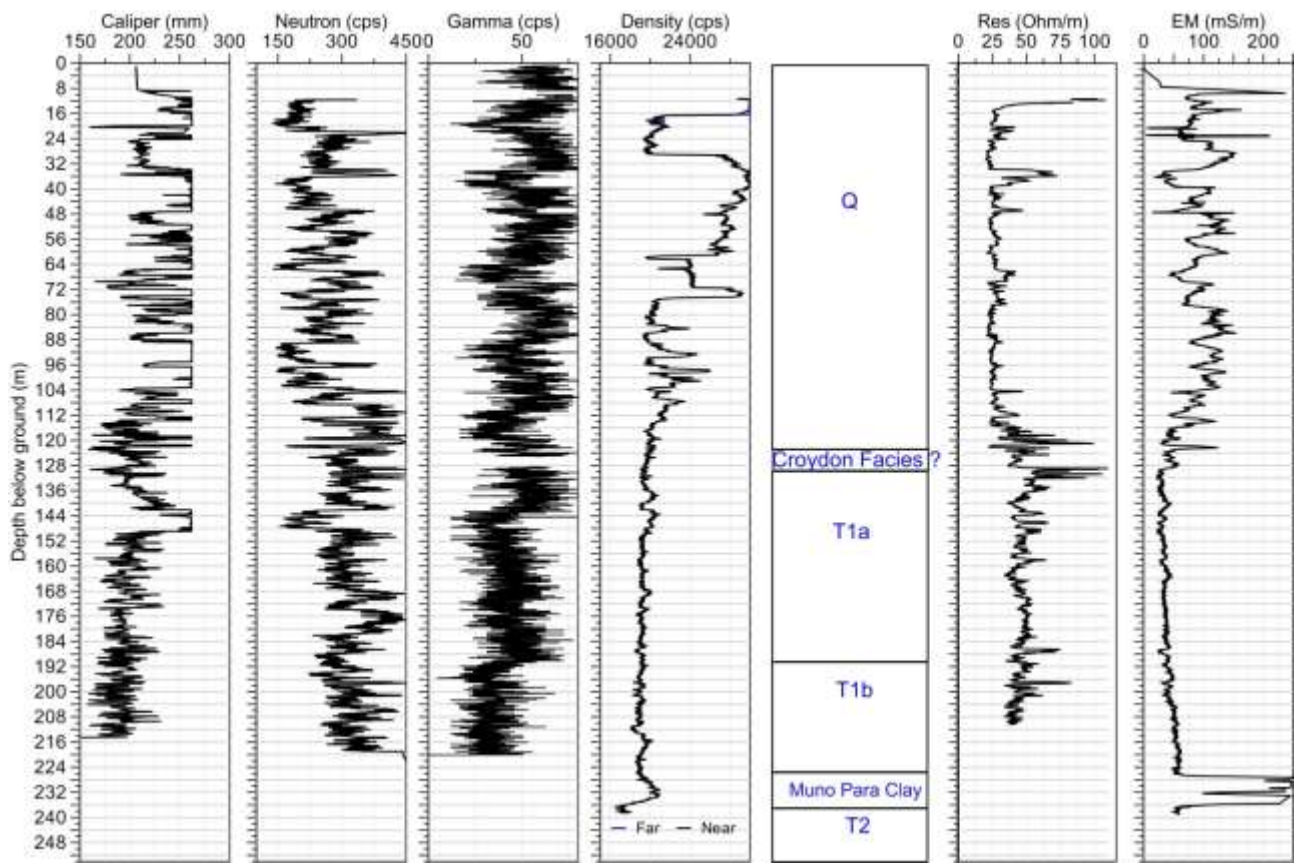
### A.5.4 WELLAND- SITE 6



Apx Figure A.7 Location map of drill site 6 at Welland.

Apx Table A.6 Drillhole strata log of deepest well (ID: 6A, PN227513) at site 6, Welland.

SCREEN INTERVAL (MBG)	AQUIFER	DEPTH FROM (MBG)	DEPTH TO (MBG)	DESCRIPTION
		0	6.00	TOPSOIL. Dark brown.
		6.00	10.00	CLAY. Mottled brown-grey clay.
		11.00	12.00	SAND. Brown fine grained sand.
		13.00	16.00	CLAY. Brown clay.
	Q1	17.00	22.00	SAND. Yellow-brown Fine-medium grained sand.
		23.00	33.00	CLAY. Red clay; light brown and more silty 31-33m
	Q2	34.00	39.00	SAND. Yellow-brown medium-coarse grained sand with some gravels (<5%); gravels increas in size and abundance 37-39m.
		40.00	45.00	CLAY. Light brown silty clay.
	Q3	46.00	48.00	SAND. Medium-coarse grained sand with some gravels.
		49.00	55.00	CLAY. Red silty clay.
	Q4	56.00	57.00	SAND. Brown fine grained sand.
		58.00	63.00	CLAY. Brown silty clay.
	Q4	64.00	70.00	SAND. Yellow-brown medium grained sand.
		71.00	72.00	GRAVELS. Fine gravels; some quartz.
	Q5	73.00	77.00	GRAVELS. Fine-coarse gravels; some quartz.
		78.00	89.00	CLAY. Red-brown clay.
		90.00	109.00	SILTY SAND. Red-brown silty fine-grained sand.
Scr: 110.5-116.5	Q6	110.00	120.00	SAND. Reddish brown fine-medium grained sand.
	Carisbrooke Sand (?)	121.00	129.00	SAND. Yellow fine-medium grained sand. Geophysics (gamma) peaks 125-128m (?)
	T1a	130.00	159.00	SHELLY SAND. Shelly grey-brown fine/medium grained sand, silt and minor clay; larger shell fragments 143-150m.
		160.00	182.00	SAND. Brown medium grained sand; minor shell fragments.
Scr: 168-174	Croydon Facies	183.00	190.00	SILTY SAND. Brown fine grained fossiliferous silty sand with minor clay.
	T1b	191.00	225.00	SILTY SAND. Brown medium grained fossiliferous silty sand.
Scr: 211-217	Munno Para	226.00	236.00	CLAY. Dark grey-blue calcareous clay.
Scr: 240-246	T2	236.00	257.00	LIMESTONE. Yellow-brown cemented to friable, highly fossiliferous limestone/sandstone.



Apx Figure A.8 Geophysical logs of deepest well (ID: 6A, PN227513) at site 6, Welland.



## A.5.5 WOODVILLE- SITE 12



Apx Figure A.9 Location map of drill site 12 at Woodville.

Apx Table A.7 Drillhole strata log of well 12 (PN227519) at site 12, Woodville.

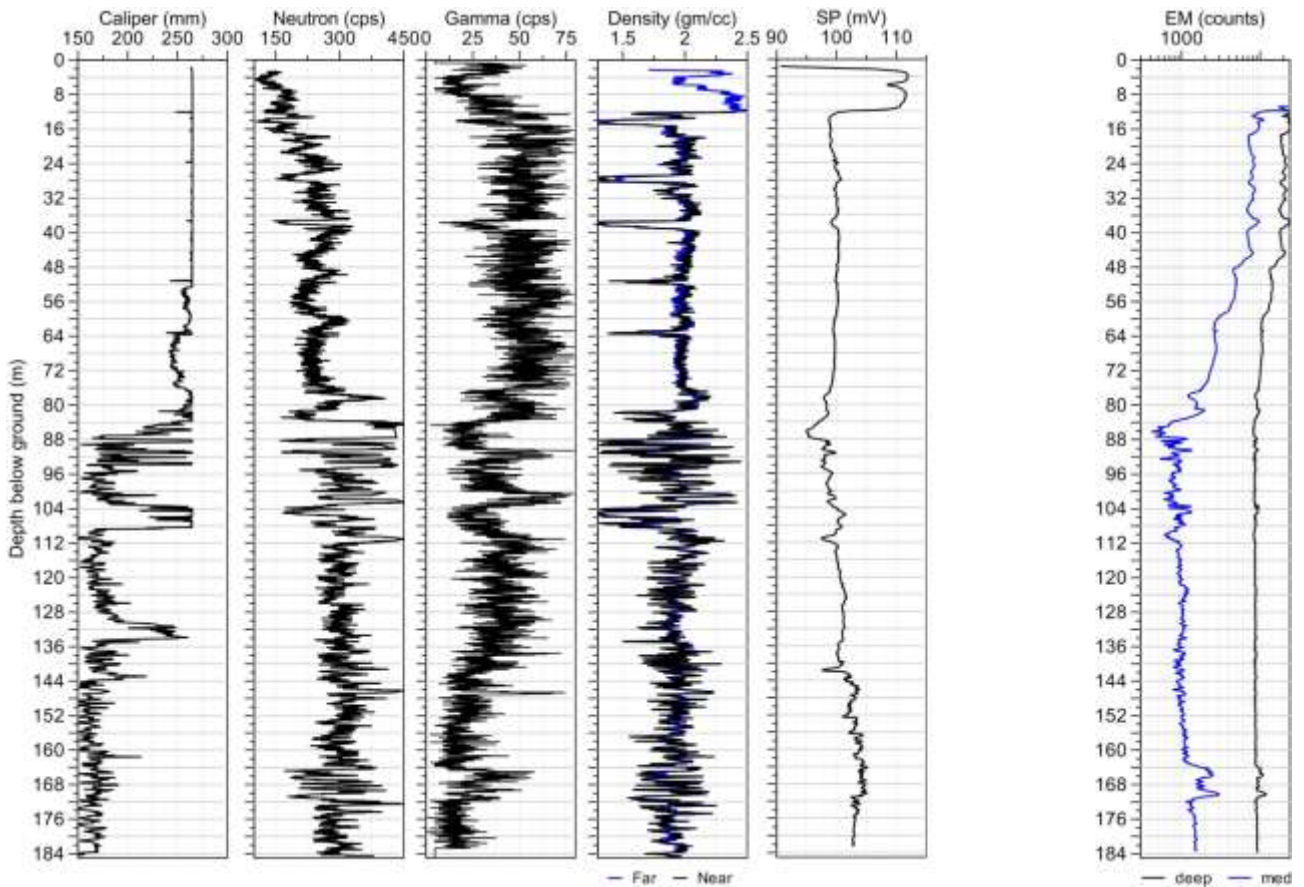
SCREEN INTERVAL (MBG)	AQUIFER	DEPTH FROM (MBG)	DEPTH TO (MBG)	DESCRIPTION
		0	2.00	TOPSOIL.
		3.00	4.00	CLAY. Dark brown clay.
		5.00	7.00	SILTY SAND. Medium brown silty sand.
		8.00	11.00	CLAY. Dark brown clay with minor fine grained sand.
		12.00	18.00	CLAY. Mottled red-grey-brown clay.
		19.00	20.00	SANDY CLAY. Medium brown sandy clay.
		21.00	23.00	SAND. Light brown medium grained sand with 10% quartz grains.
		24.00	26.00	SANDY CLAY. Medium brown sandy clay.
		27.00	29.00	SAND. Light brown medium grained sand with 10% quartz grains; finer grains ~29m.
		30.00	31.00	SANDY CLAY. Medium brown sandy clay.
		31.00	32.00	SAND. Medium brown fine grained sand.
		33.00	34.00	SANDY CLAY. Medium brown sandy clay.
		35.00	37.00	SAND. Medium brown fine grained sand.
		37.00	38.00	SANDY CLAY. Medium brown sandy clay.
		39.00	44.00	CLAY. Red-brown very stiff dense clay.
		45.00	46.00	SANDY CLAY. Medium brown sandy clay.
		47.00	48.00	SAND. Medium brown fine grained sand.
		49.00	50.00	SANDY CLAY. Medium brown clay with coarse grained sand.
		51.00	57.00	CLAY. Red-dark brown stiff clay.
		58.00	66.00	CLAY. Yellow-brown stiff clay.
		66.00	97.00	CLAY. Medium brown stiff clay.
		98.00	99.00	SANDY CLAY. Medium brown clay with fine-medium grained sand.
		100.00	110.00	SAND. Yellow-light brown fine-medium grained sand.
		111.00	121.00	SHELLY SAND. Shelly grey-brown fine/medium grained sand, silt and minor clay.
Scr: 120-128	T1	122.00	128.00	LIMESTONE. Moderately cemented, fossiliferous limestone with sand and silt bands.

No geophysical logs were undertaken at site 12, Woodville. Well completion was based on the strata log and other existing information in the nearby area.



Apx Table A.8 Drillhole strata log of deepest well (ID: 13A, PN231758) at site 13, Gilman.

SCREEN INTERVAL (MBG)	AQUIFER	DEPTH FROM (MBG)	DEPTH TO (MBG)	DESCRIPTION
		0	1.00	SAND. Yellow fine sand with rubble, dry (HCl - reactive)
		1.00	2.00	SAND. Yellow and grey fine sand with silty clay, some rubble, dry. Quartz sand angular-80%. (HCl - reactive)
		2.00	3.00	CLAY. Grey stiff clay , very plastic, fine sand and silt in last 20 cm, with shells (HCl - reactive)
		3.00	5.00	SILTY CLAY. Grey silty sand, fine angular, some coarse quartz sand , unsorted, lot of hairy things, lot of shells (HCl - reactive)
		5.00	9.00	SAND/SHELLS. White to yellow just little shells and corals, lot of hairy things ( seaweed ???), some quartz sand (HCl - reactive)
		9.00	11.00	SAND/SHELLS. Same as above but brown, silty (HCl - reactive)
		11.00	12.00	GRAVELY CLAY. Gravels and rubbles in brown clay. Gravels up to 5 cm, clay, very plastic, no more hairy things. (HCl - low reactive)
		12.00	13.00	SAND. Brown sand, quartz, unsorted, angular, from fine to coarse, little of shells (HCl - low reactive)
		13.00	14.00	SAND. Brown quartz sand, fine to coarse, unsorted, angular. In first half meter, after starting brown plastic clay (HCl - low reactive)
		14.00	36.00	CLAY/SAND/LIMESTONE. 14-15m brown plastic clay with gravel and rubble (HCl - no reactive); 15-22m limestone chips; 22-23m some medium to coarse sand ~ 20% (HCl - low reactive); 23-30m just brown clay (HCl - no reactive); 30-36m mottled brown, grey, red clay, some rock chips, limestone chips (HCl - low reactive)
		36.00	38.00	SAND. Unsorted fine to coarse quartz sand, angular. On 37.5 m start brown clay (HCl - no reactive)
		38.00	74.00	CLAY. Brown plastic clay with quartz gravel 10%. On 38m instead gravel is sand. On 40 m just greasy clay (HCl - low reactive)
		74.00	85.00	CLAY. Brown clay, plastic, with limestone chips , amount of chips raising with depth. On 85 m - 70-80 % limestone (HCl - reactive)
		85.00	86.00	CLAY. Layer of quartz coarse sand in brown clay
		86.00	91.00	SAND. Quartz medium sand with limestone content with depth raising size of grains and start brown clay (HCl - reactive)
		91.00	92.00	SHELLS. 95% shells, little brown clay and limestone chips
Scr: 94-100	T1	92.00	104.00	LIMESTONE. Grey limestone, 40% shells, some silt
		104.00	113.00	CORALS. Corals and shells some silt, fine sand
		113.00	131.00	LIMESTONE. Grey limestone and quartz medium sand 20%, little shells
		131.00	133.00	LIMESTONE. As above but more silt
		133.00	139.00	SILT. Silt with shells ( 70% shells) little quartz , medium sand and limestone
		139.00	146.00	SILT. As above, less silt more limestone ( limestone with shells and silt ), grey
		146.00	165.00	LIMESTONE. Yellow to light brown limestone with shells, some silt. 150m some quartz fine gravel subrounded. after 150 m light brown limestone with some gravel, no shells
	Munno Para	165.00	174.00	CLAY. Start dark grey plastic clay – Munno para Clay
Scr: 178-185	T2	174.00	185.00	LIMESTONE. Light brown limestone with corals, still particles of dark grey clay, after just corals , light brown (limestone made of corals)



Apx Figure A.11 Geophysical logs of deepest well (ID:13A, PN231758) at site 13, Gilman.

## A.6 References

- Gerges N (1999) The geology & hydrogeology of the Adelaide metropolitan area. PhD thesis, Flinders University of South Australia.
- Gerges N (2006) 'Overview of the hydrogeology of the Adelaide metropolitan area, South Australia.' Government of South Australia, through Department of Water, Land and Biodiversity Conservation, DWLBC Report 2006/10, Adelaide.
- National Uniform Drillers Licensing Committee (2012) 'Minimum construction requirements for water bores in Australia. Third Edition. Australian Drilling Industry Association. February 2012.'
- Zulfic H, Osei-Bonsu K, Barnett SR (2008) 'Adelaide Metropolitan Area Groundwater Modelling Project. Volume 1 - Review of Hydrogeology, and Volume 2 - Numerical model development and prediction run. South Australia.' Department of Water, Land and Biodiversity Conservation. DWLBC, Report 2008/05.

# Appendix B Review of the hydrogeological properties of aquifers and aquitards

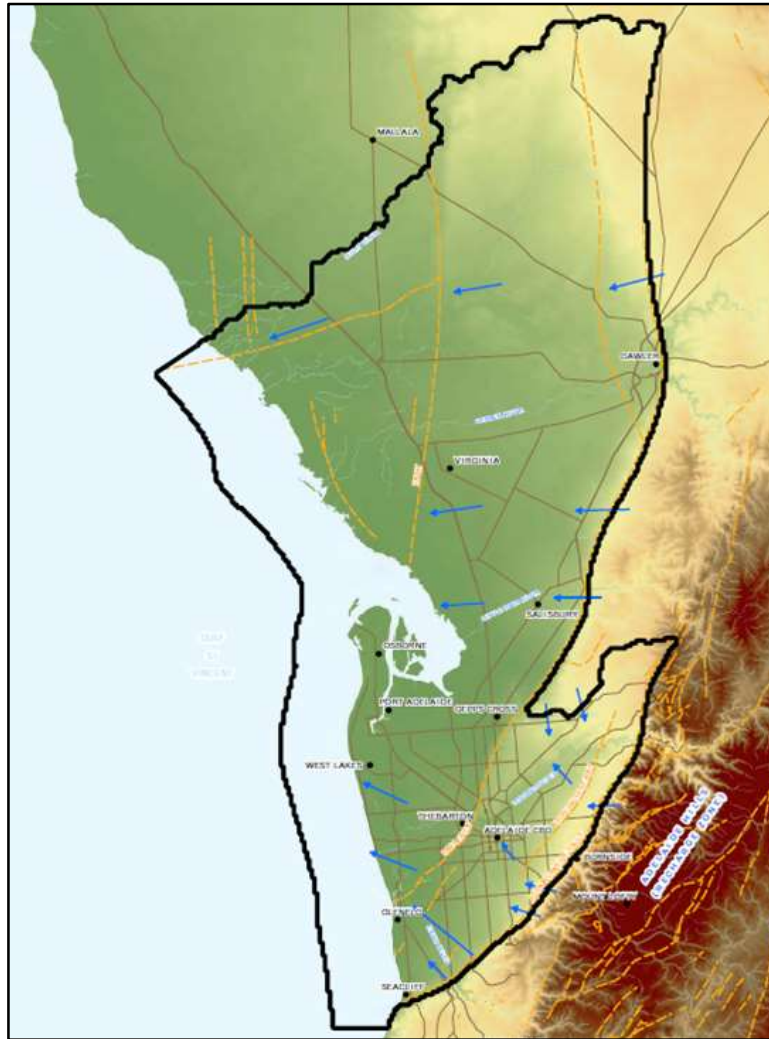
Authors: *Walkley S and Cranswick RH*

## B.1 Introduction

### B.1.1 BACKGROUND AND OBJECTIVES

The Goyder Institute for Water Research project “Assessment of Adelaide Plains Groundwater Resources” is currently being undertaken by the National Centre for Groundwater Research and Training (NCGRT), Flinders University, CSIRO and the Department of Environment, Water and Natural Resources (DEWNR). The aim of the project is to undertake research to update and improve an existing numerical groundwater model for the Adelaide Plains region. In order to have confidence in the groundwater model, certainty of the hydrogeological parameters being input into the model is required. Accordingly, values for the full range of hydrogeological parameters are required to be determined prior to the preparation of the model. During the calibration of the groundwater model, special attention will be paid to the input parameters such as hydraulic conductivity, porosity and storativity as these parameters are paramount to a sound groundwater flow model.

The focus area of the aforementioned project is the Adelaide Plains region west of the Eden-Burnside fault (which separates the plains from the Mount Lofty Ranges). The study area extends to the Light River in the north and the suburb of Seacliff in the south (Apx Figure B.1). Whilst the study area does not include the Noarlunga Embayment and Willunga Basin, as these formations lie on the boundary of the study area, information from these areas will be included within the project. The purpose for the inclusion of the Willunga Basin within the study area will make possible the transfer of research findings from the Willunga Basin to similar areas and environments within the Adelaide Plains region. There is substantial knowledge on the hydrogeology of Willunga Basin thanks to the creation of a ‘NCGRT-SuperScience site’ (“Willunga Super Science site. Research update”, October 2012, 89 pages). Due to this, the Willunga Basin has been extensively monitored (including drilling) and equipped with a monitoring well network during the last four years.



**Apx Figure B.1 Location, topography and lateral extent of the previous model boundary (Georgiou, J. et al., 2011).**

There are numerous reports available which provide varying values for the hydrogeological properties of the aquifers and aquitards underlying the Adelaide Metropolitan Area. The source of these values is not always clear, and the available information is not combined in a systematic way. As a result, the range of parameters of the various hydrogeological units (described in Section B.4), and how these vary spatially is uncertain.

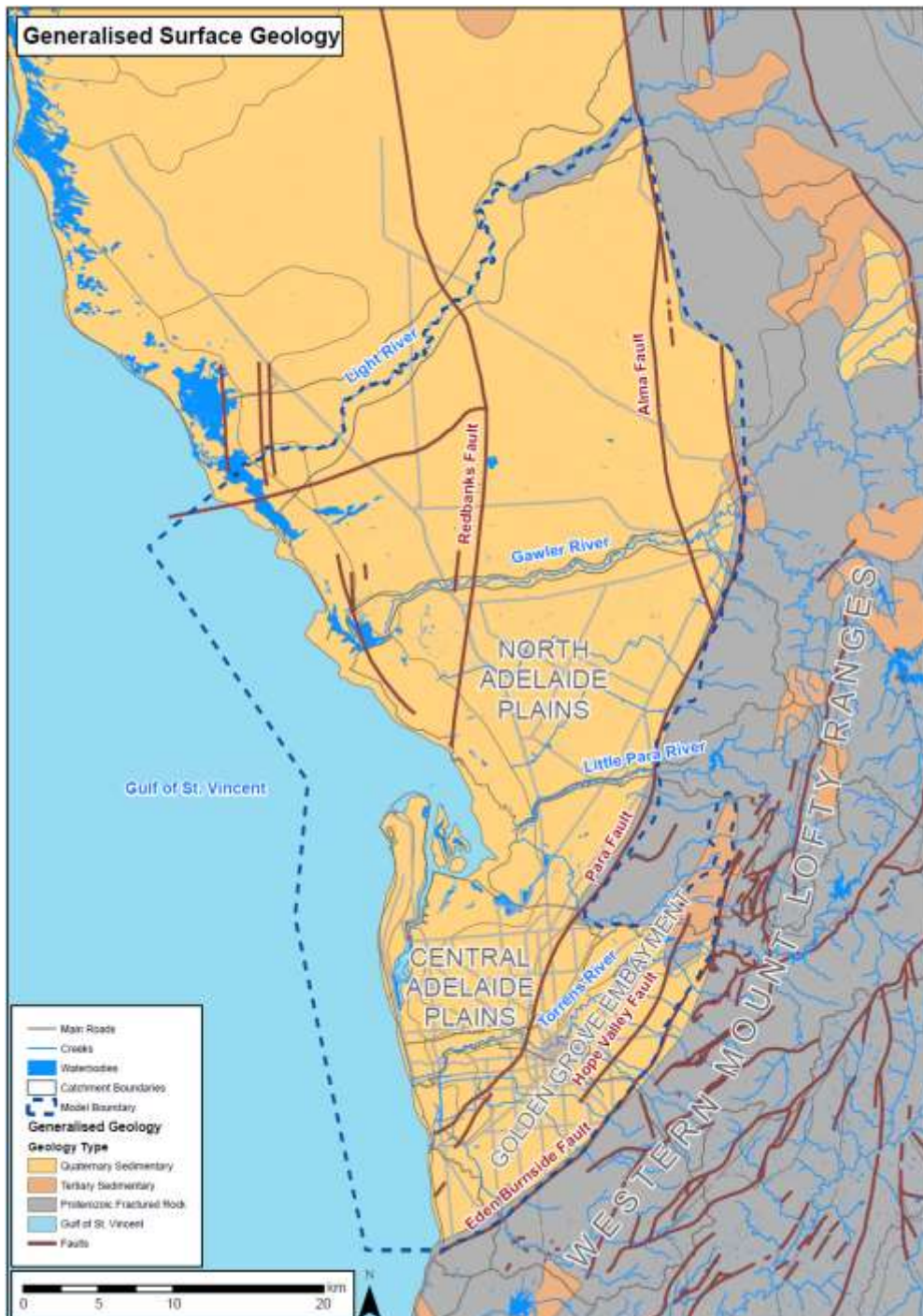
The purpose of this project is to provide a critical review of the available hydrogeological data for the study area, determine how the values for each of the parameters was calculated / sourced, extract and consolidate the relevant data and provide the data in a systematic format for inclusion in the large Goyder Institute for Water Research Project “Assessment of Adelaide Plains Groundwater Resources”.

### **B.1.2 LOCATION OF STUDY AREA AND GEOLOGICAL FEATURES**

The study area encompasses a portion of the St Vincent Basin and includes the Adelaide Plains sub-basin, the Northern Adelaide Plains and the Golden Grove Embayment (Apx Figure B.2). The study area also includes the Willunga Basin and the Noarlunga embayment. There are two major faults zones within the study area – the Eden Burnside fault which bounds the study area to the east, and the Para Fault which is located in the northern portion of the study area. In addition, there are several minor faults. The Golden Grove, Noarlunga and Willunga embayments lie between the faults and are asymmetric tectonic valleys. The hydrostratigraphy of the Golden Grove Embayment is significantly more complicated than other regions within the study area as a result of ‘erosional and depositional boundaries, lateral facies changes

and faulting' (Hodgkin, 2004). As a result, the geological formations can either form effective single aquifer systems with adjacent formations, or result in aquifers aligning against aquitards / confining beds (SKM, 2009), which strongly affects the groundwater flow regime across the boundary.

There are several rivers within the study area including the main rivers of Gawler River, River Torrens, Light River and the Sturt River. These rivers are both a source of groundwater recharge and groundwater discharge.



Apx Figure B.2 Generalised surface geology of the Adelaide Plains region.

## B.2 Methodology

A total of 31 reports were reviewed during the literature review component of this project. For ease of discussion, the reports have been grouped into two sub-sections, with only the reports considered to be relevant to the project and containing new hydrogeological data summarised separately:

- Reports that contain relevant hydrogeological data;
- Reports that do not contain hydrogeological data i.e. all data discussed is obtained from other reports being reviewed, and reports that are not relevant to the project in terms of any hydrogeological data being presented.

Details of the reports reviewed are presented in Section B.3 and a summary of the information extracted from the reports is presented in Sections B.4 and B.5.

## B.3 Literature Review

### B.3.1 REPORTS THAT CONTAIN RELEVANT HYDROGEOLOGICAL DATA

#### 3.1.1 Gerges, N., 1996, 'Overview of the Hydrogeology of the Adelaide Metropolitan Area' DWLBC DME, 491/78

This report focussed on a 560 km<sup>2</sup> area in the Adelaide metropolitan area including the Golden Grove Embayment and Adelaide Plains. The study comprised a review of historical data from previously installed groundwater wells, the drilling and installation of new groundwater wells and geophysical wireline testing to confirm the lithology information.

As a whole, the study provided an overview of the aquifer system (including confining beds). The aquifer system was divided into different stratigraphic boundaries / zones based on the lithology encountered during drilling and groundwater use areas. In addition, discussions and interpretation of hydraulic connectivity between aquifers and possible groundwater interactions between aquifers and recharge / discharge zones based on the salinity, potentiometric surface and historical data was undertaken.

Whilst the report provided data and summaries on all Quaternary and Tertiary aquifers and the fractured rock aquifer, the main focus of the report was the first Tertiary aquifer (T1). In addition, it was apparent that limited data was available for some aquifers e.g. Q4, Q5, Q6, T4 and bedrock.

The information regarding the hydrogeological framework e.g. aquifer sequence, lithology, hydrogeological parameters within the study area has been investigated and interpreted further in subsequent reports; however, remains mostly unchanged indicating that the data is sound.

#### 3.1.2 Gerges, N., 1999, 'The Geology and Hydrogeology of the Adelaide Metropolitan Area Volume 1 and Volume 2', PhD Thesis, Flinders University, Adelaide

This PhD Thesis completed in 1999 provided an extensive update on the information previously presented in 1996 by the same author as the previous report. The update was completed using a combination of data reinterpretation and additional data collection to complete, what is considered today, to be the most comprehensive study of the geology and hydrogeology of the Adelaide

metropolitan area. Whilst the 1999 PhD thesis is not as well-known as the subsequent 2006 report, it was in the PhD thesis that Gerges originally established the current conceptual understanding of the major aquifer system in the area. As part of his works, Gerges compiled historical pumping data and water levels for the major aquifers, and constructed a comprehensive groundwater numerical flow model.

It is noted that much of this data has been reviewed and reinterpreted over the years and the majority of the reports reviewed concluded a similar hydrogeological framework, with minor exceptions noted.

### **3.1.3 Gerges, N., 2006, 'Overview of the Hydrogeology of the Adelaide Metropolitan Area', DWLBC, 2006/10**

As with the 1996 report / PhD thesis compiled by Gerges relating to the Adelaide metropolitan area, this report comprised a review of historical data from previously installed groundwater wells, the drilling and installation of new groundwater wells and geophysical wireline testing to confirm the lithology information. This report follows on from the report prepared by Gerges in 1996 and the subsequent PhD thesis report prepared by Gerges in 1999.

The report refers to several of Gerges' previous investigations undertaken in the 1980s (e.g. Gerges, N.Z., (1980), 'Metropolitan Area groundwater investigations progress report No. 2' S.A. Dept. Mines and Energy Rept. Bk. 82/5 (unpublished) and Selby, J., & Gerges, N.Z., (1981), 'Saline groundwater at Waterloo Corner', Quart. Geol. Notes. Geol. Surv. S.A. 79: 16-19) and in addition, the majority of the data was likely to have been collected during the writing of Gerges' thesis in 1999 and the data is at least 15 years old as at the current date. In addition, the report notes that the historical well data is not always reliable and data has been 'cherry picked' to obtain better reliability.

Hydrogeological parameters were determined and calculated for several of the aquifers; however, the information is limited and ranges considerably between zones. Details of these parameters are set out in Tables B.3 and B.4 and discussed in Section B.5.

The information regarding the hydrogeological framework within the study area has been relied upon heavily in subsequent reports reviewed which were prepared by other agencies and individuals.

### **3.1.4 Gerges, N., 2001, 'Northern Adelaide Plains Review', DWR (2001/13)**

This report documented an investigation into the then present state of the Northern Adelaide Plains aquifers with regard to potential overuse for irrigation and industrial purposes. The main focus of the report was on the T1 and T2 aquifers; however, some discussion regarding the impacts on the overlying and underlying aquifers was also included.

The majority of the report provided an overview of information previously documented in Gerges' previous reports and limited new data was collected; however some additional information regarding transmissivity and storage coefficients (calculated using flow net method analysis or type curve matching (log/log) and Jacobs straight line (semi logarithmic)) of the T1, T2 and T4 aquifers were documented.

### **3.1.5 Osei-Bonsu, K., Gerges, N. & Zulfic, H. 'Preliminary hydrogeological investigations at Waterloo Corner', DWR (2000/21)**

The report detailed an investigation into the high reported salinity of a production well installed within the T1 aquifer at Waterloo Corner. The investigation was limited in nature; however comprised pumping tests / aquifer discharge test to confirm the presence of a hydraulic connection between the Q4 (more

saline) and T1 (less saline) aquifers and determine hydrogeological parameters of the formation and perform down hole geophysical logs to confirm the geology.

### **3.1.6 'Glenelg Golf Club Well Completion Report – Wells 8 and 9', AGT, 2005/32**

The report documents the installation of two new production wells at the Glenelg Golf Course – a hydrogeologically complex area located in the vicinity of the inferred Para Fault North Splinter. A new well was drilled and installed within each of the T1b (Gerges' zone 3) and T2 (Gerges' zone 2A) aquifers, respectively. It was noted that a production well installed within the T1 aquifer was already present on the site.

### **3.1.7 Zulfic, H, Osei-Bonsu, K. and Barnett, S., 2008, 'Adelaide Metropolitan Area Groundwater Modelling Project: Volume 1 – Review of Hydrogeology', DWLBC; and**

**Osei-Bonsu, K. and Barnett, S., 2008, 'Adelaide Metropolitan Area Groundwater Modelling Project: Volume 2 – Numerical model development and prediction run', DWLBC**

The report comprised two components. The first component (volume 1) comprised an extensive review and reinterpretation of previous hydrogeological works undertaken in the study area (mainly Gerges' previous works). Whilst no additional field work was carried out, the reinterpretation of the data provided additional information which was considered to be relevant to the project.

Following on from this review, volume 2 details the development and construction of a groundwater flow simulation model. The groundwater model was designed to determine the long-term risks to the aquifer system, and to test various management scenarios. The model incorporated the revised interpretation of the hydrostratigraphy, together with the latest available information on the hydraulic properties. The results from the model allowed interpretation of interactions between aquifers; however, as a model is only as good as the data input into it, the interpretation of the modelling results may not be accurate and these interactions are best measured and interpreted through field based tests.

### **3.1.8 Hodgkin, T., 2004, 'Aquifer Storage Capacities of the Adelaide Region', DWLBC, 2004/47**

The report detailed an assessment of the storage capacities of the sedimentary aquifer systems to determine the aquifer storage and recovery of the Adelaide Plains sub-basin and Golden Grove Embayment. Whilst this report was prepared using existing data, the data was re-used and reinterpreted to provide significantly more information regarding storativity and transmissivity of aquifers within the Adelaide region. As noted with previous reports, as the data was not collected directly by the authors and was based on reinterpretation of existing data, the reliability of the data cannot be considered to be completely reliable due to possible transcription errors with the original data, and the possibility that appropriate quality control methods were not undertaken during the original data collection.

## **B.3.2 REPORTS THAT DO NOT CONTAIN NEW OR RELEVANT HYDROGEOLOGICAL DATA**

- Merrick, N., 2010, 'Peer Review of the Adelaide Plains Numerical Groundwater Model', Heritage Computing;
- SKM, 2010, 'Adelaide Plains Model Update – Kangaroo Flat';
- Shepherd, R.G., 1975, 'Northern Adelaide Plains Groundwater Study, Stage 2 1968-1974', Department of Mines SA, 75/38.

- 'Northern Adelaide Plains Sustainable Groundwater Yield Discussion Paper', REM, 2004;
- 'Overview of the Hydrogeology in the Central Adelaide PWA', SKM, 2008;
- Pritchard, J. and Richardson, S., 2006, 'Northern Adelaide Plains Water Balance', REM;
- Martin, R. & Hodgkin, 2006, 'State and Condition of the Adelaide Plains Sub-Aquifers', DWLBC, 2005/32;
- Green, G., Alcoe, D., Watts, E. and Costar, A., 2010, 'Groundwater Flow Across Regional Scale Faults', DWLBC (unpublished);
- Richardson, S. and Haworth, D., 2006, 'Northern Adelaide Plains – ASR and Reclaimed Water Injection Schemes', REM;
- Richardson, S. and Haworth, D., 2006, 'Groundwater Modelling Scenarios for the Northern Adelaide Plains', REM;
- 'Tertiary Aquifers of the Adelaide Coastal Plains Groundwater Model: Model Conceptualisation Report', REM, 2005;
- 'Tertiary Aquifers of the Adelaide Coastal Plains Groundwater Model: Transient Model Set-up and Calibration Report', REM, 2006;
- 'Tertiary Aquifers of the Adelaide Coastal Plains Groundwater Model: Steady-state Model Set-up', REM, 2006;
- 'Northern Adelaide Plains Analysis of Trends in Groundwater Condition', REM, 2005;
- Pritchard, J. and Richardson, S., 2005 'Northern Adelaide Plains – Compilation and Summary of Hydrogeological Information to Support Estimation of Sustainable Groundwater Yield', REM;
- Zulfic, H., Wohling, D., 2004, 'Northern Adelaide Plains Prescribed Wells Area groundwater monitoring status report 2003' DWLBC, 2004/41;
- Gerges, N. and Kelly, J., 2002, 'A First Approximation of the Shallow Aquifer (Water Table) Water Balances on the Northern Adelaide Plains', NABCWM Board;
- Pritchard, J. and Richardson, S., 2006, 'Northern Adelaide Plains Water Balance', REM;
- SKM, 2009, 'State and Condition of the Underground Water Resources of the Central Adelaide PWA';
- SKM, 2009, 'Regional Groundwater Model Update';
- Evans, S. & Power, N. 1990 'Northern Adelaide Plains Review', DWLBC (unpublished);
- Yan, W., 2010, 'Review Notes of the Adelaide Plains Numerical Groundwater Model', DWLBC;
- Baird, D.J., 2010 'Groundwater Recharge and Flow Mechanisms in a Perturbed, Buried Aquifer System: Northern Adelaide Plains, South Australia', PhD Thesis, Flinders University, Adelaide
- Fisher, 1986, 'Metropolitan Region Water Resources Management Review – Groundwater Assessment', E&WS.

The purposes of these reports varied; however, generally all reports provided a qualitative hydrogeological overview of a specific section of the Study Area. The hydrogeological review comprised a desktop review and generally included a review of information from previous studies, an evaluation of the current observation well data, and an assessment of the needs of other underground water users. No additional data collection to confirm values or parameters was undertaken during the preparation of these reports. Further, whilst references were presented at the end of the report, the validity of the information was not verified by additional intrusive investigations. The data provided is only as good as the reports that the data was obtained from, and an analysis of how the data was calculated, or can be improved is not able to be recommended.

It is noted that, with the exception of the Shepherd (1975) report, any data / values provided were stated as a fact or provided as an estimated value. In most cases, no explanation was provided regarding how the data / values were calculated / obtained e.g. reasons for the variations in salinity across the aquifers and explanations as to how it is known that certain aquifers are hydraulically connected. Data gaps were identified, particularly relating to values for the yields and transmissivity of the aquifers. This may be due to the lack of readily available information for these aquifer properties. With regard to the

inclusion of the Shepherd (1975) report within this section, it was noted that the data within the report was quite dated and had been updated during Gerges' review of the Northern Adelaide Plains.

The majority of the reports provided a summary of historical and current underground water extraction, allocations etc. It is noted that the underground water extraction and incorrect allocations may lead to elevated groundwater salinities, changes in groundwater flow direction and changes in interactions between aquifers due to the formation of cones of depression (e.g. downward leakage from the Quaternary aquifer(s) into the Tertiary aquifers). In addition, several reports comprised modelling scenarios to be used as decision support tools, but in terms of the purpose of the project, are not considered relevant.

## B.4 Discussion

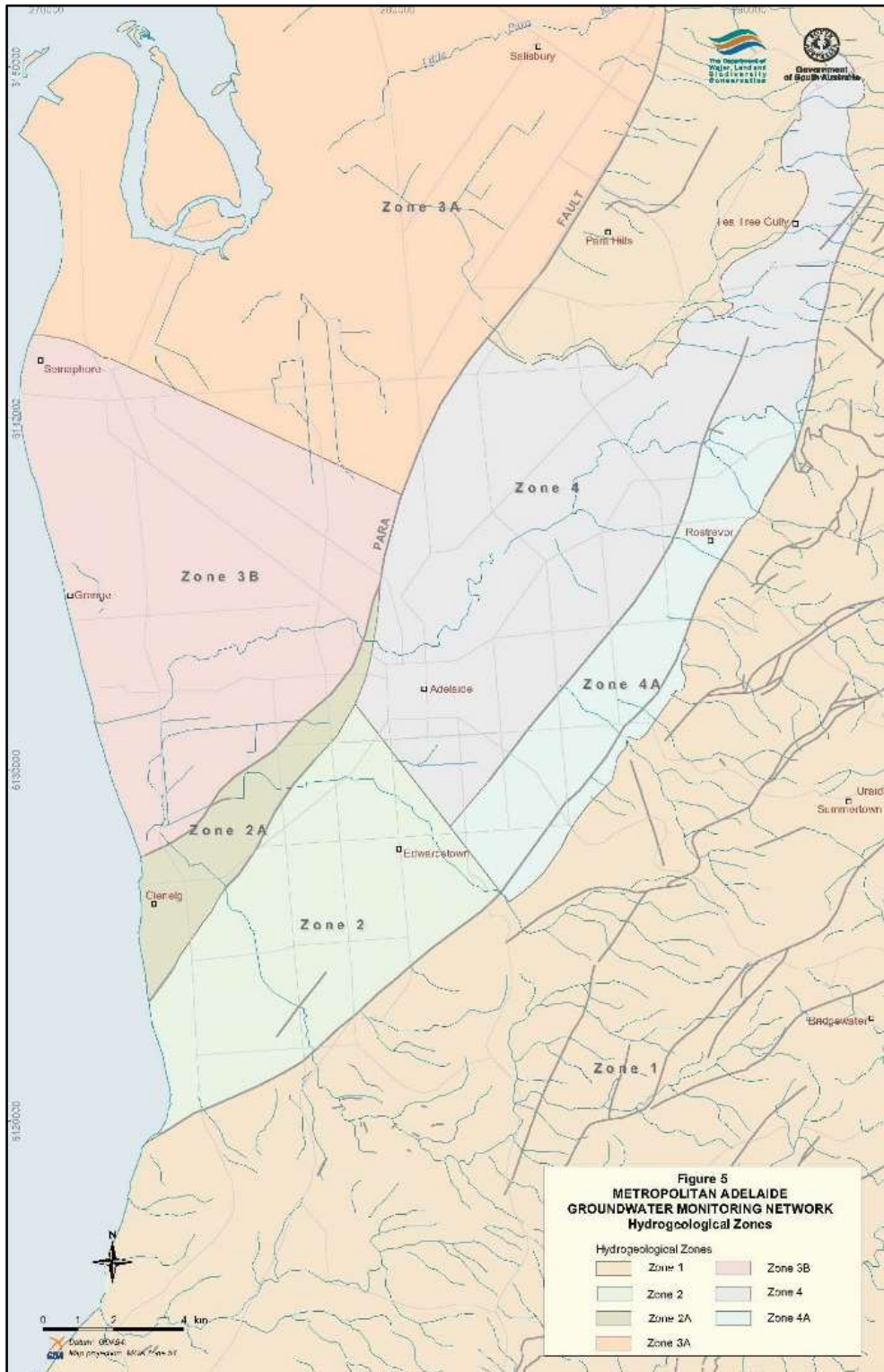
### B.4.1 HYDROGEOLOGICAL ZONES

Numerous studies have been undertaken within portions of the study area; however, a single study has not been undertaken to cover the entire study area. The most in-depth hydrogeological study of the Adelaide and surrounding areas was undertaken by Gerges as part of his PhD thesis in 1999, and revised and published in 2006. Whilst the information presented within Gerges' reports has been revised over the past 15 years, the majority of the details regarding the sequence of aquifers remain unchanged. In Gerges' 1999 PhD thesis, the majority of the study area was divided into four main hydrogeological zones. The boundaries of these hydrogeological zones were established based on geological characteristics and major groundwater extraction domains e.g. major industrial or irrigation areas extracting large volumes of groundwater. Martin and Hodgkin revised these zones in 2006 which simplified the zones to be based only on geological settings (Tables B.1 and B.2, Apx Figure B.3). The aquifer sequence within each of these 'zones' varies, with some aquifers even noted as being absent. The interconnections between each of the aquifers are controlled by the major structures and / or changes in the lithology.

**Apx Table B.1 Overview of Hydrogeological Zones (Gerges, 2006, Martin and Hodgkin, 2006).**

ZONE	GEOLOGY	HYDROGEOLOGY (TERTIARY)
1	Precambrian bedrock, shale, fractured	High hydraulic conductivity and yields.
2	Quaternary - Clays and silts Tertiary – sand with occasion thin gravel beds and thin clayey and lignitic layers	The first Tertiary aquifer (T1) consists mainly of highly permeable formations (sandy limestone) and contains water of low salinity.
2A	Quaternary – clays and silts Tertiary – sandstone, sand and limestone	Limited information is available for the deep aquifers hence interpretation of major structures is speculative.
3 and 3B	Quaternary – clays and silts Tertiary – sand, sandstone, shells, and silty sand and limestone	The first and second Tertiary aquifers are the thickest and the most productive, with relatively low salinity.
4	Quaternary – clays and silts Tertiary – fine sand, silty and clayey	Each Tertiary aquifer consists mainly of thin layers of fine sand with low yield. Most of the Quaternary and Tertiary aquifers become thin, shallow and interconnected in the vicinity of the River Torrens. The shallow fractured rock aquifer near the River Torrens contains groundwater of low salinity and significant yield.
4A	Quaternary – clays and silts Tertiary - sand with occasion thin gravel beds and thin clayey and lignitic layers	This zone is interpreted to act as a conduit for surface infiltration and groundwater flow from the fractured rock aquifers of Zone 1 into Zone 2 and Zone 4.

It is noted that the Quaternary aquifers generally low yielding (<3 L/sec) and variable, reflecting the low aquifer transmissivity and inhomogeneity. The most transmissive sections of these aquifers are usually located adjacent to major bedrock structures or surface drainage (for the shallowest aquifers).



Apx Figure B.3 Plan showing location and extent of hydrogeological zones (Martin and Hodgkin, 2006).

## B.4.2 AQUIFER SEQUENCE

There are three main aquifers within the study area: Quaternary Aquifers (identified by the symbol Q); Tertiary Aquifers (identified by the symbol T); and Precambrian age fractured Adelaidean Bedrock (identified by the symbol P).

### Quaternary Aquifers

There are up to six thin confined or semi confined aquifers within the study area designated Q1 to Q6 in order of increasing depth. The Quaternary Aquifers are relatively thin and of limited extent and generally comprise sandy / gravel consolidated layers within mottled clay and silt Quaternary sediments. They may also comprise more sandy formations adjacent the coast. In addition, perched aquifers are not uncommon. The thickness, lithology and hydraulic conductivity of the Quaternary aquifers vary across the study area, with hydraulic conductivity generally increasing near the coast and adjacent faults (Gerges, 2006). During the revision of Gerges' work in 2008 by Zulfic et al (2008), the Q4 aquifer (in the Northern Adelaide Plains and Q4/Q5 aquifer in the metropolitan area) was renamed the Carisbrooke Sand Aquifer. Whilst it is noted that the Carisbrooke Sand is a Tertiary sediment and forms a portion of the Tertiary sub aquifer T1a along the Little Para River (Gerges, 2001), Hodgkin (2004) suggested that this aquifer is in direct hydraulic connection with the underlying T1 aquifer over much of its extent. Further, it has been noted that the hydraulic characteristics of the Carisbrooke Sand formation are different from the Hindmarsh Clay Quaternary aquifers (DWLBC, 2008/05).

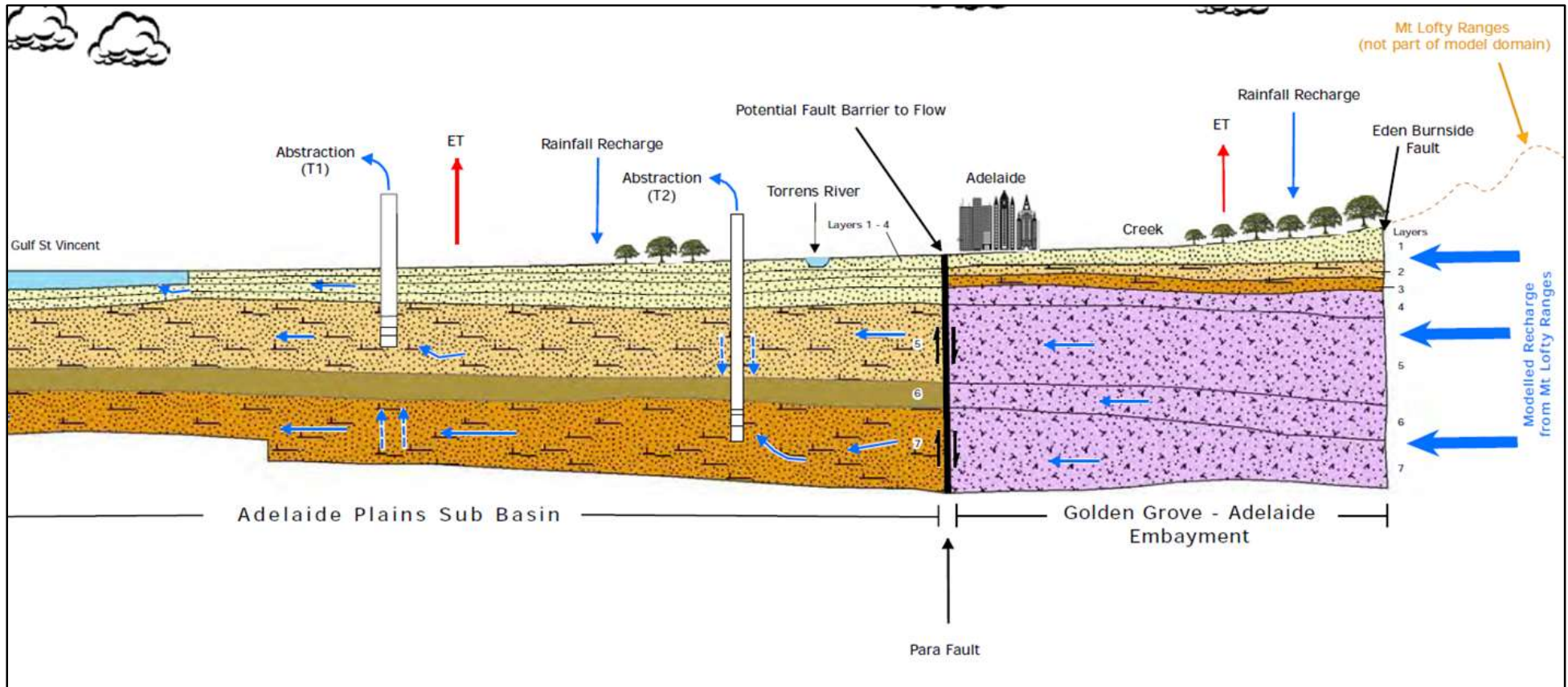
### Tertiary Aquifers

The Tertiary aquifers are designated T1 to T4 in order of increasing depth. Sub aquifers T1a and T1b have been identified in some zones within the T1 aquifer and sub-aquifers T2a to T2c have been identified within some zones within the T2 aquifers. The identification of the sub-aquifers is based lithology, yield and salinity characteristics. Each of the Tertiary aquifers is relatively independent of the geological formations, and could consist of different geological units in different hydrogeological 'zones'. As a result, the hydrogeological parameters of each of the Tertiary aquifers vary between the 'zones'. The Tertiary aquifers are distributed based on the depositional environment, major structural features, general geological history of the area and movements along the major faults.

Table B.2 provides a summary of the distribution of the Quaternary and Tertiary aquifers within each of the hydrogeological zones of the study area. An overview of the hydrogeological setting of the study area is presented as a cross section in Apx Figure B.4.

**Apx Table B.2 Overview of Hydrogeological Zones (Martin and Hodgkin, 2006, Gerges, 2006).**

ZONE	QUATERNARY AQUIFERS	TERTIARY AQUIFERS	COMMENTS
1	-	-	Basement rocks of the Adelaide Hills
2	Q1 to Q4, plus Q5 in parts	T1 to T3, T4 is well developed only near coast	T1 comprises a highly permeable formation and is used significantly.
2A	Q1 to Q4	T1 to T2 are recognised, T3 and T4 are anticipated	Hydrogeologically important zone connecting zone 2 with zone 3. Limited information regarding deeper structures.
3	Q1 to Q6	T1 to T4 are well developed in this zone	T1 used extensively for industrial and recreational use.
4	Q1, plus Q2 to Q3	T1 and T2 are thin	This area covers a portion of the Golden Grove Embayment.
4A	Q1, plus Q2 to Q5 in parts	T1 is present as one thick sandy aquifer containing several stratigraphic units	Interpreted to act as a conduit for surface infiltration and groundwater flow from fractured rock aquifer of zone 1 into zone 2 and zone 4.



Apx Figure B.4 An Overview of the Hydrogeological Setting of the Study Area (Georgiou, J. et al., 2011).

### B.4.3 CONFINING BEDS

The aquifers are generally separated by a confining bed (refer Tables B.3 and B.4). The majority of the confining beds act as an aquitard and prevent leakage between the aquifers; however, in some cases, the confining bed is absent or leaky allowing hydraulic connection between aquifers (Martin and Hodgkin, 2006). For example the confining bed separating between the sub-aquifers T1a and T1b (Croydon Facies) is considered to be a leaky confining bed (Gerges, 2001) and the Munno Para Clay (Cb9) is absent to the north of the Gawler River (as is the T1 aquifer) allowing direct hydraulic connection between the Q4 / Carisbrooke Sand aquifer and the T2 aquifer (Gerges, 2001).

As with the Tertiary aquifers, the confining beds are also independent of conventional stratigraphic units and may be represented by different stratigraphic units in different areas (Gerges, 1999).

Gerges recognised 12 confining beds (designated Cb1 to Cb12 in order of increasing depth), with up to seven (Cb1 to Cb7) separating the Quaternary aquifers from each other and the underlying Tertiary aquifers. The Tertiary confining beds (Cb8 to Cb11) separate various Tertiary aquifers, while Cb12 is combination of a Tertiary confining bed and the weathered bedrock clay. In most cases, Cb12 separates the deepest Tertiary aquifer from the underlying fractured rock aquifer. (Zulfic et al, 2008)

A summary of the confining beds within the study area and a summary of their published hydrogeological parameters is set out in Tables B.3 and B.4.

### B.4.4 REVIEW OF HYDRAULIC PARAMETERS

#### Porosity

Limited values for porosity were presented for each of the aquifers and confining beds within the reports reviewed. The porosity values that were included are presented in Table 3. It is noted that extensive testing of porosity was undertaken for the confining bed Cb7 – Munno Para Clay and there was a range of porosities reported. The variations are likely due to samples of the interbedded limestone being tested and regional variations within this confining bed. Whilst there is extensive knowledge of the geology of the study area and available published data of porosity ranges e.g. Freeze & Cherry (1979), the lack of porosity values published for the study area is considered to be a data gap and additional hydrogeological testing is required.

#### Hydraulic Conductivity

Hydraulic conductivity is a function of the geological formation and the fluid, and describes the ease with which a fluid (usually water) can move through pore spaces or fractures. It can be estimated using several different equations which utilise the parameters of permeability, density, gravity and viscosity of the fluid, hydraulic gradient, seepage velocity and the area of the formation through which the water is flowing. However, porosity is also an important controlling influence on hydraulic conductivity. In geological formations comprising well sorted sands or in fractured rock formations, higher hydraulic conductivity values are generally associated with higher porosity values. However, this correlation does not hold true with other soil types such as clay rich soils; where higher porosities are generally reported, but lower hydraulic conductivities are calculated. This is likely due to the void ratio (volume of voids / volume of the solid) as a lower void ratio will be reported for finer grained materials (Freeze and Cherry, 1979).

Hydraulic conductivity can vary horizontally and vertically within a formation. Accordingly, both vertical hydraulic conductivity ( $K_V$ ) and horizontal hydraulic conductivity ( $K_H$ ) can be calculated. If the hydraulic conductivity of a formation is independent (remains consistent) of the direction of a measurement point, the formation is considered to be isotropic at that point. If the hydraulic conductivity varies, the geological formation is considered to be anisotropic at that point. Further, if the hydraulic conductivity is independent of a position within a geological formation, the geological formation is considered to be homogenous. On the other hand, if the hydraulic conductivity is dependent on the position with the geological formation, the formation is heterogeneous (Freeze and Cherry, 1979).

The hydraulic conductivity parameters set out in Table 4 indicate that there are large variations in hydraulic conductivity between the Tertiary aquifers and the hydrogeological zones within which the Tertiary aquifers are located. As noted above, limited porosity data was provided within the reports and hydraulic conductivity is dependent, to a degree, on the porosity of the formations. It was noted that assumptions of porosity were not discussed within the reports when providing details of hydraulic conductivities. As a result, it is assumed that correct porosity value(s) for the formation type within which the tests were being undertaken were used when calculating the hydraulic conductivity for each formation / zone. Variations in hydraulic conductivity values were reported during pumping tests where the observation bore was located away from the pumping well. This suggests that aquifer parameters are spatially variable on relatively small scales which is a typical characteristic of fractured rock aquifers.

### Transmissivity

The transmissivity value is determined based on the product of the aquifer thickness and the hydraulic conductivity (i.e.  $T = bK$  where  $T$  = transmissivity,  $b$  = aquifer thickness and  $K$  = hydraulic conductivity) (Freeze & Cherry, 1979). As mentioned previously, the aquifer parameters for each of the aquifers, particularly the Tertiary aquifers are spatially variable. This is likely the case because they consist of different hydrogeological units of variable grain size, degree of consolidation and connectedness of preferential pathways in different areas. As a result, the hydraulic conductivity for each geological formation may vary. In addition, as noted in Tables 3 and 4, the thickness of each aquifer varies across the study area. Therefore, whilst the transmissivity values vary for portions of the aquifer, as the transmissivity value can be calculated based on the thickness of the aquifer, the hydraulic conductivity may be the same in each portion of the aquifer. This is demonstrated by the range of values reported in Tables 3 and 4.

Lower transmissivities are generally associated with areas of decreased aquifer thickness or geological formations with lower hydraulic conductivities e.g. the Q4 (Carisbrooke Sand) aquifer typically has a very low to low transmissivity throughout the study area as a result of limited thickness and low hydraulic conductivity (Hodgkin, 2004). Whilst there were no aquifer tests conducted, the low hydraulic conductivity is inferred to be due to the fine-grained and poorly sorted sand units that dominate the formation. The transmissivity domains shown are based entirely on aquifer thickness, which has been previously shown by Gerges (1999) to be greatest (up to 60 metres) near the Little Para River.

### Storativity

The storativity of a saturated unconfined aquifer of thickness ( $b$ ) can be defined as the volume of water that an aquifer releases from storage per unit surface area of aquifer per unit decline in the component of hydraulic head normal to that surface (Freeze and Cherry, 1979). The storativity can be calculated as  $S = S_s b$  where  $S$  represents storativity,  $S_s$  represents specific storage and  $b$  represents the thickness of aquifer. It is noted in Martin and Hodgkin (2006), the actual storativity of an aquifer

can be difficult to reliably obtain from aquifer tests. This is because the assessed value can be an “effective” value, which includes the effects of leakage from adjacent aquitards and aquifers and the effects of partial well penetration. It appears that specific storage values were more commonly reported than storativity values for this reason.

## B.5 Results and Conclusions

Values for hydrogeological parameters extracted from the reports reviewed in Section B.3 are presented in Tables B.4 and B.5 on the following pages while a summary is given in Table B.3 below.

Hydraulic parameters have been collected through a review of 31 hydrogeological investigations within the study area. Whilst many investigations provided data for Quaternary, Tertiary and fractured rock aquifers, the main focus of the reports was the first and second Tertiary aquifers (T1 and T2). In addition, it was apparent that limited data was available for some aquifers e.g. Q4, Q5, Q6, T4, bedrock and the confining beds (with the exception of the Munno Para Clay).

During the review it was clear that, whilst there were many reports available, the majority relied heavily on Nabil Gerges’ hydrogeological assessments undertaken in the mid-1990s to the mid-2000s. It was noted that additional works had been undertaken by Zulfic et al., (2008) and Hodgkin (2004).

As a result, whilst a range of parameters of the various hydrogeological units were able to be extracted, given the size of the study area, how these vary spatially is still somewhat uncertain. However, possible reasons for these variations are likely due to heterogeneity within the formations and the differing formation types within each of the aquifers.

**Apx Table B.3 Range of reported hydraulic parameter values for each of the aquifers.**

AQUIFER	ZONE	T (M2/DAY)	S	KH (M/DAY)	KV (M/DAY)
Q4 / Carisbrooke Sand Aquifer	3	-	-	1-10	1-10
T1	2	20-256	$1.3 \times 10^{-4} - 6.5 \times 10^{-4}$	1-50	
	2A		$1.3 \times 10^{-6} - 8.8 \times 10^{-5}$		
	3	51-287	-	-	
	3B	77-220	$1.16 \times 10^{-4} - 1.35 \times 10^{-3}$	2.5-80	
	4	25-40	-	120	
	4A	130-360	-	2.5	
T1A	3	69-231	$3.1 \times 10^{-4}$	-	
T1B	3	53-385	$2.3 \times 10^{-4} - 4.0 \times 10^{-4}$	1.75-2.5	
	3A	-	$1.55 \times 10^{-4} - 3.3 \times 10^{-4}$	-	
	3B	67-100	$1.76 \times 10^{-4} - 5.0 \times 10^{-4}$	3.9-4.5	
	4	-	$3.0 \times 10^{-4}$	-	
T2	NAP	91-395		-	
	3A	131-202	$1.26 \times 10^{-4} - 1.6 \times 10^{-4}$	-	
	4	-	$2.84 \times 10^{-5}$	-	

Apx Table B.4 Summary of aquifer parameters for Quaternary aquifers and confining beds.

AQUIFER / CONFINING BED	RANGE OF DEPTHS TO TOP OF FORMATION (M BGL)	HOW WAS VALUE OBTAINED?	SOURCE OF INFORMATION	KH (M/DAY)	KV (M/DAY)	HOW WAS VALUE OBTAINED?	SOURCE	SPECIFIC STORAGE	HOW WAS VALUE OBTAINED?	SOURCE
<b>Cb1</b>	Surface to 3 to 15 m bgl	Drill logs	Gerges, 1999	4.06x10-4	1.51x10-4	Test from Thebarton (ADE 190)	Gerges, 1999			
					4.7x10-4	Test from St Kilda Road	Gerges, 1999			
					2.3x10-4					
					1.2x10-4	Test from Old Virginia Primary School	Gerges, 1999			
					1.8x10-3	Chivel Road, Angle Vale	Gerges, 1999			
					3.5x10-4					
<b>Q1</b>	3 to 15	Drill logs in zone 3	Gerges, 2006							
<b>Cb2</b>					1.9x10-3	Test from Thebarton (ADE 190)	Gerges, 1999			
					1.64x10-4	Campbelltown ADE 142,143	Gerges, 1999			
					2.7x10-3	NAP St Kilda Road	Gerges, 1999			
					2.6x10-6					
					3.4x10-3	NAP Old Virginia Primary School	Gerges, 1999			
					2.5x10 -6					
					5.1x10-7					
					1.7x10-4	Chivel Road Angle Vale	Gerges, 1999			
					1.3x10-4					
					2.8x10-6					
					1.6x10-6					
9.5x10-7										
			6.04x10-3	1.00x10-3	Laboratory test on sample collected between 22.4 and 22.7 m bgl ADE 190	Gerges, 1999				
<b>Q2</b>	16 – 30	Drill logs in zone 3	Gerges, 2006							
<b>*Cb3</b>					5.8x10-5	Thebarton (ADE190)	Gerges, 1999			
					1.64x10-3	Grange (YAT123)	Gerges, 1999			
					5.8x10-7	St Kilda Road	Gerges, 1999			
					1.9x10-6					
					8.6x10-5	Chivel Road, Angle Vale	Gerges, 1999			
					5.7x10-4					
			7.17x10-5	5.79x10-5	Laboratory test on sample collected between 38.43 and 38.62 m bgl ADE 190	Gerges, 1999				
			3.46x10-5	1.64x10-3	Laboratory test on sample collected between 44.30 and 44.60 m bgl YAT 123	Gerges, 1999				
<b>Q3</b>	31 – 45	Drill logs in zone 3	Gerges, 2006							
<b>Cb4</b>					1.47x10-4	Zone 3 Thebarton (ADE190)	Gerges, 1999			
					1.8x10-4	Zone 4 Grange (YAT123)	Gerges, 1999			
					1.0x10-5(?)	St Kilda Road	Gerges,1999			
					5.2x10-6					
					2.4x10-5	Old Virginia Primary School	Gerges, 1999			
3.7x10-5	Chivel Road, Angle Vale	Gerges, 1999								

AQUIFER / CONFINING BED	RANGE OF DEPTHS TO TOP OF FORMATION (M BGL)	HOW WAS VALUE OBTAINED?	SOURCE OF INFORMATION	KH (M/DAY)	KV (M/DAY)	HOW WAS VALUE OBTAINED?	SOURCE	SPECIFIC STORAGE	HOW WAS VALUE OBTAINED?	SOURCE
				1.47x10 <sup>-4</sup>	1.81x10 <sup>-4</sup>	Laboratory test on sample collected between 59.00 and 59.17 m bgl YAT 123	Gerges, 1999			
<b>Q4 / Carisbrooke Sand Aquifer</b>	46 – 80	Drill logs in zone 3	Gerges, 2006	1 to 10	1 to 10	Estimation of value based on range of values set out in Freeze & Cherry, 1979.	Gerges, 1999	1x10 <sup>-5</sup>	Drill logs	Gerges, 1999
<b>Cb5</b>					4.89x10 <sup>-5</sup>	Thebarton (ADE190)	Gerges, 1999			
					2.98x10 <sup>-4</sup>					
					7.80x10 <sup>-6</sup>	Grange (YAT123)	Gerges, 1999			
				5.36x10 <sup>-5</sup>	4.84x10 <sup>-5</sup>	Laboratory test on sample collected between 62.33 and 62.50 m bgl ADE 190	Gerges, 1999			
				3.02x10 <sup>-3</sup>	2.90x10 <sup>-4</sup>	Laboratory test on sample collected between 63.04 and 63.25 m bgl ADE 190	Gerges, 1999			
				7.8x10 <sup>-6</sup>	7.78x10 <sup>-6</sup>	Laboratory test on sample collected between 61.80 and 62.10 m bgl YAT 123	Gerges, 1999			
<b>Q5</b>	65 to 80	Drill logs in zone 3	Gerges, 2006							
<b>Cb6</b>					3.63x10 <sup>-5</sup>	Thebarton (ADE190)	Gerges,, 1999			
					5.3x10 <sup>-5</sup>					
					5.9x10 <sup>-4</sup>					
					1.2x10 <sup>-6</sup>	Grange (YAT123)	Gerges, 1999			
					8.6x10 <sup>-7</sup>					
				6.60x10 <sup>-5</sup>	3.63x10 <sup>-5</sup>	Laboratory test on sample collected between 68.79 and 69.00 m bgl ADE 190	Gerges, 1999			
				1.38x10 <sup>-4</sup>	5.27x10 <sup>-5</sup>	Laboratory test on sample collected between 71.31 and 71.50 m bgl ADE 190	Gerges, 1999			
				7.08x10 <sup>-6</sup>	5.96x10 <sup>-6</sup>	Laboratory test on sample collected between 72.62 and 72.80 m bgl ADE 190	Gerges, 1999			
				6.48x10 <sup>-6</sup>	1.20x10 <sup>-6</sup>	Laboratory test on sample collected between 89.40 and 89.70 m bgl YAT 123	Gerges, 1999			
					8.64x10 <sup>-7</sup>	Laboratory test on sample collected between 89.70 and 90.00 m bgl YAT 123	Gerges, 1999			
				6.60x10 <sup>-5</sup>	3.63x10 <sup>-5</sup>	Laboratory test on sample collected between 68.79 and 69.00 m bgl ADE 190	Gerges, 1999			
<b>Cb6 and / or Cb7</b>				5.60x10 <sup>-6</sup>	3.10x10 <sup>-5</sup>	Laboratory test on sample collected between 92.50 and 92.80 m bgl ADE 190	Gerges, 1999			
<b>Q6</b>	90	Drill logs in zone 3	Gerges, 2006						Drill logs	
<b>Cb7</b>					3.1x10 <sup>-5</sup>	Thebarton (ADE190)	Gerges, 1999			
					5.6x10 <sup>-6</sup>					
					8.6x10 <sup>-7</sup>	Grange (YAT123)	Gerges, 1999			
<b>TQCb</b>				3.1x10 <sup>-5</sup>	3.1x10 <sup>-5</sup>	Thebarton (ADE190)	Gerges, 1999			
				1.83x10 <sup>-5</sup>	1.83x10 <sup>-5</sup>					
					8.64x10 <sup>-7</sup>	Grange (YAT123)	Gerges, 1999			
					1.6x10 <sup>-4</sup>	Campbelltown DE 142, 143	Gerges, 1999			
					1.7x10 <sup>-5</sup>	St Kilda Road	Gerges, 1999			
					?2.4x10 <sup>-5</sup>	Old Virginia Primary School	Gerges, 1999			
					3.7x10 <sup>-5</sup>	Chivel Road, Angle Vale	Gerges, 1999			

Apx Table B.5 Summary of aquifer parameters for Tertiary aquifers and confining beds

AQUIFER / CONFINING BED	ZONE	T (M2/DAY)	S	KH (M/DAY)	METHOD	SOURCE	KV (M/DAY)	KH (M/DAY)	POROSITY	METHOD	SOURCE	SS	METHOD	SOURCE
T1	2	200	5.5x10-4	50	Bailey Reserve aquifer test	Gerges, 2006								
	2	219	6.5x10-4	-	Jacob Analysis Bailey Reserve, Zone 2	Gerges, 1999								
	2	204	4.8x10-4		Type curve analysis (s vs t) 5 day test, Bailey Reserve	Gerges, 1999								
	2	190	4.12x10-4	-	Type curve analysis (s vs t/r2) 5 day test, Bailey Reserve	Gerges, 1999								
	2	256	-	-	Production Well Jacob Analysis 5 day test Bailey Reserve	Gerges, 1999								
	2	20-24	-	1	Production well Jacob analysis Step drawdown test – partial penetration – aquifer thickness 20 m Glengowrie High School	Gerges, 1999								
	2	50	-	2.5	Constant discharge test – partial penetration – aquifer thickness 20 m Glengowrie High School	Gerges, 1999								
	2	112-114	-	2.7	Step drawdown test – full penetration, aquifer thickness 42 m, Glengowrie High School	Gerges, 1999								
	2	131-135	-	3.2	Constant discharge / injection tests Glengowrie High School	Gerges, 1999								
	2	84	-	-	Production well Jacob analysis, Road Safety Council	Gerges, 1999								
	2	106-184	1.3x10-4	-	2873 minutes test at Basketball Stadium , Road Safety Council	Gerges, 1999								
	2	132-342	1.3x10-4	-	2873 minutes test at Vineyard swimming pool , Road Safety Council	Gerges, 1999								
	2A			8.8x10-5	-	Calculated using max aquifer thickness of 45 m in Morphettville	Hodgkin, 2004							
	2A			1.3x10-6	-	Calculated using max aquifer thickness of 50m in Oaklands Park	Hodgkin, 2004							
	3	85-93	-	-	-	Pump test – full penetration well Greenfields wetland	Gerges, 1999							
	3	51-55	-	-	-	Pump test – partial penetration well Greenfields wetland	Gerges, 1999							
3	244-287	-	-	-	Injection test – exceptionally high transmissivity Greenfields wetland	Gerges, 1999								
3	127	-	-	-	Pump test for 31,550 minutes G.H. Michell Ltd factory	Gerges, 1999								

AQUIFER / CONFINING BED	ZONE	T (M2/DAY)	S	KH (M/DAY)	METHOD	SOURCE	KV (M/DAY)	KH (M/DAY)	POROSITY	METHOD	SOURCE	SS	METHOD	SOURCE
	3	57-95	-	-	Step / constant drawdown tests	Gerges, 1999								
	3	120-175	2.5x10-4	60-80	Aquifer test in Kidman Park and Grange Golf Courses and flow net analysis	Gerges, 2006								
	3B	183*	4.73x10-4*	6.5*	Jacob analysis bore 2 Grange Golf Club aquifer thickness 28 m	Gerges 199								
	3B	119*	8.36x10-4*	4.25*	Type curve analysis (s vs t) bore 2 Grange Golf Club aquifer thickness 28 m	Gerges, 1999								
	3B	134*	7.5x10-4*	4.8*	Type curve analysis (s vs t/r2) bore 2 Grange Golf Club aquifer thickness 28 m	Gerges, 1999								
	3B	220*	9x10-4	4.9	Jacob analysis bore 4 Grange Golf Club aquifer thickness 45 m	Gerges, 1999								
	3B	158*	1.16x10-4*	3.5*	Type curve analysis (s vs t) bore 4 Grange Golf Club aquifer thickness 45 m	Gerges, 1999								
	3B	202*	1.35x10-3*	4.5*	Type curve analysis (s vs t/r2) bore 4 Grange Golf Club aquifer thickness 45 m	Gerges, 1999								
	3B	126*	5.87x10-4*	4.2*	Jacob Analysis bore 6 Grange Golf Club aquifer thickness ~30 m	Gerges, 1999								
	3B	77*	7.7x10-4*	2.5*	Type curve analysis bore 6 Grange Golf Club aquifer thickness ~30 m	Gerges, 1999								
	4A	130-360		120	Pump test in Hazelwood Park	Gerges, 2006								
	4	25-40		25	Estimated from within Zone 4	Gerges, 2006								
	3	231	3.1x10-4	-	Jacob analysis $\Delta S = 0.95$ m/log cycle Torrens TAFE College	Gerges, 1999						5.56x10-4	Calculated using max aquifer thickness of 77 at Torrens College	Hodgkin, 2004
<b>T1a</b>	3	142	7.4x10-4	-	Jacob analysis $\Delta S = 1.57$ m/log cycle Torrens TAFE College	Gerges, 1999								
	3	84	6.2x10-4	-	Jacob analysis $\Delta S = 2.6$ m/log cycle Torrens TAFE College	Gerges, 1999								
	3	69	-	-	Production Well Jacob analysis Torrens TAFE College	Gerges, 1999								
<b>Cb8</b> "Croydon Facies"	?						5.3x10-5						Gerges, 1999	
	NAP											7.3x10-5	Calculated using max aquifer thickness of 77 in De Ruvo, Waterloo Corner	Hodgkin, 2004
	3	53-72	-	-	Step drawdown test – full penetration of T1b in Kidman Park – aquifer thickness 36 m)	Gerges, 1999								
<b>T1b</b>	3	63	-	1.75	Jacob Analysis of pumping test data in Kidman Park – aquifer thickness 36 m	Gerges, 1999								
	3	68	2.3x10-4	1.9	Jacob Analysis of pumping test data in – aquifer thickness 36 Kidman Park	Gerges, 1999								
	3	74-90	2.8x10-4	2-2.5	Type Curve Analysis (s vs t) – aquifer thickness 36 m	Gerges, 1999								

AQUIFER / CONFINING BED	ZONE	T (M <sup>2</sup> /DAY)	S	KH (M/DAY)	METHOD	SOURCE	KV (M/DAY)	KH (M/DAY)	POROSITY	METHOD	SOURCE	SS	METHOD	SOURCE
					Kidman Park									
	3	69	2.4x10 <sup>-4</sup>	1.91	Type Curve Analysis (s vs t) – aquifer thickness 36 m	Gerges, 1999								
					Kidman Park									
	3	68	3.2x10 <sup>-4</sup>	1.9	Jacob Analysis – Aquifer thickness 36 m	Gerges, 1999						3.6x10 <sup>-4</sup>	Calculated using max aquifer thickness of 35 m in Kidman Park	Hodgkin, 2004
					Kidman Park									
	3	71	4.0x10 <sup>-4</sup>	1.97	Type Curve Analysis (s vs t) – aquifer thickness 36 m	Gerges, 1999								
					Kidman Park									
	3	69	3.3x10 <sup>-4</sup>	1.9	Type Curve Analysis (s vs t) – aquifer thickness 36 m	Gerges, 1999								
					Kidman Park									
	3B	90	5.0x10 <sup>-4</sup>	4.1	Type Curve Analysis (s vs t) – aquifer thickness 22 m	Gerges, 1999						3.4x10 <sup>-4</sup>	Calculated using max aquifer thickness of 30 in Grange Golf Club	Hodgkin, 2004
					Grange Golf Club bore 5									
	3B	100	4.0x10 <sup>-4</sup>	4.5	Jacob Analysis aquifer thickness 22, Grange Golf Club bore 5	Gerges, 1999						5.3x10 <sup>-4</sup>	Calculated using max aquifer thickness of 30 in Grange Golf Club	Hodgkin, 2004
	3B	89	4.7x10 <sup>-4</sup>	4.05	Type curve analysis (s vs t/r <sup>2</sup> ) aquifer thickness 22 m Grange Golf Club bore 5	Gerges, 1999								
	3B	78	1.76x10 <sup>-4</sup>	3.9	Jacob Analysis aquifer thickness 20 m Grange Golf Club bore 7	Gerges, 1999								
	3B	67	1.9x10 <sup>-4</sup>	3.6	Type Curve analysis (s vs t) aquifer thickness 20 m Grange Golf Club bore 7	Gerges, 1999								
	3B	91	3.75x10 <sup>-4</sup>	4.6	Jacob analysis – aquifer thickness 20 m Grange Golf Club bore 8	Gerges, 1999								
	3	123	-	5.3	Production well Jacob analysis aquifer thickness 23 m	Gerges, 1999								
	3	99	6.8x10 <sup>-4</sup>	-	Type curve analysis s vs t)	Gerges, 1999						5.35x10 <sup>-4</sup>	Calculated using max aquifer thickness of 34 in Torrens College	Hodgkin, 2004
					TAFE College									
	3	175	3.9x10 <sup>-4</sup>	-	Jacob analysis ΔS = 1.25 m/log cycle	Gerges, 1999								
					TAFE College									
	3	385	6.5x10 <sup>-4</sup>	-	Jacob analysis ΔS = 0.57 m/log cycle	Gerges, 1999								
					TAFE College									
	3B	70	1.8x10 <sup>-3</sup>	-	Type curve analysis (s vs t)	Gerges, 1999						1.8x10 <sup>-3</sup>	Calculated using max aquifer thickness of 22 in Fort Largs	Hodgkin, 2004
					Police Academy, Fort Largs									
	3B	123	-	-	Production Well Jacob Analysis	Gerges, 1999								
					Police Academy, Fort Largs									
	3A											1.55x10 <sup>-4</sup>	Calculated using max aquifer thickness of 49 in Greenfields	Hodgkin, 2004
	3A											3.3x10 <sup>-4</sup>	Calculated using max aquifer thickness of 40 m in Samcor 1974, Gepps Cross	Hodgkin, 2004
	4											3.00x10 <sup>-4</sup>	Calculated using max aquifer thickness of 43 in Coca Cola, Thebarton	Hodgkin, 2004

AQUIFER / CONFINING BED	ZONE	T (M2/DAY)	S	KH (M/DAY)	METHOD	SOURCE	KV (M/DAY)	KH (M/DAY)	POROSITY	METHOD	SOURCE	SS	METHOD	SOURCE	
	?						2.6x10-7 to 1.7x10-3			Laboratory test of core sample	Zulfic, 2008				
Cb9 'Munno Para Clay'	3A						1.5 – 1.7x10-5			Laboratory test	Gerges, 1999				
	3A						1.5x10-7	-	-	Lab test of sample collected between 174.3 and 174.6 m bgl at Wingfield	Gerges, 1999				
	3A						1.7x10-5	-	-	Lab test of sample collected between 175.2 and 175.5 m bgl at Wingfield	Gerges, 1999				
	3A						8.64x10-7	-	0.62	Lab test of sample collected between 90.6 and 90.7 m bgl at St Kilda Road	Gerges, 1999				
	3A						1.296x10-6	-	0.60	Lab test of sample collected between 91.3 and 91.4 m bgl at St Kilda Road	Gerges, 1999				
	4						7.5x10-7	1.3x10-6	0.44	Lab test of sample collected between 214.6 and 214.85 m bgl at Thebarton	Gerges, 1999				
	4						2.6x10-7	4.6x10-6	0.49	Lab test of sample collected between 217.1 and 217.4 m bgl at Thebarton	Gerges, 1999				
	4						6.6x10-6	2.76x10-6	0.51	Lab test of sample collected between 217.4 and 217.8 m bgl at Thebarton	Gerges, 1999				
	4						1.64x10-6	-	-	Lab test of sample collected between 218.35 and 218.5 m bgl at Thebarton	Gerges, 1999				
	4						1.1x10-6	-	-	Lab test of sample collected between 218.6 and 218.78 m bgl at Thebarton	Gerges, 1999				
	4						5x10-6	8.1x10-6	0.41	Lab test of sample collected between 219.7 and 220.0 m bgl at Thebarton	Gerges, 1999				
	NAP							1.123x10-6	-	0.64	Lab test of sample collected between 63.5 and 63.6 m bgl at Old Virginia Primary School	Gerges, 1999			
	NAP							1.21x10-5	-	0.54	Lab test of sample collected between 64.5 and 64.6 m bgl at Old Virginia Primary School	Gerges, 1999			
	NAP							8.47x10-7	-	0.59	Lab test of sample collected between 64.7 and 64.85 m bgl at Old Virginia Primary School	Gerges, 1999			
	NAP							0.112	-	0.37	Lab test of sample collected between 65.9 and 66 m bgl (limestone layer) at Old Virginia Primary School	Gerges, 1999			
NAP							-	1.56x10-6	0.65	Lab test of sample collected between 56.8 and 56.9 m bgl at Chivel Road, Angle Vale	Gerges, 1999				
NAP							1.73x10-6	-	0.5	Lab test of sample collected between 56.8 and 56.9 m bgl at Chivel Road, Angle Vale	Gerges, 1999				

AQUIFER / CONFINING BED	ZONE	T (M2/DAY)	S	KH (M/DAY)	METHOD	SOURCE	KV (M/DAY)	KH (M/DAY)	POROSITY	METHOD	SOURCE	SS	METHOD	SOURCE
	NAP						2.16x10-6	-	0.65	Lab test of sample collected between 59.1 and 59.3 m bgl at Chivel Road, Angle Vale	Gerges, 1999			
	NAP						1.2x10-6	-	-	Lab test of sample collected between ~97 and 110 m bgl at Andrews Farm	Gerges, 1999			
	NAP						6.0x10-6	-	-	Lab test of sample collected between ~97 and 110 m bgl at Andrews Farm	Gerges, 1999			
	NAP	91-130	-	-	Step drawdown test – full penetration	Gerges, 1999								
					Old Virginia Primary School, Northern Adelaide Plains									
	NAP	98	-	-	Step / constant drawdown test	Gerges, 1999								
					Old Virginia Primary School, Northern Adelaide Plains									
	NAP	144-190	-	-	Step / constant drawdown tests	Gerges, 1999								
					Andrew Farm, Northern Adelaide Plains									
	NAP	98-178	-	-	Step / constant injection tests	Gerges, 1999								
					Andrew Farm, Northern Adelaide Plains									
	NAP	193-395	-	-	Step drawdown tests	Gerges, 1999								
					Mawson Lakes MFP, Northern Adelaide Plains									
	NAP											2.00x10-4	Calculated using aquifer test analysis and max aquifer thickness of 70 in Virginia	Hodgkin, 2004
T2	NAP											1.13x10-3	Calculated using aquifer test analysis and max aquifer thickness of 42 in Kangaroo Flat	Hodgkin, 2004
	3A	202	-	-	Constant discharge test	Gerges, 1999								
					Mawson Lakes MFP, Northern Adelaide Plains									
	3A	131	-	-	Constant injection test	Gerges, 1999								
					Mawson Lakes MFP, Northern Adelaide Plains									
	3A	168	-	-	Constant discharge test	Gerges, 1999								
					Mawson Lakes MFP, Northern Adelaide Plains									
	3A	184	-	-	Step drawdown tests	Gerges, 1999								
					Bolivar									
	3A											1.26x10-4	Calculated using max aquifer thickness of 105 in Regency Park Golf Course	Hodgkin, 2004
	3A											1.6x10-4	Calculated using aquifer test analysis and max aquifer thickness of 95 in Mawson Lakes	Hodgkin, 2004

AQUIFER / CONFINING BED	ZONE	T (M2/DAY)	S	KH (M/DAY)	METHOD	SOURCE	KV (M/DAY)	KH (M/DAY)	POROSITY	METHOD	SOURCE	SS	METHOD	SOURCE
	4											2.84x10-5	Calculated using max aquifer thickness of 100 at Coopers	Hodgkin, 2004

\* indicates that there is no pressure cementing between T1a and T1b sub aquifers and both are interconnecting and behaving as one aquifer when obtaining these values

T1 = First Tertiary aquifer; T1a = first Tertiary aquifer (sub aquifer A); T1b = first Tertiary aquifer (sub aquifer B); T2 = second Tertiary aquifer; m bgl = metres below ground level; T = Transmissivity; S = Storativity; Ss = specific storage; K<sub>H</sub> = horizontal hydraulic conductivity; K<sub>V</sub> = vertical hydraulic conductivity

## B.6 References

- AGT (2005) Glenelg Golf Club Well Completion Report – Wells 8 and 9, Report 2005/32
- Baird DJ (2010) Groundwater Recharge and Flow Mechanisms in a Perturbed, Buried Aquifer System: Northern Adelaide Plains, South Australia, PhD Thesis, Flinders University, Adelaide
- Clarke D (2008) Overview of the Hydrogeology in the Central Adelaide PWA, SKM
- Evans S and Power N (1990) Northern Adelaide Plains Review, DWLBC (unpublished)
- Fairburn B (2004) Geological Note – Cainozoic Fluvial history of the Golden Grove Embayment, MESA Journal, issue 33, pp. 37.
- Fisher, 1986, Metropolitan Region Water Resources Management Review – Groundwater Assessment, E&WS
- Freeze RA and Cherry JA (1979) Groundwater, Prentice Hall Inc., USA
- Georgiou J, Stadter M and Purczel C (2011) Adelaide Plains groundwater flow and solute transport model. Report AP2011, RPS Aquaterra.
- Gerges N (1996) Overview of the Hydrogeology of the Adelaide Metropolitan Area DWLBC DME, 491/78
- Gerges N (1999) The Geology and Hydrogeology of the Adelaide Metropolitan Area Volume 1 & Volume 2, PhD Thesis, Flinders University, Adelaide (Gerges, 1999)
- Gerges N (2001) Northern Adelaide Plains Review, DWR (2001/13)
- Gerges N (2006) Overview of the Hydrogeology of the Adelaide Metropolitan Area, DWLBC, 2006/10
- Gerges N and Kelly J (2002) A First Approximation of the Shallow Aquifer (Water Table) Water Balances on the Northern Adelaide Plains, NABCWM Board
- Green G, Watt E, Alcoe D, Costar A and Mortimer L (2010) Groundwater flow across regional scale faults. DFW Technical Report 2010/15, Government of South Australia, through Department for Water.
- Hodgkin T (2004) Aquifer Storage Capacities of the Adelaide Region, DWLBC, 2004/47
- Jeuken B (2006) Tertiary Aquifers of the Adelaide Coastal Plains Groundwater Model: Transient Model Set-up and Calibration Report, REM
- Jeuken B (2006) Tertiary Aquifers of the Adelaide Coastal Plains Groundwater Model: Steady-state Model Set-up, REM
- Jeuken B (2005) Tertiary Aquifers of the Adelaide Coastal Plains Groundwater Model: Model Conceptualisation Report, REM
- Martin R and Hodgkin T (2006) State and Condition of the Adelaide Plains Sub-Aquifers, DWLBC, 2005/32
- Martin, R., 2009, Regional Groundwater Model Update, SKM
- Merrick N (2010) Peer Review of the Adelaide Plains Numerical Groundwater Model, Heritage Computing
- Osei-Bonsu K and Barnett S (2008) Adelaide Metropolitan Area Groundwater Modelling Project: Volume 2 – Review of Hydrogeology, DWLBC
- Osei-Bonsu K, Gerges N and Zulfic H (2000) Preliminary hydrogeological investigations at Waterloo Corner, DWR (2000/21)
- Pritchard J and Richardson S (2004) Northern Adelaide Plains Sustainable Groundwater Yield Discussion Paper, REM, 2004
- Pritchard J and Richardson S (2005) Northern Adelaide Plains – Compilation and Summary of Hydrogeological Information to Support Estimation of Sustainable Groundwater Yield, REM

- Pritchard J and Richardson S (2006) Northern Adelaide Plains Water Balance, REM
- REM (2005) Northern Adelaide Plains Analysis of Trends in Groundwater Condition, REM, 2005
- Richardson S and Haworth D (2006) Groundwater Modelling Scenarios for the Northern Adelaide Plains, REM
- Richardson S and Haworth D (2006) Northern Adelaide Plains – ASR and Reclaimed Water Injection Schemes, REM
- Shepherd RG (1975) Northern Adelaide Plains Groundwater Study, Stage 2 1968-1974, Department of Mines SA, 75/38.
- Taylor K (2009) State and Condition of the Underground Water Resources of the Central Adelaide PWA, SKM
- Taylor K (2010) Adelaide Plains Model Update – Kangaroo Flat, SKM
- Yan W (2010) Review Notes of the Adelaide Plains Numerical Groundwater Model, DWLBC.
- Zulfic H and Wohling D (2004) Northern Adelaide Plains Prescribed Wells Area groundwater monitoring status report 2003 DWLBC, 2004/41
- Zulfic H, Osei-Bonsu K and Barnett S (2008) Adelaide Metropolitan Area Groundwater Modelling Project: Volume 1 – Review of Hydrogeology, DWLBC

# Appendix C Groundwater recharge estimation – chloride mass balance approach

Authors: *Cranswick RH and Cook PG*

## C.1 Executive Summary

To estimate the groundwater recharge rate to the aquifers of the Adelaide Plains and the Willunga Basin we have applied a Chloride Mass Balance (CMB) approach. This was conducted using electrical conductivity (EC) data from the WaterConnect database and selecting only those wells with aquifer information. This data was supplemented by wells that were less than 30 m deep, which were assumed to be from the Quaternary Aquifer. This resulted in over 20 000 EC values which were then converted to approximate chloride concentrations using a previously derived relationship.

Based on the surfaces interpolated from EC-derived chloride data, there are distinct regions of low chloride groundwater. These are particularly evident for the Quaternary Aquifer in the vicinity of rivers and creeks and imply that river infiltration may be an important recharge mechanism. Also, there is some lateral continuity in chloride concentration between the FRA and the QA across the Para and Eden-Burnside Faults. This continuity was notably absent between both the T1 and T2 Aquifers and the FRA, which may suggest a lack of flow across the fault at depth. However, further analysis of vertical chloride gradients within these aquifers is required to confirm this preliminary interpretation.

The resulting median recharge estimates based on groundwater samples obtained from the Fractured Rock, Quaternary, T1 and T2 aquifers were 7.9, 3.6, 5.7 and 5.4 mm/year respectively. It is important to note, that these values represent recharge rates for the areas where these aquifers are recharged. They do not imply that the aquifers receive recharge within the Adelaide Plains region, and could indicate recharge rates within the Mount Lofty Ranges, that subsequently flows into these aquifers. Given the assumptions of rainfall chloride concentration of 5 mg/L, rainfall of 500 mm/year and negligible runoff, there is a high degree of uncertainty associated with these estimates. Because groundwater in the T1 and T2 aquifers is relatively old (i.e. 10 000 – 30 000 years or more) it is possible that rainfall chloride would have been lower at the time of recharge (because 20 000 years ago, the coast was up to 250 km offshore). Thus the palaeo recharge to these aquifers may be less than those reported here. Conversely, if recharge occurs within the Mount Lofty Ranges, and subsequently flows across the fault, then a rainfall value closer to 1000 mm/year may be more appropriate (because rainfall in the hills is higher than in the plains). It is also worth noting that river recharge is not explicitly considered by the CMB approach. Based on the spatial distribution of chloride concentration, this may be an important recharge mechanism to the Adelaide Plains aquifers.

Despite these assumptions and uncertainties, the recharge estimates derived by the CMB approach indicate that recharge to the Adelaide Plains aquifers is on the order of a few millimetres per year, or approximately 1% of rainfall.

## C.2 Introduction

The groundwater chloride mass balance (CMB) approach was first proposed by Eriksson and Khunakasem (1969) and has since been applied in a range of climatic and hydrogeological settings. It has recently been applied in the Mount Lofty Ranges to estimate groundwater recharge rates in a number of studies (e.g. Banks et al., 2007a; Banks et al., 2007b; Green et al., 2007; Guan et al., 2010; Harrington, 2002 and Harrington et al., 2004). These studies have been focussed on specific catchments and study locations and therefore have

a limited spatial coverage across the Adelaide Plains (AP) and Western Mount Lofty Ranges (WMLR). The data presented here is the first time the CMB approach has been applied more broadly across the entirety of the Western Mount Lofty Ranges, Adelaide Plains and Willunga Basin Regions.

In this chapter we use the groundwater chloride concentrations (derived from electrical conductivity data) to estimate the recharge rate of groundwater in the Adelaide Plains and Willunga Basin. Data is obtained from the Quaternary Aquifer (QA), the T1 and T2 aquifers as well as in the Fractured Rock Aquifers (FRA) of the Western Mount Lofty Ranges. The data analysis incorporates a considerable amount of uncertainty due to the assumptions of the CMB approach. However, given the broad spatial distribution of the data and the simplicity with which recharge estimates can be derived, this constitutes a good overall estimate of the likely historical groundwater recharge to the aquifers in the Region. Absolute recharge rate values should be considered within the context of the assumptions applied.

## C.3 Methodology, Data Collection and Development

### C.3.1 CHLORIDE MASS BALANCE

The CMB approach is based on a number of key assumptions about the water and solute balance of a catchment. These are:

- 1) The chloride in groundwater is derived solely from rainfall chloride;
- 2) Chloride inputs and outputs from a catchment are in steady state; and
- 3) There are no sources or sinks of chloride in the subsurface.

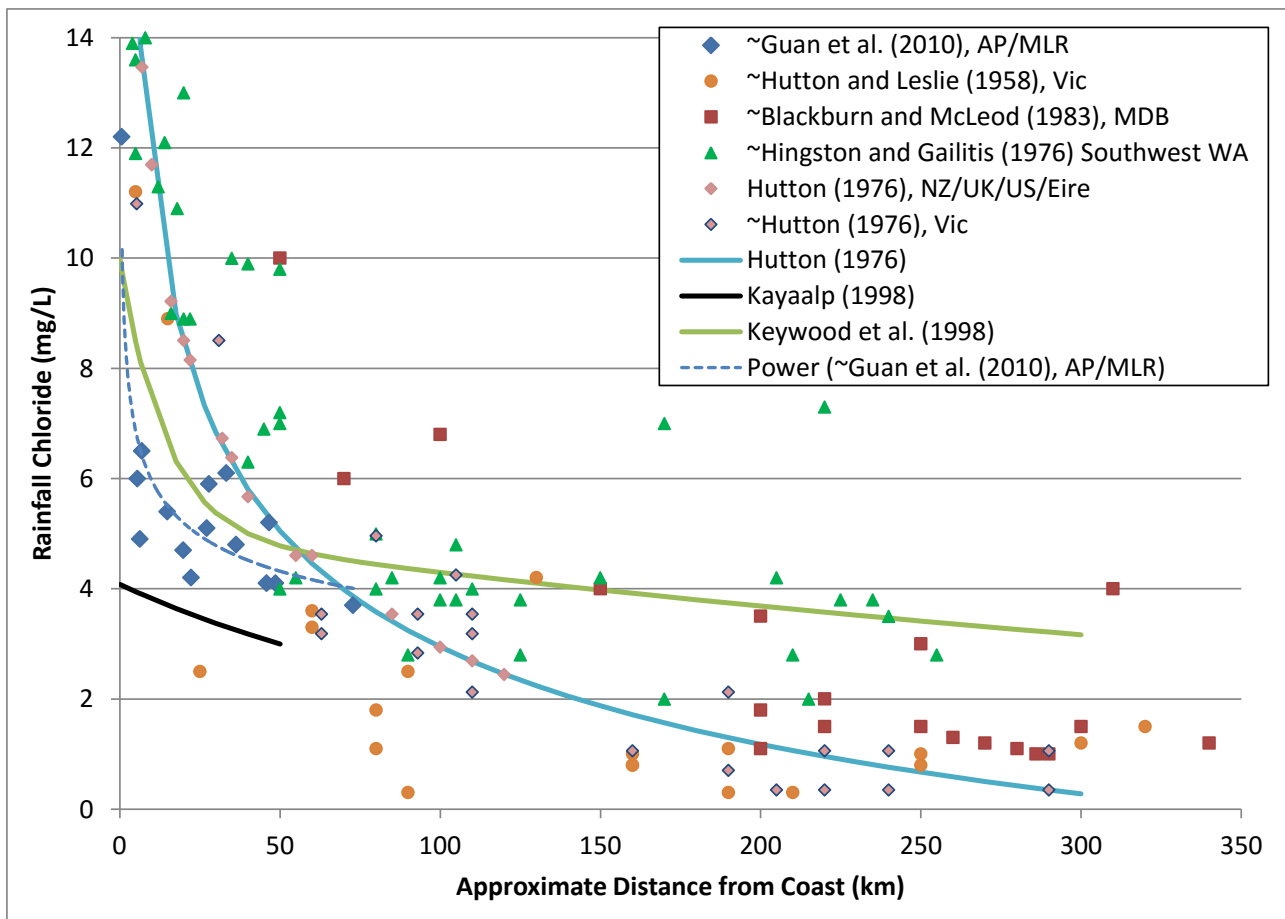
Thus a mass balance equation can be used to estimate groundwater recharge:

$$P \cdot (1 - RO) \cdot C_p = R \cdot C_{gw} \quad (1)$$

where  $P$  = precipitation (mm/year),  $RO$  = runoff coefficient (fraction of rainfall that results in streamflow),  $C_p$  = mean concentration of chloride in rainfall (mg/L),  $R$  = groundwater recharge rate (mm/year) and  $C_{gw}$  = concentration of chloride in groundwater.

A range of values have been used for the runoff coefficient in the above mentioned studies, including 0, 0.1 and 0.25 (see Table C.1). However, because the runoff coefficients between catchments are likely to be highly variable we have chosen to use a value of 0. If, for example, a value of 0.1 was used, the estimate of groundwater recharge rate would be reduced by 10%. This is considered to be a small error compared the uncertainty of rainfall chloride concentration and rainfall at the time of recharge.

Rainfall chloride concentrations have been the subject of a number of studies in Australia. Authors have attempted to relate the rainfall chloride concentration to distance from the coast. They have shown that very high concentrations are found near the coast (due to the capture of sea spray), and that these values decrease with distance inland. A number of exponential regressions have been proposed based on available data (e.g. Hutton, 1976; Keywood et al., 1998). The results of these and other studies (including raw data where available) are displayed in Apx Figure C.1.



**ApX Figure C.1** The change in rainfall chloride concentration with approximate distance from the coast in the direction of the major weather systems. This includes both raw data and relationships that have been derived based on this and other data not displayed. Where data was not presented in table format, values were approximated from graphs and so may contain some error. This error is considered to be small and not relevant for the purposes of this study.

Previous studies using the CMB approach have applied a wide range of rainfall and rainfall chloride concentrations based on available local data. We have summarised this in Table C.1. In this study, we have adopted a rainfall chloride concentration of 5 mg/L and rainfall of 500 mm/year for all aquifers. Variations to these values will result in a proportional change in the recharge values. For example, if we consider that recharge to the T1 and T2 aquifers (via recharge in the WMLR) occurred sometime in the past, it may be appropriate to reconsider the values used in the CMB approach. Preliminary age dating of the T1 and T2 aquifers suggests that groundwater in these aquifers is between 10 000 and 30 000 years old (see Appendix E: Groundwater Hydrochemistry). At this time the coastline would have been at or near the continental shelf (Drexel and Preiss, 1995) located approximately 250 km to the west of Adelaide. Thus it may be that rainfall chloride was lower than modern rainfall chloride observations. Therefore we could consider using a value of say 2.5 mg/L for rainfall chloride deposition, which would result in recharge estimates that are a factor of 2 smaller than those reported here.

Similarly, rainfall at higher elevations in the WMLR may be greater than 500 mm/year and so recharge estimates to the fractured rock aquifers reported here may be underestimates. If a rainfall value of 1000 mm/year were to be used, recharge rates would increase by a factor of 2. This would also apply to the AP aquifers if their primary recharge mechanism is lateral flow across faults from the FRA.

It is important to note that recharge via infiltration from creeks and rivers flowing across the AP is not explicitly accounted for in this simple application of the CMB approach.

**Apx Table C.1 Details of CMB parameters used in previous studies in the Western Mount Lofty Ranges, Adelaide Plains and Willunga Basin.**

REFERENCE	STUDY LOCATION	RAINFALL CL (mg/L)	RAINFALL (mm/year)	RUNOFF %	RECHARGE RATE (mm/year)
Banks et al., 2006	Eastern MLR	4, 5.5	300-500, 450-850	10, 10	<3, 1-59
Banks et al., 2007	Tookyerta Catchment	7.2	570-884	25	190
Green et al., 2006	Western MLR	7.9	500-1000	10	13-114
Guan et al., 2010	AP and MLR	2.1-4.3	574-871	-	27
Guan et al., 2013	Cox Ck Catchment	4.6	1054	0	30, 108
Harrington, 2002	Willunga Basin	7	572	0	4.7-8.8
Harrington, 2004	Scott Ck, Tookyerta and Marne Catchments	5-10, 4-8	534, 845	10	69-83, 3-10.5, 35-124
Zulfic, 2006	South Para Catchment	4.1-7.1	456-576	0	4.8-11.5
Zulfic et al., 2003	Upper Onkaparinga Catchment	4.2-8.5	750-977	0	5-30
This Study	All western draining areas	5	500	0	7.9, 3.9, 6.1, 5.4

### C.3.2 DATA COLLECTION

Groundwater chloride data was collected from the WaterConnect database on 31/07/2014 by selecting all wells with salinity data that intersected the western draining catchments from Cape Jervis in the south to the northern part of the Adelaide Plains. This resulted in a selection of 25 818 wells of which 13 366 had aquifer classifications and were extracted for use in this study. For the Quaternary Aquifer there were 703 wells with salinity data and aquifer name which was considered insufficient for this analysis. A further selection was made of wells that had maximum drilled depths of less than 30 m across the Adelaide Plains Willunga Basin and a section of Quaternary sediments in the hills, which resulted in an additional 7182 wells. It is considered very likely that these wells are screened in Quaternary Aquifers and so they are referred to below as part of the QA dataset. Where multiple EC and chloride values were available, the value with the latest sampling date was selected. The relationship between electrical conductivity (EC) and chloride determined by Guan *et al.* (2010) was used to convert EC data to approximate chloride concentrations as per the equation:

$$[Cl] = 0.0457 \cdot EC^{1.211} \quad (3)$$

where  $[Cl]$  is chloride concentration in mg/L and  $EC$  is electrical conductivity in  $\mu\text{Scm}^{-1}$ .

While there is a degree of uncertainty within this relationship (i.e. scatter in the data), any errors due to individual data points are considered to be outweighed by the large dataset and the use of median values in the following discussion. The resultant EC-derived Cl dataset is summarised in Table C.2 and the histograms for each aquifer are shown in Apx Figure C.2 and Figure C.3. From within this dataset, measured chloride data was also available but was far less adequate in representing the spatial variability ( $n = 1004$ ). The measured chloride data is summarised in the Table C.1 and histograms shown in Apx Figure C.12 and Apx Figure C.13 of section C.5 Additional Information. For the purposes of this study the measured chloride data has not been discussed further as the EC derived chloride is considered to be more spatially representative.

### C.3.3 SPATIAL ANALYSIS

A number of spatial datasets, shape files and layer files were created in ESRI ArcGIS v10.1, as part of the analysis in this chapter and are listed below along with a brief description of the procedures used:

- 1) Data Selection – The EC-derived chloride data for each aquifer was selected based on aquifer name for the T1, T2 and Fractured Rock Aquifers. Wells representing the Quaternary Aquifer were selected using a definition query based on aquifer name and additionally, by selecting wells with maximum drilled depths that were > 0 m and < 30 m. Where the aquifer name field contained more than one aquifer the upper aquifer was chosen (i.e. T1+T2 = T1). These wells were then extracted for each respective aquifer and used in all further analysis.
- 2) Aquifer Boundaries – New shapefiles were created for the inferred extent of the Quaternary Aquifers and Fractured Rock Aquifers. The QA extent was bounded in the west by the coastline and in the east by the outcropping hard rock geology. Additionally, there was a collection of Quaternary sediments in the hills and these were also digitised as part of the QA extent shapefile. For the FRA extent, the western boundary was either inferred based on the location of wells with aquifer names classified as bedrock geology, where hard rock geology was expressed as surface geology or along the Para or Eden-Burnside Faults. Where there was a conflict between these western boundaries due to low resolution base shapefiles, the western-most boundary was taken. The eastern boundary was approximately derived from the surface expression of hard rock geology and lies to the east of the data frame. FRA wells were then sub-selected based on a lasso selection to include a limited number of wells located to the east of the topographic divide for the purposes of interpolation. Boundaries for T1 and T2 Aquifers were provided by DEWNR (NAP and CAP) and NCGRT (Willunga). The T2 Aquifer extent in the NAP and CAP was created by dissolving and slightly altering the T2 boundary in the CAP with the NAP Prescribed Wells Area. The eastern extent of the T2 Aquifer in the north was then altered to run along the Para Fault rather than the PWA boundary.
- 3) Interpolation – Inverse Distance Weighting (IDW) was used to interpolate a spatially representative surface of the EC derived chloride concentration for each aquifer. A power of 2 and cell size of 100 m was selected while the search radius used 12 points. Other interpolation techniques produced similar surfaces (i.e. Kriging) but did not allow individual values to be as conspicuous (which in this case was desired in order to identify potential outliers visually). These surfaces were then extracted using a mask of the relevant aquifer boundary, reclassified appropriately and then saved as layer files.
- 4) Differencing – selected EC derived chloride surfaces were subtracted from each other to determine the difference in chloride concentration between aquifers. This was done by firstly subtracting the T1 Aquifer surface from the QA surface and secondly, by subtracting T1 Aquifer surface from the T2 Aquifer surface. The resulting surface could only be created where the two aquifer extents overlapped and may be used to infer the potential for inter-aquifer leakage or lack thereof.

## C.4 Results and Discussion

### C.4.1 EC DERIVED CHLORIDE CONCENTRATIONS

The median values for EC-derived chloride (referred to hereafter as chloride) for the FRA, QA, T1 and T2 aquifers are 318, 701, 436 and 460 mg/L respectively (Table C.2). These are lower than the mean values indicating that the means are skewed towards some very high salinity groundwater samples. This is also reflected in the 90<sup>th</sup> percentile values for each of the aquifers, particularly for the Quaternary Aquifers whose 90<sup>th</sup> percentile is approximately double that of the other aquifers. The T1 and T2 Aquifers have very similar

chloride statistics with the T2 Aquifer having slightly higher values for all statistics. Meanwhile groundwater in the FRA generally has the lowest chloride concentrations.

The histograms shown in Apx Figure C.2 and Apx Figure C.3 show the distribution of chloride concentrations in each aquifer. The FRAs have mostly very low chloride concentrations but a relatively long tail towards higher concentrations. The QA chloride concentrations have a wider distribution with a higher mean and a considerable number of very high chloride concentrations. The histograms of T1 and T2 aquifers show a very similar distribution with few very low concentrations and an extended tail towards higher concentrations.

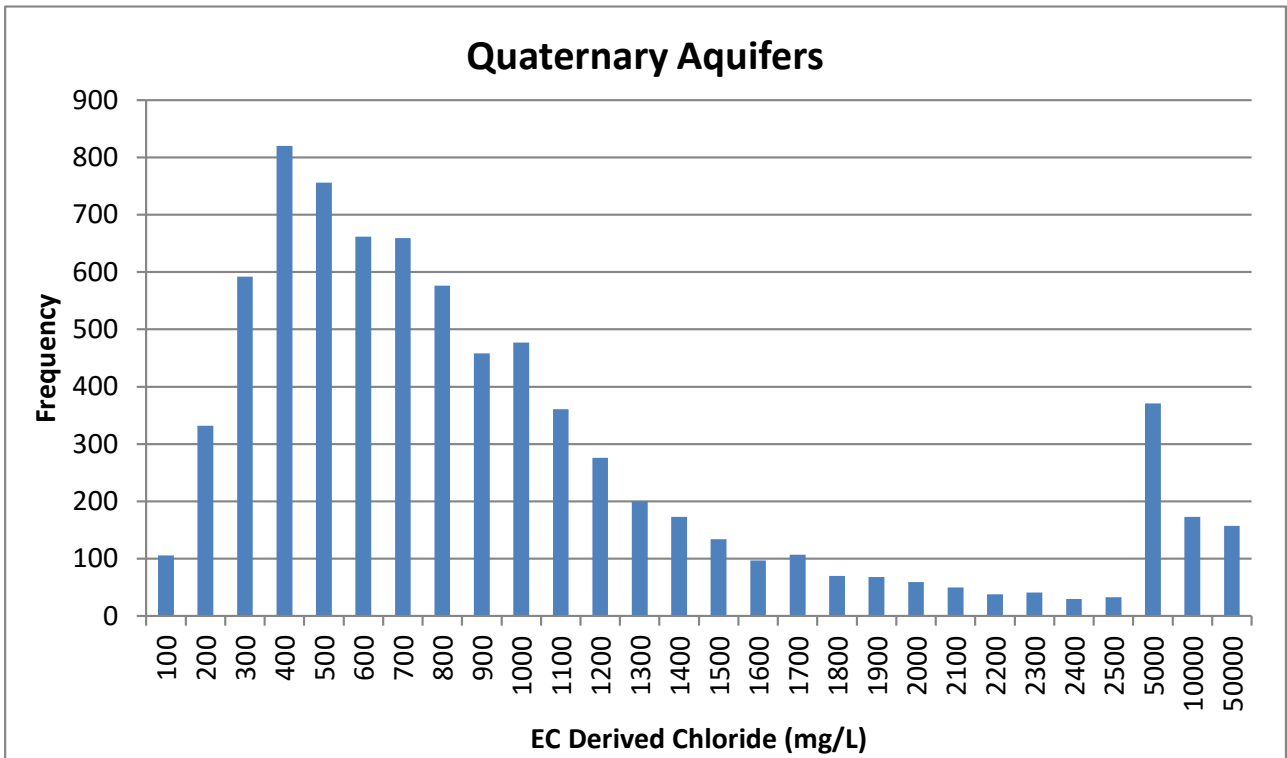
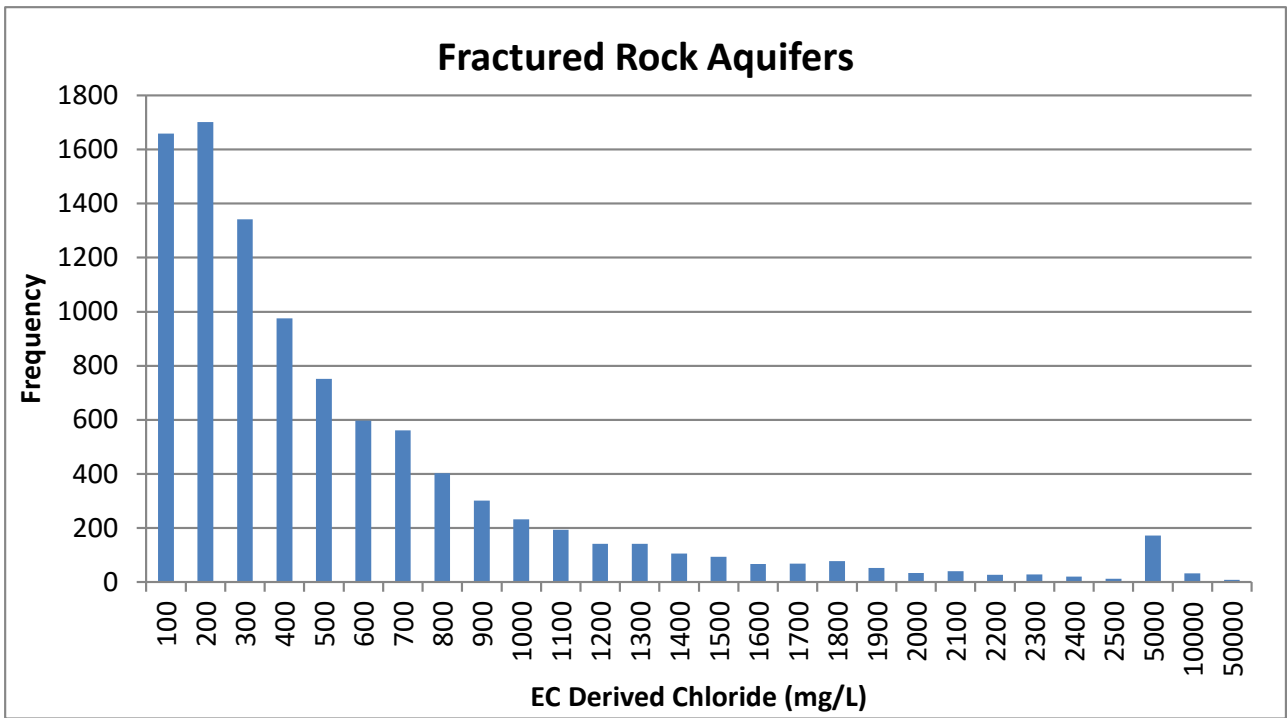
**Apx Table C.2 Summarised EC derived chloride values from selected wells with aquifer names.**

AQUIFERS	COUNT	MEAN (mg/L)	MEDIAN (mg/L)	90 <sup>TH</sup> PERCENTILE (mg/L)	10 <sup>TH</sup> PERCENTILE (mg/L)
Fractured Rock	9837	550	318	1197	65
Quaternary	7885	1477	701	2271	267
T1	1149	794	436	1013	230
T2	1426	911	460	1149	266
Total	20 297				

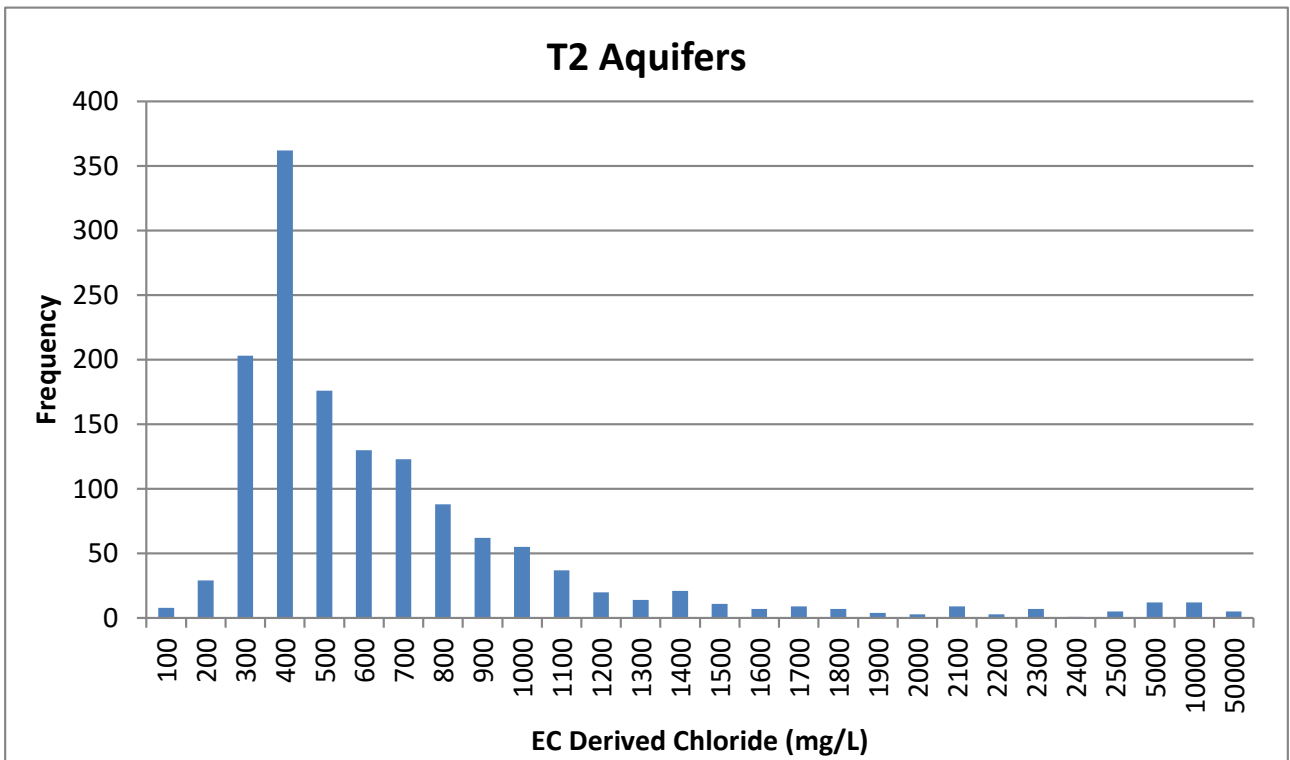
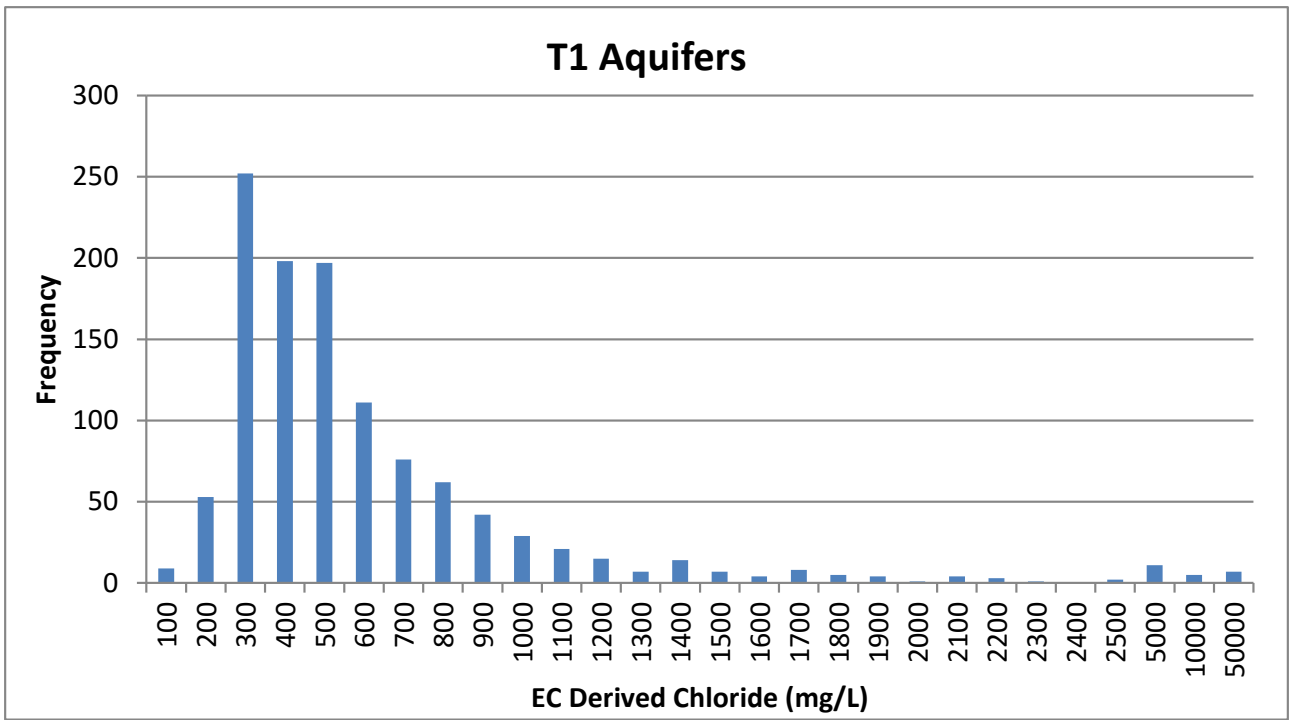
The spatial distribution of chloride concentration in each aquifer can be seen in Figures 4-7. Broadly speaking, the lowest chloride concentrations are in the FRA in the central hills area which suggests the potential for high recharge rates. Additionally, there are some lower chloride values in the Adelaide Plains aquifers in the vicinity of the Gawler River and other creeks draining from the WMLR, most notably in the QA. These include reaches along the Little Para River, Brownhill Creek, First, Second, Third and Fifth Creeks and lower reaches of Fourth Creek. These low groundwater concentrations suggest that river infiltration may be an important recharge mechanism on the Adelaide Plains (as is discussed further in Appendix D: Groundwater – Surface Water Exchange). The lower chloride concentrations in the T1 and T2 aquifers occur in the vicinity of the Gawler, Little Para and Torrens Rivers as well as near Brownhill Creek. This could suggest that recharge is associated with river loss or leakage from overlying QA in this area.

High chloride concentrations are found to the north of the Gawler River and in an east-west section between the Gawler and Little Para Rivers in QA, T1 and T2 aquifers. Additionally, higher chloride concentrations occur in the QA and T2 Aquifer between the Para Fault and the Barker Inlet. Relatively high chloride concentrations are found in the FRA in the upper reaches of the Gawler River, near the surface water divide between the Western and Eastern MLR and to the east of the Willunga Basin. These higher chloride concentrations indicate lower recharge rates and/or mixing with more saline aquifers.

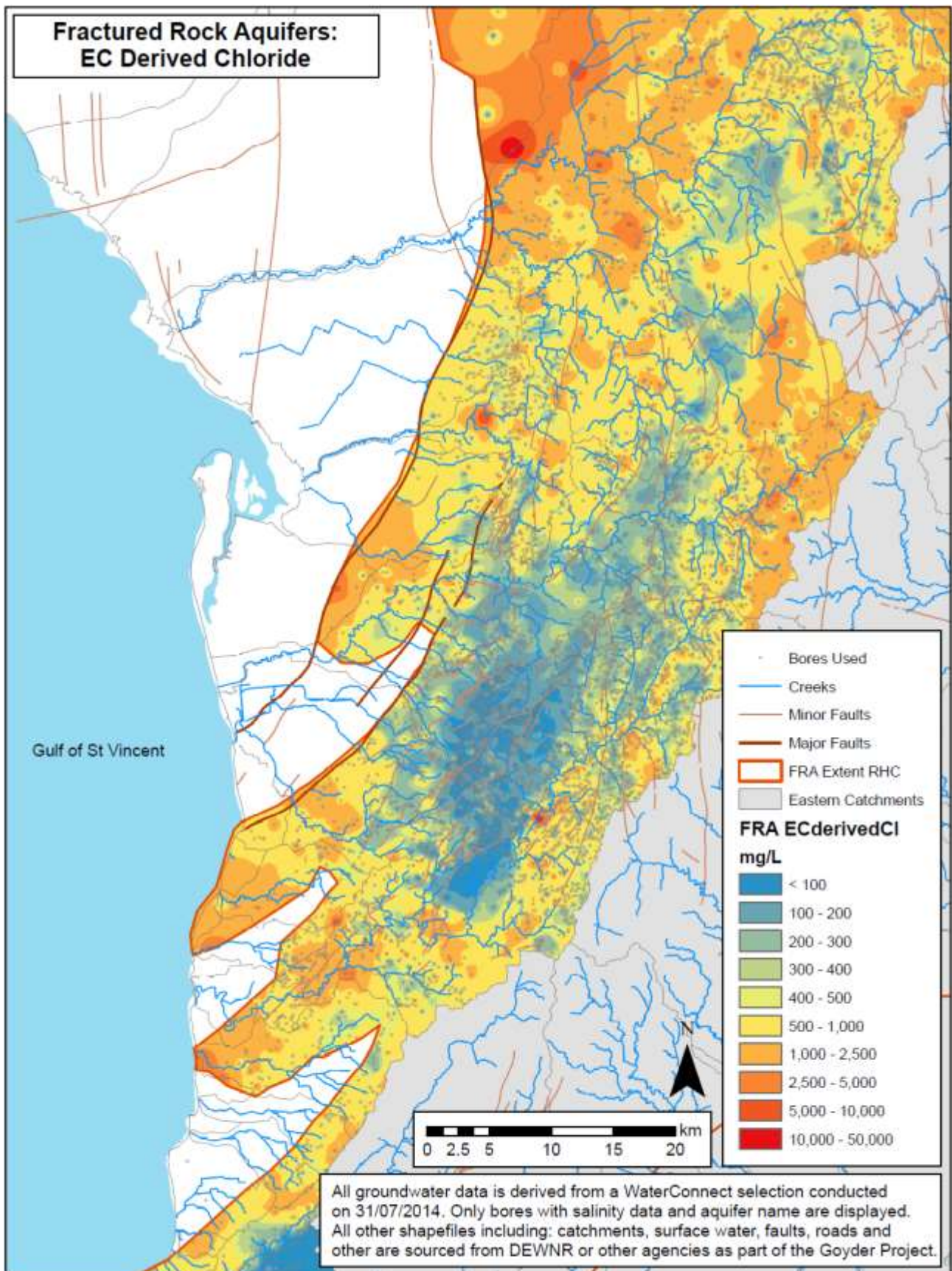
Chloride difference maps were created by subtracting the values of the T1 Aquifers from the QA (Apx Figure C.8) and also the T2 Aquifers from the T1 Aquifers (Apx Figure C.9). Areas in blue shading indicate that the upper aquifer is fresher than the lower aquifer while red shading indicates that the upper aquifer is more saline than the lower aquifer. Where the area is yellow, the chloride concentration of these aquifers is similar and may indicate historical and or modern aquifer–aquifer interaction. These areas of similar chloride concentration are particularly evident in the vicinity of Brownhill Creek and First, Second, Third and Fifth Creeks, parts of the Gawler River and along the Little Para River (Apx Figure C.8). Although chloride is not a definitive indication of inter-aquifer mixing and potential flowpaths, this data would support such conclusions.



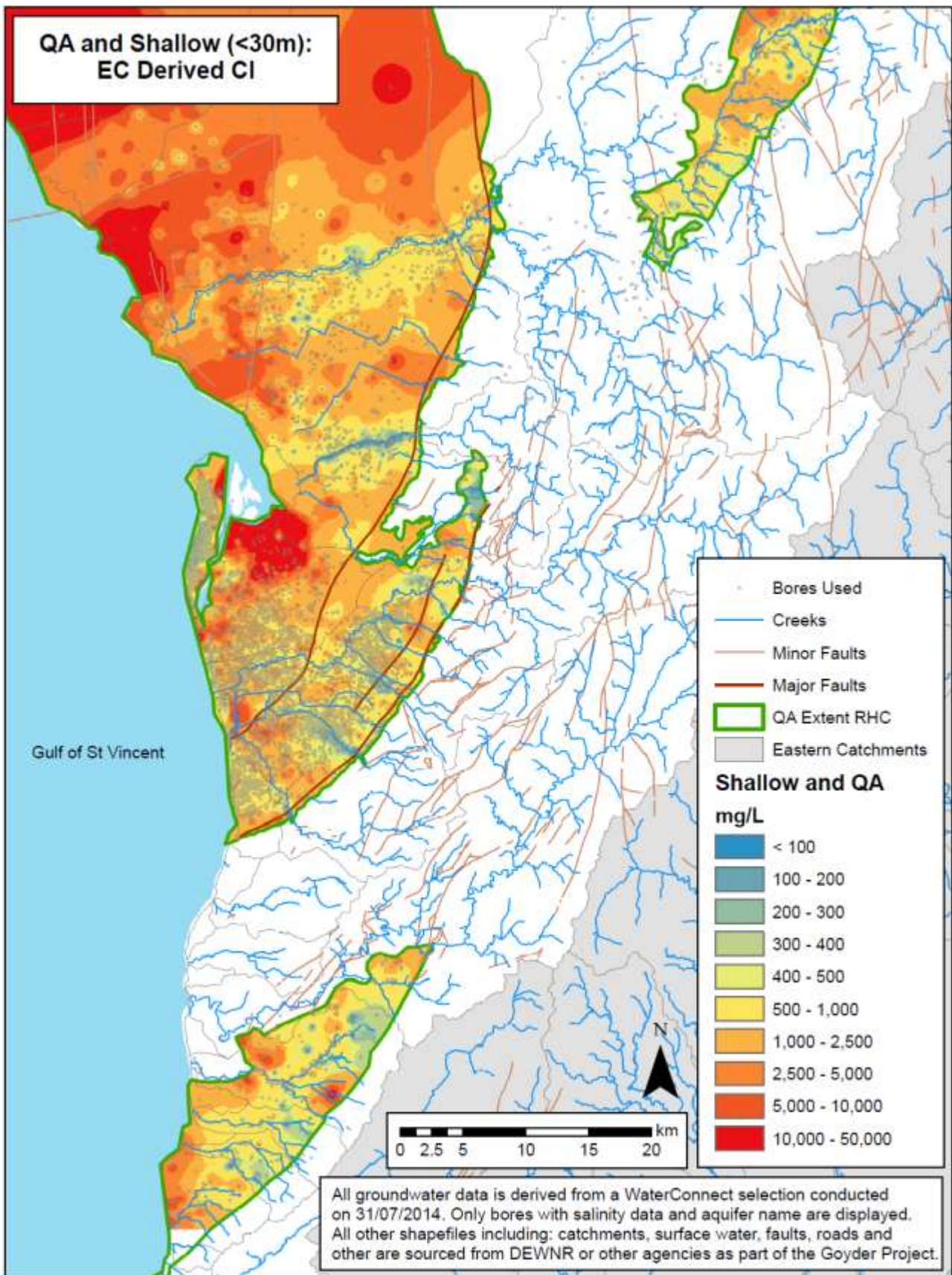
Apx Figure C.2 Latest EC derived chloride values from Fractured Rock and Quaternary Aquifers. Note that the bin ranges are increased for the right-most three categories.



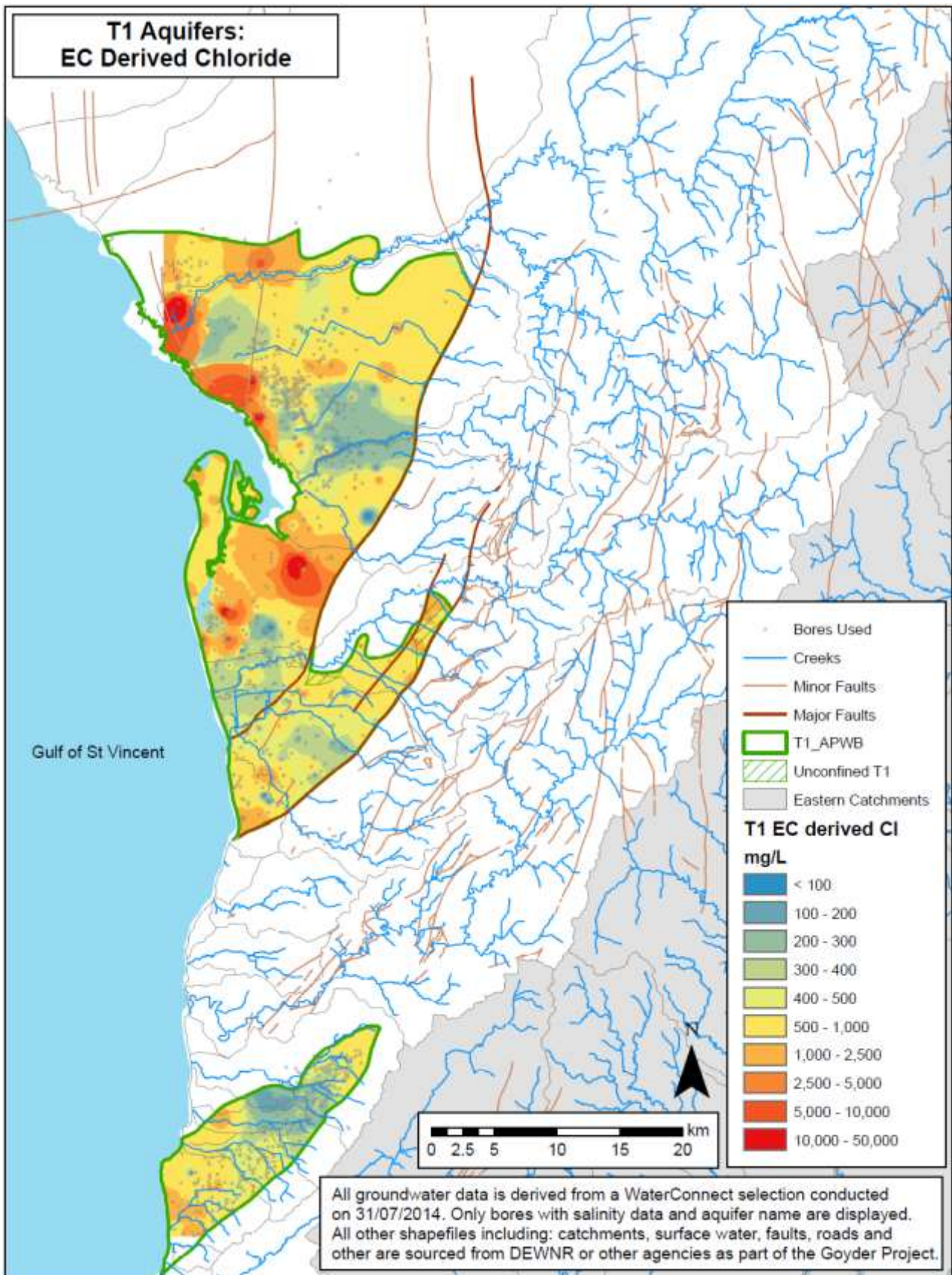
Apx Figure C.3 Latest EC derived chloride values from T1 and T2 Aquifers. Note that the bin ranges are increased for the right-most three categories.



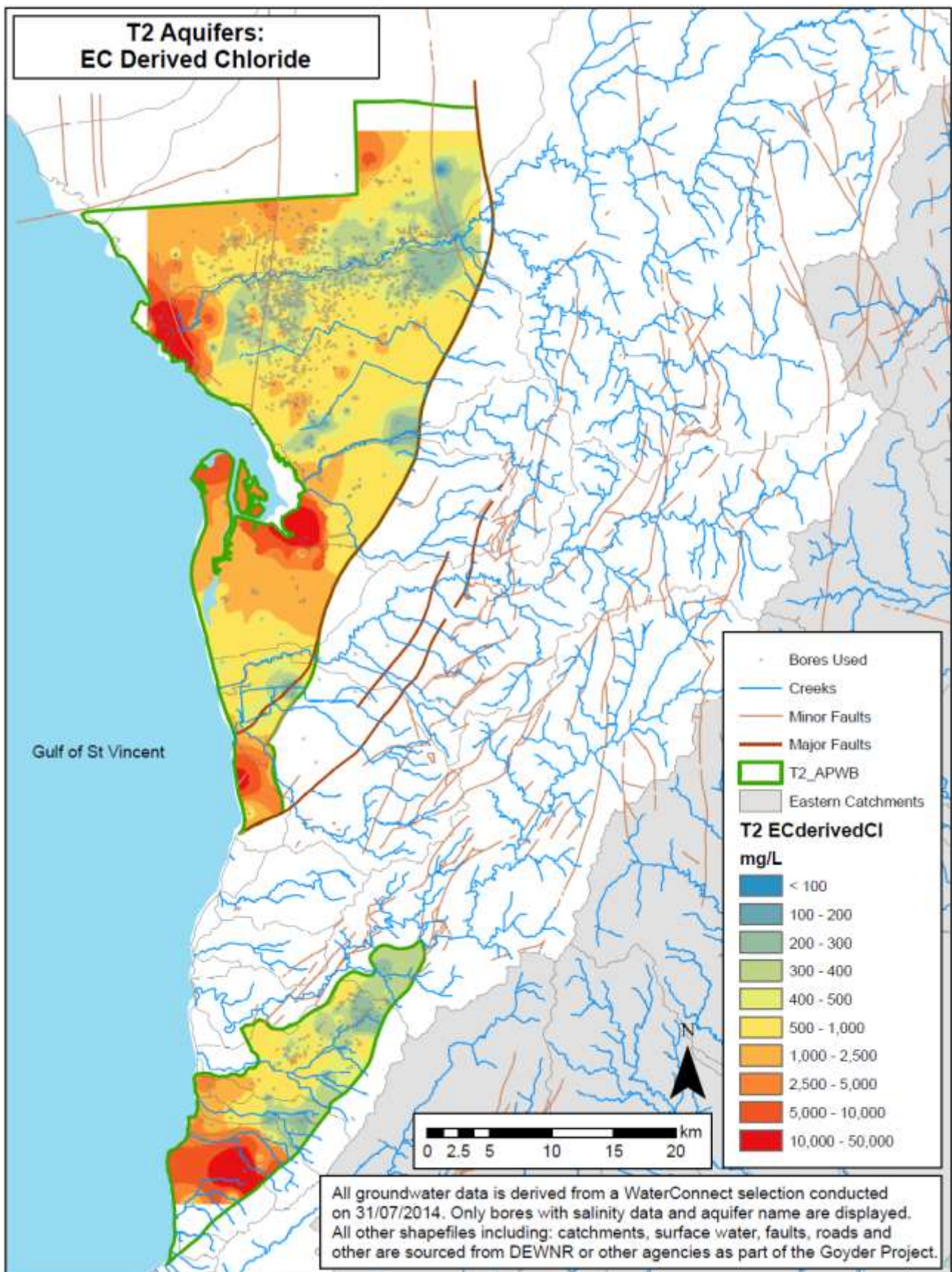
Apx Figure C.4 Interpolated EC derived chloride from the Fractured Rock Aquifers.



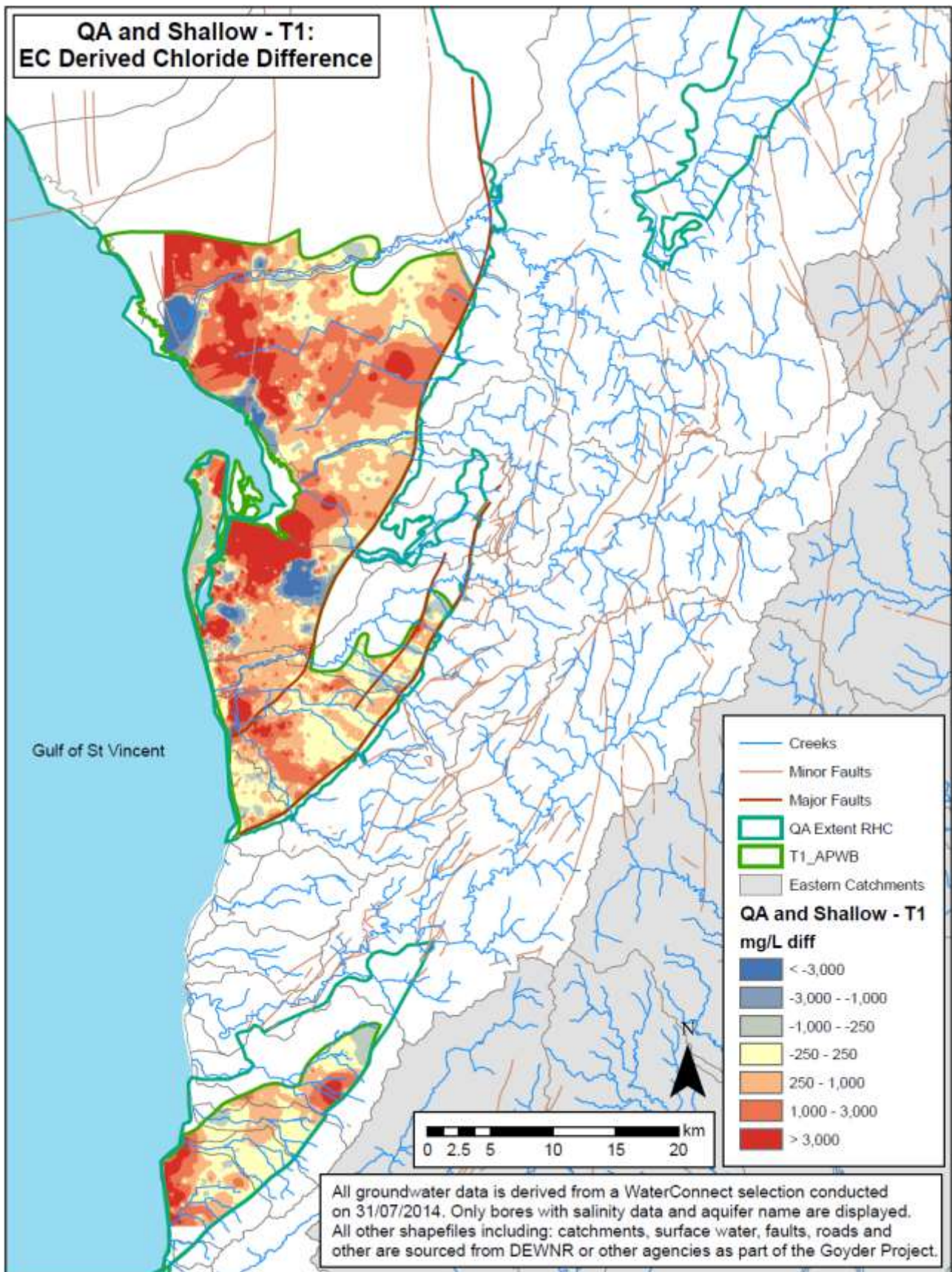
Apx Figure C.5 Interpolated EC derived chloride from the Quaternary Aquifers.



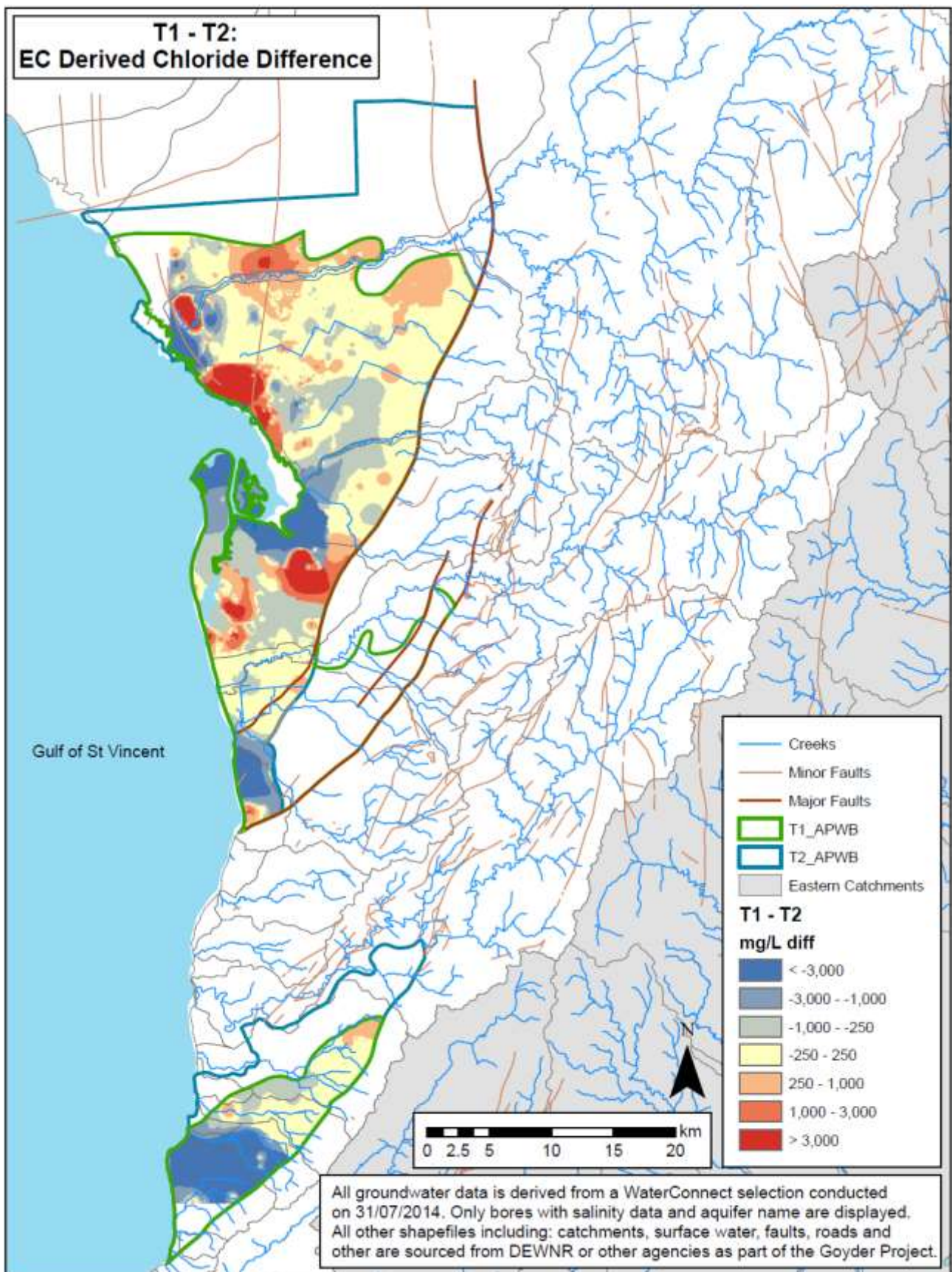
Apx Figure C.6 Interpolated EC derived chloride from the T1 Aquifers.



Apx Figure C.7 Interpolated EC derived chloride from the T2 Aquifers.



Apx Figure C.8 Interpolated EC derived chloride difference between the QA and T1 Aquifers.



Apx Figure C.9 Interpolated EC derived chloride difference between the T1 and T2 Aquifers.

## C.4.2 CMB GROUNDWATER RECHARGE RATES

Recharge rates derived from the CMB approach are shown in Table C.4 with histograms shown in Apx Figure C.8 and Apx Figure C.9. The median recharge rates for the FRA, QA, T1 and T2 aquifers are 7.9, 3.6, 5.7 and 5.4 mm/year respectively. The median recharge rates for the T1 and T2 Aquifers appear to be very similar at 5 to 6 mm/year. Recharge rates to the QA are lower than the T1 and T2 aquifers while recharge to the FRA is notably higher (and higher still if different rainfall values are used – see later discussion). The recharge estimates for the AP aquifers are seen to represent 1-2% of rainfall.

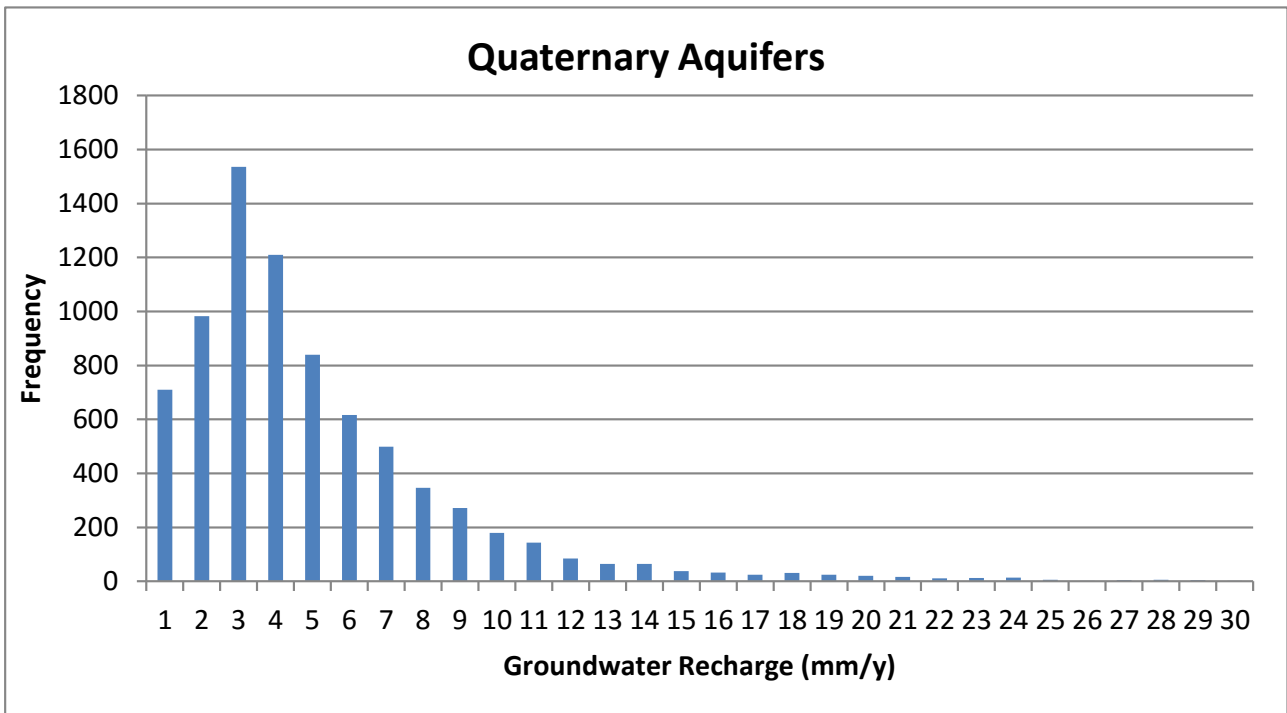
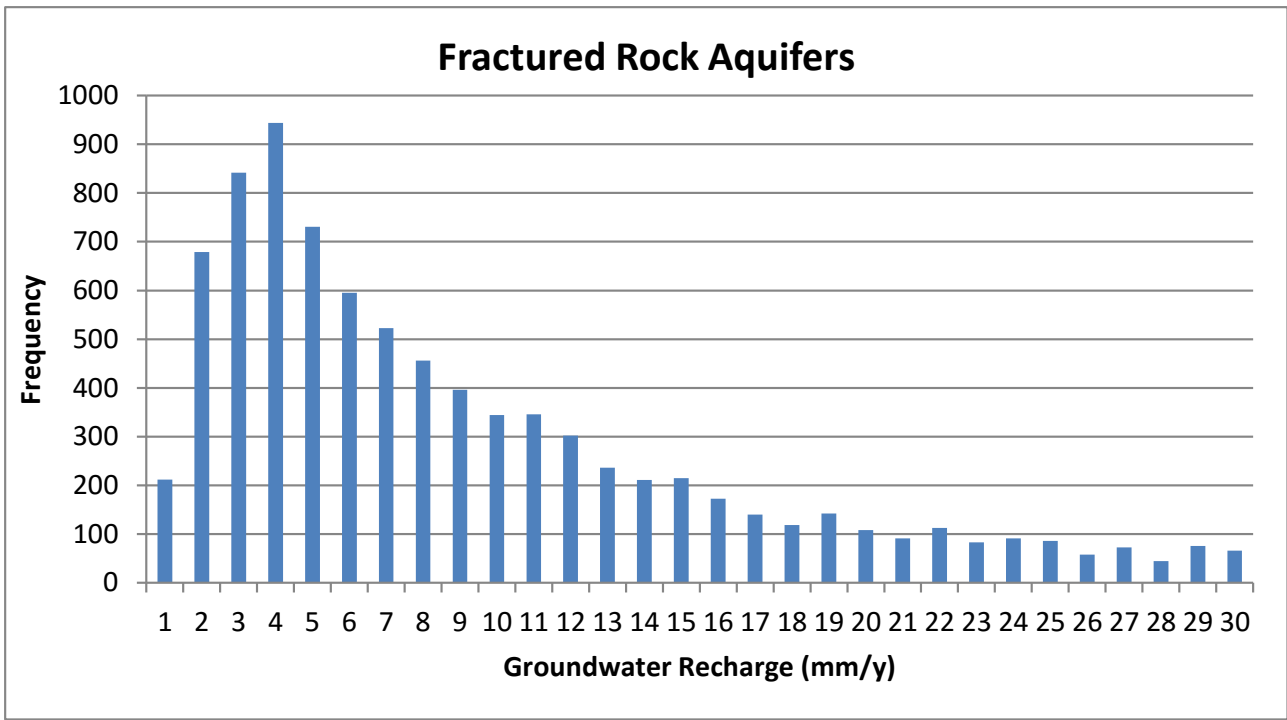
**Apx Table C.3 Summarised recharge rate estimations for all Aquifers.**

AQUIFERS	COUNT	MEAN (mm/y)	MEDIAN (mm/y)	90 <sup>TH</sup> PERCENTILE (mm/y)	10 <sup>TH</sup> PERCENTILE (mm/year)
Fractured Rock	9837	15.9	7.9	38.6	2.1
Quaternary	7885	5.4	3.6	9.4	1.1
T1	1149	7.1	5.7	10.8	2.5
T2	1426	6.0	5.4	9.4	2.2
Total	20 297				

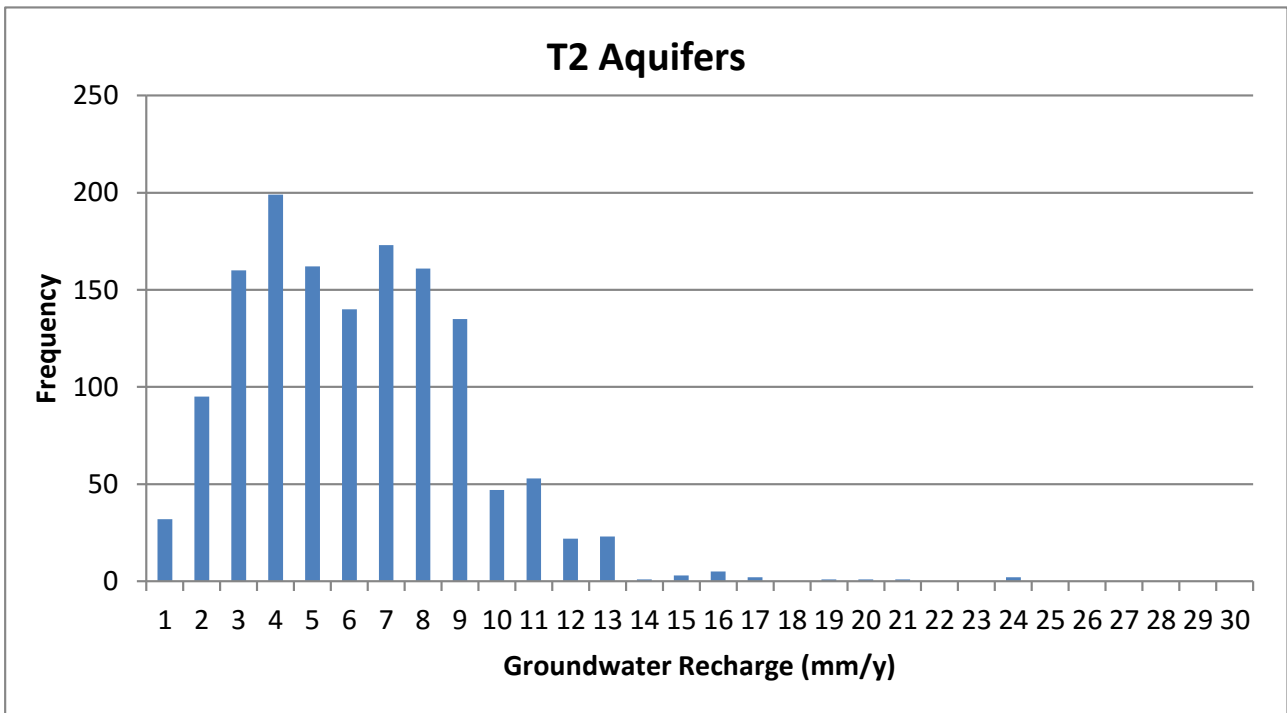
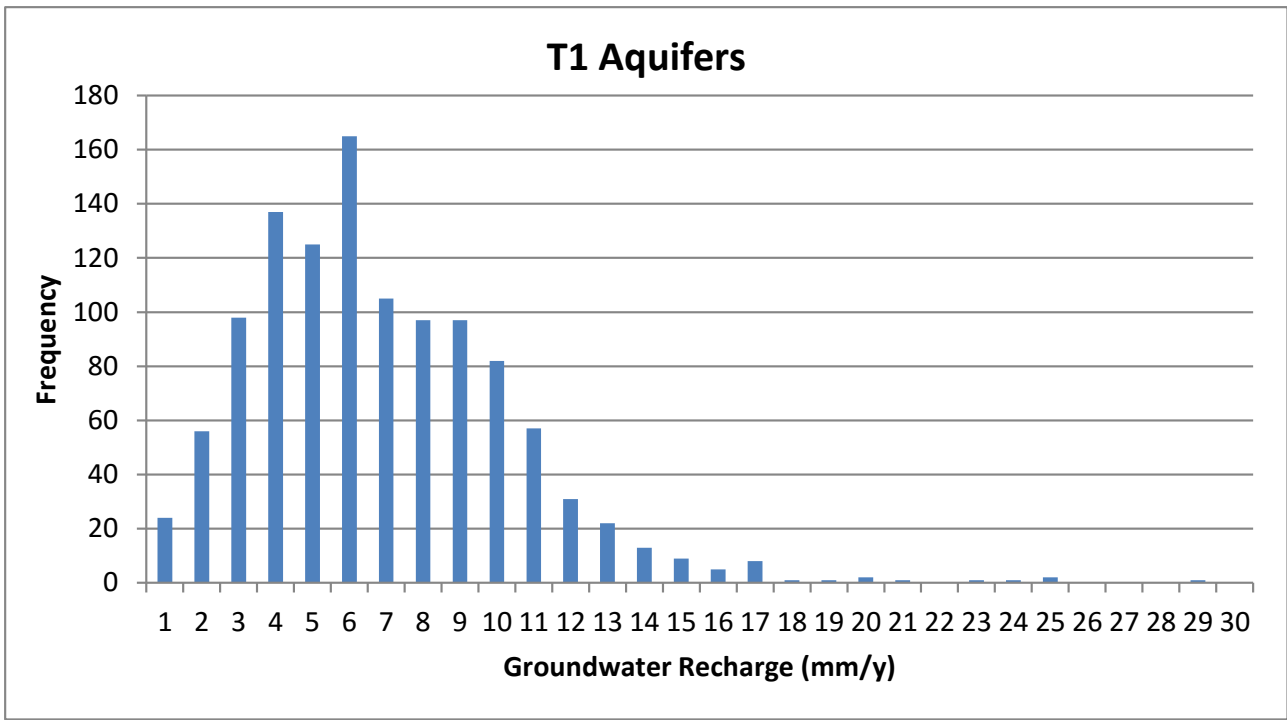
It is possible that data from the AP aquifers has a spatial bias, particularly with regard to the QA. The wells drilled and subsequently selected, are more densely located in areas of lower salinity (e.g. adjacent to the Gawler, Little Para, Torrens and Sturt Rivers as well as in the vicinity of Brownhill and First through Fifth Creeks). This would result in the weighting of recharge rates towards higher values than if additional data from more saline areas was available (see Apx Figure C.5). We acknowledge that higher salinities are found elsewhere for the QA and thus our estimate may be an overestimate compared to a regionally weighted estimate.

As suggested above, it is possible that due to the age of the groundwater in the T1 and T2 Aquifers (i.e. 10 000 – 30 000 years), that rainfall chloride values at the time of recharge may have been lower than 5 mg/L. If they were for example, 2.5 mg/L, due to the coast being approximately 250 km further offshore, the recharge rate estimates would be reduced by a factor of 2.

Recharge estimates for the FRAs are higher than the AP Aquifers as a result of their lower chloride concentrations. As mentioned previously, considerable uncertainty in the recharge estimates is introduced by the assumptions of the CMB approach. If we assume that recharge to the AP aquifers occurs via lateral flow across the faults, the recharge estimates for these aquifers should also be doubled (if rainfall is increased to 1000 mm/y as mentioned above).



Apx Figure C.10 Histograms of the CMB groundwater recharge estimates for the Fractured Rock and Quaternary Aquifers. Note that the histogram of the FRA recharge rates has been truncated at 30 mm/year. The tail of this distribution for FRA includes 143 recharge estimates that are > 100 mm/year (i.e. from very fresh groundwater samples).



Apx Figure C.11 Histograms of the CMB groundwater recharge estimates based on data from the T1 and T2 Aquifers, where we assume recharge originally occurred in the WMLR and entered the T1 and T2 via lateral flow.

## C.6 Conclusions

To estimate the groundwater recharge rate to the aquifers of the western draining Mount Lofty Ranges, the Adelaide Plains and the Willunga Basin we have applied a Chloride Mass Balance (CMB) approach. This was conducted using an extraction of all available electrical conductivity data from the WaterConnect database and selecting only those wells with aquifer information, supplemented by wells that less than 30 m deep (classified as Quaternary Aquifers). This resulted in over 20 000 EC values which were then converted to approximate chloride concentrations using a previously derived relationship.

Based on the surfaces interpolated from EC-derived chloride data, there are distinct areas of low chloride groundwater. These are particularly evident for the Quaternary Aquifers in the vicinity of rivers and creeks and imply that river infiltration may be an important recharge mechanism. River infiltration is not explicitly included in the CMB, although these low chloride values are included in calculation of mean values for each of the aquifers.

The median recharge estimates for the Fractured Rock Aquifers, Quaternary Aquifers, T1 and T2 Aquifers were 7.9, 3.6, 5.7 and 5.4 mm/year respectively. Given the assumptions of rainfall chloride concentration of 5 mg/L, rainfall of 500 mm/year and a runoff coefficient of 0, there is a large degree of uncertainty associated with these estimates. It is also important to note that these recharge rates relate to the location where the aquifers are recharged, and do not imply that this occurs within the AP region. It is possible that recharge occurs within the Mount Lofty Ranges, and subsequently flows across the fault into the sedimentary aquifers. If this is the case, then the recharge rates could be up to double those reported here, because a rainfall value representative of the Mount Lofty Ranges should be used in the analysis.

Nevertheless, the recharge estimates derived by the CMB approach indicate that recharge to the Adelaide Plains aquifers is on the order of millimetres per year, which is 1-2% of rainfall.

## C.8 Additional Information

### C.8.1 MEASURED CHLORIDE

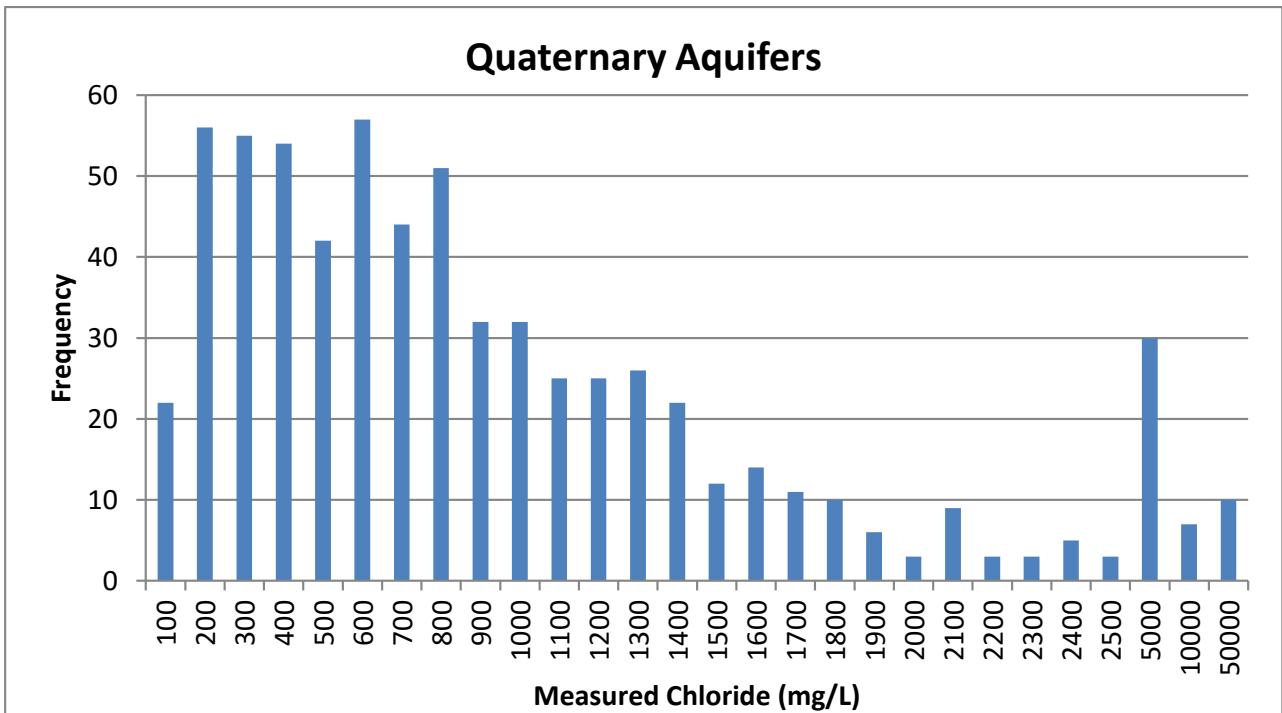
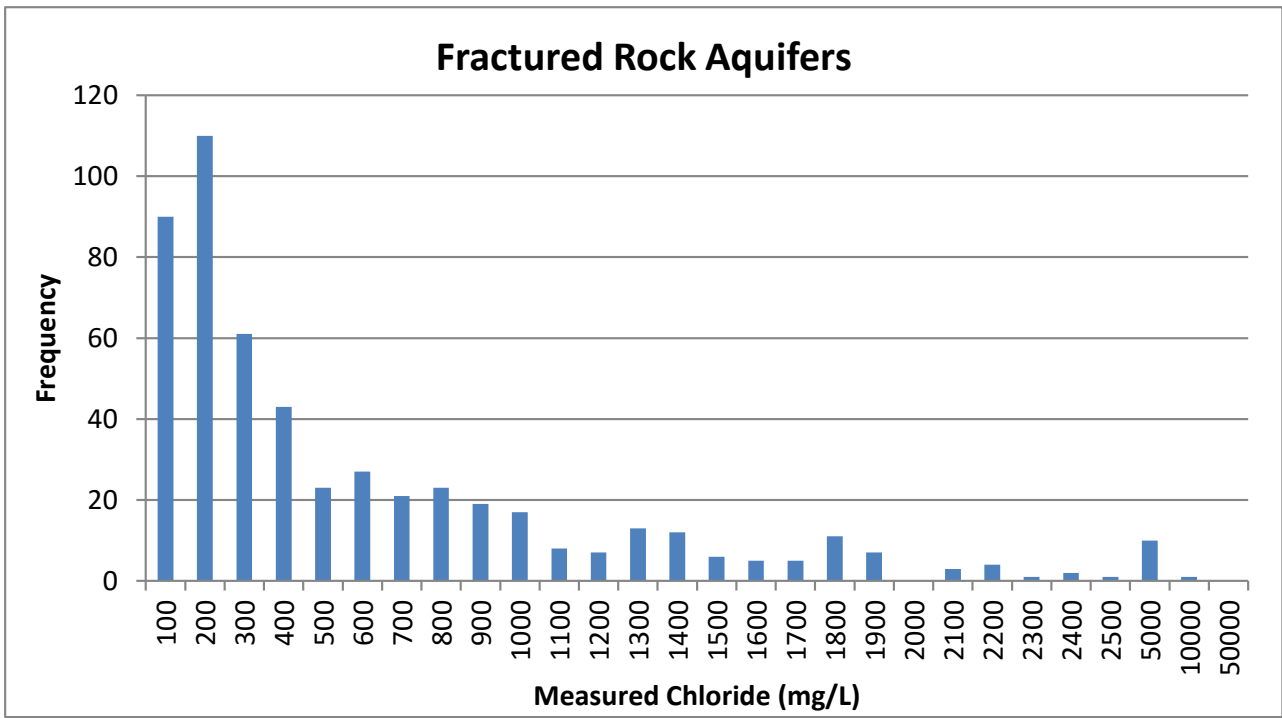
The latest measured chloride concentrations available from WaterConnect are summarised in Table C.4, Apx Figure C.12 and Apx Figure C.13. This dataset, other historical data collected from a range of sources and more recent work done in Willunga Basin and as part of the Goyder Project could be added to the data presented above. However, these potential inclusions are unlikely to improve the spatial coverage enough to warrant their inclusion (compared to EC derived chloride data). Additionally, the EC data from these WaterConnect wells are already included in the analysis of EC derived chloride discussed above.

Apx Table C.4 Summarised measured chloride values from selected wells.

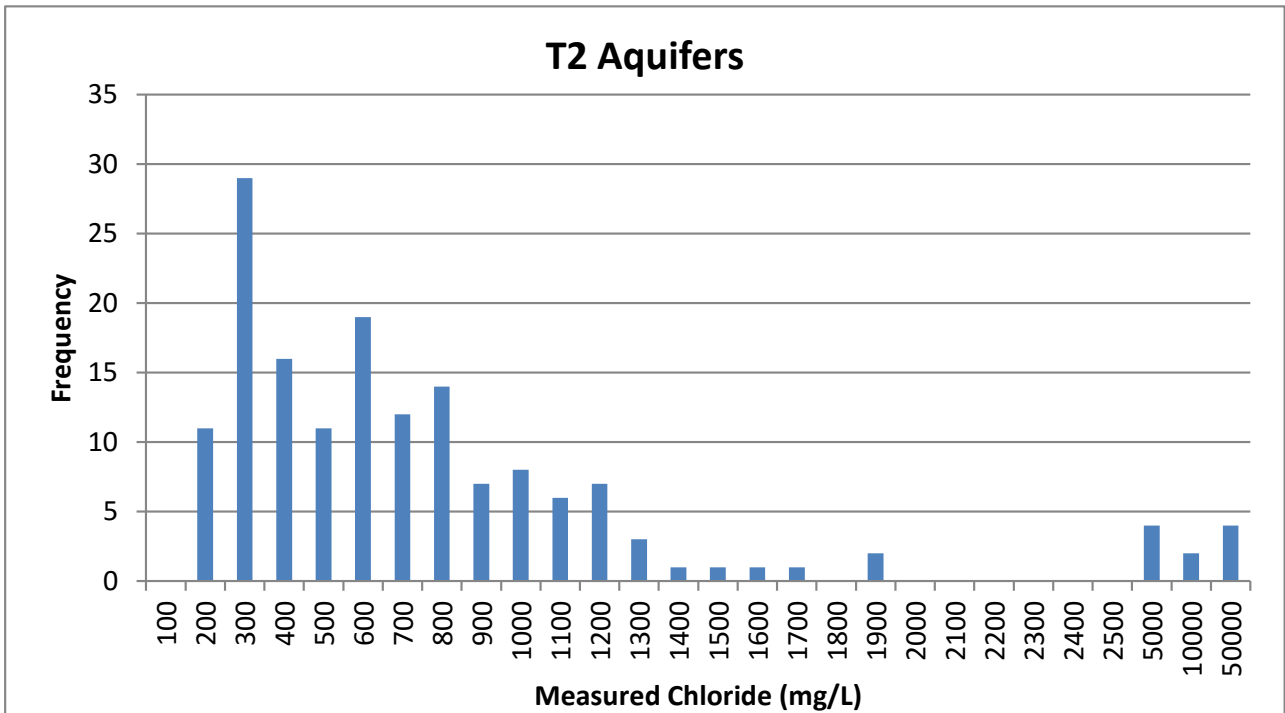
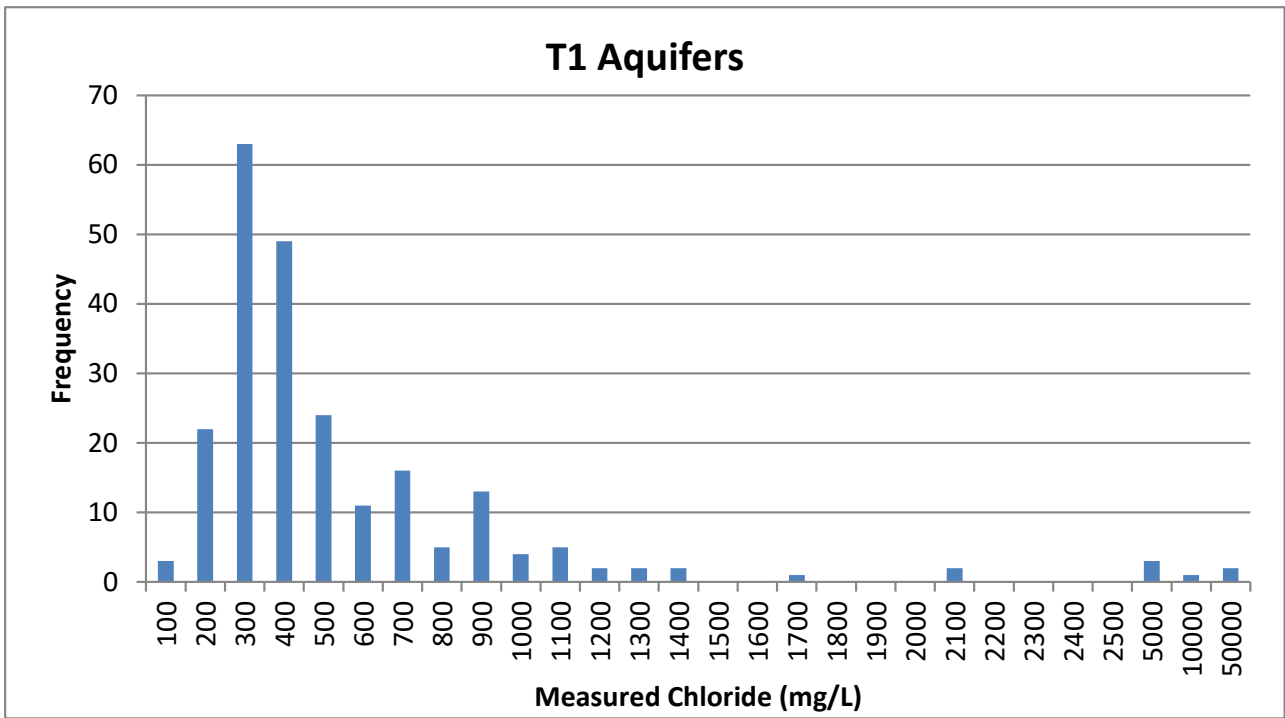
AQUIFERS	COUNT	MEAN (mg/L)	MEDIAN (mg/L)	90TH (mg/L)	10TH (mg/L)
Fractured Rock	530	589	305	1484	70
Quaternary	669	1203	707	2036	182
T1	230	776	339	917	195
T2	159	1389	560	1274	215
Total	1588				

### C.8.1 CHLORIDE ACROSS THE FAULTS MAP SERIES

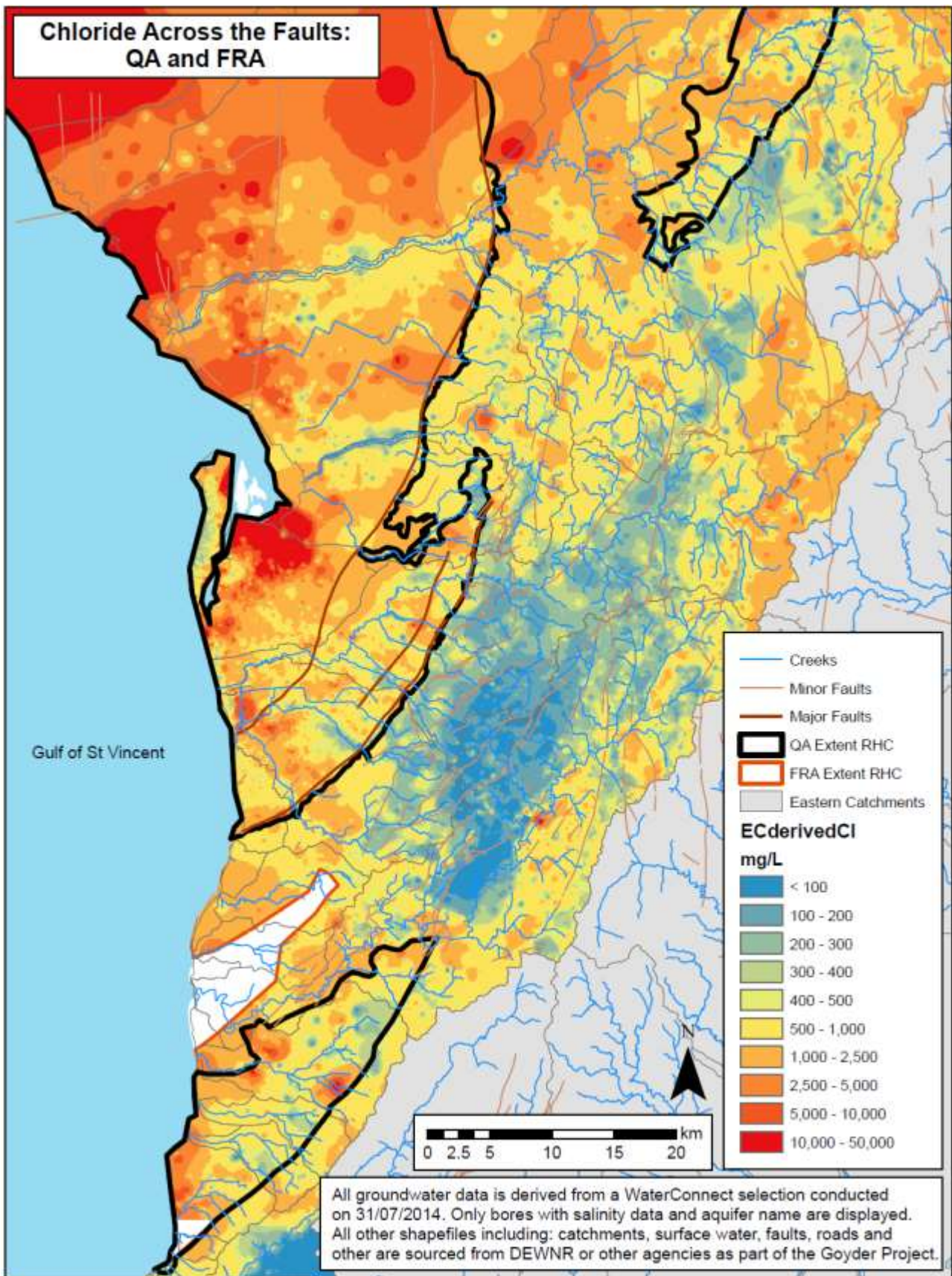
Figures C14-C16 show the interpolated EC derived chloride surfaces of the QA, T1 and T2 Aquifers relative to that of the FRA to the east of the Para and Eden–Burnside Faults. There appears to be relatively sharp concentration gradients in a number of locations, implying a lack of flow across the fault, or the presence of significant recharge at or near the fault. This is particularly noticeable for the regions where chloride is < 400 mg/L in the T1 and T2 Aquifers in both the AP and Willunga Basin and much higher in the FRA. There appears to be more continuity in chloride concentration across the faults between the QA and FRA than with the Tertiary Aquifers. This may indicate that shallow fluxes are more significant than deeper fluxes, although further work is required to confirm this preliminary interpretation.



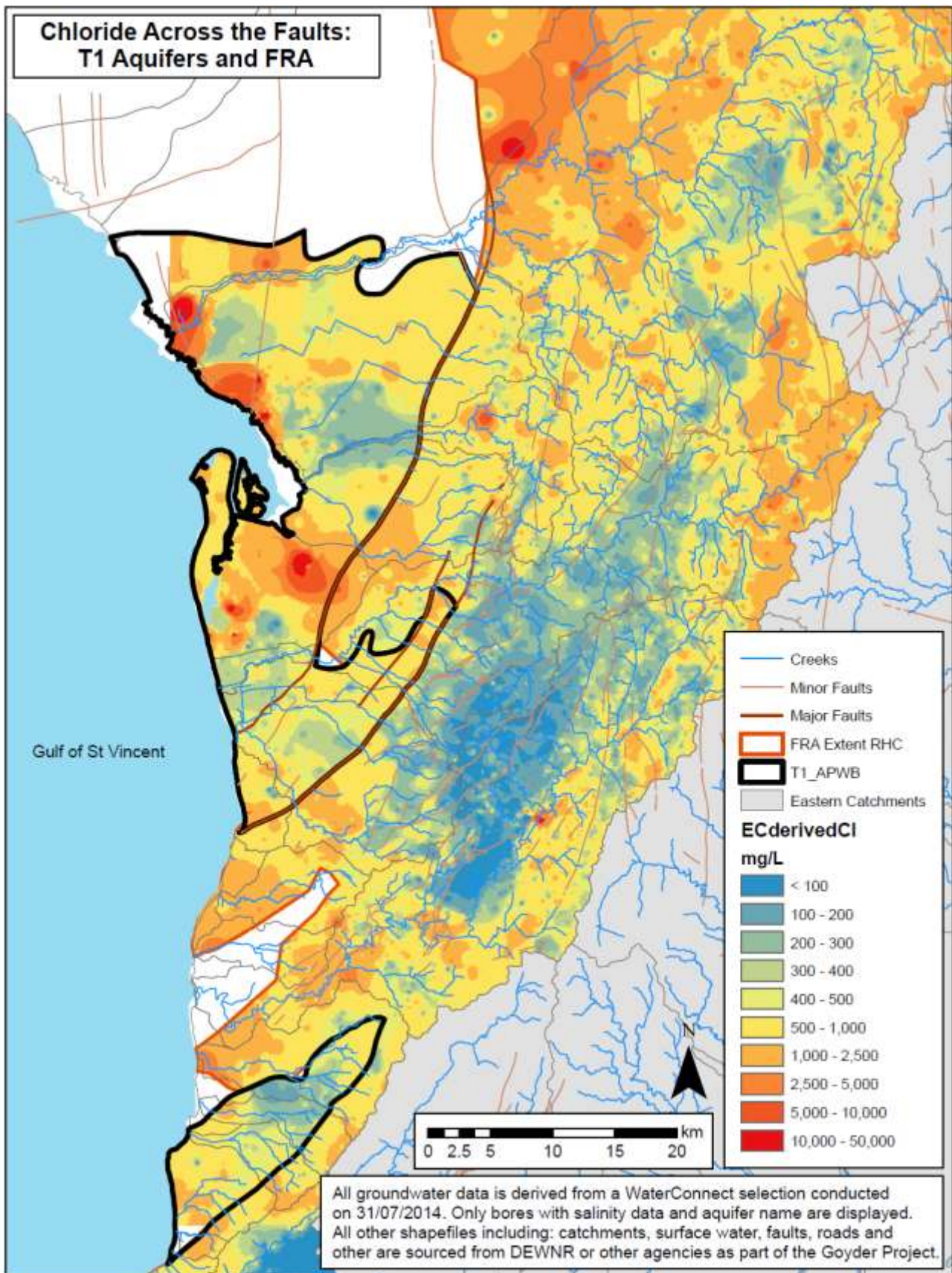
Apx Figure C.12 Latest measured chloride values from Fractured Rock and Quaternary Aquifers. Note that the bin ranges are increased for the right-most three categories.



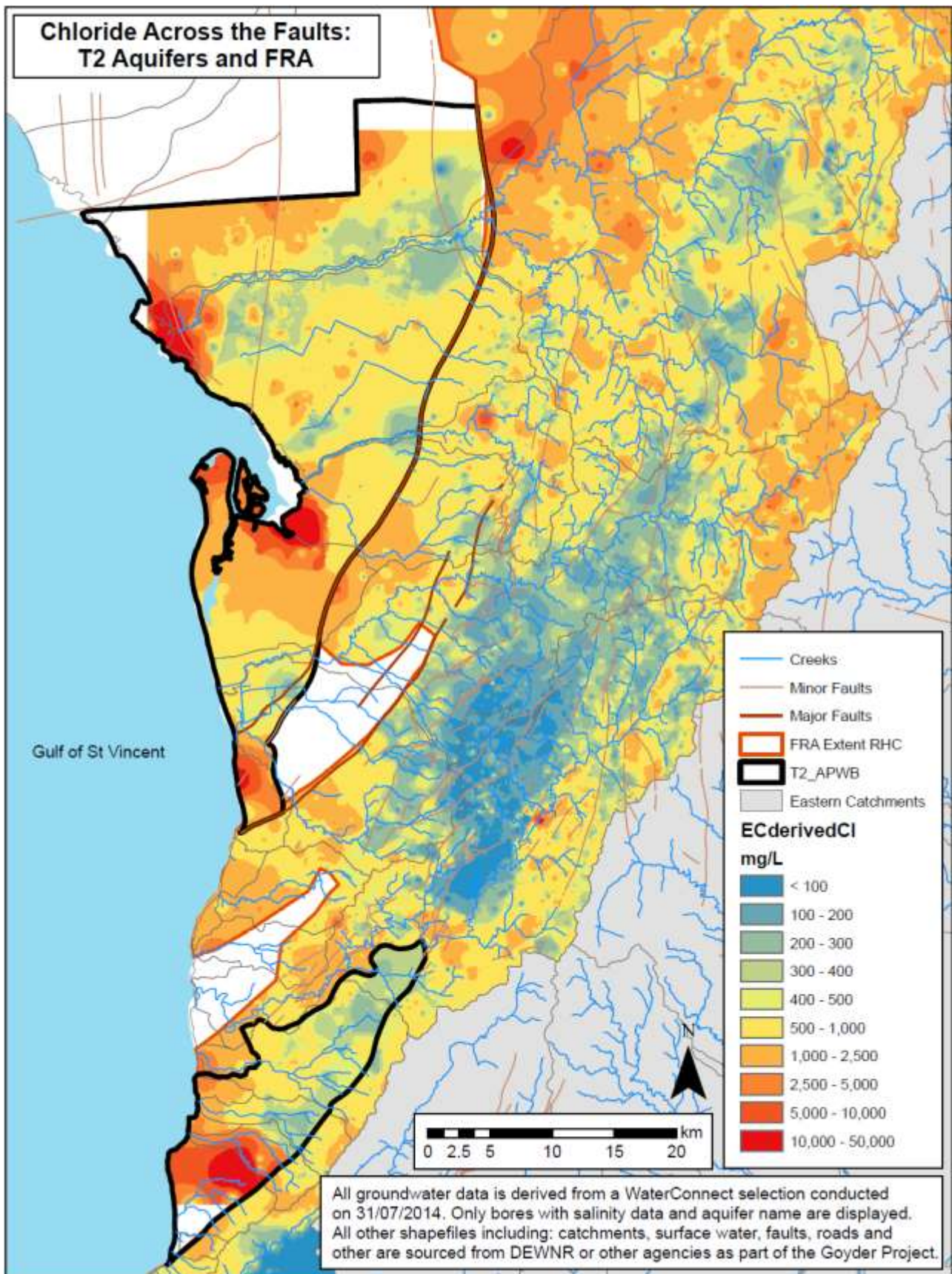
Apx Figure C.13 Latest measured chloride values from T1 and T2 Aquifers. Note that the bin ranges are increased for the right-most three categories.



Apx Figure C.14 Interpolated chloride surface of the Quaternary and Fractured Rock Aquifers, separated by Faults.



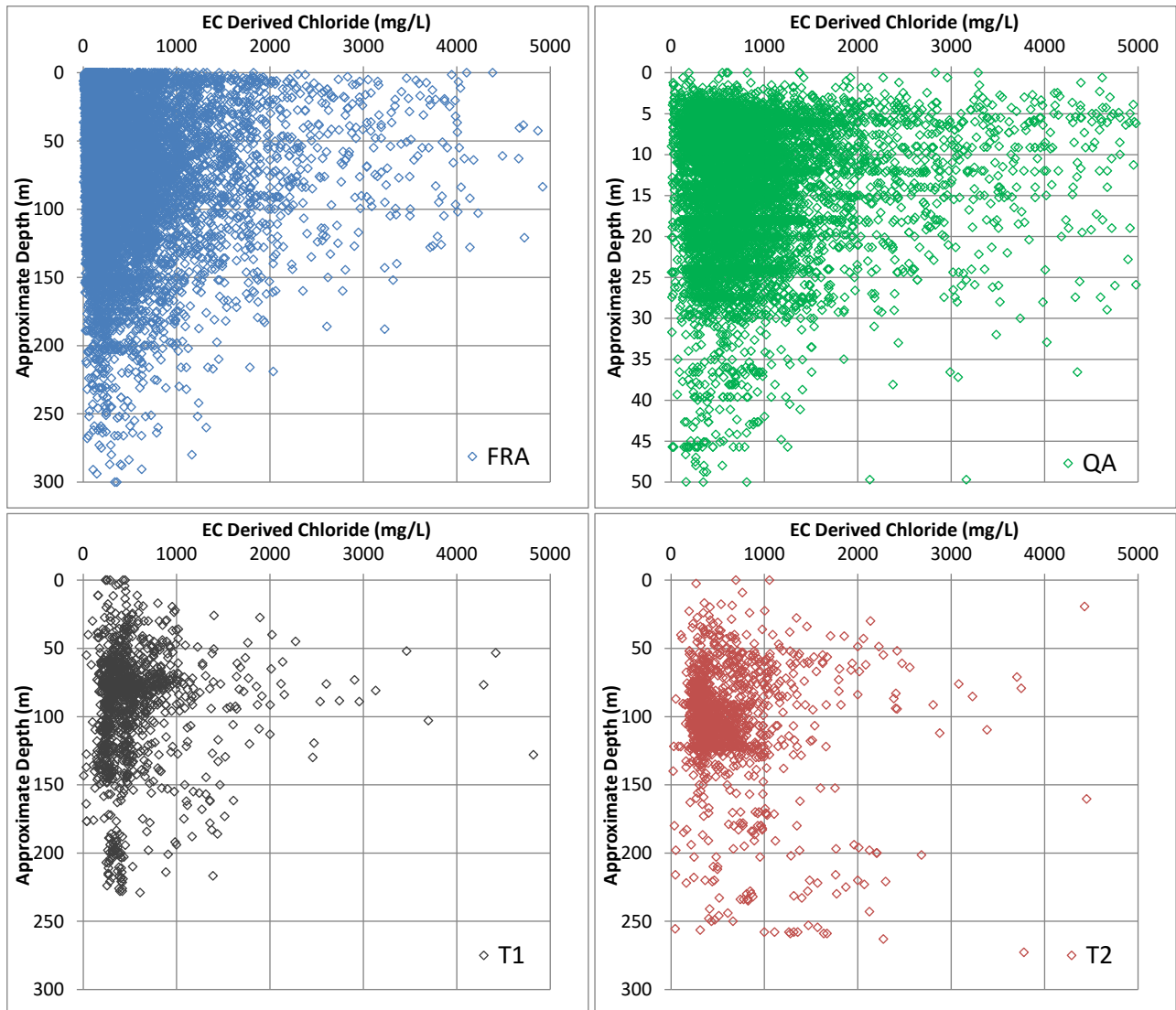
Apx Figure C.15 Interpolated chloride surface of the T1 and Fractured Rock Aquifers, separated by Faults.



Apx Figure C.16 Interpolated chloride surface of the T2 and Fractured Rock Aquifers, separated by Faults.

### C.8.1 EC DERIVED CHLORIDE VS MAXIMUM DRILLED DEPTH

The below figures show scatter plots of drilled depth vs EC-derived chloride for each aquifer. The depth value was derived by preferentially selecting the latest open depth, cased to depth and maximum drilled depth if no depth value was available for the other fields. There does not appear to be any clear vertical gradient trends for any of the four aquifers based on this broad approach. The scatter seen for the shallower depths of FRA and QA is thought to reflect the greater number of wells drilled to shallower depths. However, it is likely that vertical gradients in chloride concentration do exist at particular field sites depending on changing recharge rates in response to changes in climatic trends and / or landuse change. A proximity analysis or other more detailed analysis is considered beyond the scope of this chapter.



Apx Figure C.17 Scatter plots of depth vs EC derived chloride. Note the different y-axis on the QA scatter plot.

## C.9 References

- Banks EW, Wilson T, Green G and Love AJ (2006) Groundwater recharge investigations in the Eastern Mount Lofty Ranges, South Australia. Report DWLBC 2007/20, Government of South Australia, through Department of Water, Land and Biodiversity Conservation, Adelaide.
- Banks EW, Zulfic D and Love AJ (2006) Groundwater recharge investigation in the Tookayerta Creek Catchment, South Australia. DWLBC Report 2007/14, Government of South Australia, through Department of Water, Land and Biodiversity Conservation, Adelaide.
- Blackburn G, and McLeod S (1983) Salinity of Atmospheric Precipitation in the Murray-Darling Drainage Division, Australia. *Australian Journal of Soil Research*, 21, 411-434.
- Drexel JF and Preiss WV (Eds) (1995) *The geology of South Australia. Vol. 2. The Phanerozoic.* South Australia Geological Survey, Bulletin, 54.
- Green G, Banks E, Wilson T and Love A (2006) Groundwater recharge and flow investigations in the Western Mount Lofty Ranges, South Australia. DWLBC Report 2007/29, Government of South Australia, through Department of Water, Land and Biodiversity Conservation, Adelaide.
- Green G and Zulfic D (2008) Summary of groundwater recharge estimates for the catchments of the Western Mount Lofty Ranges Prescribed Water Resources Area. DWLBC Technical note 2008/16, Government of South Australia, through Department of Water, Land and Biodiversity Conservation, Adelaide.
- Guan H, Love AJ, Simmons CT, Hutson J and Ding Z (2010) Catchment conceptualisation for examining applicability of chloride mass balance method in an area with historical forest clearance. *Hydrolo. Earth Syst. Sci.*, 14, 1233-1245. DOI: 10.5194/hess-14-1233-2010.
- Guan H, Hutson J, Ding Z, Love A, Simmons CT and Deng Z (2013). Principal component analysis of watershed hydrochemical response to forest clearance and its usefulness for chloride mass balance applications, *Water Resour. Res.*, 49, doi:10.1002/wrcr.20357.
- Harrington GA (2002) Recharge mechanisms to Quaternary sand aquifers in the Willunga Basin, South Australia. South Australia. Department of Water, Land and Biodiversity Conservation. Report, DWLBC 2002/016.
- Harrington G (2004) Hydrogeological Investigation of the Mount Lofty Ranges, Progress Report 4: Groundwater – surface water interactions in the Scott Creek, Marne River and Tookayerta Creek Catchments. DWLBC Report 2004/11, Government of South Australia, through Department of Water, Land and Biodiversity Conservation, Adelaide.
- Hingston FJ and Gailitis V (1976) The Geographic Variation of Salt Precipitated over Western Australia. *Australian Journal of Soil Research*, 14, 319-335.
- Hutton JT (1976) Chloride in Rainwater in Relation to Distance from Ocean. *Search*, 7, 207-208.
- Hutton JT and Leslie TI (1958) Accession of non-nitrogenous ions dissolved in rainwater to soils in Victoria. *Aust. J. Agric. Res.* 9:492-507
- Keyword MD, Fifield LK, Chivas AR and Cresswell RG (1998). Fallout of chlorine 36 to the Earth's surface in the southern hemisphere. *Journal of Geophysical Research*, 103 (D7), 8281-8286.
- Zulfic D, Barnett SR and van den Akker J (2002) Mount Lofty Ranges Groundwater Assessment, Upper Onkaparinga Catchment. South Australia. Department of Water, Land and Biodiversity Conservation. Report, DWLBC 2002/29.
- Zulfic D (2006) Mount Lofty Ranges groundwater assessment — South Para River Catchment. Report DWLBC 2005/41, Government of South Australia, through the Department of Water, Land and Biodiversity Conservation, Adelaide.

# Appendix D Groundwater – surface water exchange

Authors: Cranswick RH and Cook PG

## D.1 Executive Summary

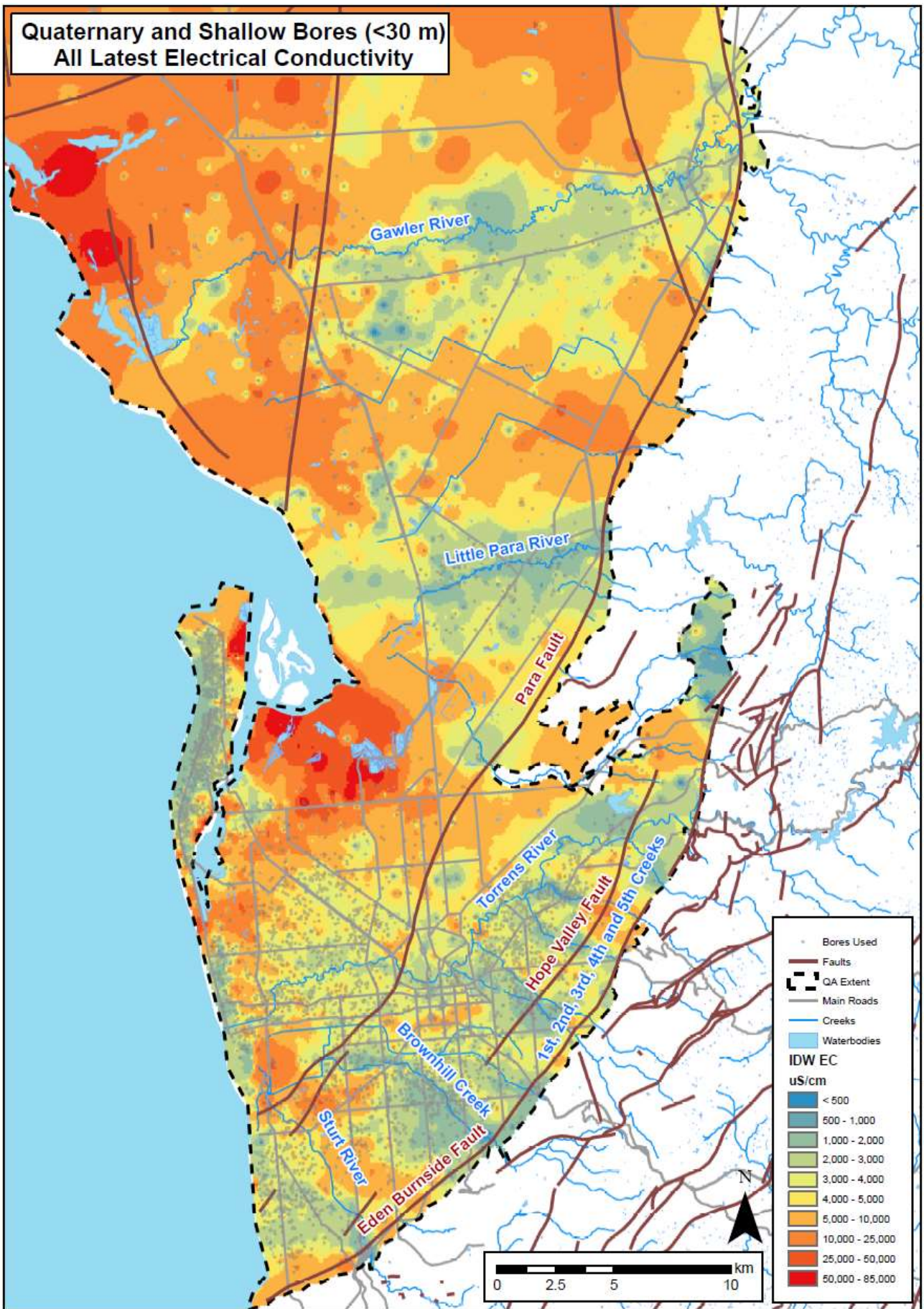
The western draining creeks of the Mount Lofty Ranges flow ephemerally across the Adelaide Plains. However, due to the large downward hydraulic gradients between the creeks and the underlying aquifers after they cross the Eden Burnside fault, they may provide a source of recharge to the Quaternary and potentially Tertiary aquifers. Evidence of this has been previously proposed by Gerges (1999; 2006) and others. The current study has quantified groundwater – surface water exchange rates using longitudinal stream gauging. General conceptual trends of gaining above the fault and losing below the fault suggested in studies such as Gerges (2006), Green *et al.* (2010) and Currie *et al.* (2011) were generally shown to hold true. However the groundwater – surface water exchange was found to be variable both spatially and temporally for all creeks gauged. When adjusted for riparian evapotranspiration, the average loss rates for Brownhill Creek and First through Fifth Creeks ranges from -2 to -6.1 L/s/km during baseflow conditions. This equates to approximately 1319 ML/year of river recharge assuming that these rates occur for 6 months of the year along 3 km of creek length from the Eden Burnside fault to the west. When similar exchange rates are applied to the Sturt, Little Para and Gawler Rivers an additional 3380 ML/y of river recharge is likely to be added to the shallow AP aquifers. Together these ephemeral surface water features add approximately 4700 ML/year to the overall water balance of the Adelaide Plain groundwater resources. It is likely that this represents a conservative value of river recharge because loss rates can be larger during periods of higher creek/river flow. River recharge of this magnitude provides the most plausible explanation for the fresh groundwater seen in the Quaternary aquifers in the vicinity of the creeks and rivers of the Adelaide Plains (see Figure D.1). Inter-aquifer leakage from the Quaternary to the Tertiary aquifers seems plausible given the downward hydraulic gradients between the two and broadly similar salinity in many locations, particularly in the vicinity of surface water features.

## D.2 Introduction

Many of the creeks draining from the Western Mount Lofty Ranges (WMLR) flow for just a few months of the year across the Adelaide Plains (AP) though they may be perennial in their upper reaches in the Western Mount Lofty Ranges. Infiltration from these creeks may recharge the aquifers of the Adelaide Plains. Gerges (1999; 2006) suggested that the distribution of lower salinity groundwater in the Quaternary aquifers was likely a result of creek losses (Apx Figure D.1). However few attempts have been made to quantify these potential exchanges. Green *et al.* (2010) conducted a series of flow measurements on Brownhill Creek and First – Fifth Creeks to determine their hydraulic state (gaining or losing) as they crossed the Eden Burnside fault (referred hereafter as the EB fault or the fault). They found that the creeks were mostly gaining before the fault, and either losing or gaining downstream of the fault. Green *et al.* (2010), estimated that infiltration from Brownhill, First and Fifth creeks contributes approximately 890 ML/year to the shallow aquifers of the AP whilst Second – Fourth creeks were found to be receiving groundwater discharge. Teoh (2006) found loss rates of 1370 ML/year from Brownhill Creek alone and suggested large losses from the Sturt River based on hydrological modelling.

In this chapter we repeat the gauging of Green *et al.* (2010), but measure flow at more locations to better resolve the variation in groundwater – surface water exchange. We primarily use a dilution gauging method that is more accurate for measuring low flow rates in small creeks. We also examine electrical conductivity of the shallow aquifers adjacent to the major creeks, and infer flow directions (i.e. gaining or losing) from the

difference between the surface water stage and the head in the underlying aquifers. This enables a discussion of the likely role of these creeks as a recharge source for the Quaternary and Tertiary aquifers of the AP.



ApX Figure D.1 Electrical conductivity interpolation for the AP Quaternary and shallow aquifers (<30 m).

## D.3 Methodology

### D.3.1 DILUTION GAUGING

Common gauging methods that measure flow velocity in small or shallow turbulent streams, can result in discharge estimates with considerable uncertainty (i.e. > 10%). Dilution gauging is a useful alternative for estimating flow in small streams because the highly variable velocity is not measured. The method is in fact best applied in small rivers where flow is shallow and turbulent and has been applied successfully in many mountain streams (Kilpatrick and Cobb, 1985). Dilution gauging is a mass balance approach whereby a brine (salt solution in water) or dye solution of known concentration is injected into a stream at a known rate using a peristaltic pump or a mariotte container. The injected solution is then allowed to mix over a length of stream. The flow rate can then be calculated when the initial stream concentration and mixed concentration are determined according to:

$$Q = q \cdot \frac{c_b}{c_m - c_0} \quad (1)$$

where  $Q$  = creek discharge (L/s),  $q$  = brine injection rate (L/s),  $C_b$  = brine concentration (mg/L),  $c_m$  = mixed creek concentration (mg/L) and  $c_0$  = the background creek concentration (mg/L).

In this study we have used a brine solution of sodium bromide (NaBr) and analyzed for bromide (Br). Background concentrations were collected at each location and subtracted from the mixed concentration. Samples were sent to the CSIRO Analytical Services Laboratory, Waite Campus and analyzed using Ion Chromatography. A standard brine solution (50 kg of NaBr in approximately 500 L of water) was used for all measurements, and this was subsampled for injection and analysis ( $n = 5$ ) to obtain a more accurate concentration value. The standard deviation of analysis for low concentration and brine samples are < 5% and < 1% respectively.

A peristaltic pump was used for injection, and the flow rate was calibrated before and after each injection period using a graduated cylinder and a stopwatch. The error of injection flow rate is estimated by assuming an error of +/- 1 second over the time taken to fill the graduated cylinder (500 mL). These errors were calculated for each gauging, was outlined in the following section.

On 13/08/2014, a trial gauging was conducted at a number of locations along Brownhill Creek to test the method (Table D.1). This proved successful although errors were initially relatively large due to the use of different brines at different sites and the use of a small graduated cylinder to measure the injection flow rate (100 mL). These errors were reduced for subsequent dilution gaugings.

**Apx Table D.1 Details of trial dilution gauging on Brownhill Creek (13/08/2014) including potential errors.**

LOCATION	$q$ (L/s)	ABSOLUTE ERRORS (L/s)			TOTAL Q	TOTAL Q ERROR %
		$q_{inj}$	$c_m$	$c_b$		
Site 1b	52.8	2.5	0.6	1.4	4.6	8.6
Site 1a	50.7	2.4	0.6	2.3	5.3	10.4
Site 2	67.2	3.2	1.0	1.2	5.4	8.0
Site 3	64.3	3.1	0.8	1.8	5.7	8.8
Site 4	56.1	2.7	0.8	1.0	4.5	8.0

Additional errors may exist due to the dilution of tracer from inflowing hyporheic or groundwater fluxes that occur during the injection period over the mixing length. However these are considered to be negligible due to the relatively short stream reaches and time periods over which the gaugings are conducted (i.e. commonly < 50 metres and < 20 minutes).

Because we are mainly concerned with the groundwater – surface water exchange along the Adelaide Plains, dilution gauging was only conducted at one or two sites above the Eden-Burnside Fault. Where access was possible, electrical conductivity was measured and flow approximated by eye at some upstream sites. These

flow estimates are considered indicative only and are attributed with a 50% error. It is important to note, however, that the sites where flow was visually estimated are all in the upper reaches of the creeks, and so do not effect estimates of loss rate downstream of the fault.

The net exchange rate can be estimated using a simple mass balance equation:

$$\frac{dQ}{dx} = q_{in} - q_{out} - ET \cdot w \quad (2)$$

where  $dQ$  = the difference between upstream and downstream discharge rates ( $m^3/s$ ),  $dx$  = the reach length (m),  $q_{in}$  = the gross groundwater input ( $m^2/s$ ),  $q_{out}$  = the gross creek loss ( $m^2/s$ ),  $ET$  = the approximate evapotranspiration of the riparian vegetation (m/s) and  $w$  = the approximate width of the riparian zone (m).

The net exchange rate is therefore calculated along each stream reach as:

$$Q_{ex} = (q_{in} - q_{out}) = (Q_{us} - Q_{ds})/\Delta x - ET \cdot w \quad (3)$$

where  $Q_{us}$  and  $Q_{ds}$  are the upstream and downstream gaugings, and  $\Delta x$  is the river distance between these locations.

For the purposes of this analysis, the evapotranspiration for the riparian zone was estimated at 4 mm/day over a 20 m wide section of the creek. This equates to approximately 0.9 L/s/km and is considered to be significant when dealing with creek discharge differences on the order of litres per second. The net exchange rates for all values calculated in this study have been adjusted by this amount.

### D.3.2 ENVIRONMENTAL TRACERS

The net exchange rate can also be estimated if environmental tracers are used in combination with creek flow data (after Cook *et al.*, 2006). In the case of electrical conductivity, the mass balance equation can be written:

$$\frac{\partial Qc}{\partial x} = q_{in}c_{in} - q_{out}c + wETc \quad (4)$$

The electrical conductivity of the creek is denoted by  $c$  (uS/cm) while that of the groundwater is  $c_{in}$  (uS/cm) and other terms are defined as above. The terms on the right hand side of equation (4) represent changes in the total mass of creek EC due to groundwater inflow, river loss and evapotranspiration respectively. This equation is solved numerically. The creek was discretised into 10 m sections where the uppermost creek measurements are at  $x = 0$ .

### D.3.3 SPATIAL ANALYSIS

A number of spatial datasets, shapefiles and layer files were created in ESRI ArcGIS v10.1, as part of the analysis in this chapter and are listed below along with a brief description of the procedures used:

- 5) *Data Selection* – Bores representing the Quaternary aquifer were selected from the WaterConnect download as described in **Appendix C: Groundwater Recharge Estimation – Chloride Mass Balance Approach**. Bores in the QA with EC values were selected using a definition query based on aquifer name and additionally, by selecting bores with maximum drilled depths that were  $> 0$  m and  $< 30$  m.
- 6) *Gauging Data* – the location of dilution gauging measurements were collected using a handheld GPS and entered into the spreadsheets relevant for each measurement. These and the gauging results were imported and converted into a shapefile to be appropriately classified based on flow rate.
- 7) *Groundwater – Surface Water Exchange Rates* – Exchange rates were calculated in excel and attributed to the appropriate creek reach. These were classified based on the exchange fluxes into 5 categories for display purposes.

- 8) *EC Interpolation* – Inverse Distance Weighting (IDW) was used to interpolate a spatially representative surface of the electrical conductivity for the QA. A power of 2 and cell size of 100 m was selected while the search radius used 12 points. Other interpolation techniques produced similar surfaces (i.e. Kriging) but did not allow individual values to be as conspicuous (which in this case was desired in order to identify potential outliers visually). This surface was then extracted using a mask of the QA boundary, reclassified appropriately and then saved as a layer file.
- 9) *RWL Interpolation* – Kriging was used to determine the most spatially representative RWL surface for the QA using available data found in the EC dataset. This consisted of 5293 values from a range of dates. It is thought that due to the large spatial coverage and interpolation method used, any seasonal or decadal variation in water level would be essentially averaged and thus all data was used.

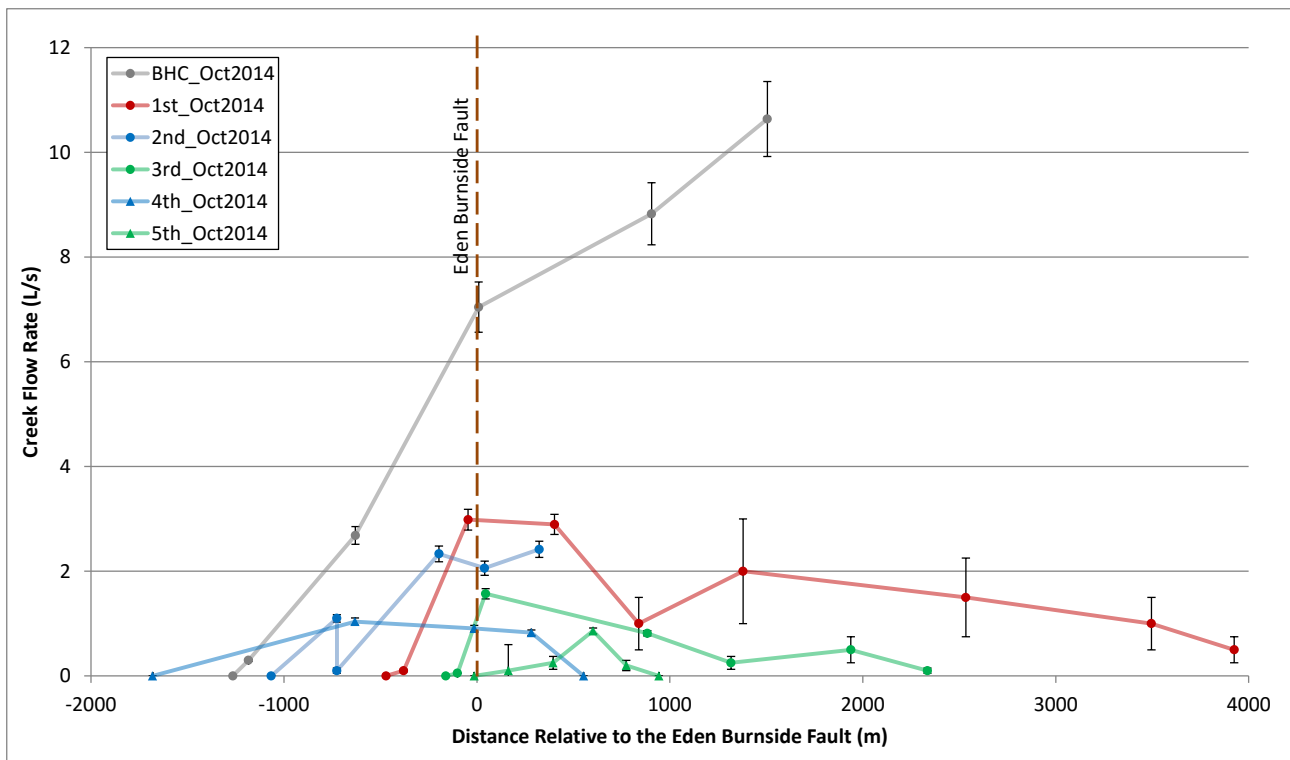
## D.4 Results and Discussion

### D.4.1 CREEK DISCHARGE RATES

Dilution gauging measurements were made on a selection of the western draining creeks along the WMLR as outlined in Table D.2. Brownhill Creek was gauged on three occasions (August 2014, October 2014 and January 2015) while the other creeks were gauged twice (October 2014 and January 2015). The results from October 2014 are considered representative of flow towards the end of the flow period for each creek. The gauging in January 2015 was conducted when the flow rates were declining following a week of high summer rainfall.

In October 2014 Brownhill Creek has decreasing flow both above and below the fault. First and Third creeks have decreasing flow below the EB fault while Second and Fourth creeks have decreasing flow after a short reach of increasing flow. All creeks are dry within 2 km of the fault (Apx Figure D.2). At the time of gauging, Fifth creek had ceased to flow before the fault. These trends below the EB fault are generally similar to those of Green *et al.* (2010), although some differences in interpretation can be explained by the increased spatial resolution of sampling in the current study. In particular, Green *et al.* (2010) showed an apparent increase in flow across the EB fault for Second, Third and Fourth creeks, whereas it is possible in some cases for this to be explained by large gains above the fault and then a small loss below the fault. This is particularly likely for Third Creek, where the upstream location of Green *et al.* (2010) is approximately 714 m above the fault. Second and Fourth creeks also had decreasing flows above of the fault in Green *et al.* (2010) while we found the flow to be increasing in the October 2014 gauging. Conversely, we found that Brownhill Creek flow was decreasing towards the fault in October and January 2014 while it was increasing in August 2014 and at the time of gauging in Green *et al.* (2010). It is apparent that groundwater – surface water exchange in all creeks is temporally variable.

The rates of decreasing flow below the fault appear similar for Brownhill, First, Second and Third Creeks while a slower decline is seen for Fourth and Fifth creeks (Apx Figure D.2). The increase in flow from 0.1 L/s to 1.10 L/s that occurs below the fault in Second Creek was due to tributary inflow.

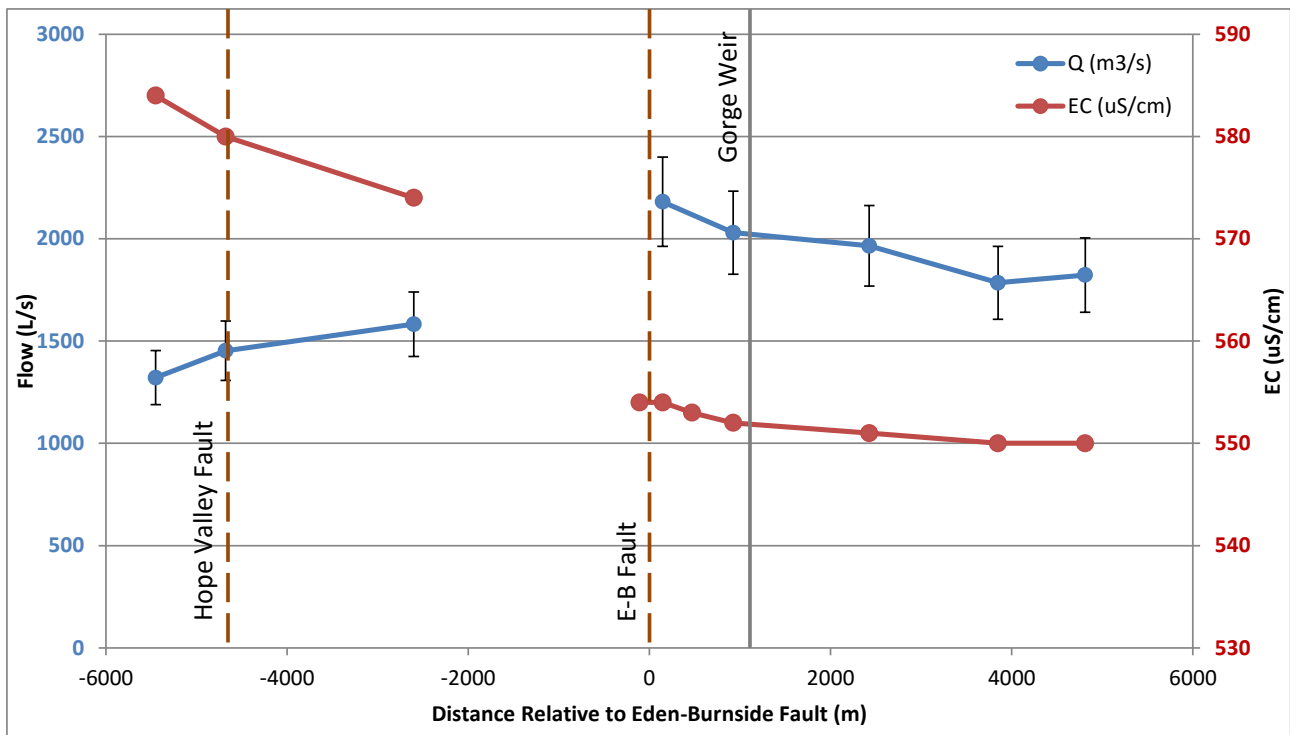


Apx Figure D.2 Longitudinal gauging for selected western draining creeks, October 2014. River flow is from right to left.

Longitudinal gauging of the Torrens River was conducted (using 3 point velocity measurements along river cross sections) during what was hoped to be a day of stable release from Kangaroo Creek Reservoir. However it was later found that the release was increased, as recorded at the Torrens River Gorge Weir (A5040501), from 1671 L/s at 8:40 am to 1899 L/s at 10 am to a new stable rate. The flow measurements for the three most downstream sites were conducted before or during this change in flow while the other measurements collected upstream were measured after the new flow was stable at Gorge Weir. This limits the potential for robust interpretation of the measured flow rates upstream and downstream of the E-B Fault. There appears to be an increase in both flow and EC from upstream towards the fault in the new stable flow period suggesting groundwater discharge is occurring (Apx Figure D.3). However the potential influence of bank storage mobilizing salt or variable flow release from the reservoir meant that we have not attempted to quantify the apparent groundwater – surface water exchange over this upstream reach. Similarly due to the change in flow, the apparent loss rate below the EB and Hope Valley faults cannot be clearly attributed to GW-SW exchange on this occasion.

Apx Table D.2 Dilution and other gauging details.

Creek	Date	Site	Easting	Northing	Q (L/s)	Absolute Errors (L/s)				Total Q	Total Q Error %
						q	c <sub>m</sub>	c <sub>b</sub>			
Brownhill	13/08/2014	1a	281545	6127365	50.7	2.4	0.6	2.3	5.3	10.4	
		1b	281623	6127326	52.8	2.5	0.6	1.4	4.6	8.6	
		3	282855	6126525	67.2	3.2	1.0	1.2	5.4	8.0	
		4	283395	6125890	64.3	3.1	0.8	1.8	5.7	8.8	
		5	283649	6125423	56.1	2.7	0.8	1.0	4.5	8.0	
	30/10/2014	1	282081	6126852	0.30	0.002	0.003	0.014	0.02	6.4	
		2	282425	6126629	2.83	0.016	0.026	0.135	0.18	6.3	
		3	282425	6126629	2.68	0.015	0.024	0.128	0.17	6.3	
		4	282934	6126498	8.25	0.092	0.075	0.396	0.56	6.8	
		5	282934	6126498	7.04	0.079	0.064	0.338	0.48	6.8	
		6	283407	6125865	8.83	0.088	0.080	0.425	0.59	6.7	
		7	283664	6125427	10.64	0.109	0.096	0.513	0.72	6.7	
	15/01/2015	1	283409	6125857	8.00	0.174	0.385	0.072	0.63	7.9	
		2	283659	6125429	8.23	0.082	0.397	0.074	0.55	6.7	
	First	30/10/2014	1	286084	6131308	0.1				0.01	11
2			286295	6131069	2.98	0.028	0.027	0.143	0.20	6.6	
3			286601	6130786	2.89	0.027	0.026	0.138	0.19	6.6	
4			287251	6130062	2				1	50	
5			288059	6128311	1				0.5	50	
6			288200	6127925	0.5				0.25	50	
7			287694	6129140	1.5				0.75	50	
8			286872	6130450	1				0.5	50	
9			286524	6130942	0.5				0.25	50	
16/01/2015		1	286296	6131086	2	0.017	0.072	0.014	0.10	6.8	
		2	286763	6130572	2.8	0.030	0.132	0.025	0.19	6.8	
Second		29/10/2014	1	286356	6132007	1.10	0.009	0.010	0.053	0.07	6.5
			2	286356	6132007	0.1				0.05	50
			3	286812	6131836	2.33	0.019	0.021	0.111	0.15	6.5
			4	287038	6131772	2.06	0.019	0.019	0.098	0.14	6.6
	5		287184	6131539	2.42	0.018	0.022	0.116	0.16	6.4	
	16/01/2015	1	286354	6132006	0.83				0.08	10	
		2	287043	6131768	2.68	0.029	0.128	0.024	0.18	6.8	
	Third	29/10/2014	3	287231	6131497	3.38	0.037	0.162	0.031	0.23	6.8
			1	288374	6134225	1.57	0.011	0.014	0.075	0.10	6.4
			2	289165	6134012	0.82	0.006	0.007	0.039	0.05	6.4
3			289712	6133159	0.5				0.25	50	
4			289652	6132778	0.1				0.05	50	
5			289431	6133678	0.25				0.13	50	
16/01/2015		6	288244	6134275	0.05	0.000	0.000	0.002	0.00	6.2	
		1	288366	6134224	0.40	0.004	0.019	0.004	0.03	6.8	
Fourth		29/10/2014	1	288062	6136621	0.25				0.13	50
			2	288359	6136441	0.25				0.13	50
	3		288665	6136263	1.04	0.010	0.009	0.049	0.07	6.7	
	4		289161	6135955	0.91	0.007	0.008	0.043	0.06	6.4	
	5		289445	6135873	0.83	0.006	0.007	0.039	0.05	6.4	
	16/01/2015	1	289446	6135866	2.90	0.028	0.139	0.026	0.19	6.7	
		2	290118	6135314	5.75	0.060	0.289	0.065	0.41	7.2	
Fifth	31/10/2014	1	289842	6137960	0.1				0.05	50	
		2	290262	6137305	0.1				0.05	50	
		3	290448	6137157	0.25				0.13	50	
		4	290587	6137036	0.86	0.008	0.008	0.041	0.06	6.6	
		5	290739	6137033	0.2				0.1	50	



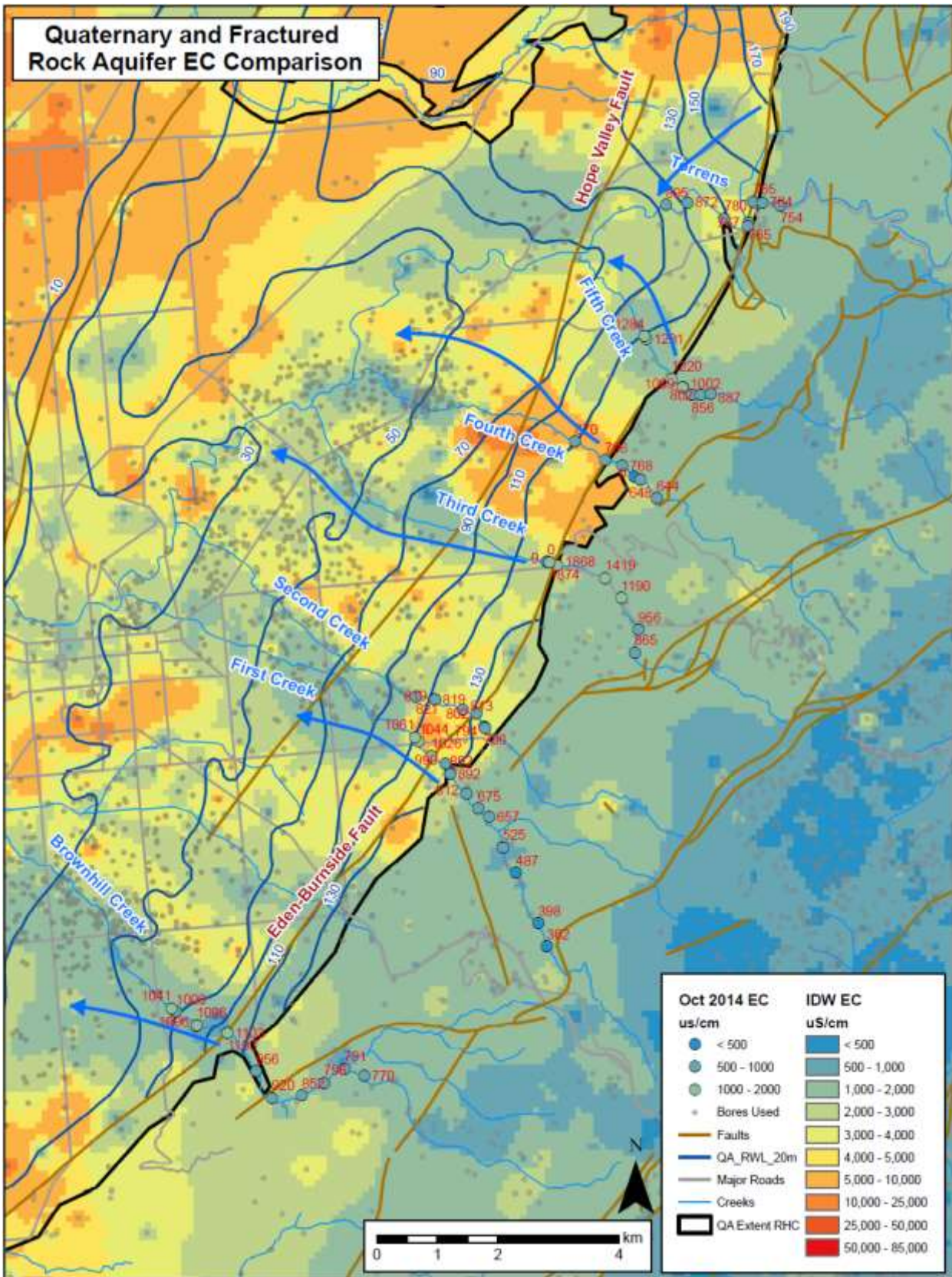
Apx Figure D.3 Longitudinal gauging for the Torrens River, December 2014. River flow is from right to left and EC measurements are shown in red while flow measurements are shown in blue.

#### D.4.2 CREEK AND GROUNDWATER ELECTRICAL CONDUCTIVITY

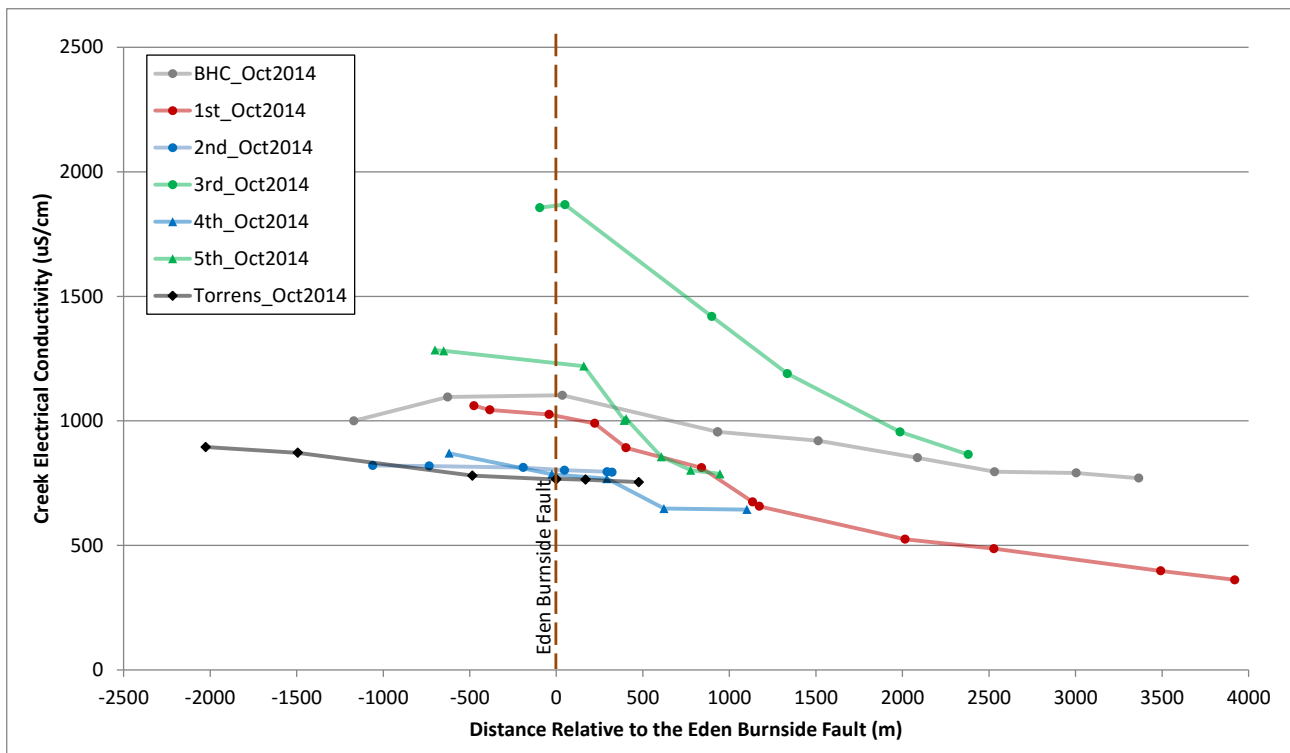
The groundwater electrical conductivity (EC) of the Quaternary Aquifer can also be used as supporting evidence of creek infiltration or groundwater discharge (Apx Figure D.4). This map (in addition to Apx Figure D.1) was constructed using all available EC data from a WaterConnect database selection as further discussed in Appendix C. Groundwater of lower EC is clearly associated with the drainage lines of the western draining creeks. These areas of lower EC tend to extend to the west and southwest of the drainage lines and may indicate the direction of groundwater flow. The creek EC during the October 2014 and January 2015 gauging events are similar to the lowest groundwater EC in the vicinity of each creek. This is further evidence that some volume of water is infiltrating from these creeks as recharge to the QA.

EC data collected in the creeks in October 2014 shows that the EC increases downstream towards the E-B Fault (Apx Figure D.5, see also Apx Figure D.12 for January 2015 data in Section D.6 Additional Information). These trends are similar to those found in creek EC surveys done by Currie *et al.* (2011) in late March 2011. The increases in creek EC likely represent groundwater discharge to the creek along the upstream reach.

Since flow data was not collected in sufficient detail upstream of the EB fault for most creeks, a more detailed analysis to constrain both  $ET$  and the  $Q_{ex}$  is not possible (with the exception of First Creek and Brownhill Creek – see later discussion). It should also be noted that the EC increases more slowly after the EB Fault, suggesting a decrease or absence of groundwater discharge. The slight rise in EC downstream seen in some creeks may be due to evapotranspiration. In contrast, the EC of the Torrens River appears to increase after 500 m downstream of the Fault, suggesting groundwater discharge is occurring in October 2015. The EC of Brownhill and Second Creeks in October 2014 and Jan 2015, respectively, appear to decrease after the fault which may be due to a freshening from garden/urban runoff or irrigation that flows to the creeks. The general trend of slowly increasing EC downstream of the EB fault (compared to more rapid increase upstream of the Fault) generally agrees with the findings of Currie *et al.* (2011).



Apx Figure D.4 Quaternary and Fractured Rock aquifer EC, Quaternary aquifer RWL and inferred groundwater flow direction.



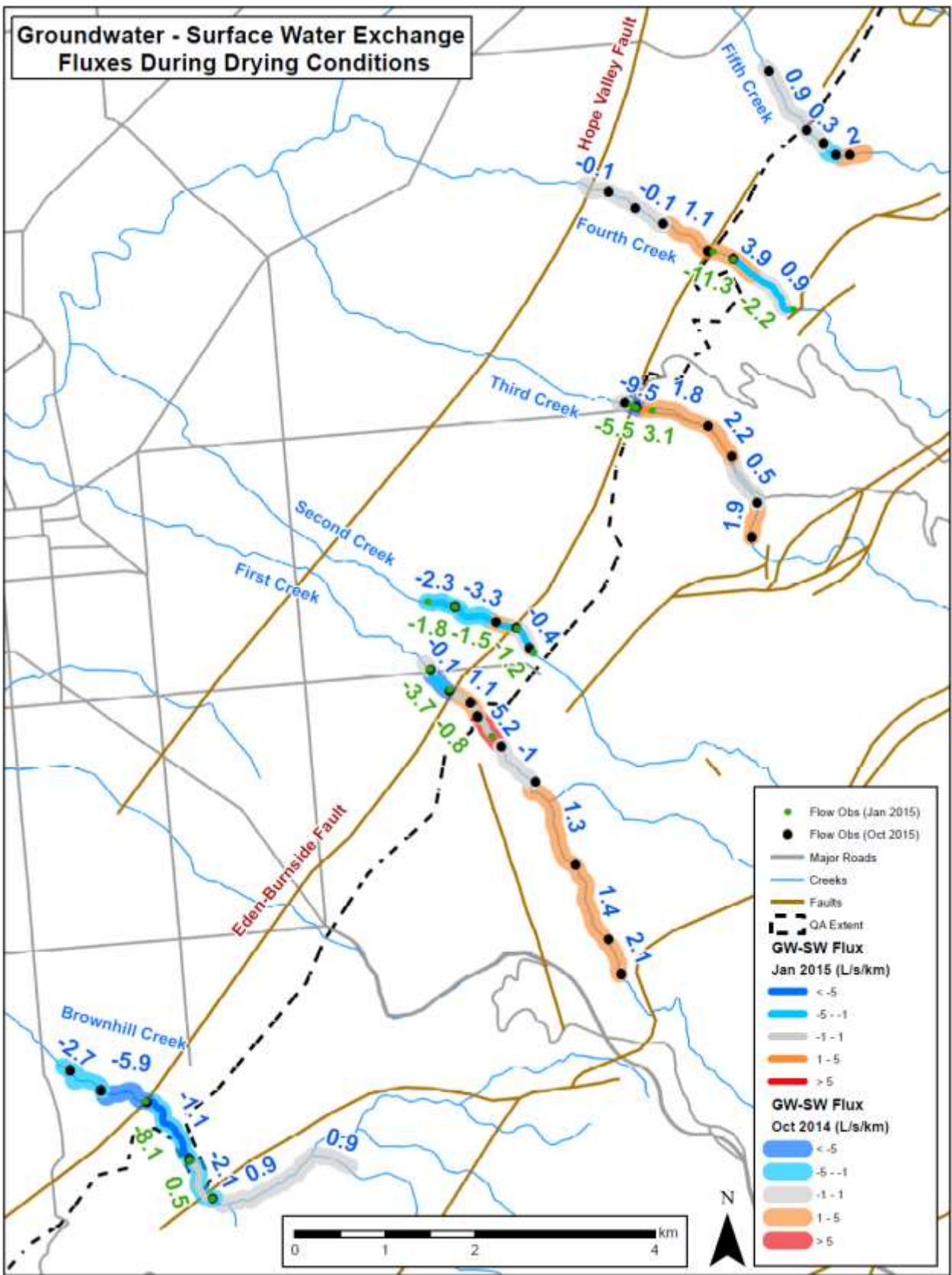
Apx Figure D.5 creek electrical conductivity relative to the Eden Burnside fault, October 2014. River flow is from right to left.

### D.4.3 QUANTIFYING GROUNDWATER – SURFACE WATER EXCHANGE

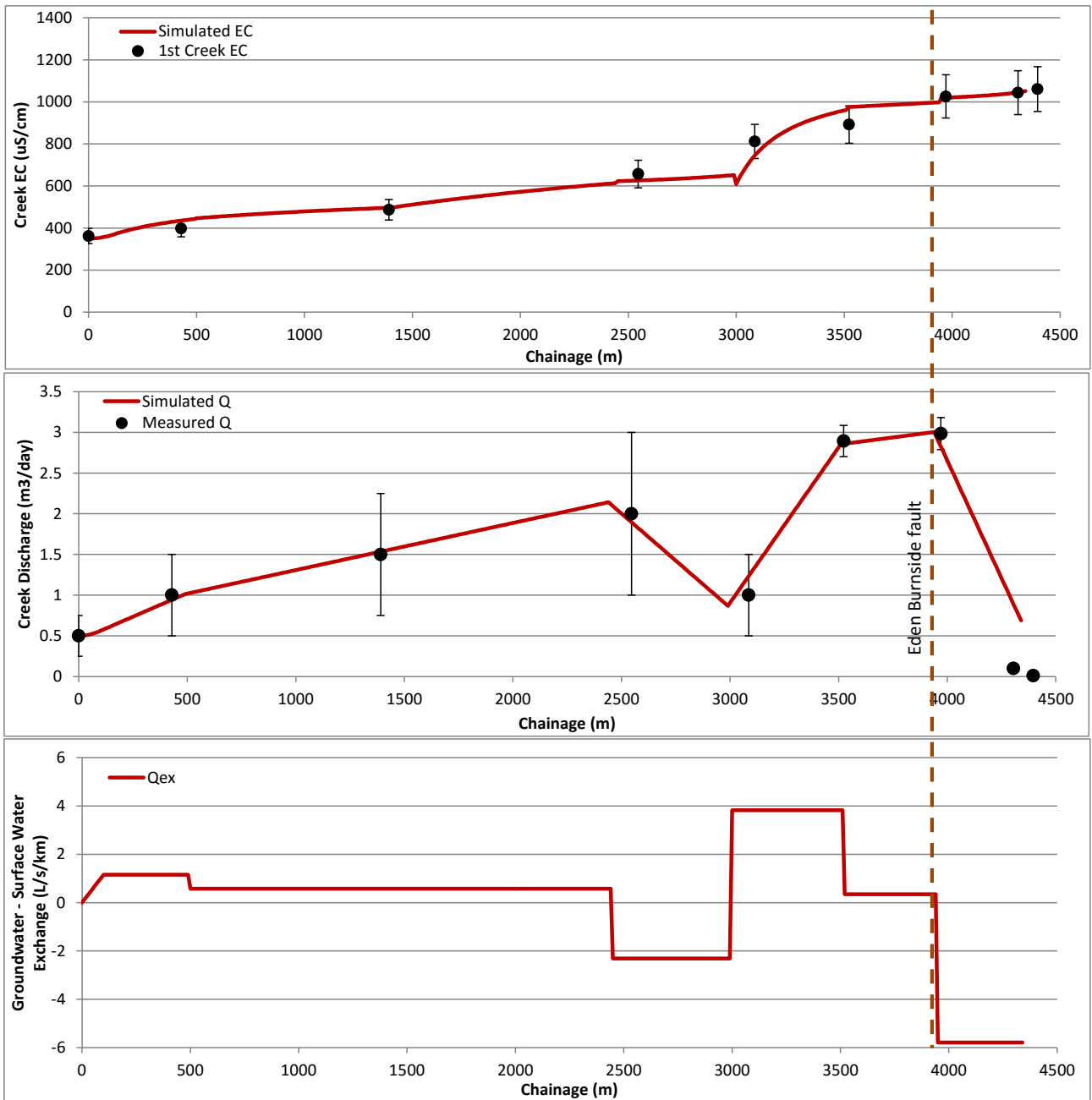
#### (I) SPATIAL VARIABILITY

Simple estimates of groundwater – surface water exchange have been made for each of the creeks where flow gauging was conducted using equation (3). The exchange fluxes have been categorised into two losing, two gaining and a neutral condition as shown in Apx Figure D.6. Generally, the creeks are gaining above the Eden Burnside Fault and losing below the Fault. However, when riparian evapotranspiration is also considered, some reaches appear as gaining or neutral despite flow decreasing downstream. This occurs in the lower reaches of Third, Fourth and Fifth Creeks.

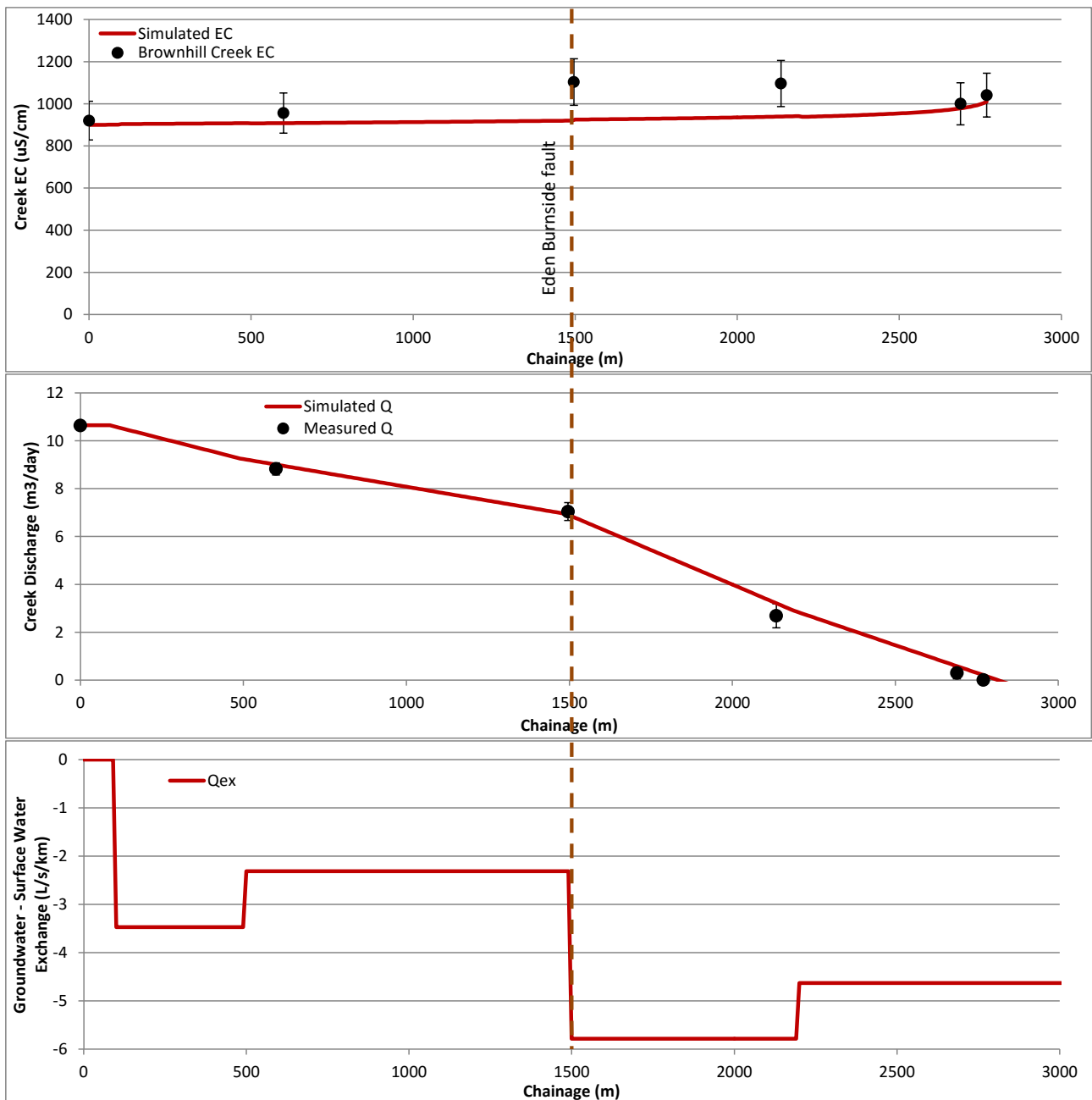
Where creek discharge and EC are measured it is possible to apply the simple numerical model presented by Cook *et al.* (2006) to better constrain the exchange fluxes. The results of the longitudinal groundwater – surface water exchange flux and model fits are shown in Apx Figure D.7 and D.8 for First Creek and Brownhill Creek respectively. These estimates of GW-SW exchange should have a lower degree of uncertainty than the results found using equation (3) in isolation because these are constrained by the EC of the creek as well as creek flow rate. However, the groundwater EC adjacent to the creeks is not well characterised and is likely to be spatially variable (i.e. see Apx Figure D.4). We have loosely based the values on available data from WaterConnect but some manual adjustments were made in order to better fit the simulated values with the measured EC and Q values. The resulting exchange fluxes are very similar to those determined using equation (3).



Apx Figure D.6 Groundwater – surface water exchange rates (L/s/km) in October 2014 and January 2015. Numerals represent measured exchange rates (positive in gain and negative is loss), and their relative magnitudes are also indicated by colours of the creek reaches.



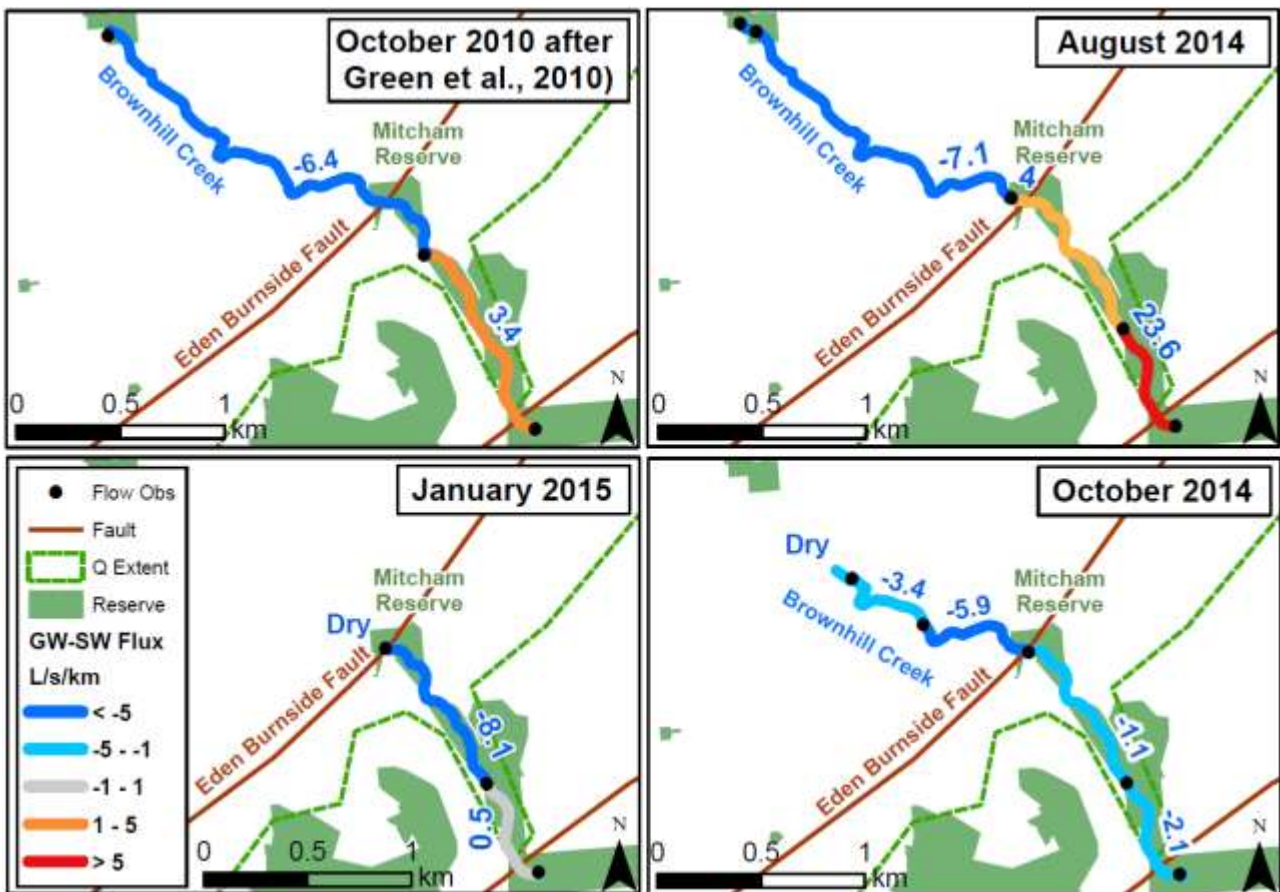
Apx Figure D.7 First Creek mass balance for October 2014 gauging (after Cook *et al.*, 2006).



Apx Figure D.8 Brownhill Creek mass balance for October 2014 gauging (after Cook *et al.*, 2006).

## (II) TEMPORAL VARIABILITY

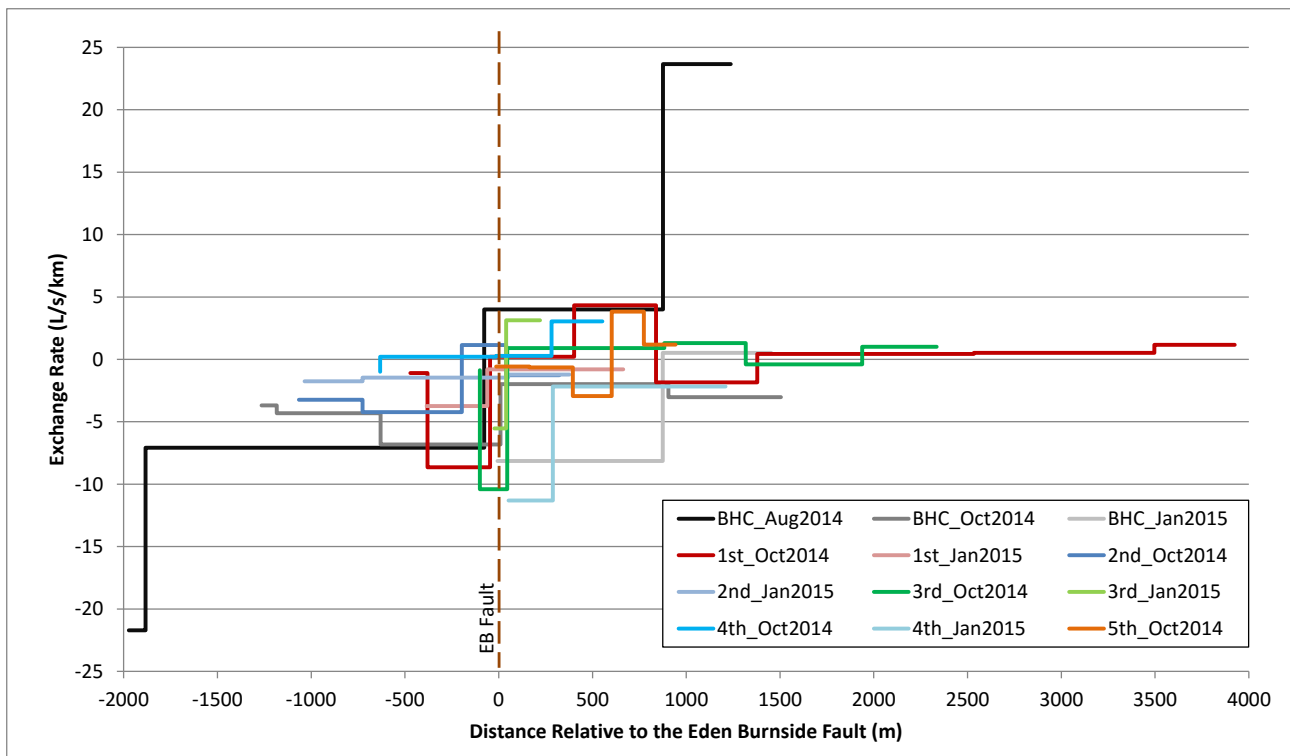
To identify any temporal trends of groundwater – surface water exchange along Brownhill Creek, we have also included the data from Green *et al.* (2010). Apx Figure D.9 shows the groundwater – surface water exchange rates (corrected for ET) for the longitudinal gauging that occurred in January 2015, October 2014, August 2014 and October 2010. The loss rate in Brownhill Creek below the fault appears to occur at a relatively consistent rate between -3.4 and -7.1 L/s/km for all gauging events. The gaining section seen in the October 2010 and August 2014 above the fault was shown to be a losing reach during the October 2014 and January 2015 gauging events. This suggests that as the creek discharge decreases towards the summer months, that the state of connection changes from gaining to losing above the fault.



Apx Figure D.9 Groundwater – surface water exchange for Brownhill creek at four gauging times. Numerals represent measured exchange rates (positive in gain and negative is loss), and their relative magnitudes are also indicated by colours of the creek reaches.

The exchange condition of other creeks is also likely to be seasonally variable as indicated by the minor differences between October 2014 and January 2015 gauging events (Apx Figure D.6 and Apx Figure D.10). Losing conditions are seen consistently below the EB fault at varying rates while there are variably gaining and losing conditions in the vicinity of and above the fault. The spatial and temporal variability between October 2014 and January 2015 pairs can be seen for First – Fourth Creeks and between the three latest gauging events for Brownhill Creek (Apx Figure D.10).

These exchange patterns are considered representative of baseflow conditions close to the time when flow ceases across the AP. It is possible that when flow rates are higher in the winter months, the loss rates could be greater than during baseflow conditions (Cranswick and Cook, 2015). Multiple gauging events during different types of flow conditions would help to better characterize this temporal variability and further establish any spatially consistent trends.



Apx Figure D.10 Groundwater – surface water exchange rates for all creeks relative to the EB fault. River flow is from right to left.

#### D.4.4 HYDRAULIC STATE OF GROUNDWATER – SURFACE WATER INTERACTION

The interaction between surface water and groundwater can also be assessed by comparing river stage with groundwater levels. Currie *et al.* (2011) used a digital elevation model to calculate river stage, and compared inferred creek elevations with nearby observation bore water levels, and found that the creeks of the AP are likely to be losing downstream of the E-B Fault. The potential error in the creek bed elevation (i.e. how incised the creek is compared to the land surface) however makes this conclusion indicative only (Currie *et al.*, 2011).

To confirm this generalisation, a number of comparisons between the hydrographs of state observation wells and creek hydrographs (or approximate creek bed elevations) are also made in section D.6 Additional Information. These comparisons show that there are large downward hydraulic gradients of generally greater than 10 m, between the creek level and underlying aquifers (with the exception of the Torrens River as it flows across the fault). This hydraulic condition is also seen for the Little Para and Gawler Rivers across the North Adelaide Plain where similarly large differences exist between the rivers and underlying aquifers. These hydrograph comparisons and water level differences are summarised in a series of figures and Table D.4 found in section D.6 Additional Information.

#### D.4.5 RECHARGE VIA CREEK INFILTRATION

Given the continuous downward hydraulic gradients and therefore losing conditions found adjacent to the EB fault (and both the Para and Alma faults in the North Adelaide Plains), the total annual volume of creek recharge can be calculated from the duration of flow for each creek, the length of creek over which that loss occurs and by assuming that the rates of exchange are relatively consistent temporally and spatially across the hills zone of the AP. If we assume that First – Fifth and Brownhill Creeks flow on average for 6 months of the year, across 3 km of the AP, this equates to 1319 ML/year (see Table D.3). For equivalent creeks this recharge value is similar to the 890 ML/year estimated by Green *et al.* (2010) from Brownhill

Creek, First Creek and Fifth Creek. Meanwhile an estimate of 1370 ML/year was made by Teoh (2006) for Brownhill Creek alone between the Scotch College and Keswick gauging stations. This equates to a loss rate of -6.1 L/s/km over the approximate 9.5 km reach between these gauges, and is similar to the mean exchange flux determined in this study and in Green *et al.* (2010) (Table D.3). The approximations of total reach length and flow duration make the comparisons between studies indicative only, however the mean rates of exchange for Brownhill Creek downstream of the fault appear consistent.

**Apx Table D.3 Mean  $Q_{ex}$  and creek Loss below or near the E-B Fault.**

Creek	Mean $Q_{ex}$ (L/s/km) <sup>1</sup>	Mean $Q_{ex}$ (L/s/km) <sup>2</sup>	Mean $Q_{ex}$ (L/s/km) <sup>3</sup>	Mean $Q_{ex}$ (L/s/km) <sup>4</sup>	Recharge (ML/y) <sup>*1</sup>	Recharge (ML/y) <sup>**3</sup>	Recharge (ML/y) <sup>***4</sup>
Brownhill	-6.1	-5.2	-6.4	-6.1	-290	-500	1370
First	-5.7	-5.8	-6.5	-	-271	-300	-
Second	-2.0	-	5.7	-	-95	-	-
Third	-7.5	-	1.9	-	-355	-	-
Fourth	-4.5	-	11.7	-	-213	-	-
Fifth	-2.0	-	-0.9	-	-95	-90	-

<sup>1</sup> Estimates of Mean  $Q_{ex}$  made using equation 3.

<sup>2</sup> Estimates of Mean  $Q_{ex}$  made using equation 4.

<sup>3</sup> after Green *et al.* (2010).

<sup>4</sup> after Teoh (2006).

\* Recharge calculations assume 6 months of flow along a 3 km reach onto the AP.

\*\* Recharge calculation assumes 365 days of flow along the reach downstream of the fault.

\*\*\* Recharge calculation assumes 8 months of flow and reach distances between Scotch College and Keswick gauges (~9.5 km).

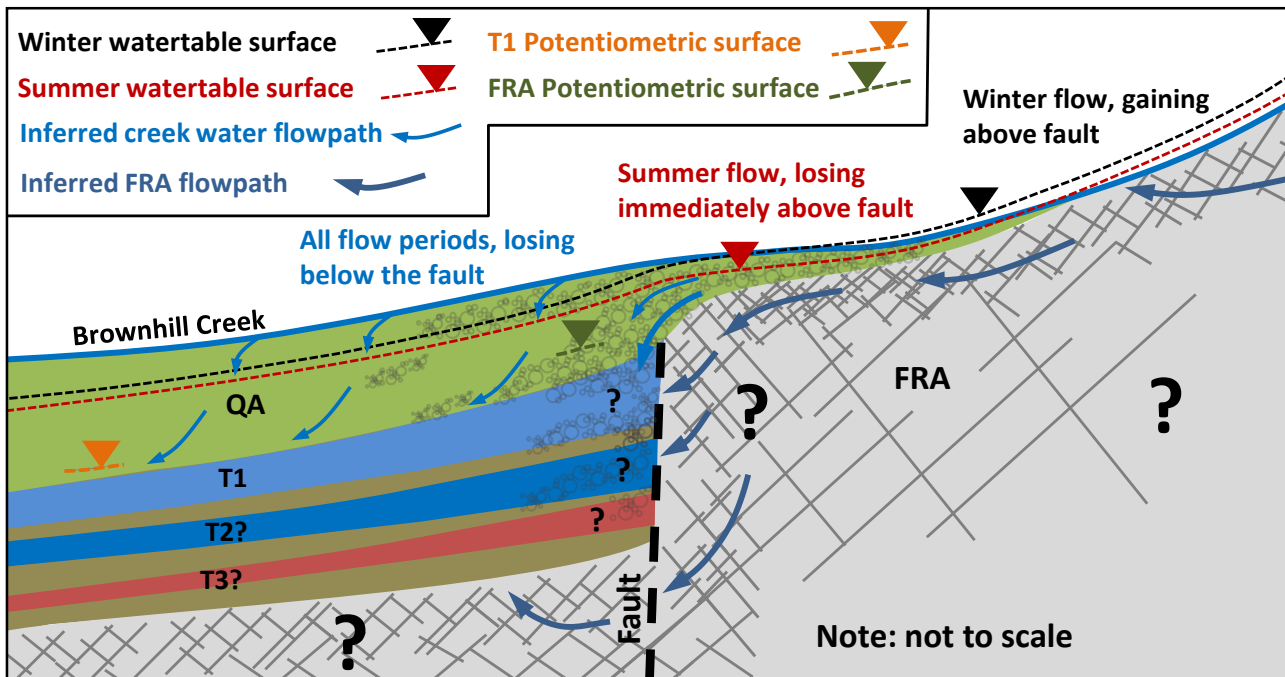
If the average exchange rate for Brownhill creek below the EB fault (-6.1 L/s/km) was applied to the Sturt, Little Para and Gawler rivers for 6 months of flow duration and 5, 10 and 20 km of river reach, this would result in river recharge of 483, 966 and 1932 ML/y respectively. This upscaling approach contains a high degree of uncertainty since no longitudinal gauging was conducted in this study. Nevertheless the hydraulic state (i.e. groundwater levels well below the riverbed elevation) and similar sediment types allow us to reasonably assume that the exchange rates may be similar. Furthermore, because the flow in these rivers is generally higher than that of Brownhill Creek, even higher loss rates are considered likely (Cranswick and Cook, 2015). Hence the sum of loss for all creeks and rivers mentioned above is approximately 4700 ML/year and represents a conservative estimate of river recharge to the AP. Recharge of this magnitude is strongly supported by the low salinity of shallow groundwater seen in the vicinity of creeks and rivers and the large downward hydraulic gradients adjacent to the hills face zone.

## D.5 Conceptual Model

The river-aquifer exchange along Brownhill Creek has been investigated in the most detail within this study and a conceptual model has been developed based on this work (in addition to the hydrographs presented in section D.6). During winter flow periods, the creek is thought to be gaining in its upper reaches and losing as it flows onto the Adelaide Plains (Apx Figure D.11). Meanwhile, as flow declines into the summer months, the state of connection is seen to change immediately above the EB fault to losing conditions. Regional groundwater discharge from the FRA in the hills still flows towards the bottom of the valley but the waterlevel surface is no longer above the creek bed elevation. Hence any creek flow gained from upstream reaches becomes losing towards the EB fault during this flow period (Apx Figure D.11). This could be caused by an

increase in the transmissivity of the alluvial sediments though a combination of the deposition of coarse grained sediments and an increase in their thickness.

Groundwater throughflow derived from the FRAs could occur across the EB fault via these coarser grained alluvial sediments which are thought to extend laterally and perhaps vertically onto the Adelaide Plains. Hence the recharge mechanisms to the AP aquifers may be a combination of creek loss as it flows across the plains, in addition to throughflow occurring preferentially through the coarser alluvial sediments deposited in the vicinity of the downthrow side of the EB fault (Apx Figure D.11). The fate of this shallow groundwater is not well understood but it could contribute to the recharge of deeper T1 and T2 aquifers (see further discussion in Appendix L).



Apx Figure D.11 An alternative conceptual model of groundwater flow and groundwater – surface water exchange in the vicinity of Brownhill Creek.

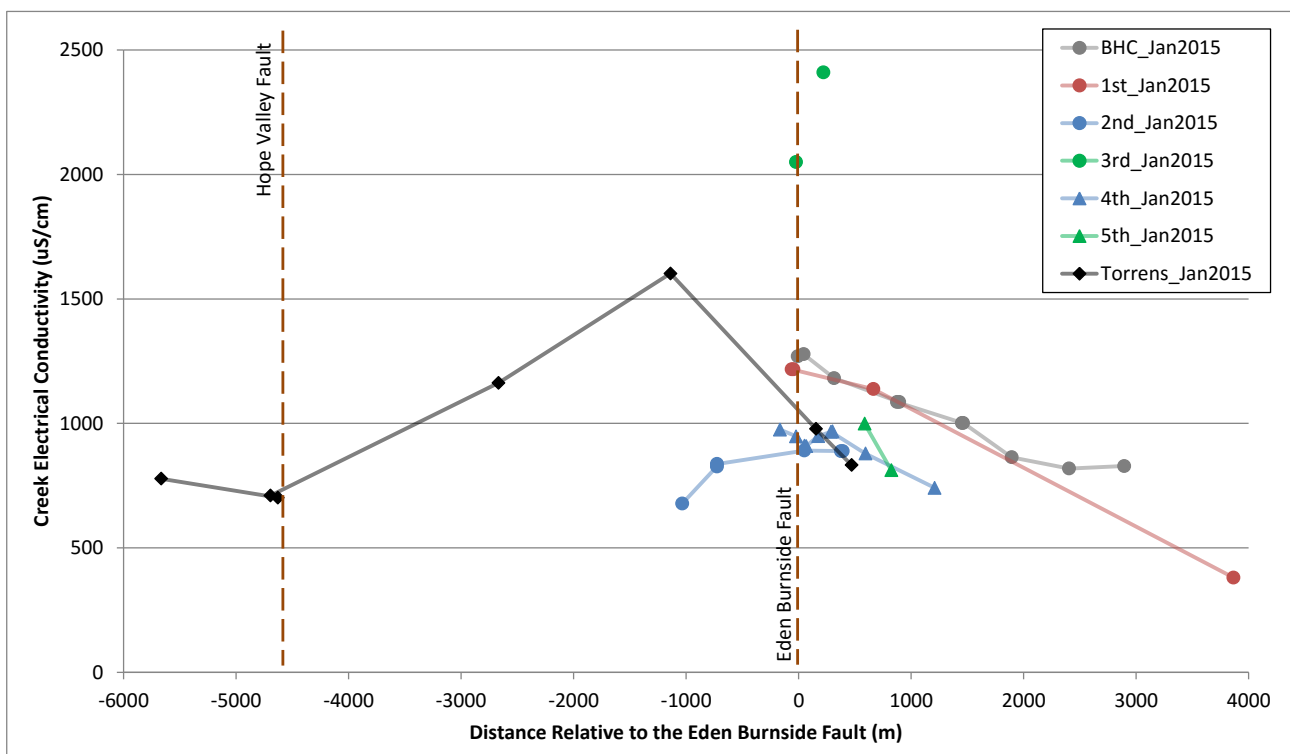
## D.6 Conclusions

The current study has quantified the groundwater – surface water exchange rates using a longitudinal gauging approach. In general, creeks are gaining above the fault and losing below the fault, as previously suggested by Gerges (2006), Green *et al.* (2010) and Currie *et al.* (2011). When adjusted for riparian evapotranspiration, the average loss rates for Brownhill Creek and First – Fifth Creeks ranges from -2 to -6.1 L/s/km during baseflow conditions. This equates to approximately 1319 ML/year of river recharge assuming that these rates occur for 6 months of the year along 3 km of creek length from the Eden Burnside fault to the west. When similar exchange rates are applied to the Sturt, Little Para and Gawler Rivers, an additional 3380 ML/y of river recharge is conservatively estimated. Together these ephemeral surface water features add approximately 4700 ML/year to the overall water balance of the Adelaide Plain groundwater resources. River recharge of this magnitude provides the most plausible explanation for the fresh groundwater seen in the Quaternary aquifers in the vicinity of the creeks and rivers of the AP (see Apx Figure D.1).

## D.8 Additional Information

The following figures and tables act as additional supporting information to the discussion of previous sections. These are not described in detail but indicate the general trends of downward hydraulic gradients from surface water features to the underlying aquifers. Inter-aquifer vertical gradients can also be seen by comparing the hydrographs of the Quaternary, Tertiary and Fractured Rock aquifers. Across the central AP there appears to be very large downward gradients between the Quaternary aquifer and the underlying Tertiary and Fracture Rock aquifers, suggesting that the Quaternary may be a perched aquifer (i.e. at least in the vicinity of Brownhill, First, Fourth and Fifth creeks where hydrograph comparisons were made (see Table D.4).

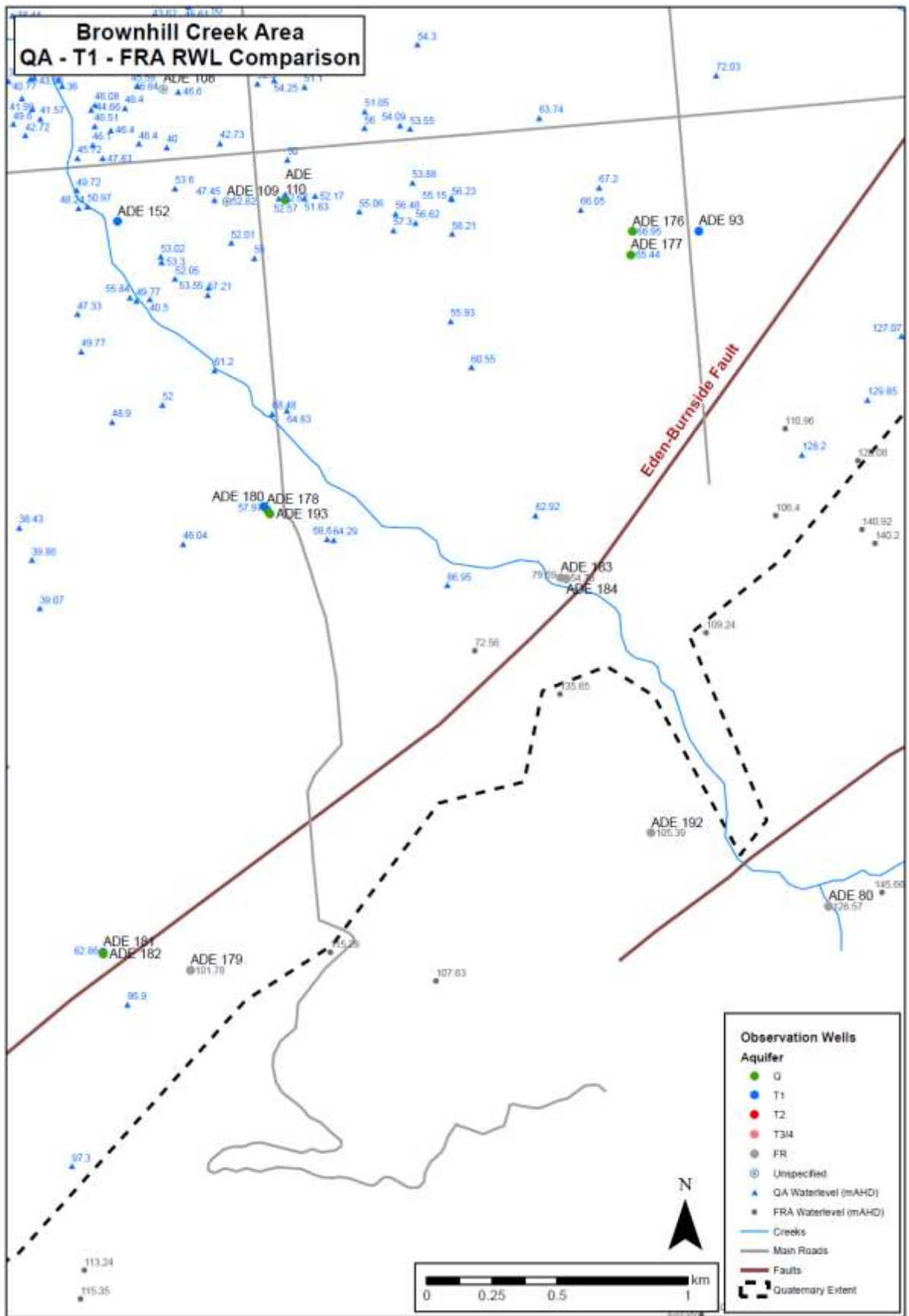
Downward hydraulic gradients were generally seen between vertically separated sedimentary aquifers (Quaternary and Tertiary) across the Adelaide Plains. Meanwhile, upward hydraulic gradients were apparent within the Fractured Rock aquifer near Brownhill creek and between the FRA and T1 between Fourth and Fifth creeks (Apx Figure D.14, Apx Figure D.20 and Apx Figure D.21 respectively). This implies that there is at least the potential for upward vertical recharge to occur from the FRA in addition to the lateral recharge most commonly assumed (see further discussion in Appendices E and I).



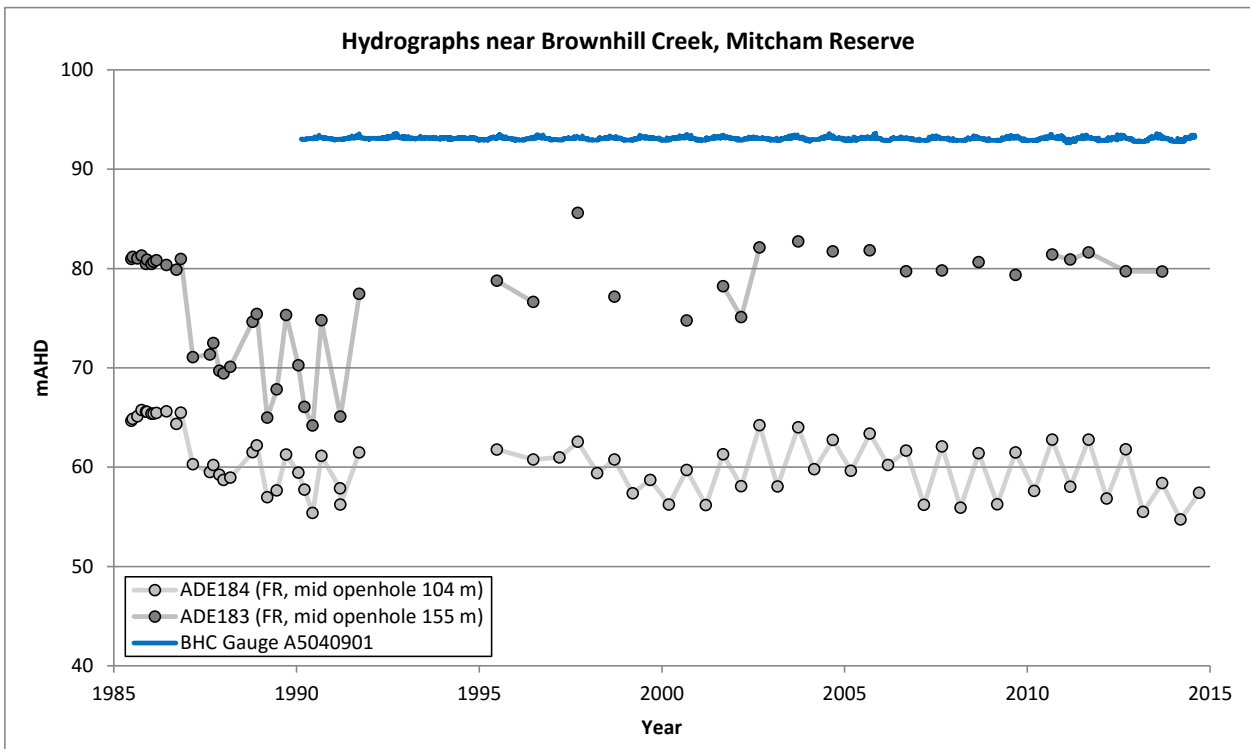
Apx Figure D.12 creek electrical conductivity relative to the Eden Burnside fault, January 2015. River flow is from right to left.

**Apx Table D.4 Summary of flow direction and approximate head difference between from creeks/ivers to aquifers, positive values indicates downward while negative values indicates upward difference. Note that the ranges of head difference values.**

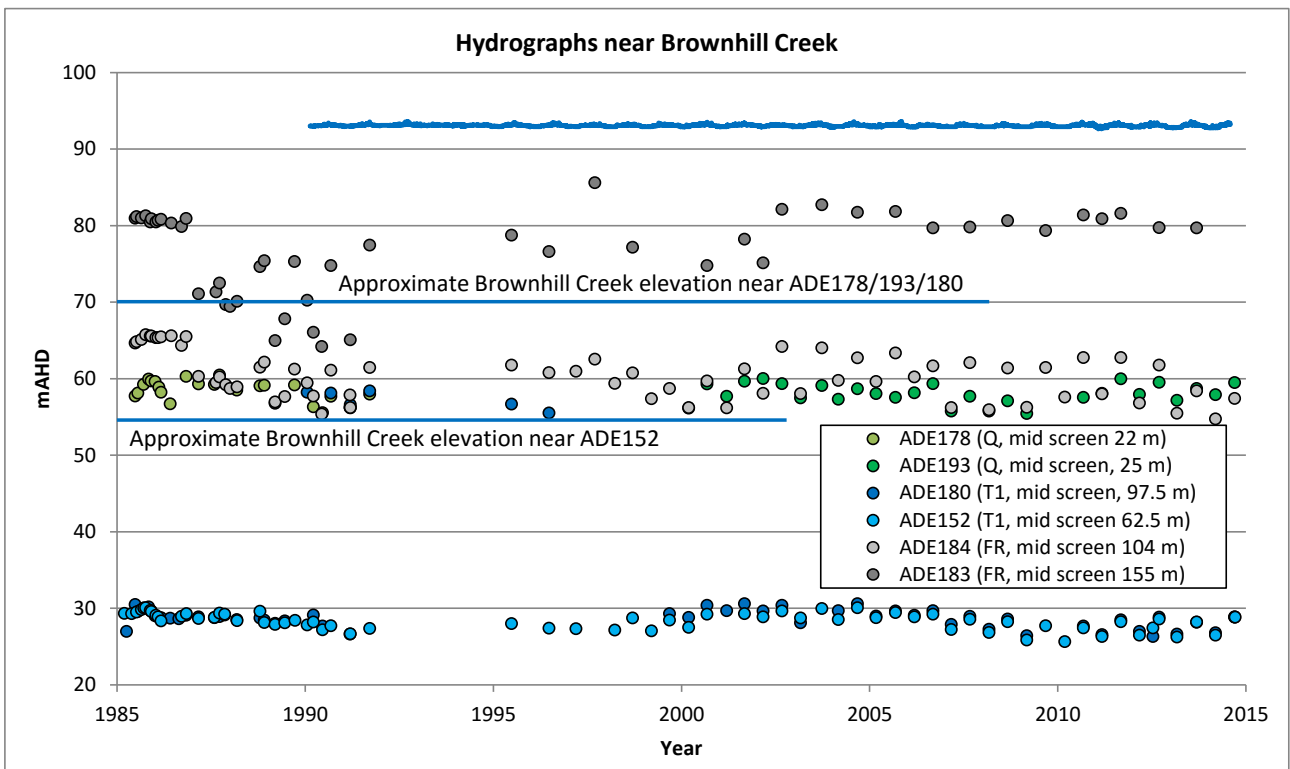
Creek/River	Direction of gradient to nearest aquifer	Approximate head difference (m)	
		Near the fault (to aquifer)	Away from the fault (to aquifer)
Brownhill	Down	30 (FRA)	25 (T1), 40 (T1)
First	Down	5 to 10 (Q)	1 to 5 (Q), 55 (T1)
Second	Down	5 to 10 (Q)	5 to 10 (Q)
Third	Down	10 (Q)	
Fourth	Down	10 (Q)	
Fifth	Down	5 (Q), 55 (FRA)	10 (Q), 50 (FRA)
Sturt	Down	10 (Q)	
Torrens	Across	>-30 (Q)	-5 (FRA), -10 (Q)
Little Para	Down	15 (Q1), 20 (Q2), 40 (Q3/T1/T2)	25 (Q4/T2), 10 (Q3) 15 (Q4/T1)
Gawler	Down	5 to 10 (Q), 10 (T2)	5 to 15 (Q) 5 to 25 (T2), 5 to 20 (Q), 5(Q) 20 to 50 (T2)



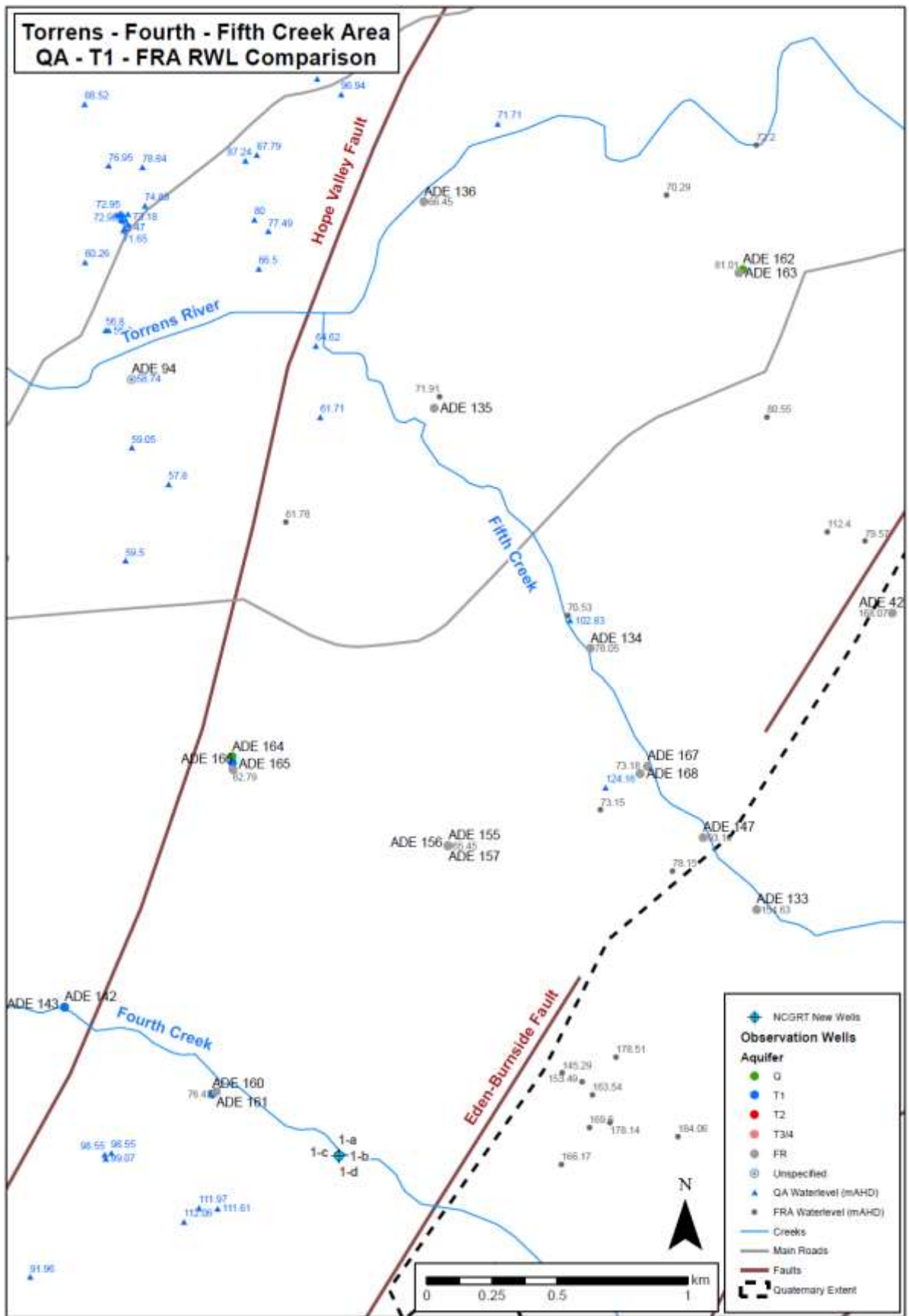
Apx Figure D.13 Reference map for Brownhill Creek hydrograph comparisons. Blue numerals indicate hydraulic heads (m AHD) in the shallow Quaternary aquifer while grey numerals are hydraulic heads in the fractured rock aquifer.



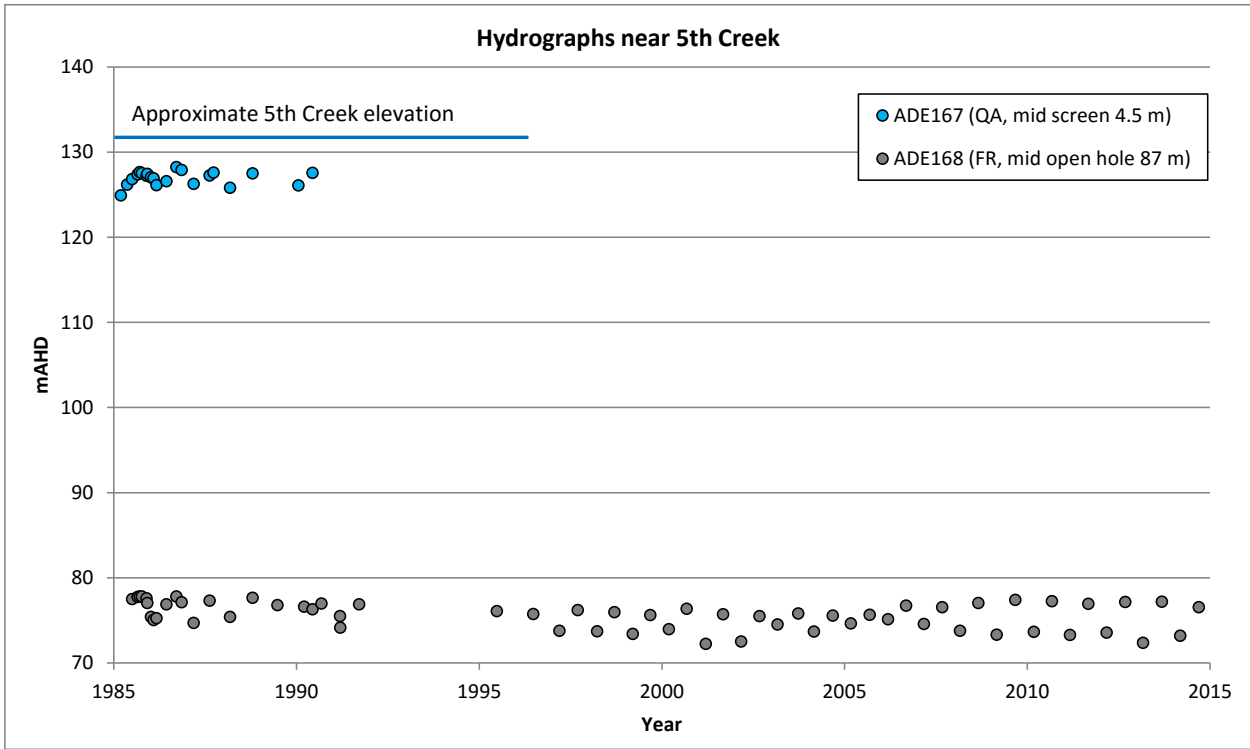
Apx Figure D.14 Hydrograph comparisons between Brownhill creek and the FRA.



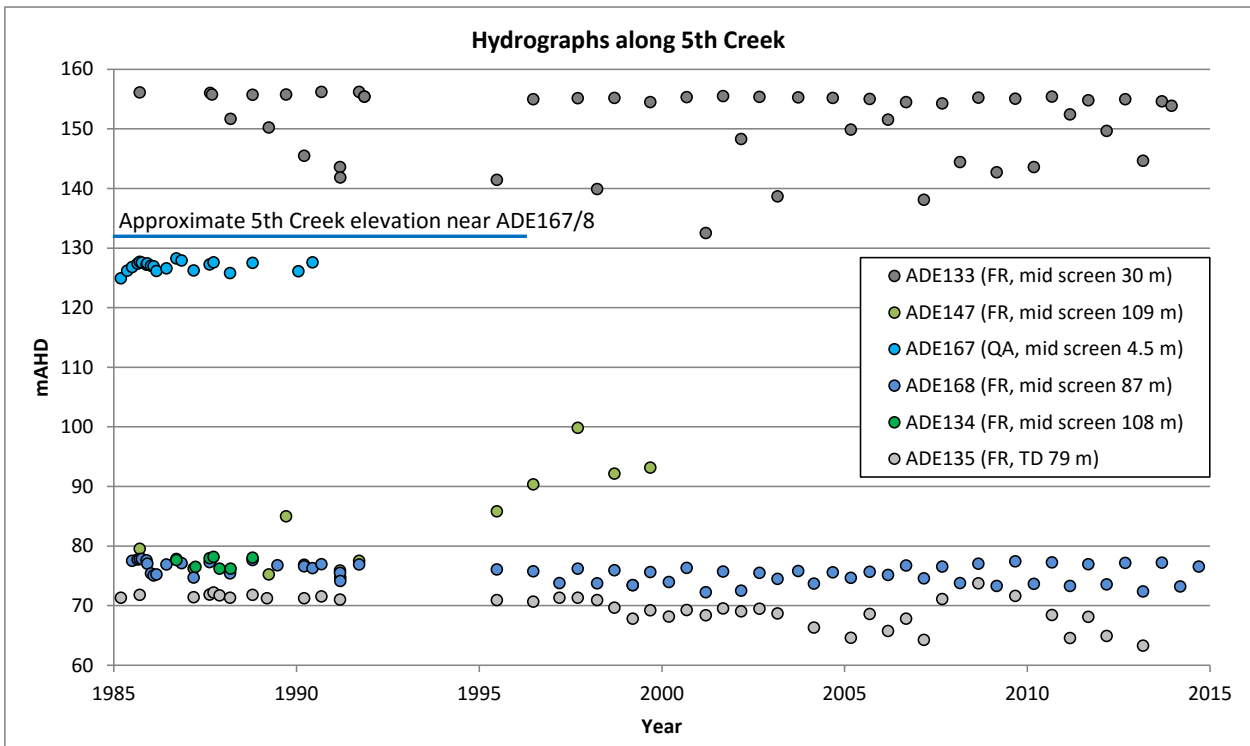
Apx Figure D.15 Hydrograph comparisons between Brownhill creek and nearby aquifers.



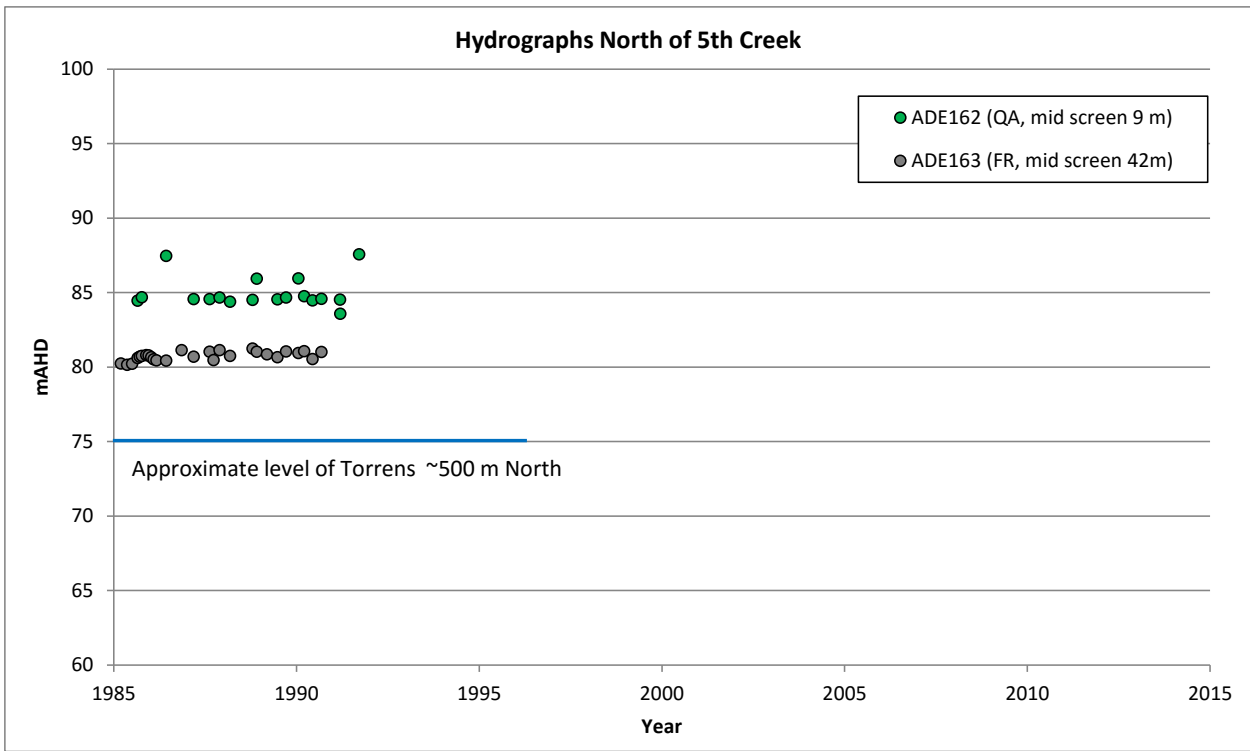
ApX Figure D.16 Reference map for Torrens River, Fourth and Fifth Creek hydrograph comparisons. Blue numerals indicate hydraulic heads (m AHD) in the shallow Quaternary aquifer while grey numerals are hydraulic heads in the fractured rock aquifer.



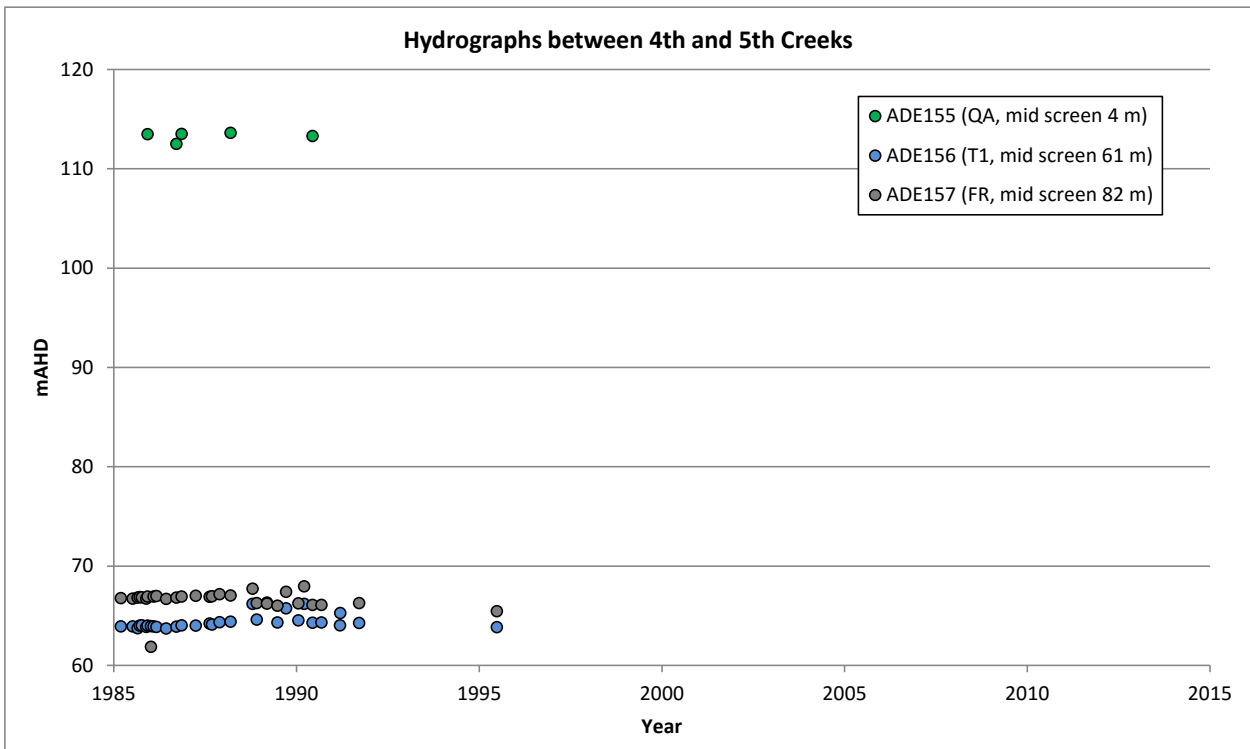
Apx Figure D.17 Hydrograph comparisons between Fifth creek and underlying QA and FRA.



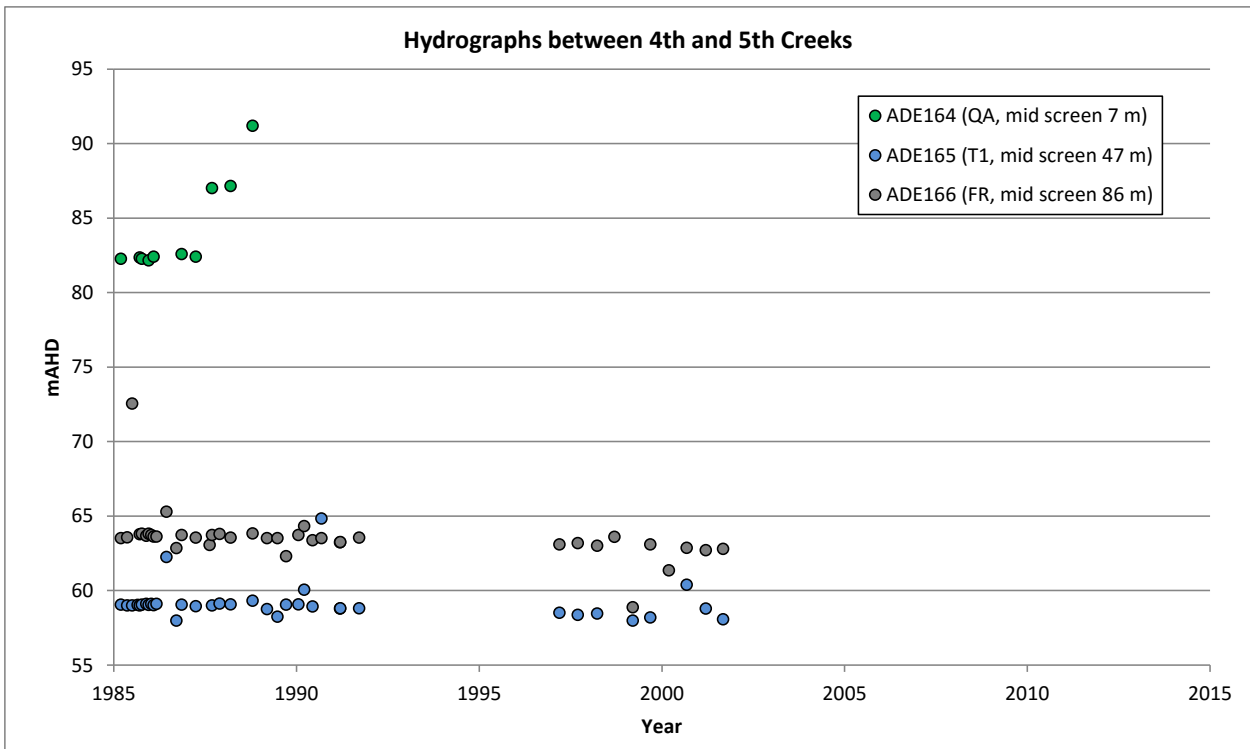
Apx Figure D.18 Hydrograph comparisons between Fifth creek and nearby aquifers.



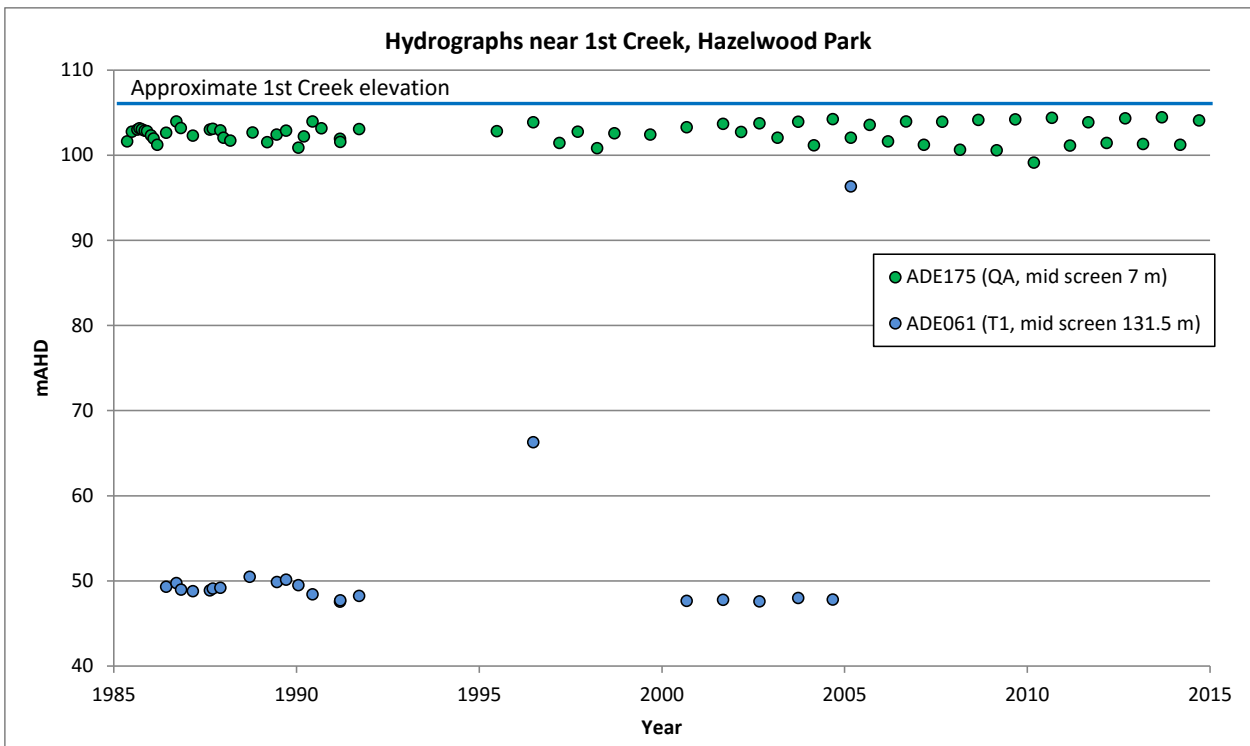
Apx Figure D.19 Hydrograph comparison between the Torrens river and nearby aquifers.



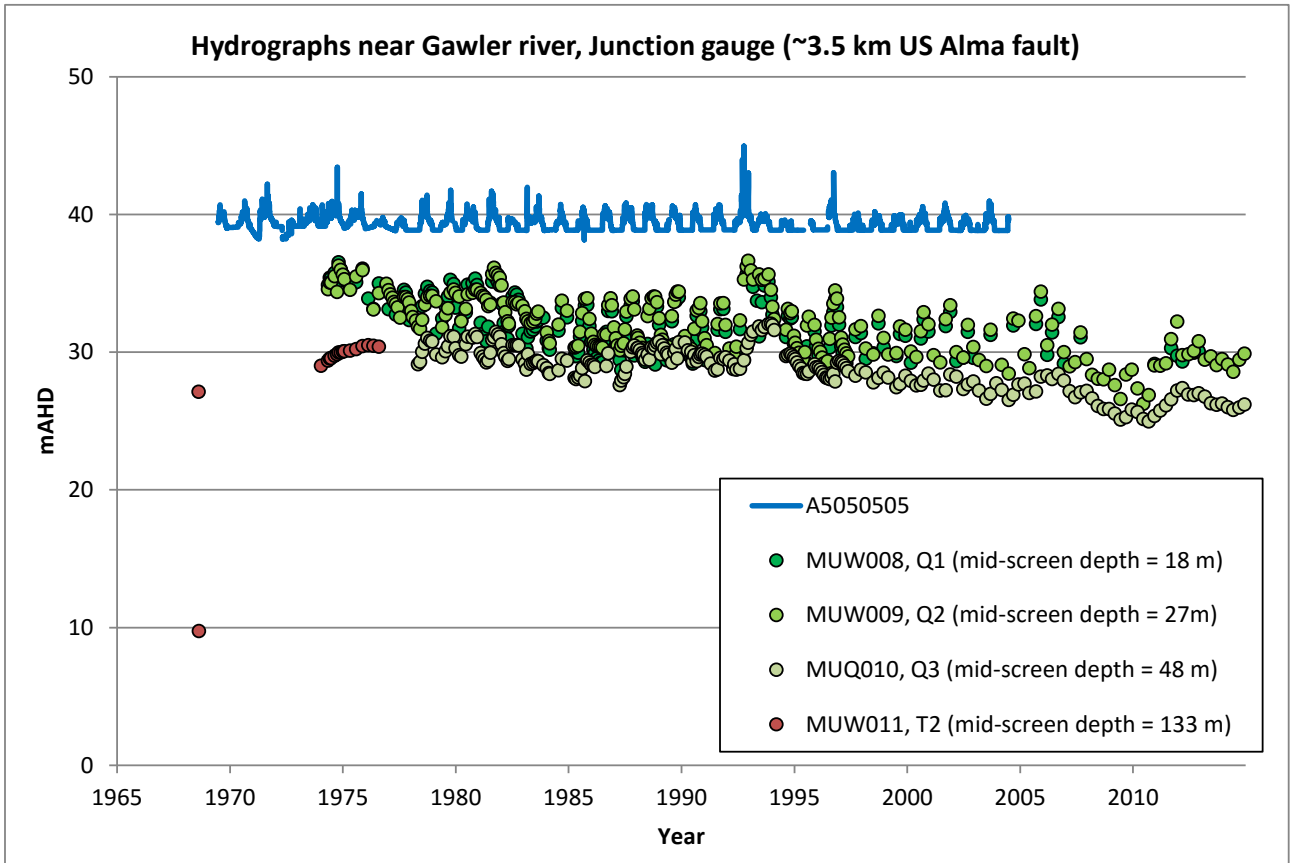
Apx Figure D.20 Hydrograph comparison between the aquifers between Fourth and Fifth creeks.



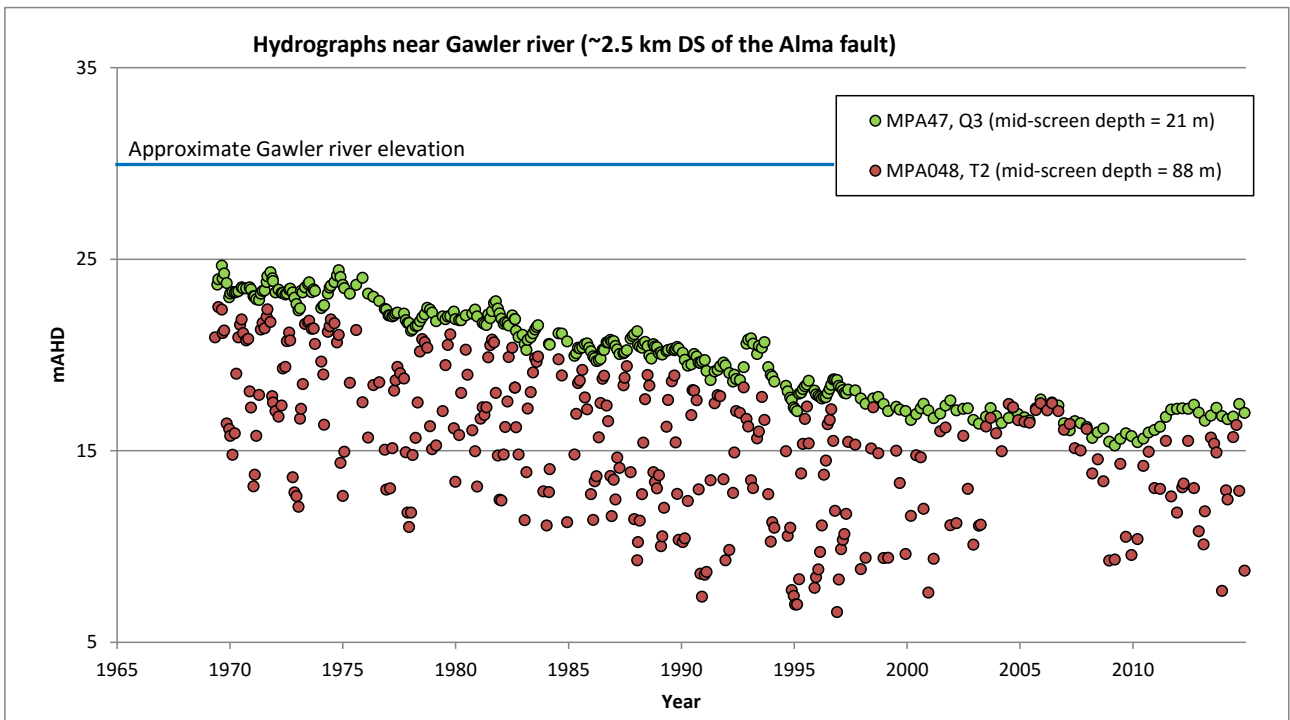
ApX Figure D.21 Hydrograph comparison for the aquifers between Fourth and Fifth creeks near the Hope Valley fault.



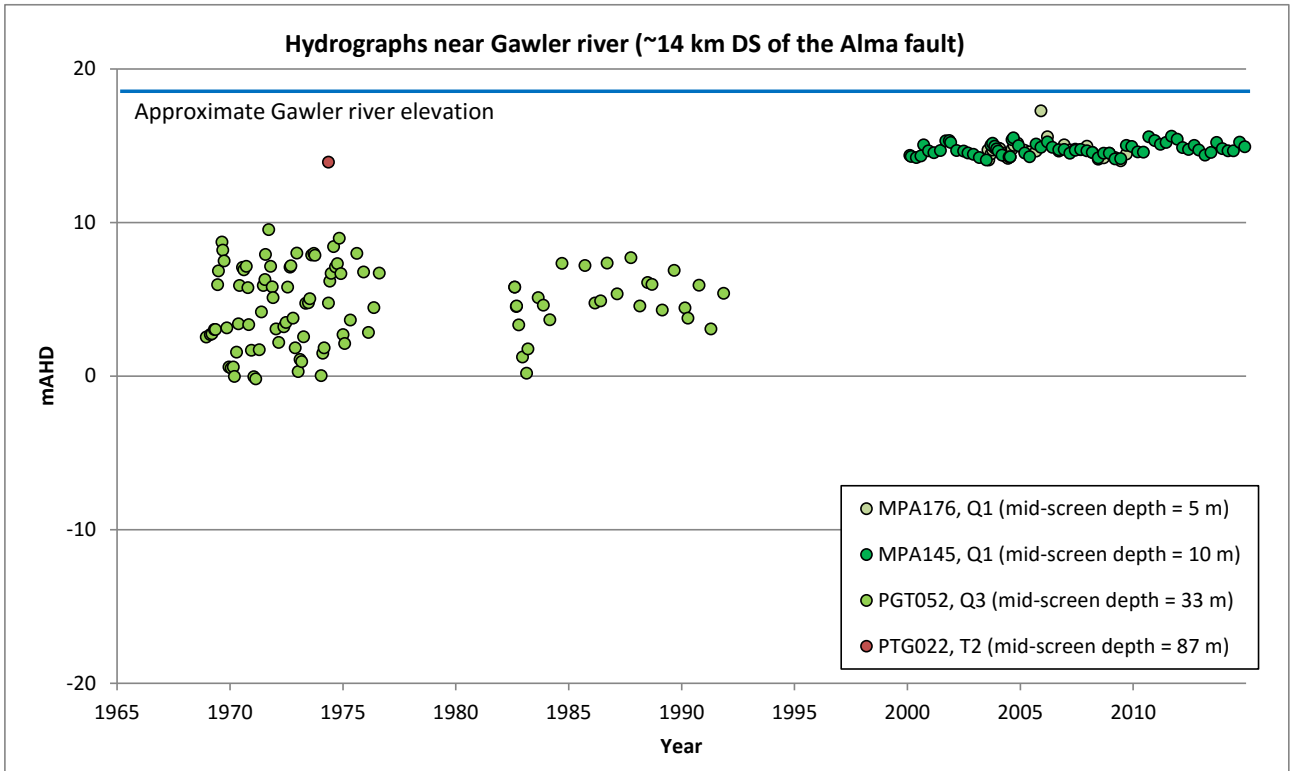
ApX Figure D.22 Hydrograph comparison between the aquifers near First creek.



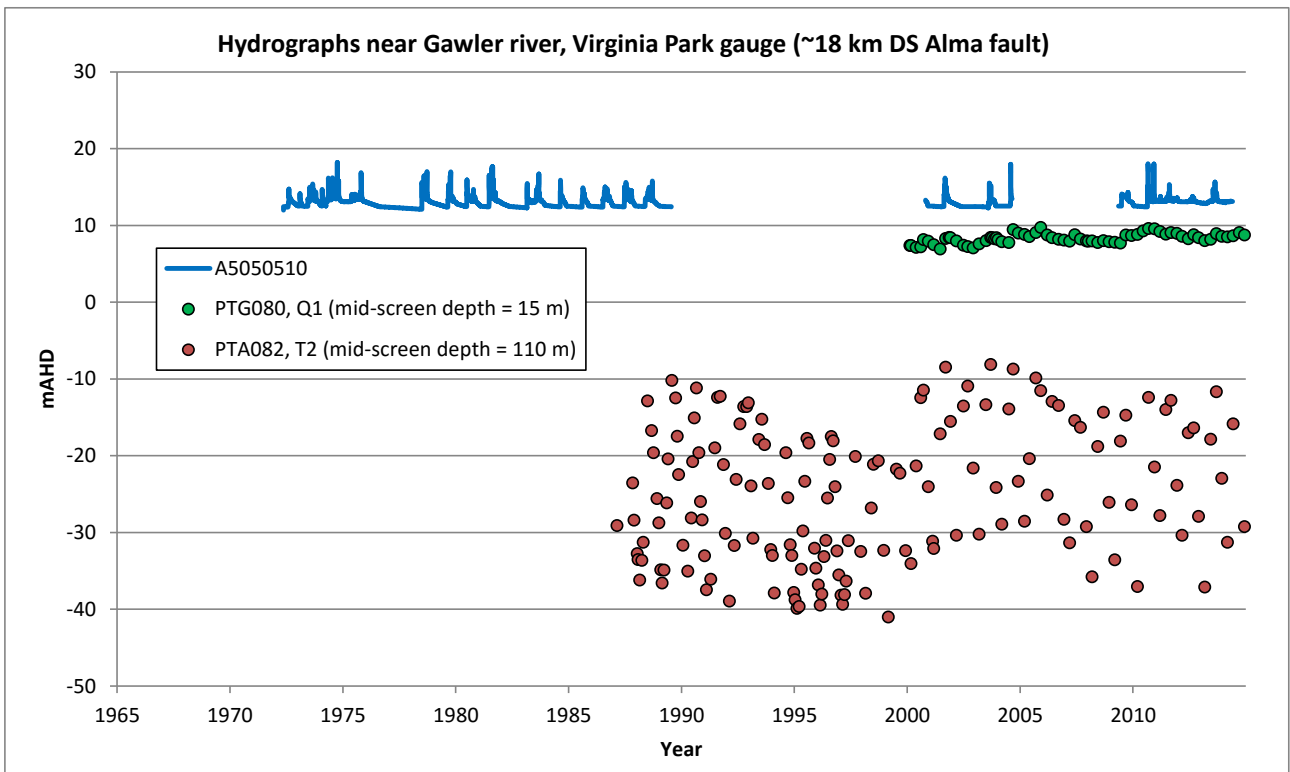
Apx Figure D.23 Hydrographs near the Gawler river, approximately 3.5 km upstream of the Alma fault.



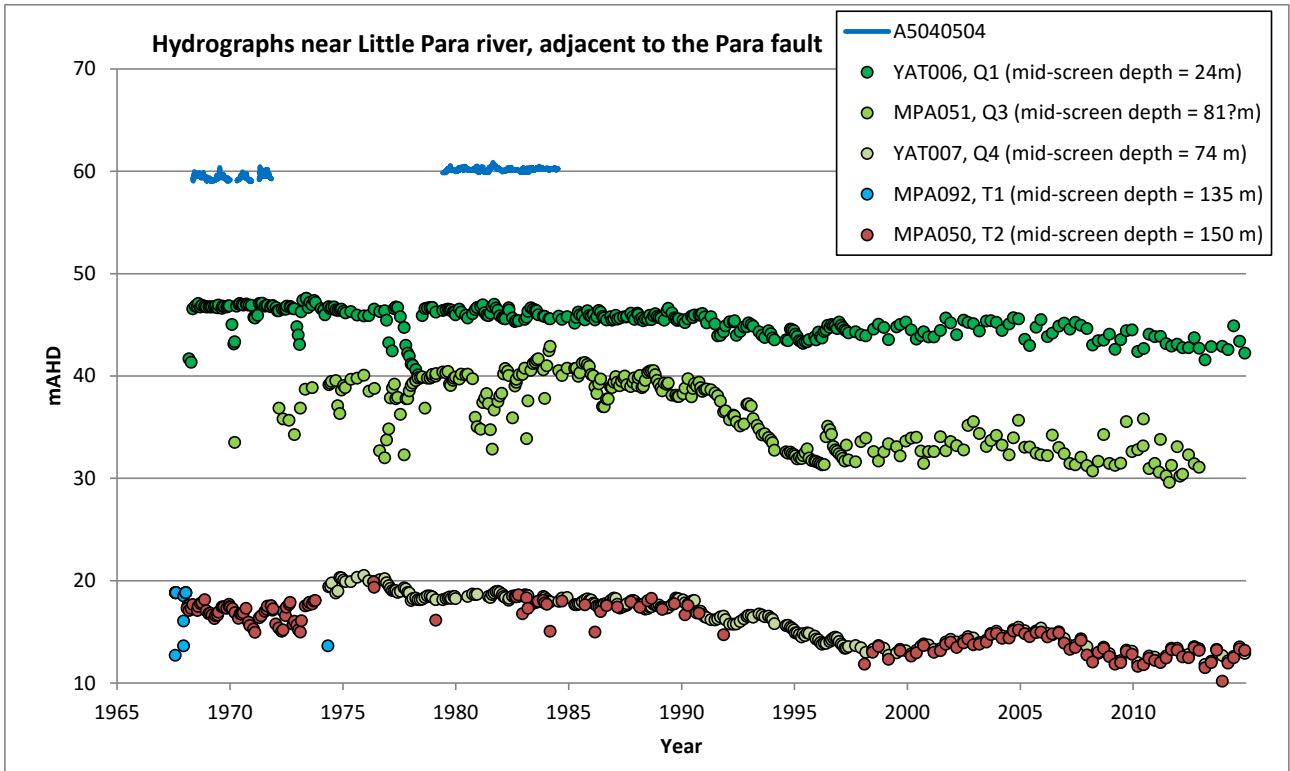
Apx Figure D.24 Hydrographs near the Gawler river, approximately 2.5 km downstream of the Alma fault.



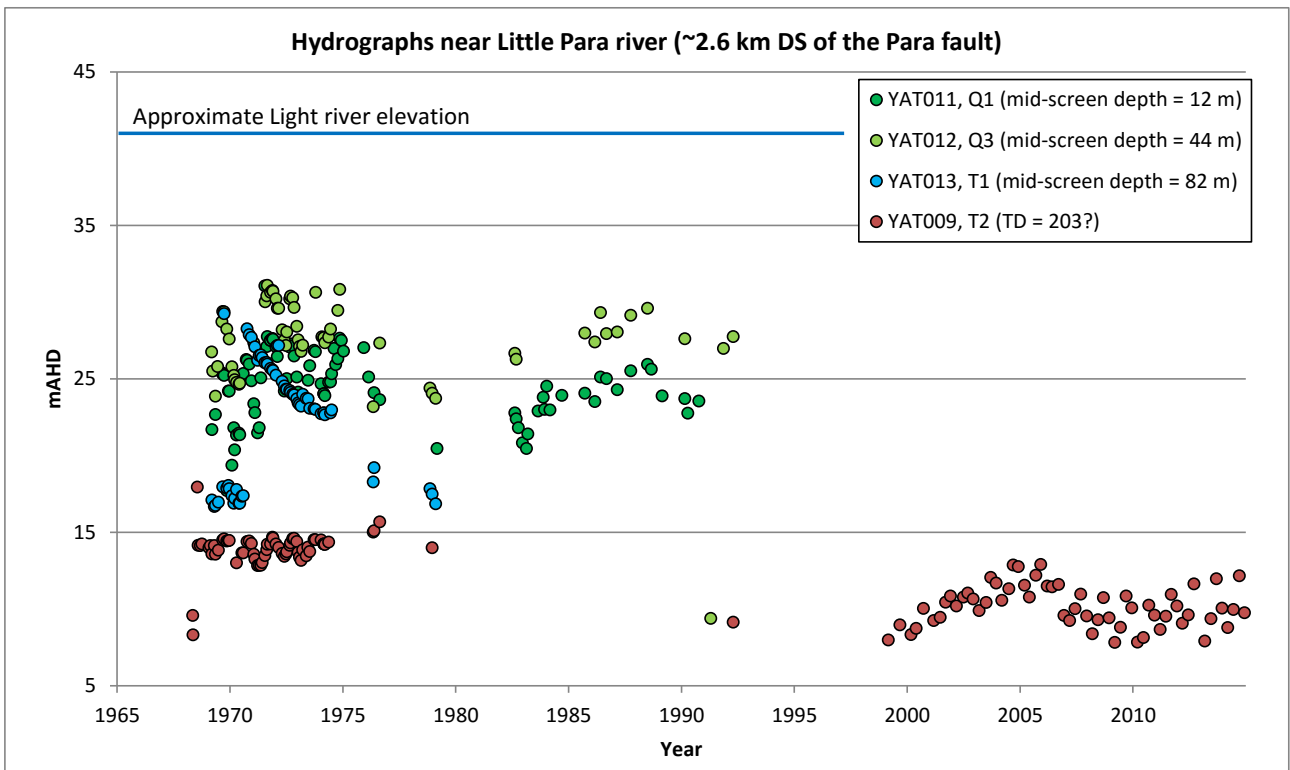
Apx Figure D.25 Hydrographs near the Gawler river, approximately 14 km downstream of the Alma fault.



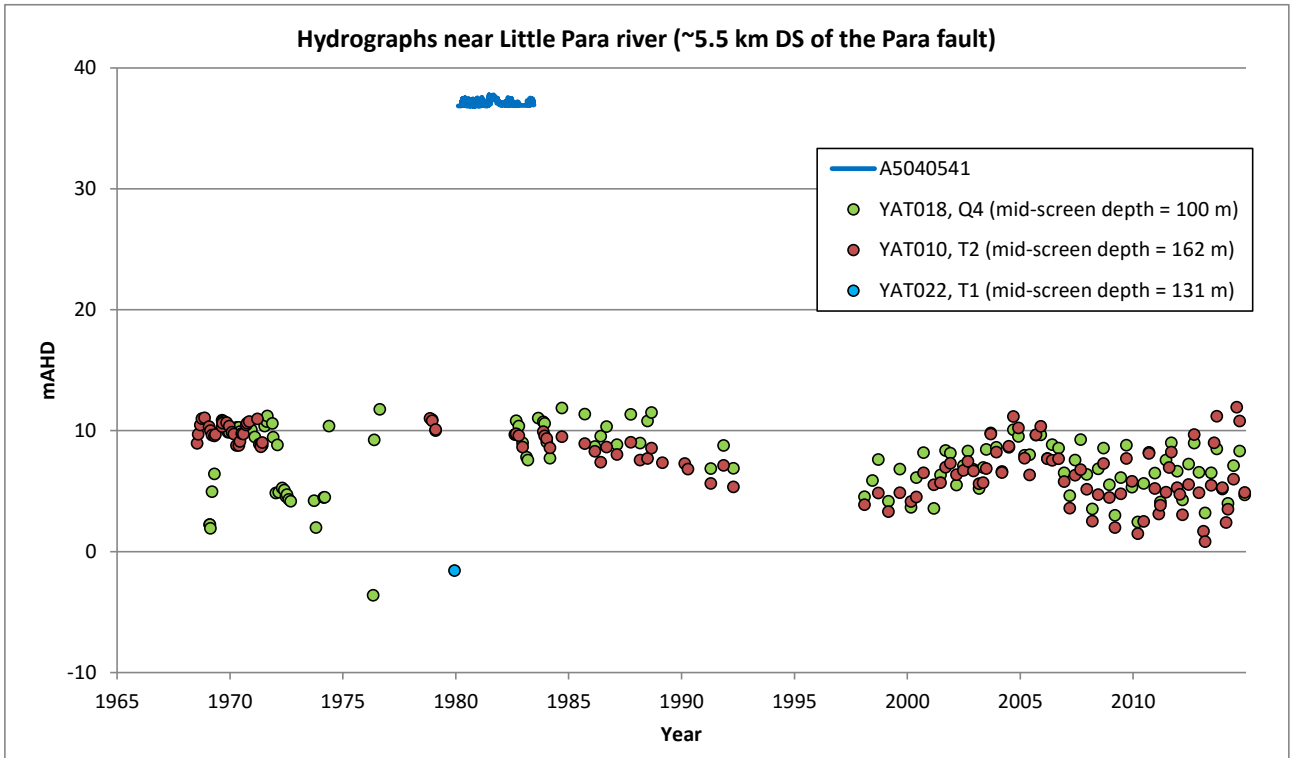
Apx Figure D.26 Hydrographs near the Gawler river, approximately 18 km downstream of the Alma fault.



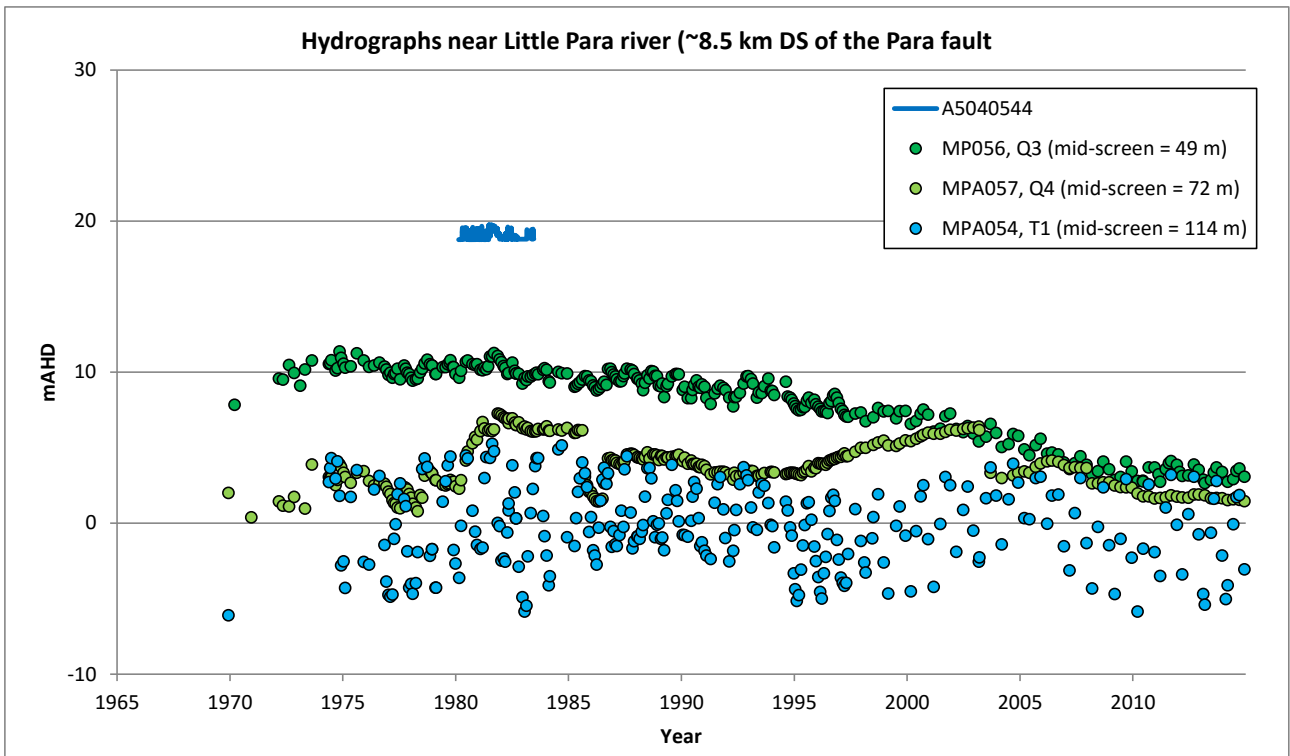
Apx Figure D.27 Hydrographs near the Little Para river, adjacent to the Para fault.



Apx Figure D.28 Hydrographs near the Little Para river, approximately 2.6 km downstream of the Para fault.



Apx Figure D.29 Hydrographs near the Little Para river, approximately 5.5 km downstream of the Para fault.



Apx Figure D.29 Hydrographs near the Little Para river, approximately 8.5 km downstream of the Para fault.

## D.9 References

- Cook PG, Lamontagne S, Berhane D and Clark JF (2006) Quantifying groundwater discharge to Cockburn river, southeastern Australia, using dissolved gas tracers  $^{222}\text{Rn}$  and  $\text{SF}_6$ . *Water Resources Research*, 42, W10411, DOI:10.1029/2006WR004921.
- Cranswick RH and Cook PG (2015) Scales and magnitude of hyporheic, river-aquifer and bank storage exchange fluxes. *Hydrological Processes*, DOI: 10.1002/hyp.10421
- Currie D, Braithwaite H and McCallum C (2011) Adelaide Plains Groundwater Investigation Projects part 3: Surface water / groundwater interactions. Prepared by Sinclair Knight Merz for the Adelaide and Mount Lofty Natural Resource Management Board.
- Gerges N (1999) The Geology and Hydrogeology of the Adelaide Metropolitan Area. PhD Thesis, Flinders University, Adelaide, 243 pp.
- Gerges N (2006) Overview of the hydrogeology of the Adelaide metropolitan area. South Australia. Department of Water, Land and Biodiversity Conservation. DWLBC Report 2006/10.
- Green G, Watt E, Alcoe D, Costar A and Mortimer L (2010) Groundwater flow across regional scale faults. DFW Technical Report 2010/15, Government of South Australia, through Department for Water, Adelaide.
- Kilpatrick FA and Cobb ED (1985) Measurement of Discharge Using Tracers, Book 3, Chapter A16 in: *Techniques of Water-Resources Investigations of the United States Geological Survey*. USGS, Denver CO.
- McCallum JL, Cook PG, Berhane D, Rumpf C, McMahon GA (2012) Quantifying groundwater flows to streams using differential flow gaugings and water chemistry. *Journal of Hydrology* 416: 118–132. DOI: 10.1016/j.jhydrol.2011.11.040.
- Teoh K (2006) Assessment of Surface Water Resources of Patawalonga Catchment and the Impact of Farm Dam Development. DWLBC Report 2007/09, Government of South Australia, through Department of Water, Land and Biodiversity Conservation, Adelaide.

# Appendix E Groundwater hydrochemistry

Authors: Cook PG and Banks EW

## E.1 Introduction

Geochemical methods can provide important insights into hydrological processes. The chemical composition of a water sample provides information on the processes that have occurred over the entire flow path of the sample. Thus it is possible to obtain information on regional scale processes from a relatively small number of geochemical measurements.

Available geochemical methods fall into a number of different categories. The first category comprises of those tracers that provide information on water age or residence time. This includes radioactive tracers, such as  $^{14}\text{C}$ , in which the radioactivity of the tracer provides an inbuilt clock, so that decreases in concentration can be directly related to residence time. In the case of  $^{14}\text{C}$ , the half-life is approximately 5730 years, and so the tracer can be used to determine the residence time of water of timescales of approximately 200 – 40,000 years. For shorter residence times, there are a number of anthropogenic tracers, including  $^3\text{H}$ , CFCs and  $\text{SF}_6$  (Cook and Solomon, 2000; Plummer and Busenberg, 2000) These tracers were produced and released to the atmosphere by industrial activity, and have well-defined input concentrations, so that the time of recharge can be determined by matching measured concentrations with the known history. Another type of residence time tracer is the accumulating tracer. These are tracers whose concentration in groundwater increases over time due to radioactive decay of other elements. Concentrations of these tracers provide qualitative information on residence time, that can become semi-quantitative if information can be obtained on the tracer's rate of production and release (and hence the accumulation rate). The most widely used accumulating tracer is the dissolved gas helium, which is produced as part of the uranium-thorium decay process (Solomon, 2000). The groundwater velocity along a flowpath is equal to the distance between points divided by the travel time, and hence residence time tracers are particularly useful for estimating groundwater velocities and aquifer recharge rates (e.g., Verhagen, 1992; Cook et al., 1995).

While residence time tracers provide one of the most powerful tools for quantitatively determining flow velocities and recharge rates in aquifers, there are a number of other tracers that can provide information on recharge processes and sometimes on rates of recharge. Concentrations of noble gases in groundwater provide information on air temperature and pressure at the time of recharge (Aeschbach-Hertig et al., 1999), and  $^2\text{H}$  and  $^{18}\text{O}$  can provide information on rainfall patterns producing recharge, elevation of recharge and distance from the ocean, and the extent of evapotranspiration before recharge (Gat, 1996). The ratio of the concentration of chloride in groundwater to that in rainfall can also provide information on the fraction of rainfall that evaporated prior to recharge. This approach, termed the chloride mass balance, has been widely used to estimate rates of recharge, particularly in arid zones where evaporation rates are greatest (Allison et al., 1994; Harrington et al., 2002). Of course, interpretation of all of these tracers can be complicated by other processes that may affect concentrations. Such processes include rock-water interaction, which can affect concentrations of  $^{14}\text{C}$ ,  $\text{SF}_6$  and chloride, and degradation, which can affect CFC concentrations. A thorough understanding of the geochemistry of the aquifer is therefore required as part of such studies.

This paper presents geochemical data for the Adelaide Plains aquifers, and uses this information to infer information about past and present-day flow systems. Some early measurements of  $^{14}\text{C}$  and  $^2\text{H}$  in the southern part of the aquifer system were presented by Dighton et al. (1994), and these values were also used in the study of Gerges (1999). Subsequently, Baird obtained  $^{14}\text{C}$ ,  $^3\text{H}$ ,  $^{18}\text{O}$  and  $^2\text{H}$  data from the Northern Adelaide Plains as part of his PhD thesis (Baird, 2010), and Green et al. (2010) measured  $^{18}\text{O}$ ,  $^2\text{H}$  and chlorofluorocarbons in the southeastern corner of the plains and the adjacent Mount Lofty Ranges. The current study supplements this data with measurements of  $^{14}\text{C}$ ,  $^2\text{H}$  and  $^{18}\text{O}$  across the entire Adelaide Plains

region, and also presents the first measurements of dissolved helium concentrations in groundwater in the Adelaide Plains aquifers. The data are used to infer flow processes and flow velocities.

## E.2 Methods

Groundwater sampling was conducted at 44 new and existing monitoring wells across the Adelaide and Mount Lofty Ranges region between October 2013 and October 2014 (Figure 1). Sampled wells are mostly located along three transects, each of which extends from the Mount Lofty Ranges through to St Vincent Gulf (Apx Figure E.1). Samples were collected from each of the main four aquifers: Quaternary, T1, T2 and fractured rocks, although work focussed on the T1, T2 and fractured rock systems.

A YSI® multi-parameter meter was used to measure pH, specific electrical conductance (SEC), dissolved oxygen (DO), redox (ORP) and temperature during purging of the monitoring wells using a flow-through cell. Alkalinity (as CaCO<sub>3</sub>) and dissolved oxygen were measured in the field using HACH titration kits. Prior to sampling, the static water level was measured from top of casing (TOC) using an electric water level indicator. Groundwater samples were collected after purging three well volumes or once the physical parameters of temperature, SEC and pH did not change by more than 5% within a half hour period, indicating that the sample was representative of the section of the aquifer sampled.

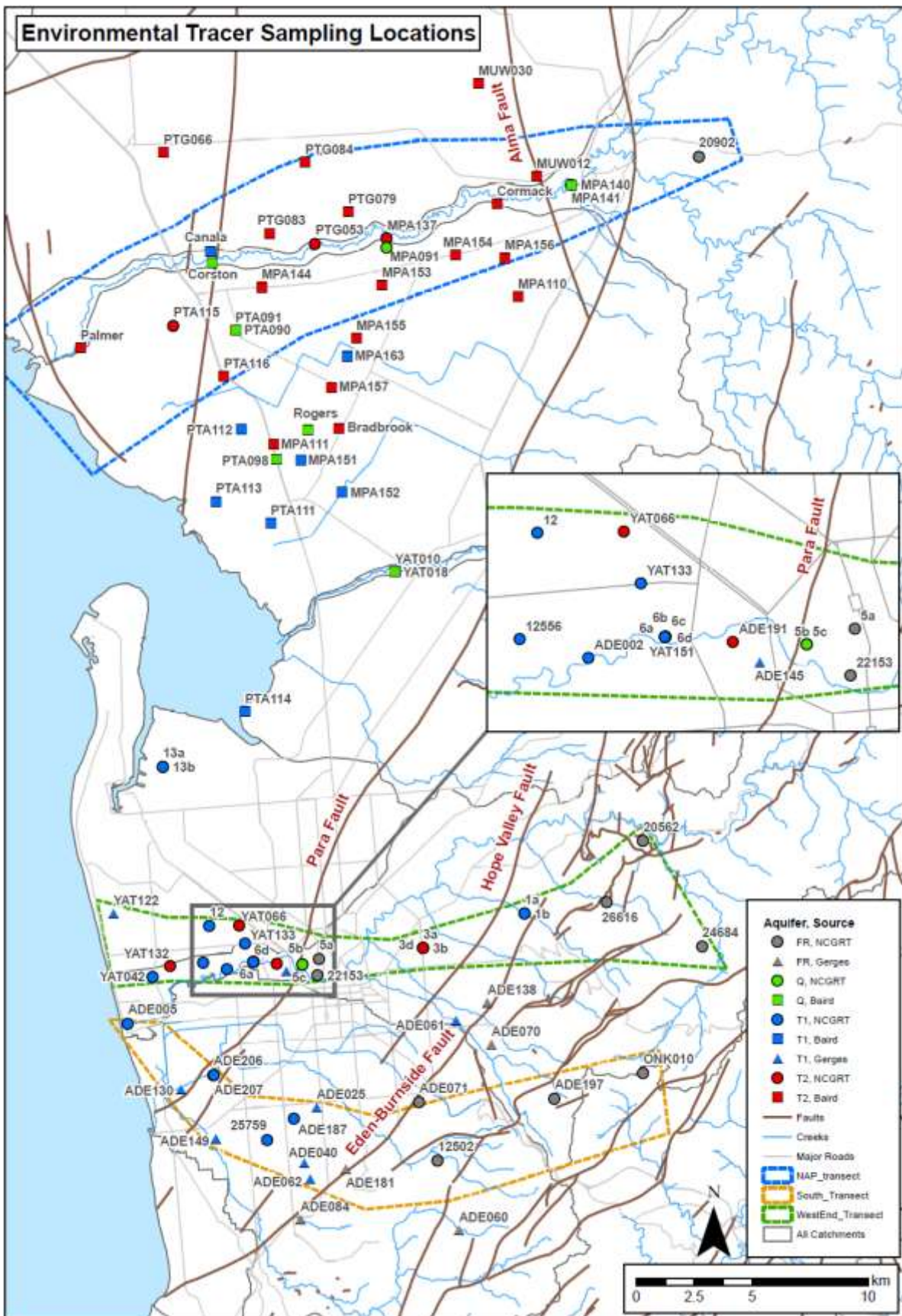
Major element analyses were conducted on groundwater samples that were filtered through a 0.45µm membrane filter in the field into 50 ml plastic bottles. Major cation and trace element samples were acidified with nitric acid (1% v/v HNO<sub>3</sub>) and analysed by a Spectro CIROS Radial Inductively Coupled Plasma Optical Emission Spectrometer at CSIRO Land and Water Analytical Services, Adelaide, South Australia. Major anions were analysed using a Dionex ICS-2500 Ion Chromatograph. All ion balances were typically better than ± 5 %.

The stable isotope ratios of hydrogen and oxygen (<sup>2</sup>H/<sup>1</sup>H and <sup>18</sup>O/<sup>16</sup>O) were measured by a Picarro L2130-i δ<sup>18</sup>O/δ<sup>2</sup>H Ultra High Precision Isotopic Water Analyser at School of Environment, Flinders University, South Australia using duplicate groundwater samples collected in 2 ml glass vials. The results are reported as a deviation from Vienna Standard Mean Ocean Water (vs. VSMOW) in per mil (‰) difference using delta (δ) notation. The analytical precision for δ<sup>18</sup>O and δ<sup>2</sup>H is ± 0.025 ‰ and ± 0.1 ‰, respectively.

Groundwater samples were collected for carbon isotope (<sup>13</sup>C/<sup>12</sup>C and <sup>14</sup>C) analysis in 1 L plastic bottles (with zero head space and no preservative) and analysed using accelerator mass spectrometry (AMS) at the Rafter radiocarbon laboratory, GNS Science, New Zealand. Carbon-13 isotope data (δ<sup>13</sup>C) are reported in delta notation, as per mil (‰) and Carbon-14 data are reported as percent modern carbon (pmC) according to the convention described in Stuiver and Polach (1977).

Samples for helium (He), neon (Ne), argon (Ar) and nitrogen (N<sub>2</sub>) analysis were collected using passive gas diffusion samplers (Gardner and Solomon, 2009) installed at screen depth for a minimum of 7 days or collected in copper tubes during well sampling. (Ar and N<sub>2</sub> values are only reported for samples collected using diffusion samplers.) Samples were analysed at the CSIRO Environmental Isotope Laboratory with a Stanford Research Systems RGA 220 quadrupole mass spectrometer with cryogenic separation (Poole et al., 1997). Precision of He and Ar measurements is approximately ± 5 %. (Ne and N<sub>2</sub> precision is not reported by the laboratory.)

A number of piezometers across the Adelaide region were also sampled and analysed for major ion chemistry and environmental isotopes by Dighton et al. (1994), Baird (2010) and Green et al. (2010). (The results of Dighton et al. (1994) are also reported by Gerges (1999).) Dighton et al. (1994) sampled a total of 19 piezometers south of the city and analysed them for <sup>14</sup>C, <sup>13</sup>C and <sup>2</sup>H, and Baird (2010) sampled 55 piezometers within the Northern Adelaide Plains for <sup>18</sup>O, <sup>2</sup>H, <sup>14</sup>C and <sup>13</sup>C analyses. Green et al. (2010) sampled 65 piezometers in the Adelaide hills and southeastern Adelaide suburbs for <sup>18</sup>O, <sup>2</sup>H and chlorofluorocarbons (CFC-11 and CFC-12). (Not all analyses were performed on all samples in each of these studies.) Some of these results are compared with results obtained in the current study. A total of six of the earlier wells sampled by Dighton et al. (1994) and Baird (2010) were resampled in the current project.



Apx Figure E.1 Map showing locations of transects and sampled wells. The symbol colours represent the different aquifers sampled, and shapes represent the source of the data. Locations of the three transects are indicated by broken lines.

## E.3 Results

Results of field measurements and major ion analyses are given in Apx Table E.1, and environmental isotope and dissolved gas results are given in Apx Table E.2. Of the 44 piezometers sampled, six of these had been previously sampled. Piezometers ADE071 and ADE187 were sampled in 1994 for measurement of  $^{14}\text{C}$ ,  $^{13}\text{C}$  and  $^{18}\text{O}$  (Dighton et al., 1994), and MPA137, MPA140, Palmer and PTA115 were sampled in 2003 for measurement of  $^{14}\text{C}$ ,  $^{13}\text{C}$ ,  $^{18}\text{O}$  and  $^2\text{H}$  (Baird, 2010). In most cases, agreement between the two sampling times was very good. All  $^2\text{H}$  results were within 1.5 ‰,  $^{18}\text{O}$  within 0.5 ‰, and  $^{13}\text{C}$  within 2.9 ‰. Four of the resampled wells had  $^{14}\text{C}$  activities within 1 pmC of the original results, and other values were 2.4 and 14.9 pmC greater. The most significant change was for ADE071, which was 48.1 pmC in 1994 and 63.0 pmC when resampled in 2013. The reason for this difference is uncertain.

### E.3.1 MAJOR IONS

The plots of the major ions versus chloride for the groundwater samples from the Adelaide Plains and Mount Lofty Ranges show broad linear trends of increasing individual ion concentrations relative to increased chloride concentration (Apx Figure E.2). The trends in  $\text{Ca}^{2+}$ ,  $\text{Mg}^{2+}$ ,  $\text{Na}^+$  and  $\text{HCO}_3^-$  lie slightly above the seawater dilution line implying some degree of water–rock interaction and that the weathering of primary carbonate and silicate minerals is likely to be an important control on groundwater chemistry in this system. The pH of all groundwater samples were close to neutral (average 7.4) with a total range from 5.9 to 8.6. There is greater variation in the Quaternary and fractured rock samples compared to the closely grouped T1 and T2 aquifer samples, and they also tend to have higher concentrations, which suggest that the T1 and T2 aquifers are less evaporated than the Quaternary and fractured rock samples. The three samples from the fractured rock aquifer that have the highest chloride concentrations do show a distinct hydrochemical composition that is different from the other samples. These particular groundwater samples show similar characteristics to the brine end member that was identified in the Port Willunga Formation in the Willunga Embayment, which appears to be from another source and/or climatic regime (Appendix G). The piper plot shows that the majority of groundwater samples from each of the main aquifers are sodium-chloride type waters. This reflects a predominantly seawater composition of rainfall, which is expected given the areas proximity to the coast (Apx Figure E.3). However, some of the fractured rock and Quaternary samples are calcium-bicarbonate type waters. Saturation indices show that all aquifers are at or above saturation with aqueous aragonite, calcite and dolomite and typically below saturation for anhydrite and gypsum (Apx Table E.3).

The distribution of chloride along the three transects is depicted in Apx Figure E.4. In general, concentrations are higher in the Quaternary aquifer than in the T1, T2 and fractured rock aquifers. This suggests higher rates of evaporation for the Quaternary aquifer, and hence lower rates of recharge. It also suggests that leakage from the Quaternary to the Tertiary aquifers is a relatively small component of the T1 and T2 aquifer water balances. Median concentrations for each of the aquifers for the piezometers shown in Figure 4 are 1054, 346, 294 and 212 mg/L for the Quaternary, T1, T2 and fractured rock aquifers, respectively. For comparison, Appendix C estimated the median chloride concentrations within these aquifers across the entire Adelaide Plains region based on a relationship between chloride concentration and electrical conductivity. The resulting median concentrations were 701, 436, 460 and 318 mg/L for the Quaternary, T1, T2 and fractured rock aquifers respectively. Considering the limited sampling, the median values obtained from the transect piezometers are similar to these regional values. A few piezometers along the transect that are screened within the fractured rock, however, contain high concentrations, with values of 5035, 8114 and 10172 measured in piezometers 5a, 22153 and 5b, respectively, in the central transect.

Apx Table E.1 Field parameters and major ion analyses on groundwater samples.

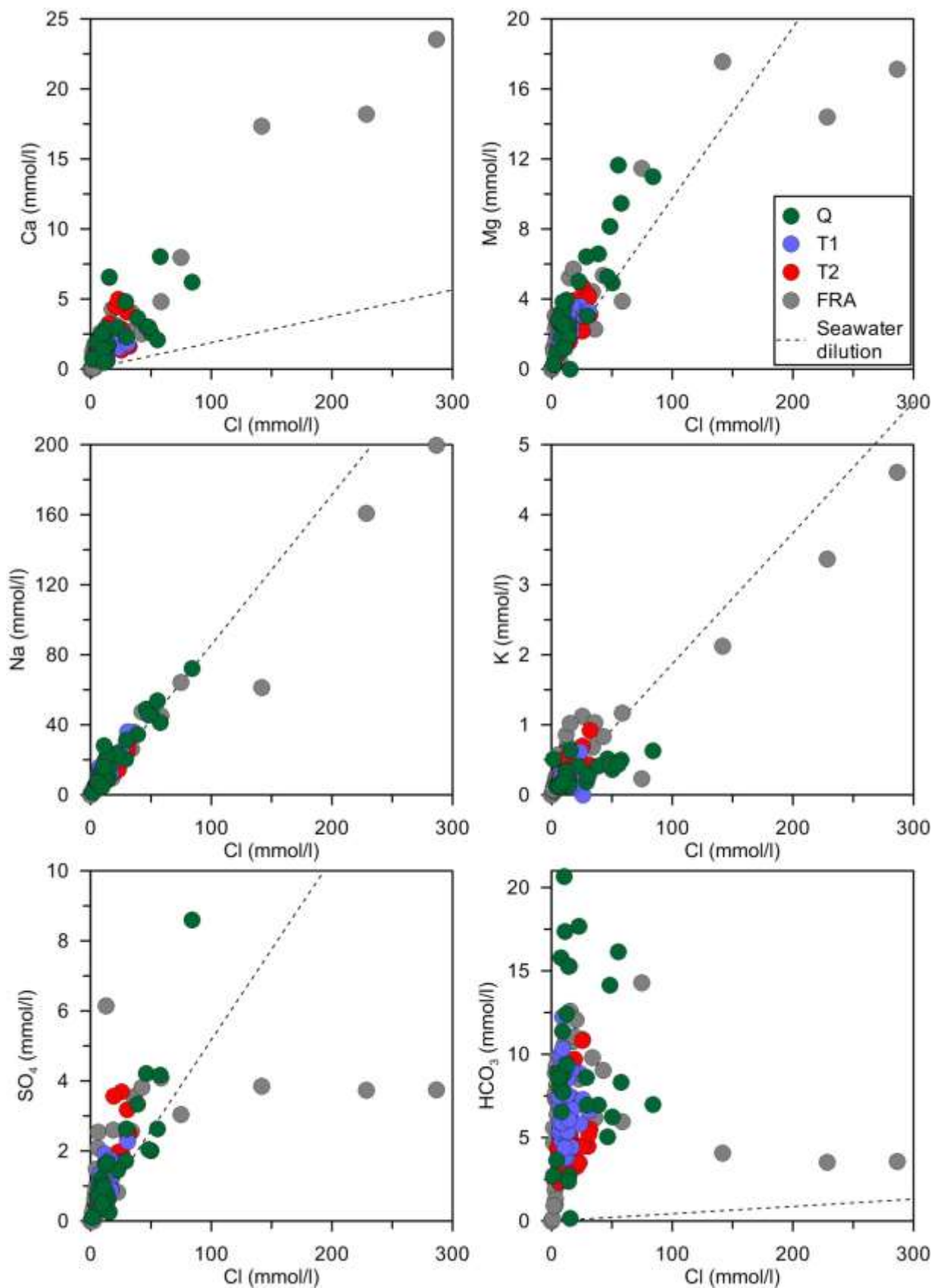
ID	AQUIFER	DATE	FIELD PARAMETERS						LABORATORY MEASUREMENTS										
			EC (µS/cm)	PH	ALK (mg/L)	EC (µS/cm)	PH	ALK (mg/L)	Cl (mg/L)	HCO <sub>3</sub> (mg/L)	Br (mg/L)	NO <sub>3</sub> (mg/L)	SO <sub>4</sub> (mg/L)	Ca (mg/L)	K (mg/L)	Mg (mg/L)	Na (mg/L)	S (mg/L)	
MPA091	Q	24.04.14	2040	6.9	128	1960	7.6	2.7	508	166	1.5	4.9	59	68	8.5	55	258	20	
3-d	Q	14.05.14	3834	7.7	536	4040	7.9	10.9	906	660	2.6	55	188	114	27	115	575	59	
3-e	Q	09.05.14	4596	12.0	731	4430	11.9	12.6	549	10	1.4	18	26	263	25	0	367	9.2	
5-c	Q	24.09.14	5280	7.2	601	4831	8.0		1203	598.4	3.3		246	163	17	173	603		
12556	T1	16.04.14			250	1760	8.2	5.4	347	321	1.0	0.23	118	55	8.8	42	269	39	
25759	T1	10.12.13	2610	7.28	377	2581	8.33	7.6	590	452	1.80	2.20	120	63.1	13.8	56.8	384	37.5	
13-b	T1	09.10.14	5160	7.9	321	4959	8.2		1275	377.3	4.0		342	113	25	90	826		
6-c	T1	18.09.14	1404	7.6	360	1336	8.4		203	390.0	0.6		76	44	6	31	204		
ADE002	T1	23.04.13	1635	7.6	258	1560	8.3	6.0	262	356	0.72	0.03	108	40	7.9	34	269	37	
ADE005	T1	02.12.13	1415	7.41	240	1417	7.72	4.8	290	293	0.85	0.22	66	49.5	7.36	35.9	183	20.8	
ADE187	T1				342	1359	8.46	7.1	230	420	0.58	0.59	54	53.3	6.14	37.1	188	17.4	
ADE207	T1	22.11.13	2010	7.00	336	2009	7.51	6.5	440	397	1.20	9.60	73	68.5	9.13	61.4	244	22.3	
YAT042	T1	09.12.13	1672	7.48	320	1660	8.17	6.4	300	388	0.96	0.09	110	38.9	7.43	36.8	258	32.9	
YAT133	T1		1646	7.64	180	1727	8.21	3.9	450	231	1.30	0.23	33	59.4	12.8	47	204	10.3	
YAT-151	T1	15.09.14	4229	8.0	332	1176	8.5		183	355.1	0.5		46	39	14	36	162		
6-d	T1	17.09.14	1165	9.1	271	1114	8.3		240	148.6	0.7		57	23	11	17	176		
6-b	T1	16.09.14	1939	8.8	287	2153	8.6		453	308.2	1.2		173	32	15	78	310		
12	T1	10.09.14	1539	7.7	287	1474	8.3		279	330.4	0.9		73	51	12	47	182		
13-a	T2	07.10.14	7380	7.0	307	7178	7.8		2075	364.4	6.6		392	193	29	152	1040		
1-b	T2	08.05.14	1910	6.5	369	2240	7.6	7.4	421	448	1.1	0.03	184	90	11	78	289	63	
3-b	T2	09.05.14	1995	7.3		2180	7.6	6.9	429	418	1.1	0.03	154	111	21	78	248	54	
6-a	T2	17.09.14	2030	7.9	108	1941	8.3		386	357.5	1.0		124	46	15	49	289		
ADE191	T2	09.01.14	1982	7.13	268	1979	7.99	5.5	440	331	1.30	0.16	130	63.8	10.6	47.8	264	38.8	
ADE206	T2	29.11.13	1716	7.34	250	1722	7.59	5.1	370	313	1.00	0.14	87	52.9	11.1	52.8	212	27.6	
MPA137	T2	18.12.13	1311	7.21	248	1308	7.97	5.0	250	304	0.68	0.19	72	61.9	5.62	28.5	169	23	
MPA140	T2	18.12.13	980	6.45	108	978	7.41	2.3	230	142	0.56	0.27	43	27.3	6.25	26.4	127	13.6	
Palmer	T2	15.1.14	2140	7.61	218	2060	8.04	4.5	520	270	1.60	0.13	88	70.8	10.1	50.8	261	27.2	
PTA115	T2	17.12.13	1219	7.20	202	1224	7.94	4.2	240	251	0.66	0.25	75	64.9	7.11	27.7	142	24.1	

PTG053	T2	17.12.13	1669	7.17	223	1661	7.87	4.6	370	278	1.10	0.26	91	82.9	7.37	35.4	201	28.8
YAT066	T2	12.12.13	1717	7.39	269	1730	7.85	5.3	370	319	1.10	0.14	90	55.3	10.1	54.5	213	28.7
YAT132	T2	11.12.13	2360	7.30	350	2330	8.30	6.4	510	382	1.60	0.18	140	49.2	10.5	49.3	369	45.1
22153	FRA	25.09.14	23900	6.9	247	23048	7.8		8114	216.0	24.0		359	730	82	563	3700	
5-a	FRA	23.09.14	15370	6.9	225	14912	7.7		5035	249.4	15.2		370	695	52	687	1410	
5-b	FRA	24.09.14	29300	6.8	172	28285	7.7		10172	218.9	31.9		360	944	112	670	4590	
12502	FRA	23.04.14	1510	7.42	355	1460	8.0	7.2	224	437	0.61	0.07	86	65	8.4	76	153	29
20562	FRA	07.05.14			377	1100	8.2	7.7	127	462	0.34	0.03	32	66	9.7	55	111	11
20902	FRA	24.04.14			427	5840	7.8	9.1	1513	552	5.2	12	366	101	33	130	1090	123
24684	FRA	01.05.14	1098	7.40	373	1040	8.0	7.6	106	456	0.29	0.03	43	49	6.7	74	85	15.1
26616	FRA	30.04.14	1102	7.34	359	1060	8.0	7.4	123	444	0.34	0.03	21	53	6.1	58	107	7.4
1-a	FRA	02.05.14	3000	7.83	306	2880	7.9	6.0	460	363	1.3	0.03	590	115	17	86	425	203
3-a	FRA	05.05.14	2185	7.14	312	2170	7.6	6.5	436	392	1.1	0.03	157	90	16	78	252	54
ADE071	FRA	29.11.13	1460	7.35	373	1454	7.77	7.3	250	441	0.69	0.14	52	66.7	6.99	66.3	133	16.6
ADE197	FRA	30.04.14			291	492	7.2	1.0	106	61	0.29	0.11	22	5	5.6	14	77	7.6
ONK010	FRA	30.04.14	546	6.55	162	481	7.6	2.5	70	153	0.13	1.7	11	24	2.5	24	45	3.6

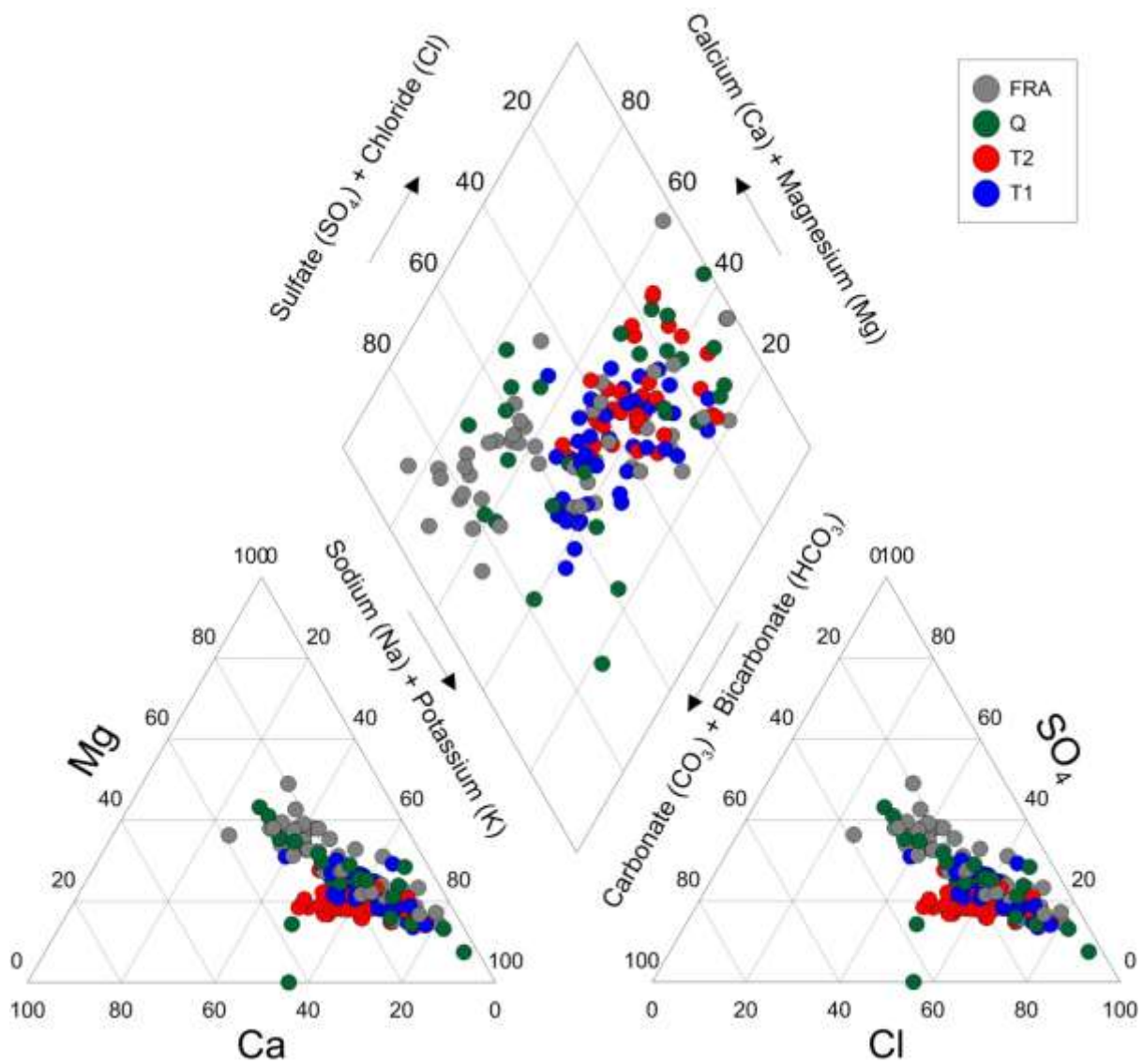
Apx Table E.2 Results of environmental isotope and dissolved gas analyses on groundwater samples.

ID	UNIT NO.	AQUIFER	<sup>2</sup> H (‰)	<sup>18</sup> O (‰)	<sup>14</sup> C (pmC)	<sup>13</sup> C (‰)	He (cm <sup>3</sup> /g)	Ne (cm <sup>3</sup> /g)	N <sub>2</sub> (cm <sup>3</sup> /g)	Ar (cm <sup>3</sup> /g)
MPA091	6628-01473	Q	-26.3	-4.7	83.2	-12.0				
3-d	6628-27257	Q	-21.6	-3.9	91.0	-13.4				
3-e		Q	-17.8	-3.1						
5-c	6628-27435	Q	-19.3	-3.2	86.4	-13.0	2.58 × 10 <sup>-7</sup>	2.17 × 10 <sup>-7</sup>	1.33 × 10 <sup>-2</sup>	3.30 × 10 <sup>-4</sup>
12556	6628-12556	T1	-27.7	-5.1	3.18	-5.42				
25759	6628-25759	T1	-26.4	-4.9	14.7	-9.06	9.86 × 10 <sup>-6</sup>	3.01 × 10 <sup>-7</sup>		
13-b	6628-27503	T1			4.17	-8.5	3.47 × 10 <sup>-7</sup>	2.00 × 10 <sup>-7</sup>	1.16 × 10 <sup>-2</sup>	3.07 × 10 <sup>-4</sup>
6-c		T1	-26.6	-5.1	2.56	-7.23	3.64 × 10 <sup>-7</sup>	3.23 × 10 <sup>-7</sup>	1.53 × 10 <sup>-2</sup>	3.58 × 10 <sup>-4</sup>
ADE002	6628-07538	T1	-26.9	-5.1	3.51	-6.96				
ADE005	6628-19725	T1	-26.3	-5.0	1.33	-6.63	3.17 × 10 <sup>-7</sup>	2.42 × 10 <sup>-7</sup>	1.69 × 10 <sup>-2</sup>	3.93 × 10 <sup>-4</sup>
ADE187	6628-13482	T1	-25.3	-5.0	36.8	-10.1				
ADE207	6628-25428	T1	-25.9	-5.1	24.6	-8.74	4.47 × 10 <sup>-8</sup>	1.39 × 10 <sup>-7</sup>	9.66 × 10 <sup>-2</sup>	2.57 × 10 <sup>-4</sup>
YAT042	6628-07388	T1	-29.5	-5.3	2.83	-6.9	3.48 × 10 <sup>-7</sup>	2.48 × 10 <sup>-7</sup>	1.86 × 10 <sup>-2</sup>	4.33 × 10 <sup>-4</sup>
YAT133	6628-07484	T1	-24.8	-4.8	37.5	-11.4	4.17 × 10 <sup>-7</sup>	2.77 × 10 <sup>-7</sup>		
YAT-151	6628-25604	T1	-28.0	-5.4	5.09	-7.15	5.64 × 10 <sup>-7</sup>	2.46 × 10 <sup>-7</sup>	1.52 × 10 <sup>-2</sup>	3.39 × 10 <sup>-4</sup>
6-d		T1	-23.7	-4.6	28.0	-11.3	4.36 × 10 <sup>-7</sup>	3.78 × 10 <sup>-7</sup>	2.47 × 10 <sup>-2</sup>	5.99 × 10 <sup>-4</sup>
6-b		T1	-25.4	-4.7	1.54	-5.11	2.71 × 10 <sup>-7</sup>	2.75 × 10 <sup>-7</sup>	1.79 × 10 <sup>-2</sup>	3.93 × 10 <sup>-4</sup>
12	6628-27253	T1	-25.1	-4.7	5.73	-6.66	4.94 × 10 <sup>-8</sup>	1.92 × 10 <sup>-7</sup>	1.15 × 10 <sup>-2</sup>	3.07 × 10 <sup>-4</sup>
13-a	6628-27436	T2			0.41	-9.31	2.27 × 10 <sup>-6</sup>	2.41 × 10 <sup>-7</sup>	1.43 × 10 <sup>-2</sup>	3.44 × 10 <sup>-4</sup>
1-b	6628-27218	T2	-29.3	-5.3	35.6	-12.4	4.89 × 10 <sup>-8</sup>	1.83 × 10 <sup>-7</sup>	1.11 × 10 <sup>-2</sup>	3.05 × 10 <sup>-4</sup>
3-b	6628-27255	T2	-27.2	-4.7	4.09	-12.1	4.72 × 10 <sup>-8</sup>	1.88 × 10 <sup>-7</sup>	1.16 × 10 <sup>-2</sup>	3.18 × 10 <sup>-4</sup>
6-a		T2	-27.7	-5.0	0.82	-3.8	1.47 × 10 <sup>-6</sup>	3.48 × 10 <sup>-7</sup>		
ADE191	6628-14266	T2	-27.1	-4.8	1.98	-3.92	7.63 × 10 <sup>-7</sup>	2.02 × 10 <sup>-7</sup>	2.58 × 10 <sup>-2</sup>	4.81 × 10 <sup>-4</sup>
ADE206	6628-25427	T2	-26.9	-5.1	4.27	-6.76	2.35 × 10 <sup>-6</sup>	2.60 × 10 <sup>-7</sup>	1.73 × 10 <sup>-2</sup>	4.57 × 10 <sup>-4</sup>
MPA137	6628-18941	T2	-22.8	-4.3	14.2	-8.7	3.23 × 10 <sup>-7</sup>	2.60 × 10 <sup>-7</sup>	1.83 × 10 <sup>-2</sup>	4.31 × 10 <sup>-4</sup>
MPA140	6628-16713	T2	-21.8	-4.0	81.1	-11.0	2.85 × 10 <sup>-6</sup>	2.99 × 10 <sup>-7</sup>	2.05 × 10 <sup>-2</sup>	5.09 × 10 <sup>-4</sup>
Palmer	6528-02069	T2	-29.0	-4.8	1.57	-9.04	1.55 × 10 <sup>-6</sup>	3.26 × 10 <sup>-7</sup>		
PTA115	6628-20666	T2	-25.9	-4.8	1.45	-9.71	4.94 × 10 <sup>-7</sup>	3.14 × 10 <sup>-7</sup>	1.96 × 10 <sup>-2</sup>	5.19 × 10 <sup>-4</sup>
PTG053	6628-01066	T2	-23.8	-4.5	2.26	-9.29	2.00 × 10 <sup>-7</sup>	2.83 × 10 <sup>-7</sup>		
YAT066	6628-11385	T2	-24.7	-4.7	1.67	-3.59	2.33 × 10 <sup>-6</sup>	2.33 × 10 <sup>-7</sup>	1.68 × 10 <sup>-2</sup>	4.20 × 10 <sup>-4</sup>

YAT132	6628-11153	T2	-29.5	-5.5	1.21	-2.76	$4.32 \times 10^{-6}$	$2.00 \times 10^{-7}$	$1.52 \times 10^{-2}$	$3.87 \times 10^{-4}$
22153	6627-22153	FRA	-30.4	-5.2	1.15	-10.8	$1.02 \times 10^{-4}$	$3.31 \times 10^{-7}$	$1.96 \times 10^{-2}$	$4.06 \times 10^{-4}$
5-a	5-a	FRA	-30.8	-5.2	1.16	-10.7	$6.81 \times 10^{-6}$	$2.32 \times 10^{-7}$	$1.30 \times 10^{-2}$	$3.64 \times 10^{-4}$
5-b	5-b	FRA	-30.3	-5.0	1.46	-8.60				
12502	6628-12502	FRA	-27.9	-5.0	41.1	-8.98				
20562	6628-20562	FRA	-29.1	-5.4	14.7	-9.80				
20902	6628-20902	FRA	-21.8	-3.3	58.5	-9.62				
24684	6628-24684	FRA	-29.8	-5.8	34.2	-10.1				
26616	6628-26616	FRA	-28.1	-5.4	28.8	-12.5				
1-a	6628-27503	FRA	-31.2	-5.6	4.38	-11.2	$2.55 \times 10^{-6}$	$3.09 \times 10^{-7}$	$1.95 \times 10^{-2}$	$4.35 \times 10^{-4}$
3-a	6628-27212	FRA	-27.6	-4.8	1.08	-12.2	$1.17 \times 10^{-7}$	$1.94 \times 10^{-7}$	$1.13 \times 10^{-2}$	$3.10 \times 10^{-4}$
ADE071	6628-12020	FRA	-26.1	-5.1	63.0	-11.5	$1.32 \times 10^{-7}$	$4.29 \times 10^{-7}$		
ADE197	6628-21639	FRA	-28.9	-5.7	89.5	-11.9				
ONK010	6628-10954	FRA	-26.9	-5.3	77.7	-9.12				



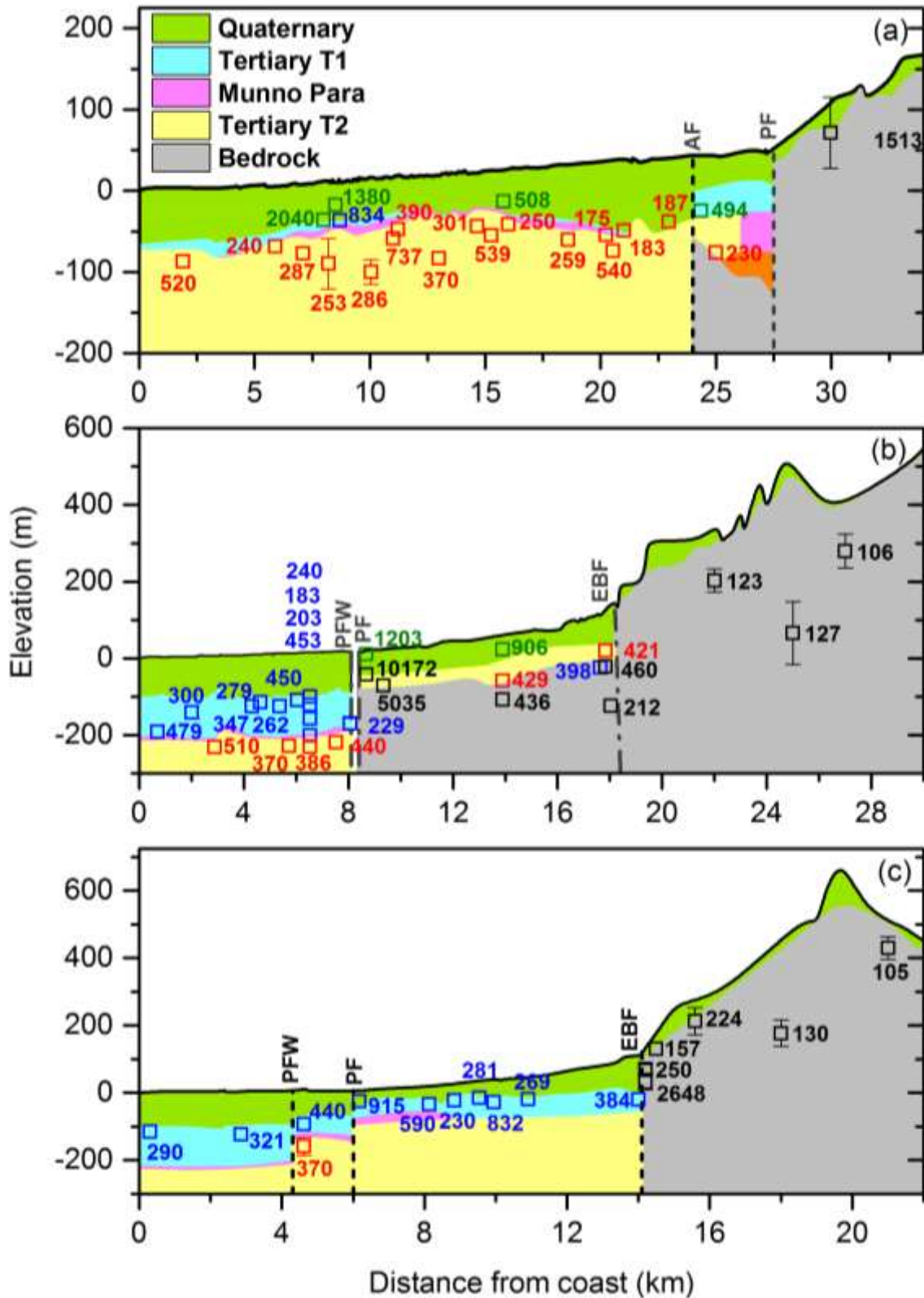
Apx Figure E.2 Major ion concentrations versus chloride concentrations showing groundwater samples from the Quaternary, T1, T2 and FRA aquifer systems. Both data obtained during the present study and data of Baird (2010) and Green et al. (2010) are shown.



Apx Figure E.3 Piper plot showing groundwater samples from the Quaternary, T1, T2 and fractured rock (FRA) aquifer systems. Both data obtained during the present study and data of Baird (2010) and Green et al. (2010) are shown.

Apx Table E.3 SI saturation indices for the Quaternary, T1, T2 and fractured rock (FRA) aquifer systems.

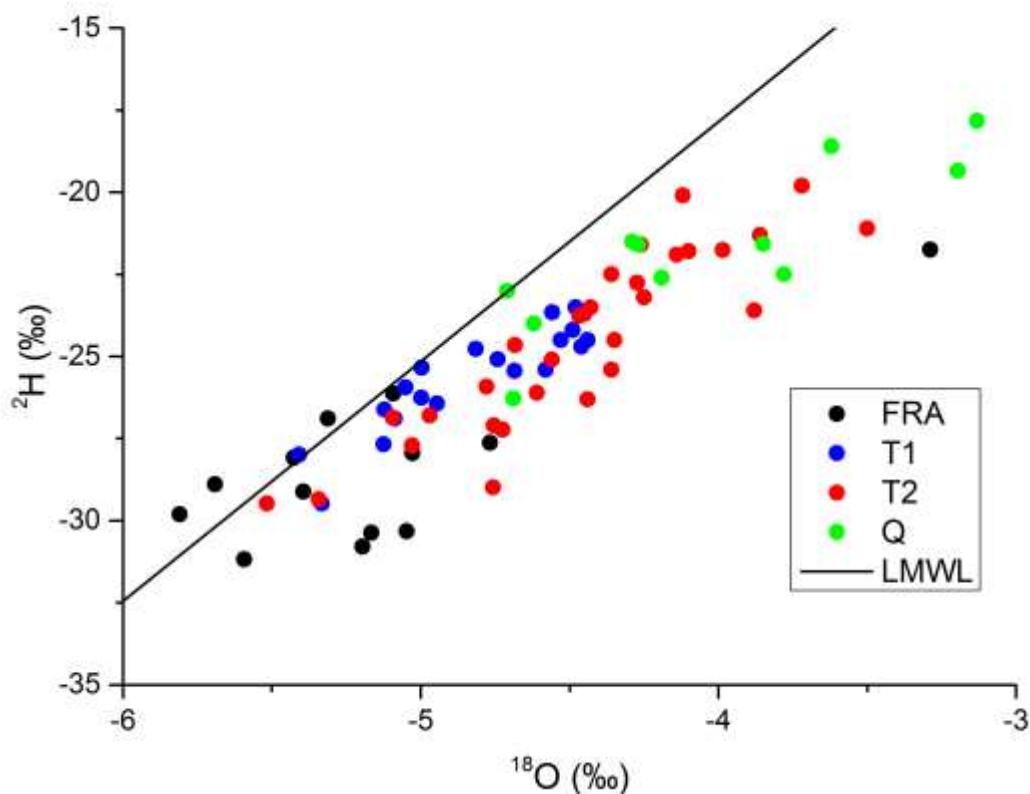
		Anhydrite	Aragonite	Halite	Calcite	CO <sub>2</sub> (g)	Dolomite	Gypsum
Q	MIN	-3.2	-1.5	-7.3	-1.4	-2.4	-2.5	-3.0
	MAX	-1.1	1.1	-4.0	1.2	-0.9	2.8	-0.8
	MEDIAN	-2.0	0.2	-5.4	0.4	-1.6	1.2	-1.8
T1	MIN	-2.6	-0.8	-6.1	-0.6	-3.2	-1.1	-2.4
	MAX	-1.5	1.3	-4.6	1.4	-0.7	3.0	-1.3
	MEDIAN	-2.1	0.0	-5.7	0.1	-2.2	0.3	-1.8
T2	MIN	-2.6	-1.5	-6.2	-1.4	-2.8	-2.5	-2.4
	MAX	-1.2	0.9	-4.4	1.1	-1.3	2.4	-1.0
	MEDIAN	-2.1	0.1	-5.6	0.3	-2.1	0.6	-1.8
FRA	MIN	-5.4	-4.4	-7.4	-4.2	-2.6	-7.9	-5.2
	MAX	-1.1	1.0	-3.1	1.1	-0.5	2.6	-0.9
	MEDIAN	-2.2	0.3	-6.1	0.5	-1.9	1.2	-2.0



Apx Figure E.4 Distribution of chloride (mg/L) along the three transects: (a) North Transect, (b) Central Transect, and (c) South Transect. Screen intervals for piezometers are shown using vertical bars only when screen lengths exceed the size of the symbols. Vertical broken lines indicate the approximate locations of the major faults: Alma Fault (AF), Para Fault (PF), Para Fault West (PFW), and Eden-Burnside Fault (EBF).

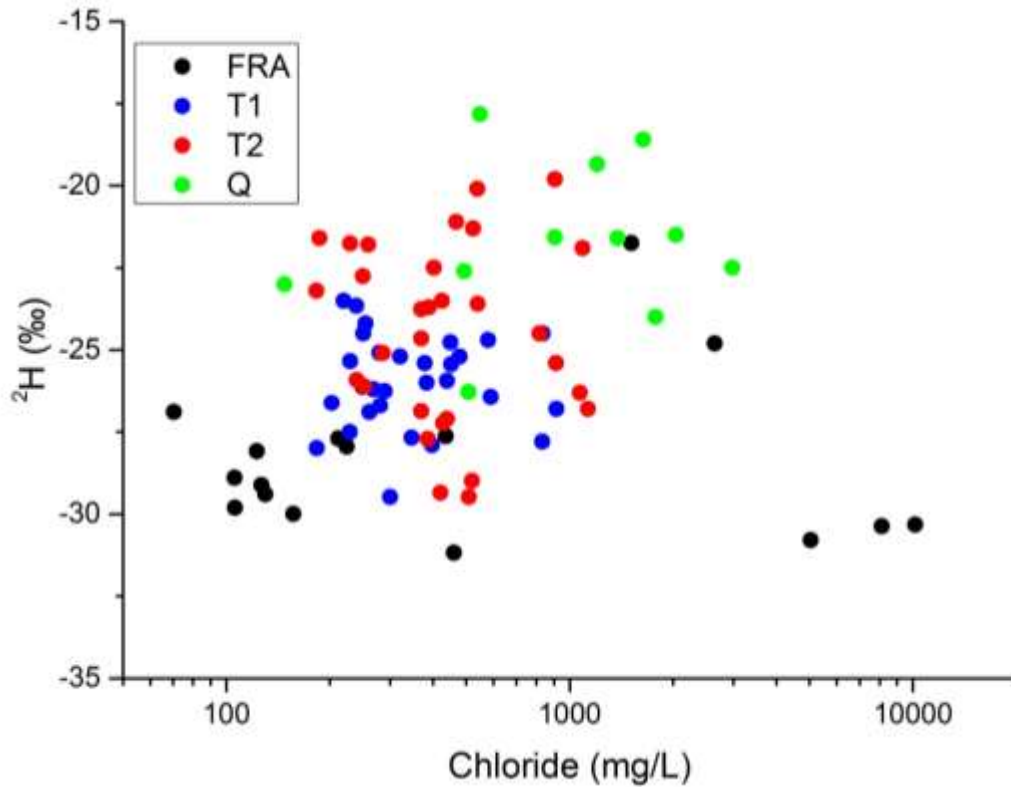
### E.3.2 STABLE ISOTOPES OF WATER

Apx Figure E.5 shows the relationship between  $^{18}\text{O}$  and  $^2\text{H}$  for piezometers sampled during the present study, and those sampled previously by Dighton et al. (1994) and Baird (2010). Results are also compared to the Local Meteoric Water Line (LMWL), which describes the approximate relationship between  $^{18}\text{O}$  and  $^2\text{H}$  values in Adelaide rainfall (Liu et al., 2010). Most groundwater samples fall to the right of the LMWL, which is consistent with evaporation of rainfall prior to recharge.



Apx Figure E.5 Relationship between oxygen-18 and deuterium ( $^2\text{H}$ ) values in groundwater. Both data obtained during the present study and data of Baird (2010) are shown. (Where piezometers were sampled in both studies, the most recent values are plotted.) The Local Meteoric Water Line (LMWL; Liu et al., 2010) is shown for comparison.

Apx Figure E.6 shows the relationship between  $^2\text{H}$  and chloride concentration for groundwater from the different aquifer units. In general, samples from the Quaternary aquifers have higher chloride concentrations and are more enriched in  $^2\text{H}$  than other groundwaters. This is consistent with evaporation and low rates of recharge to these aquifers. Samples from the fractured rock aquifers mostly have relatively low chloride concentrations and are relatively depleted in  $^2\text{H}$  and  $^{18}\text{O}$ . However, some of the samples from the fractured rock aquifers have higher chloride concentrations and more enriched  $^2\text{H}$  and  $^{18}\text{O}$  values. The piezometers with highest chloride concentrations are screened with the fractured rock aquifer (piezometers 5a, 5b and 22153), and are also depleted in stable isotopes (bottom right of Apx Figure E.6).



Apx Figure E.6 Relationship between deuterium values and chloride concentration for groundwater from different aquifer systems. Both data obtained during the present study and data previously obtained by Dighton et al. (1994) and Baird (2010) are shown. (Where piezometers were sampled more than once, the most recent values are plotted.).

### E.3.3 CARBON ISOTOPES

$\delta^{13}\text{C}$  values in groundwater samples range between -2.8 and -15.2 ‰, and  $^{14}\text{C}$  activities range from 0.4 to 91 pmC (Apx Figure E.7).  $^{14}\text{C}$  values in excess of 70 pmC are associated with  $\delta^{13}\text{C}$  values between approximately -9 and -15 ‰.  $\delta^{13}\text{C}$  values of -12 ‰ to -15 ‰ are consistent with a  $\delta^{13}\text{C}$  value for soil  $\text{CO}_2$  of approximately -22 ‰ and a +8 ‰ fractionation between gaseous  $\text{CO}_2$  and dissolved bicarbonate (Clark and Fritz, 1997). These values are therefore likely to reflect groundwater within the recharge areas. Higher  $\delta^{13}\text{C}$  values likely result from interaction with carbonate in the aquifer matrix.  $^{14}\text{C}$  values associated with  $\delta^{13}\text{C}$  above -12 ‰ have therefore been corrected for exchange with matrix carbonate using

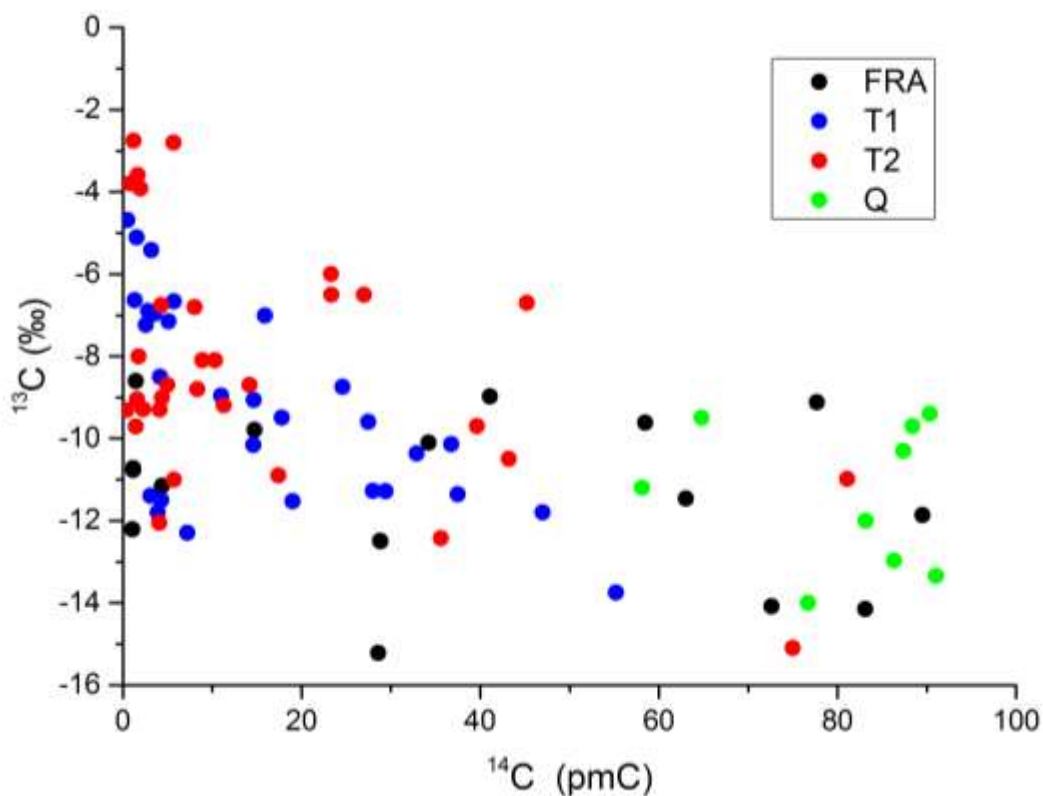
$$^{14}\text{C}_{\text{corr}} = ^{14}\text{C}_{\text{uncorr}} \frac{\delta^{13}\text{C}_{\text{rech}} - \delta^{13}\text{C}_{\text{carb}}}{\delta^{13}\text{C}_{\text{TDIC}} - \delta^{13}\text{C}_{\text{carb}}} \quad (1)$$

where  $^{14}\text{C}_{\text{corr}}$  is the corrected  $^{14}\text{C}$  activity,  $^{14}\text{C}_{\text{uncorr}}$  is the measured  $^{14}\text{C}$  activity on TDIC,  $\delta^{13}\text{C}_{\text{DIC}}$  is the measured  $\delta^{13}\text{C}$  activity on TDIC,  $\delta^{13}\text{C}_{\text{rech}} = -12$  ‰ is the assumed initial  $\delta^{13}\text{C}$  ratio in groundwater recharge and  $\delta^{13}\text{C}_{\text{carb}} = 0$  ‰ is the assumed  $\delta^{13}\text{C}$  ratio of carbonate in the aquifer matrix.

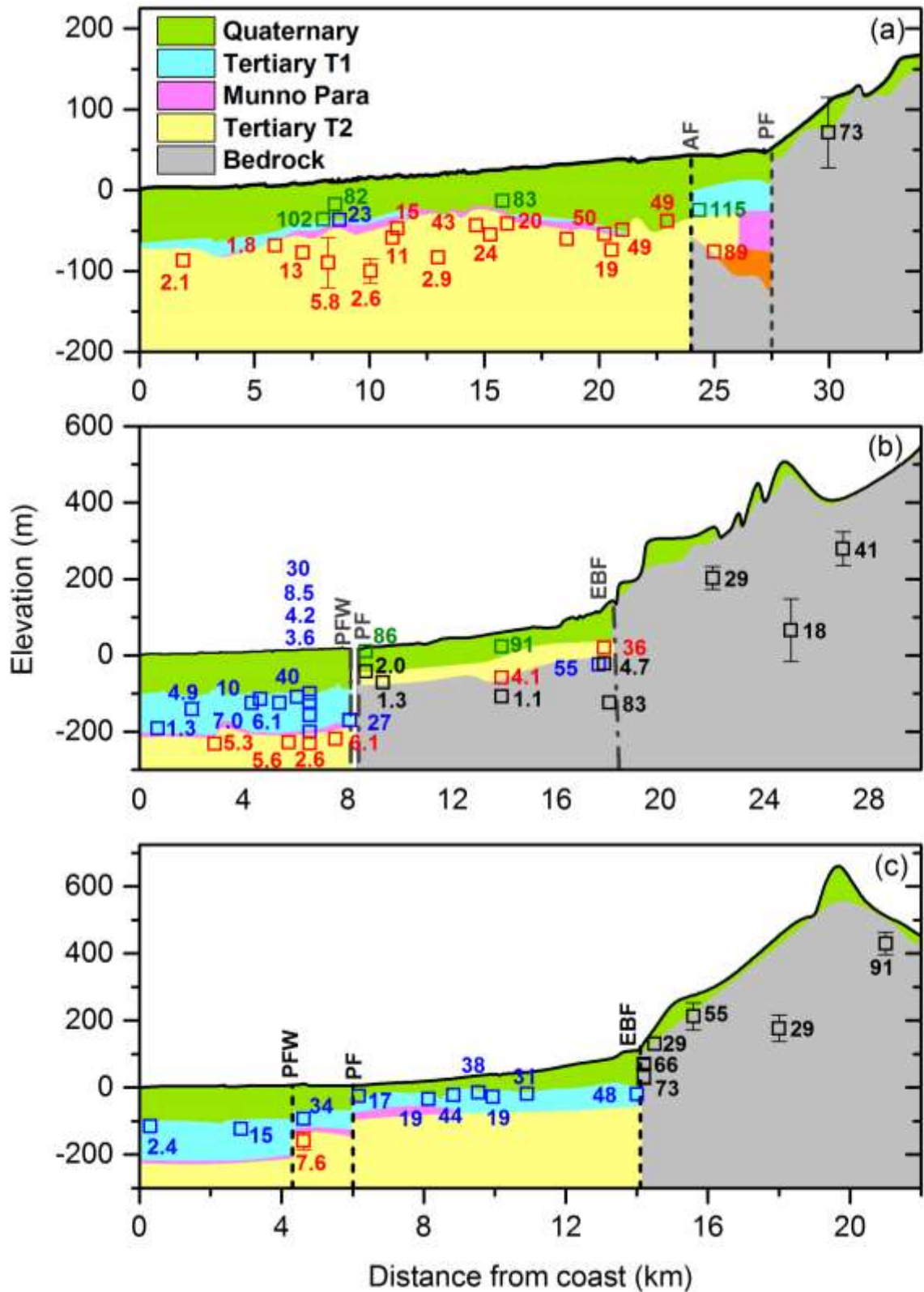
Apx Figure E.8 shows the distribution of corrected  $^{14}\text{C}$  activity along the three transects. Corrected  $^{14}\text{C}$  activities within the Quaternary aquifers are usually high (86 – 115 pmC), indicating that this water is relatively young. Within the main Tertiary aquifers,  $^{14}\text{C}$  activity decreases with depth and with distance from the Mount Lofty Ranges. This is most apparent along the central and southern transects in the T1 aquifer and along the northern transect in the T2 aquifer.

Apx Figure E.9 shows the distribution of apparent  $^{14}\text{C}$  age with depth and distance along the flow line within the T2 aquifer along the north transect. A clear increase in age with depth is apparent in the most up gradient piezometers (those between 20 and 25 km from the coast), and between the piezometers in the centre of the flow system (between 7 and 13 km from the coast). Leakage from the Quaternary into the T2 aquifer within the Adelaide Plains would be expected to lead to younger water at the top of the aquifer. However this is not apparent in Apx Figure E.9, and at all depths there appears to be a consistent increase in age between 20-25 km and 7-13 km. The increase in age between these two groups of piezometers is approximately 8000 years, giving a mean flow velocity of 1.1 m/y.

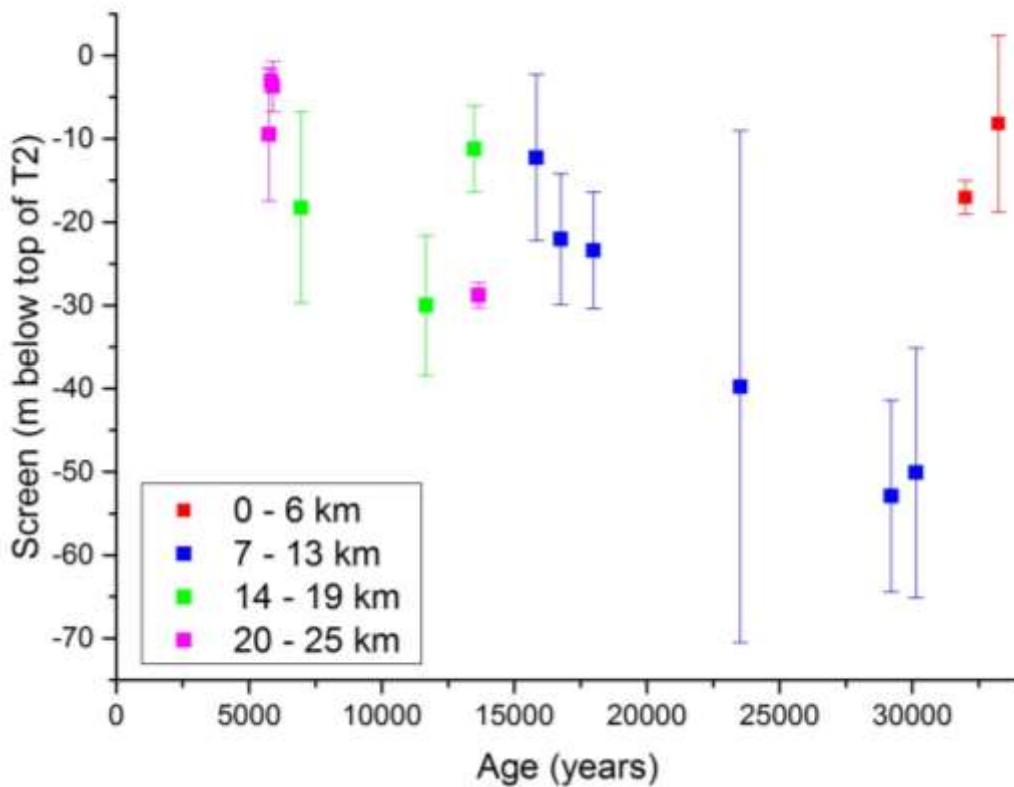
Apx Figure E.10 shows the relationship between distance from the coast and  $^{14}\text{C}$  age for all aquifers and all three transects. Although this figure groups together piezometers screened at different depths, an increase in age along the flow line is still apparent – particularly in the T2 aquifer in the north transect and the T1 aquifer in the south transect. In the south transect, the groundwater flow velocity within the T1 aquifer appears to decrease west of the Para Fault. The rate of increase in age with distance is approximately 1.8 y/m between the Eden-Burnside Fault and the Para Fault, giving a mean flow velocity of 0.6 m/y. West of the Para Fault, the rate of increase in age with distance is approximately 5.9 y/m, giving a flow velocity of 0.2 m/y, although data in this part of the system is limited, and this flow velocity is dependent on the  $^{14}\text{C}$  derived groundwater age at a single piezometer (ADE005). The apparent decrease in velocity may be partly due to an increase in aquifer thickness to the west of the Para Fault, but could also indicate loss of water to the overlying Quaternary aquifer and/or the underlying T2 aquifer. Although modern head gradients do not indicate leakage in these directions (Appendix G), current gradients would have been impacted by pumping and so do not reflect the flow directions under pre-development conditions. Although there is more scatter, an apparent increase in age with distance is also apparent in the T1 aquifer west of the Para Fault in the central transect. The apparent  $^{14}\text{C}$  age increases from close to 10,000 years near the fault to over 35,000 years near the coast, a rate of increase of approximately 3.6 y/m, giving a flow velocity of approximately 0.3 m/y.



Apx Figure E.7 Relationship between  $^{14}\text{C}$  activity and  $^{13}\text{C}$  value for groundwater samples. Both data obtained during the present study and data previously obtained by Dighton et al. (1994) and Baird (2010) are shown. (Where piezometers were sampled more than once, the most recent values are plotted.)



Apx Figure E.8 Distribution of corrected  $^{14}\text{C}$  activity (pmC) along the three transects: (a) North Transect, (b) Central Transect, and (c) South Transect. Screen intervals for piezometers are shown using vertical bars, only when screen lengths exceeded the size of the symbols. Vertical broken lines indicate the approximate locations of the major faults: Alma Fault (AF), Para Fault (PF), Para Fault West (PFW), and Eden-Burnside Fault (EBF).

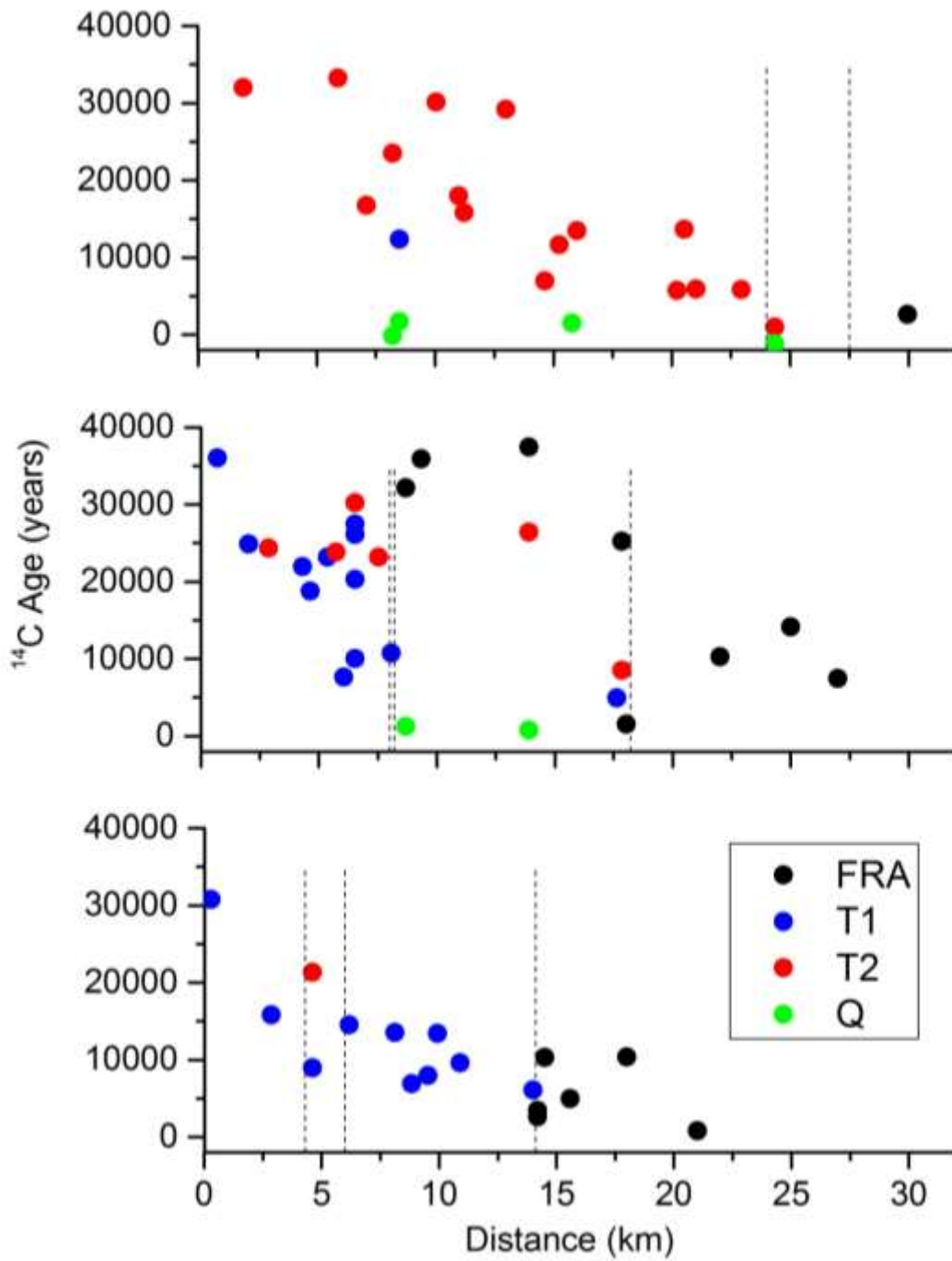


Apx Figure E.9 Relationship between corrected  $^{14}\text{C}$  age and location within the T2 aquifer along the north transect. The corrected  $^{14}\text{C}$  age is plotted versus the location of the piezometer screen below the top of the T2 aquifer at that location. (Vertical bars denote the length of the piezometer screen.) Piezometers are grouped according to their horizontal distance along the transect (0 – 6, 7 – 13, 14 – 19 and 20 – 25 km from the coast). Both data obtained during the present study and data previously obtained by Dighton et al. (1994) and Baird (2010) are shown. Where piezometers were sampled more than once, the most recent values are plotted.

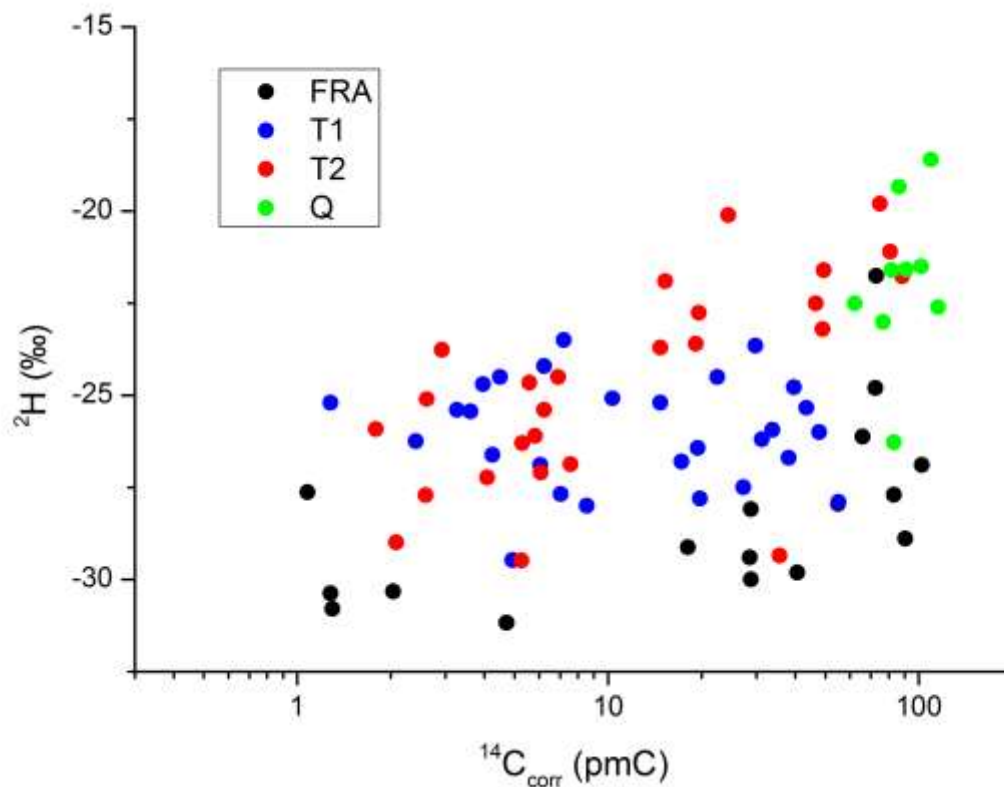
There is no clear pattern of increasing  $^{14}\text{C}$  age with distance in the central transect, although the oldest sample occurs closest to the coast. It appears likely that this transect does not represent a flowline, and that there is little flow in the T2 aquifer between the Eden-Burnside Fault and the Para Fault in this part of the system. Rather, flow within the T1 aquifer west of the Para Fault is likely derived from areas further north and south, with these flowlines converging west of the fault.

It is noteworthy that some very high  $^{14}\text{C}$  activities (young  $^{14}\text{C}$  ages) were measured close to the faults that separate the Mount Lofty Ranges from the plains (the Para Fault in the north, and the Eden-Burnside Fault in the south). This may indicate preferential movement of groundwater across the fault onto the plains, and suggests that this flow may occur at significant depth. Thus a  $^{14}\text{C}$  activities of 89 pmC was measured on MPA140, located between the Para and Alma Faults on the north transect and screened at 112-125 m depth, and a  $^{14}\text{C}$  activity of 83 pmC was measured on ADE138 screened at 277-287 m depth in the fractured rock immediately west of the Eden-Burnside Fault on the central transect.

Apx Figure E.11 shows the relationship between corrected  $^{14}\text{C}$  activity and  $^2\text{H}$ . Although there is considerable scatter, there is a trend for decreasing  $^2\text{H}$  values with decreasing  $^{14}\text{C}$  activity. This may indicate that some of the older samples were recharged under a colder climate.



Apx Figure E.10 Relationship between corrected  $^{14}\text{C}$  activity and distance from the coast along the three transects. Scales are the same for all three transects to permit easy comparison. Both data obtained during the present study and data previously obtained by Dighton et al. (1994) and Baird (2010) are shown. Where piezometers were sampled more than once, the most recent values are plotted.



Apx Figure E.11 Relationship between corrected  $^{14}\text{C}$  activity and  $^2\text{H}$  values in groundwater. Both data obtained during the present study and data previously obtained by Dighton et al. (1994) and Baird (2010) are shown. Where piezometers were sampled more than once, the most recent values are plotted.

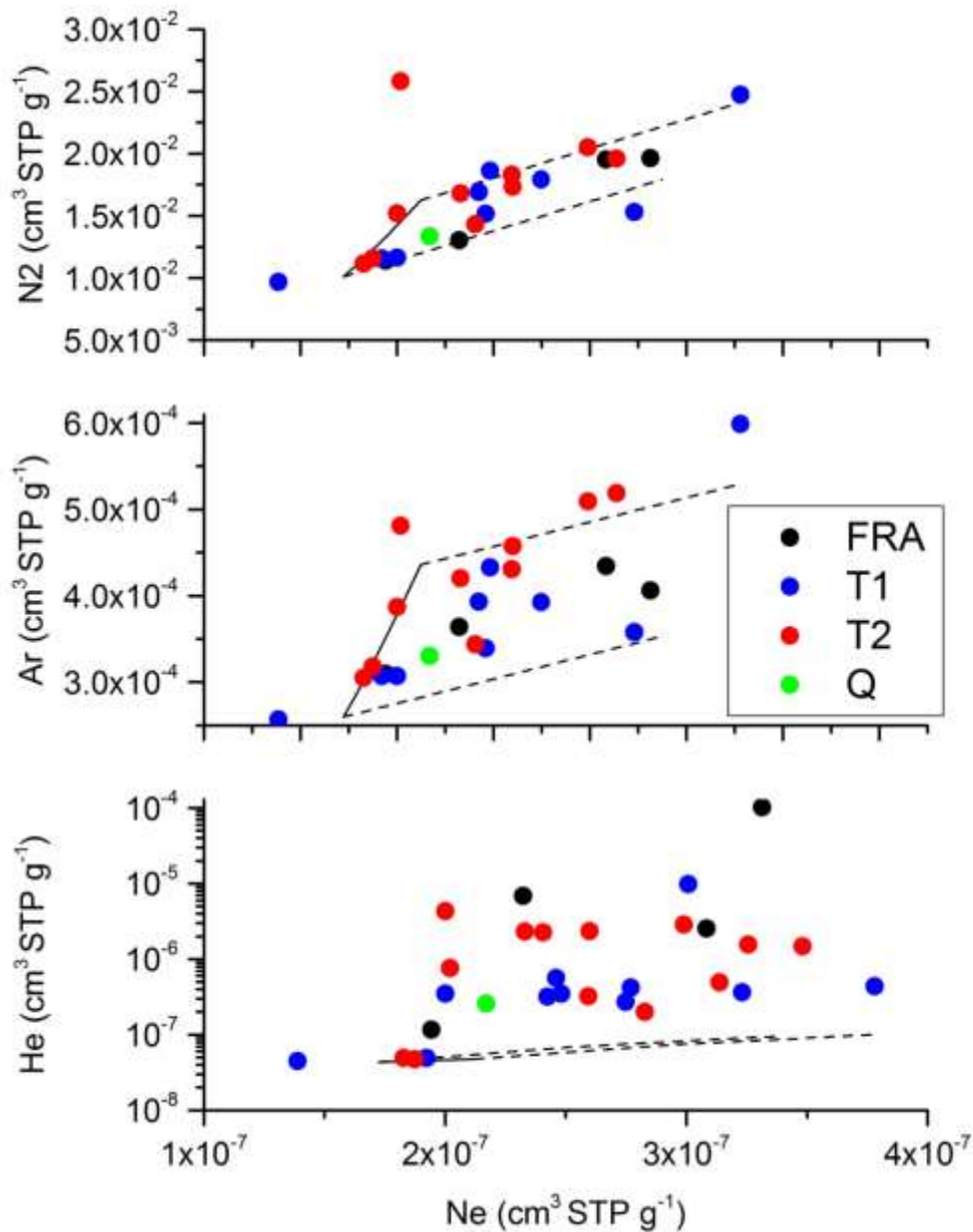
### E.3.4 NOBLE GASES AND $\text{N}_2$

Atmospheric noble gases dissolve in water in accordance with their solubility. The dissolved concentration is therefore a function of recharge temperature, pressure and salinity, as these affect the gas solubility. In some cases, elevated concentrations of all gases occur due to entrapment and subsequent dissolution of air bubbles in recharging groundwater. This process (termed *excess air*) is believed to be most significant where recharge occurs very rapidly (Heaton and Vogel, 1981). Subsequent to recharge,  $\text{N}_2$  concentrations can be affected by geochemical processes (e.g., denitrification), and He concentrations can increase due to subsurface production of He by radioactive decay of uranium and thorium within the aquifer matrix. Ar concentrations can also increase due to subsurface production associated with radioactive decay of  $^{39}\text{K}$ , but this is usually insignificant.

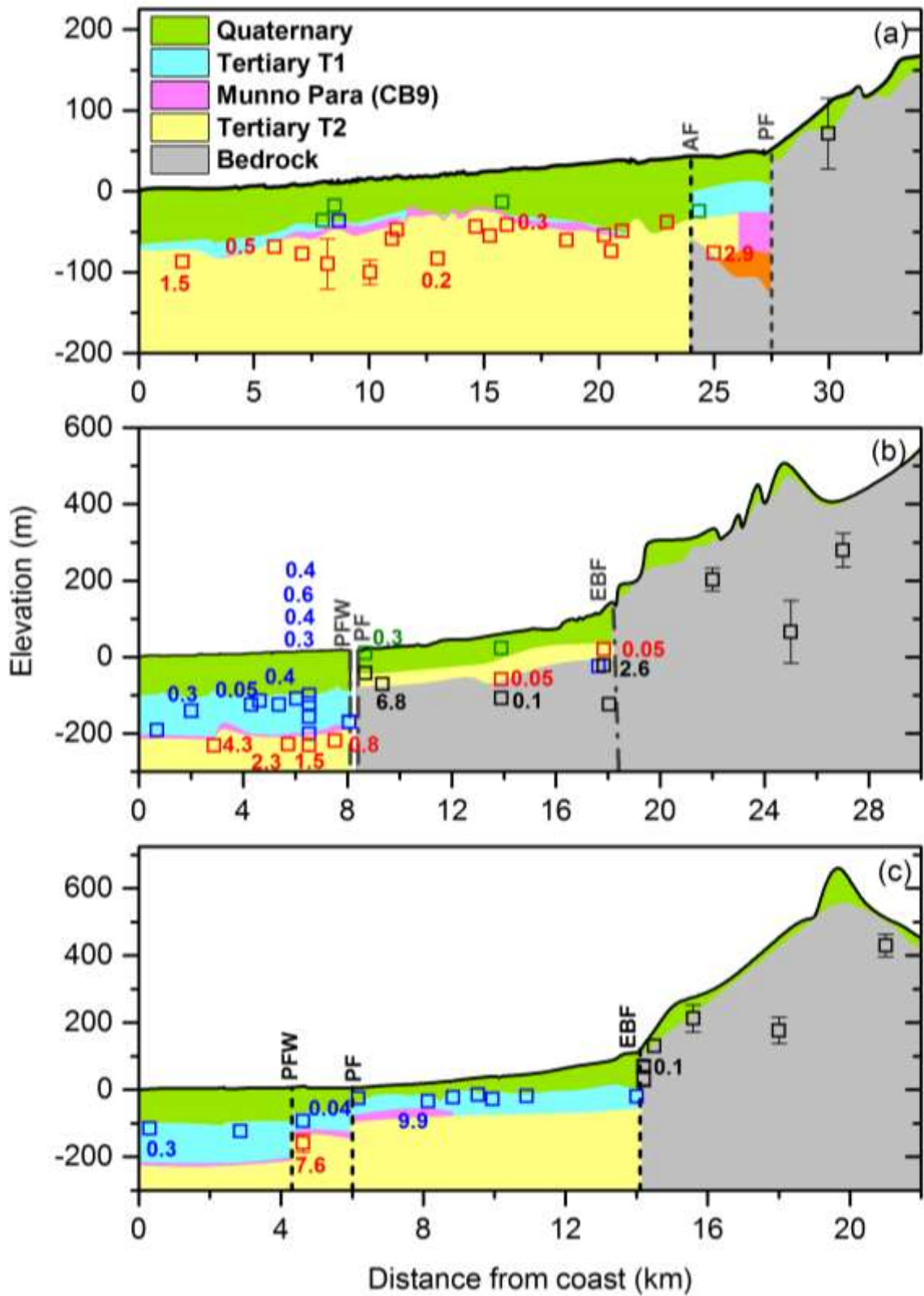
Apx Figure E.12 compares measured noble gas and  $\text{N}_2$  concentrations in groundwater with expected concentrations based on recharge temperatures between 5 and 30°C and excess air of less than 10  $\text{cm}^3 \text{kg}^{-1}$ . Most samples fall within these envelopes. Exceptions to this include piezometer ADE207, which has a low Ne concentration – possibly indicating loss of gas during sampling or analysis. A small number of other samples also have unusually high argon concentrations. These are piezometers 6d, PTA115, MPA140 and ADE191, and resampling of these wells is needed to confirm the results.

Almost all He concentrations are greater than can be explained by equilibrium with atmospheric He at the time of recharge, and indicate subsurface production of He within the aquifer. Based on recharge temperatures between 5 – 30°C and up to 10  $\text{cm}^3 \text{kg}^{-1}$  of excess air, equilibrium He concentrations should be between  $4.35 \times 10^{-8} \text{ cm}^3/\text{g}$  and  $9.99 \times 10^{-8} \text{ cm}^3/\text{g}$ . Values for four samples fall within this range, but others show concentrations up to three orders of magnitude higher.

Apx Figure E.13 shows the distribution of He along the three transects. The greatest number of measurements were made in the central transect, and the helium concentrations in the T2 aquifer show a progression along the flow line. East of the Para Fault, helium concentrations in the T2 aquifer are close to equilibrium with the atmosphere ( $4.7 - 4.9 \times 10^{-8} \text{ cm}^3/\text{g}$ ). West of the Para Fault, however, helium concentrations increase from  $7.6 \times 10^{-7} \text{ cm}^3/\text{g}$  to  $4.3 \times 10^{-6} \text{ cm}^3/\text{g}$  over a distance of less than five kilometres.  $^{14}\text{C}$  data from this part of the aquifer do not show the same trend of increasing age with distance along the flow line. However, uncorrected  $^{14}\text{C}$  ages are very low ( $< 2 \text{ pmC}$ ; corrected values  $2 - 7 \text{ pmC}$ ). For such low values, analytical uncertainty becomes significant, as does uncertainty in the correction, and hence the calculated  $^{14}\text{C}$  ages are likely to be unreliable.



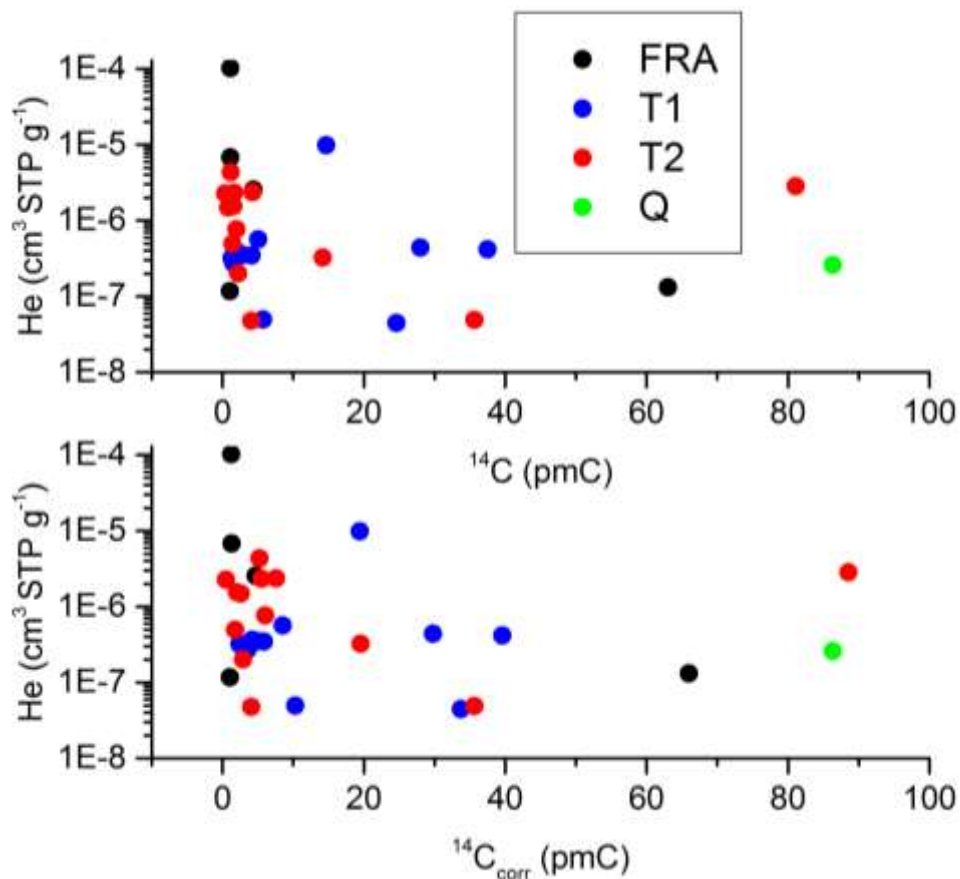
Apx Figure E.12 Comparison of measured concentrations of neon, argon, helium and nitrogen in groundwater, with expected concentrations based on equilibrium solubility of atmospheric gases in water at temperatures between 5 and 30°C, and excess air volumes up to  $10 \text{ cm}^3 \text{ kg}^{-1}$ . (The solid line indicates the relationship between gas concentrations based on water temperatures between 5 and 30°C, with lower concentrations at higher temperatures. Broken lines indicate the effect of  $0 - 10 \text{ cm}^3 \text{ kg}^{-1}$  excess air.) Note that helium is plotted on a logarithmic scale, whereas the scale for the other gases is linear.



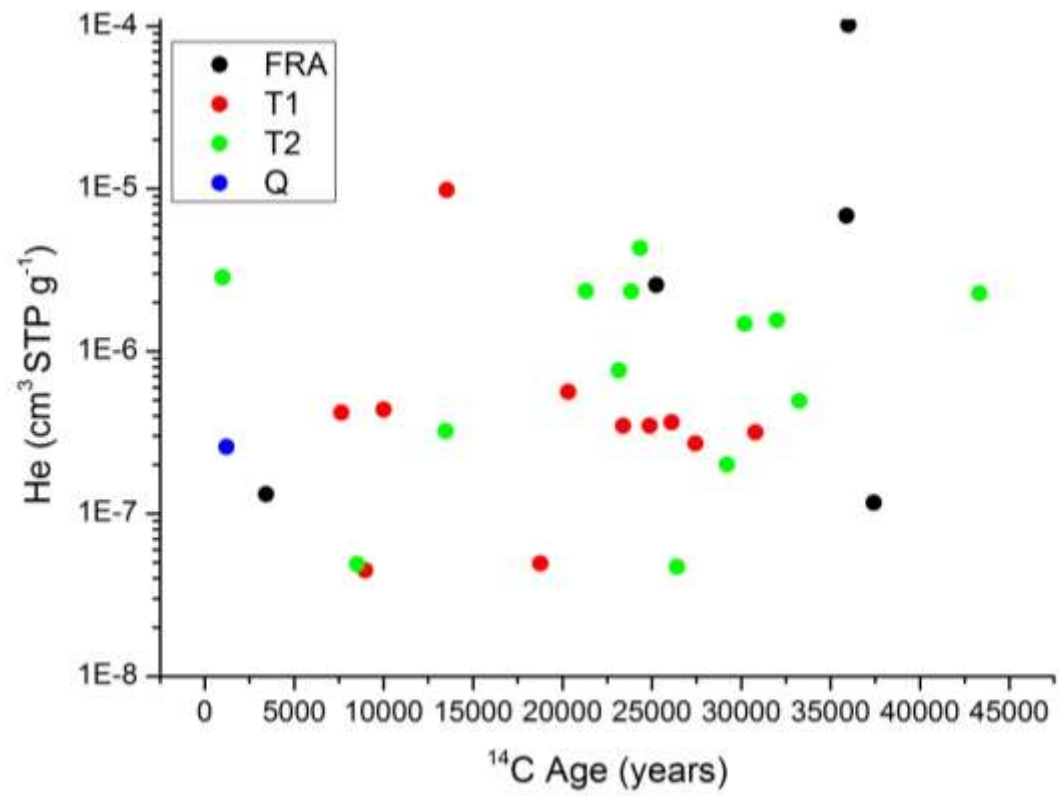
Apx Figure E.13 Distribution of helium ( $10^{-6} \text{ cm}^3/\text{g}$ ) along the three transects: (a) North Transect, (b) Central Transect, and (c) South Transect. Screen intervals for piezometers are shown using vertical bars, only when screen lengths exceeded the size of the symbols. Vertical broken lines indicate the approximate locations of the major faults: Alma Fault (AF), Para Fault (PF), Para Fault West (PFW), and Eden-Burnside Fault (EBF).

Apx Figure E.14 shows He versus both corrected and uncorrected  $^{14}\text{C}$  activity. If the elevated He concentration are due to subsurface production, then a relationship between He and  $^{14}\text{C}$  would be expected. Although Apx Figure E.14 indicates that the highest He concentrations are generally associated with low  $^{14}\text{C}$  values, there is no clear relationship between He concentration and  $^{14}\text{C}$  activity. Apx Figure E.15 compares He concentrations and  $^{14}\text{C}$  ages. A constant rate of He production would produce a linear relationship between He and  $^{14}\text{C}$  age. This is not apparent in Apx Figure E.15, even when individual aquifers are considered. This suggests that other processes are affecting either the He concentrations or  $^{14}\text{C}$  activities.

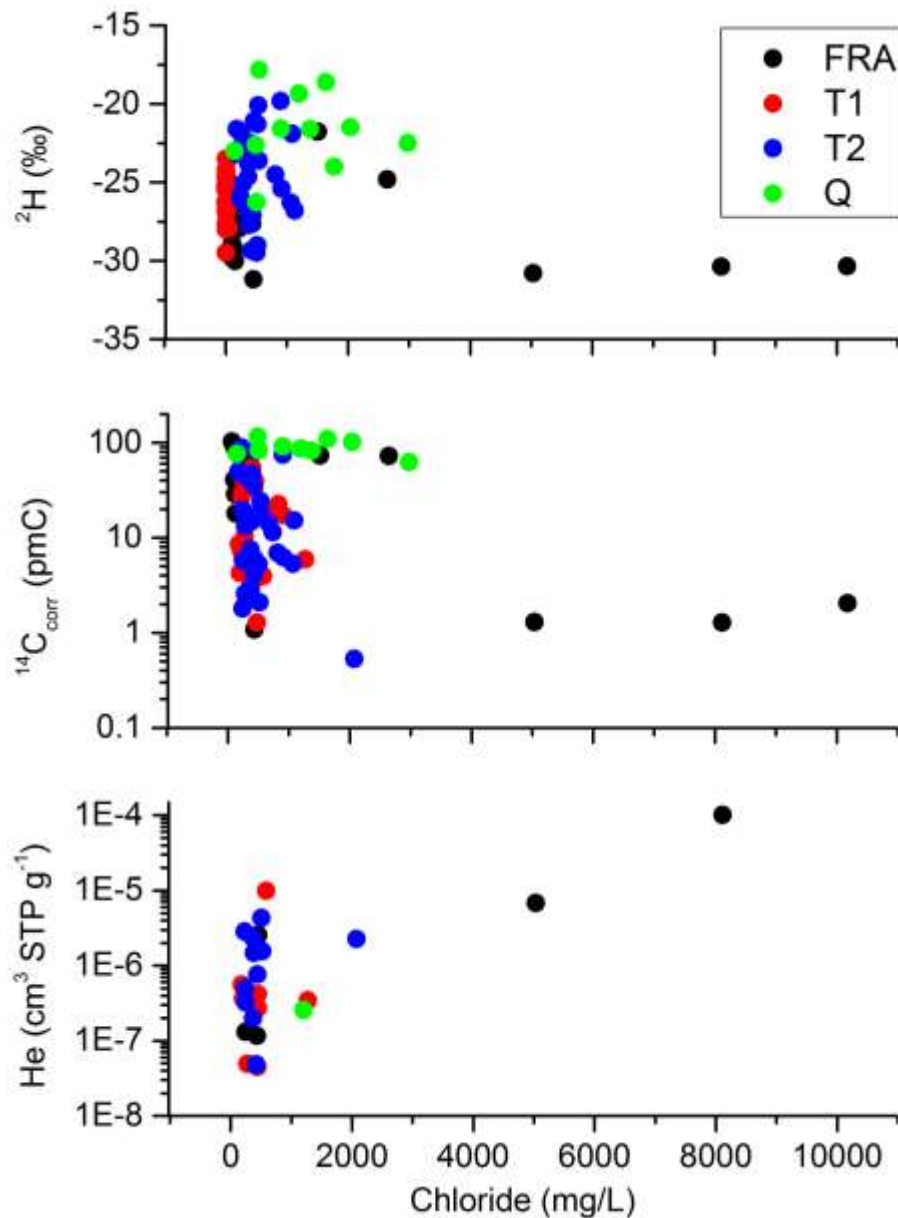
Figure 16 compares chloride concentrations with  $^2\text{H}$  values, corrected  $^{14}\text{C}$  activities and He concentrations for wells sampled as part of the current study. Four samples stand out from the others as having high chloride and helium concentrations, depleted  $^2\text{H}$  values and low  $^{14}\text{C}$  activities: 5a, 5b, 22153 from the fractured rock aquifer and 13a from the T2. (Helium and  $^2\text{H}$  were only analysed on three of these four piezometers.) These samples suggest the existence of old, saline groundwater in parts of the aquifer. Post et al. (Appendix G) have also identified the existence of brines beneath the Willunga Basin aquifers, and suggested that they are not linked to seawater intrusion processes. Three of these piezometers occur close to the Para Fault, and may indicate either old groundwater that has become isolated from the flow system by displacement of the aquifers, or upward leakage of brines from basement aquifers.



Apx Figure E.14 Relationship between corrected and uncorrected  $^{14}\text{C}$  activity and dissolved helium concentration.



Apx Figure E.15 Helium concentrations versus estimated <sup>14</sup>C ages in groundwater.



Apx Figure E.16 Helium, corrected  $^{14}\text{C}$  and deuterium versus chloride.

## E.4 Discussion

Estimating flow velocities in confined aquifers from groundwater age data requires information on both the vertical and horizontal distribution of groundwater ages. Despite extensive sampling for  $^{14}\text{C}$  and He in the Adelaide Plains aquifers, the data is still sparse relative to the complexity of the aquifer systems. The best data set is from the T2 aquifer along the north transect, which shows decreases in  $^{14}\text{C}$  activity (and hence increases in  $^{14}\text{C}$  age) with increasing depth, and with increasing distance from the Mount Lofty Ranges. There is a consistent increase in age at all depths between piezometers located between 20 – 25 km from the coast (3 – 8 km from the edge of the ranges) and those 7-13 km from the coast (15 – 21 km from the ranges). The increase in age between these two groups of piezometers is approximately 8000 years, giving a mean flow velocity of 1.1 m/y. When piezometers screened at all depths are plotted versus distance from the coast, an increase in age with distance is also apparent in the T1 aquifer in the central and southern transects. (There is insufficient data to determine relationships in other aquifers.) Along the central transect, the apparent  $^{14}\text{C}$  age in the T1 aquifer increases from close to 10,000 years near the fault to over

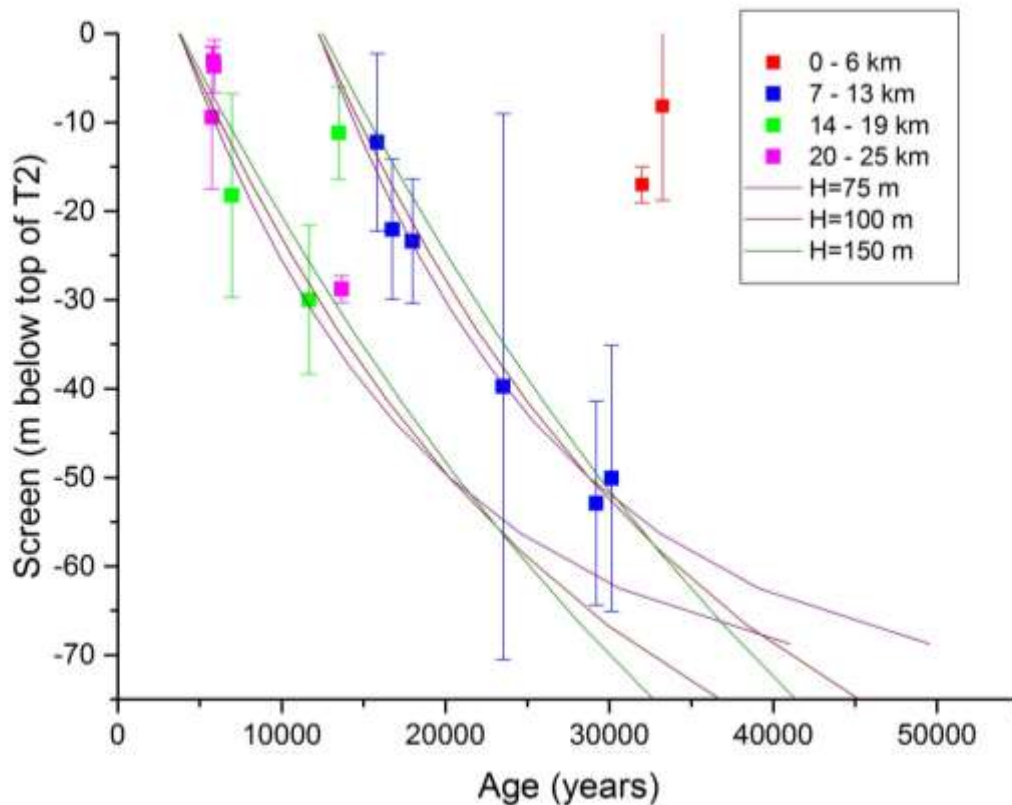
35,000 years near the coast, giving a flow velocity of approximately 0.3 m/y. Along the south transect, the flow velocity in the T1 aquifer between the Eden-Burnside Fault and the Para Fault is estimated to be approximately 0.6 m/y, although west of the Para Fault this decreases to 0.2 m/y. The slower flow velocity west of the Para Fault along both transects may indicate loss of water to the Quaternary aquifer (and subsequent loss from the Quaternary aquifer by evapotranspiration).

The presence of old water near the top of the T2 aquifer in the north transect suggests against significant leakage into the aquifer from the overlying Quaternary aquifers within the Adelaide Plains region. On this basis, we have modelled the T2 aquifer as a confined aquifer with flow derived entirely from the Mount Lofty Ranges. In such an aquifer, the groundwater age distribution will be a function of the recharge rate in the area where the confined aquifer is recharged, and the length of the flow system in both the unconfined and confined parts of the system. This can be simply expressed as

$$t = \frac{H\varepsilon}{R} \ln\left(\frac{H}{H-z}\right) + \frac{x^*H\varepsilon}{Rx} \quad (2)$$

where  $t$  is the groundwater age,  $H$  is the aquifer thickness,  $R$  is the recharge rate in the unconfined part of the aquifer,  $x$  is the length of the unconfined recharge zone,  $x^*$  is the distance along the confined part of the aquifer,  $\varepsilon$  is porosity and  $z$  is the depth (Cook and Bohlke, 2000). This model assumes that the aquifer is of constant thickness, and uniform porosity and hydraulic conductivity, and that no leakage occurs into the aquifer in the confined part of the system. It also considers only advective ages, and ignores the influence of diffusion and dispersion on the tracer distribution (Weissmann et al., 2002). Nevertheless, although the model is highly simplified, it can be useful for interpreting age distributions.

If we have groundwater age profiles at different locations within a confined aquifer, then it is possible to use Equation 2 to constrain aquifer parameters. Apx Figure E.17 shows the best fit to the data from the T2 aquifer along the north transect. Since the aquifer thickness is uncertain, we have estimated parameters for three different aquifer thicknesses (Apx Table E.4). If the aquifer is thinner then high values of  $R/\varepsilon$  and lower values of  $x^*$  are required to fit the data. Values of  $R/\varepsilon$  for the three models vary between 0.0036 and 0.004 m/y. Based on a porosity of  $\varepsilon = 0.3$ , this gives recharge rates of 11 and 15 mm/y within the Mount Lofty Ranges. (Note that these are pre-development recharge rates.) However, some of the recharge must travel significant distances within the Mount Lofty Ranges, because the water at the base of the Tertiary aquifers close to the fault is relatively old. If recharge occurs over only a relatively small area, then we would expect to see much less variation in groundwater age with depth. All of these models give a horizontal groundwater velocity of approximately 1.45 m/year. Estimated volumes of flow from the Mount Lofty Ranges to the plains are dependent upon the assumed aquifer thickness, and range between 33 and 65 m<sup>2</sup>/y. Assuming that similar flow rates occur along the boundary between the ranges and the plains in other areas, this equates to a total flow of between  $2 \times 10^6$  and  $4 \times 10^6$  m<sup>3</sup>/y (2 – 4 GL/y).



Apx Figure E.17 Comparison between measured apparent  $^{14}\text{C}$  ages in the T2 aquifer along the North Transect and results of the advective model (Equation A.1) based on different values of aquifer thickness (H).

Recharge rates can also be determined using a chloride mass balance approach. The median chloride concentrations within the fractured rock aquifer is 318 mg/L (see Appendix C). Based on a mean chloride concentration in rainfall of 5 mg/L and rainfall of 1000 mm/y (representative of a recharge location within the Mount Lofty Ranges rather than within the Adelaide Plains), we estimate a recharge rate of approximately 16 mm/y. This is in excellent agreement with the values determined from the vertical  $^{14}\text{C}$  age profiles.

Apx Table E.4 Best fit values for the advective model.

	H (m)	$R/\varepsilon$ (m/y)	x (km)
Scenario 1	75	0.005	22
Scenario 2	100	0.0042	35
Scenario 3	150	0.0036	60

Groundwater in the T2 aquifer west of Para Fault was sampled in the central transect but is beyond the limit of reliable  $^{14}\text{C}$  dating. An increase in groundwater age along the flow path in the central transect, however, is apparent from the He data. Unfortunately, it is not possible to estimate a groundwater age from helium, because the release rate of helium from aquifer material is unknown. Often, it is possible to estimate the release rate based on a relationship between He concentration and  $^{14}\text{C}$  age determined from groundwater that is within the limits of  $^{14}\text{C}$  dating (Castro et al., 2000). However, in this study no such relationship could be established. The lack of a relationship is unlikely to be the result of small-scale heterogeneity in the helium production and release rate. Along low flow paths the dissolved helium concentration should reflect the average release rate and not be affected by small-scale variations. The rate

of helium production and release can therefore not be accurately determined. It is likely that the poor relationship between helium concentration and  $^{14}\text{C}$  activity is due to mixing with very old groundwater in deeper parts of the aquifer. A small number of groundwater samples have high chloride concentrations and these also have low  $^{14}\text{C}$  activities and high He concentrations. Mixing of a small amount of very old water into samples of younger water will have less effect on  $^{14}\text{C}$  age, because the  $^{14}\text{C}$  activity of water older than 50,000 years is close to zero.

## E.5 Conclusions

Geochemical analysis of groundwater within the Adelaide Plains region, and adjacent areas of the Mount Lofty Ranges suggests:

1. Groundwater within the Adelaide Plains Tertiary aquifers (T1 and T2) originates from recharge within the Mount Lofty Ranges. Recharge rates within the Mount Lofty Ranges are 10 – 15 mm/year.
2. Flow across the Alma Fault from the Mount Lofty Ranges into the Northern Adelaide Plains is estimated to be between 33 and 65  $\text{m}^2/\text{y}$ . Assuming that similar flow rates occur along the boundary between the ranges and the plains further south, this equates to a total flow from the Mount Lofty Ranges to the plains across the region of between  $2 \times 10^6$  and  $4 \times 10^6$   $\text{m}^3/\text{y}$  (2 – 4 GL/y).
3. In the central and southern areas, groundwater flow velocities west of the Para Fault are much slower than those between the Eden-Burnside Fault and the Para Fault. This may indicate inter-aquifer leakage either associated with the Para Fault, or in downgradient areas. It is possible that some of this leakage was to the Quaternary aquifers, from where it was subsequently lost to evapotranspiration.
4. Pockets of very old groundwater (possibly exceeding hundreds of thousands of years old) occur close to some of the major fault zones. Mixing between such very old groundwater, and relatively young groundwater flowing from the Mount Lofty Ranges affects the utility of helium as a groundwater dating tool in this environment.

## E.6 References

- Aeschbach-Hertig W., Peeters F., Beyerle U. and Kipfer R. (1999) Interpretation of dissolved atmospheric noble gases in natural waters. *Water Resour. Res.*, 35(9):2779-2792.
- Allison G.B., Gee G.W. and Tyler S.W. (1994) Vadose-zone techniques for estimating groundwater recharge in arid and semi-arid regions. *Soil Sci. Soc. Am. J.*, 58:6-14.
- Baird D.J. (2010) Groundwater recharge and flow mechanisms in a perturbed, buried aquifer system: Northern Adelaide Plains, South Australia. PhD Thesis, Flinders University .
- Castro M.C., Stute M. and Schlosser P. (2000) Comparison of  $4\text{He}$  ages and  $^{14}\text{C}$  ages in simple aquifer systems: implications for groundwater flow and chronologies. *Applied Geochemistry*, 15: 1137-1167.
- Clark I.D. and Fritz P. (1997) *Environmental Isotopes in Hydrogeology*. Lewis, Boca Raton. 328p.
- Cook P.G. and Bohlke J.K. (2000) Determining timescales for groundwater flow and solute transport. In P.G. Cook and A.L. Herczeg (ed.) *Environmental Tracers in Subsurface Hydrology*. Kluwer, Boston, pp.1-30.
- Cook P.G., Solomon D.K., Plummer L.N., Busenberg E. and Schiff S.L. (1995) Chlorofluorocarbons as tracers of groundwater transport processes in a shallow, silty sand aquifer. *Water Resour. Res.*, 31: 425-434.

- Dighton J.C., Herczeg A.L., Leaney F.W., Lennard R.P., Love A.J. and Gerges N.Z. (1994) Stable isotope and radiocarbon data for groundwaters from the Adelaide metropolitan area. Centre for Groundwater Studies, Report No. 56.
- Gardner P. and Solomon D. (2009) An advanced passive diffusion sampler for the determination of dissolved gas concentrations. *Water Resour. Res.*, 45(6).
- Gat JR (1996) Oxygen and hydrogen isotopes in the hydrologic cycle. *Annu. Rev. Earth Planet. Sci.*, 24: 225-262.
- Gerges N.Z. (1999) The geology and hydrogeology of the Adelaide metropolitan area. PhD thesis, Flinders University, Adelaide.
- Green G, Watt E, Alcoe D, Costar A and Mortimer L (2010) Groundwater flow across regional scale faults. Department for Water, Technical Report DFW 2010/15.
- Heaton T.H.E. and Vogel J.C. (1981) 'Excess air' in groundwater. *J. Hydrol.*, 50: 201-216.
- Harrington G.A., Cook P.G. and Herczeg A.L. (2002) Spatial and temporal variability of ground water recharge in central Australia: a tracer approach. *Ground Water*, 40(5):518-527.
- Liu J., Fu G., Song X., Charles S.P., Zhang Y., Han D. and Wang S. (2010) Stable isotope compositions in Australian precipitation. *J. Geophys. Res.*, 115(D23):D23307.
- Poole J.C., McNeill G.W., Langman S.R. and Dennis F. (1997) Analysis of noble gases in water using a quadrupole mass spectrometer in static mode. *Applied Geochemistry*, 12(6): 707-714.
- Plummer L.N. and Busenberg E. (2000) Chlorofluorocarbons. In P.G. Cook and A.L. Herczeg (ed.) *Environmental Tracers in Subsurface Hydrology*. Kluwer, Boston, pp.441-478.
- Solomon D.K. and Cook P.G. (2000)  $^3\text{H}$  and  $^3\text{He}$ . In P.G. Cook and A.L. Herczeg (ed.) *Environmental Tracers in Subsurface Hydrology*. Kluwer, Boston, pp.397-424.
- Solomon D.K. and Cook P.G. (2000)  $^4\text{He}$  in groundwater. In P.G. Cook and A.L. Herczeg (ed.) *Environmental Tracers in Subsurface Hydrology*. Kluwer, Boston, pp.425-439.
- Stuiver M. and Polach H.A. (1977) Discussion: Reporting of  $^{14}\text{C}$  data. *Radiocarbon*, 19(3): 355-363.
- Vergagen B.T. (1992) Detailed geohydrology with environmental isotopes. A case study at Serowe, Botswana. *Isotope Techniques in Water Resource Development 1991*, pp. 345-362. IAEA, Vienna.
- Weissmann G.S., Zhang Y., LaBolle E.M. and Fogg G.E. (2002) Dispersion of groundwater age in an alluvial aquifer system. *Water Resources Research*, 38(10), 1198, doi:10.1029/2001WR000907.

# Appendix F Leakage estimation across the Munno Para Clay

Authors: *Smith SD, Banks EW, Turnadge C and Cook PG*

## F.1 Executive Summary

Leakage of groundwater between aquifers separated by a lower conductive unit can result from a change in pressure gradient between aquifers. This can cause contamination of the groundwater resource between aquifers of different water quality and also result in poor accounting and management of the resource. The Munno Para Clay Member separates the heavily utilised T1 and T2 aquifers in the Central and Northern Adelaide Plains. Environmental tracers were used to determine rates of inter-aquifer leakage across the Munno Para Clay. During the drilling of new observation wells in Welland and Gillman, core samples were collected for the analysis of helium, chloride and the stable isotopes of water. The distribution of these conservative tracers from the T1 aquifer through the Munno Para Clay and into the T2 aquifer were used to calibrate models of fluid velocity, however, because of apparent transient conditions, it was difficult to perfectly fit the data to a given fluid velocity. Regardless of these transient conditions, the helium data showed that the vertical flux is less than 1 mm/year and the Munno Para Clay has a vertical hydraulic conductivity of  $3.9 \times 10^{-11}$  m/s. This information, when combined with updated T1-T2 gradient maps for the Central Adelaide PWA and the North Adelaide Plains PWA indicate a potential upward leakage from the T2 into the T1 aquifer of 366 ML/year and a potential downward leakage from the T1 into the T2 aquifer of 1190 ML/year. The majority of the potential leakage occurs near Virginia where the head gradient is high due to a thin aquitard and significant drawdown related to pumping. This potential leakage rate is significantly greater than previous estimates and results from higher hydraulic gradients between the T1 and T2 aquifers due to pumping and also a higher estimate of hydraulic conductivity for the clay. These findings show that pumping has created the potential for significant amounts of inter-aquifer leakage. This highlights the importance of knowing aquitard properties in systems with multiple aquifers and in the Adelaide Plains there is an ongoing need to monitor changes in water quality that may be related to leakage.

## F.2 Introduction

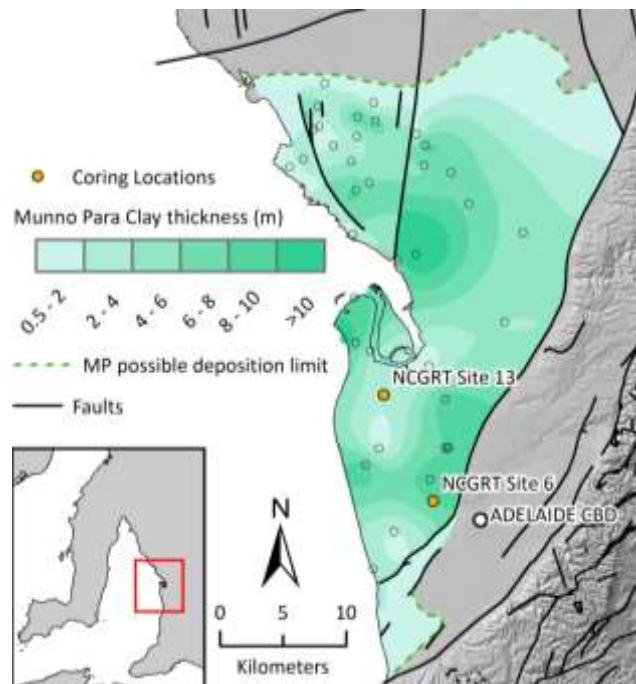
Inter-aquifer leakage can be a very important groundwater process at the regional scale, but there is usually little information to quantify this process. In industrial settings where fluids are being extracted and/or injected into reservoirs, it is crucial to know if these reservoirs are sufficiently isolated from adjacent aquifers. In an urban setting, such as the Adelaide Plains, inter-aquifer leakage rates need to be known because groundwater resources are in high demand and there needs to be an understanding about how processes including injection and pumping in a given aquifer will affect the adjacent aquifers. If inter-aquifer leakage is occurring at a significant rate, water resources can be over-allocated, contaminated, or degraded by other processes resulting from poor management. With an understanding of leakage rates, groundwater flow models can be calibrated to accurately represent the complex layered aquifer systems. This can lead to more effective resource management.

The estimation of inter-aquifer leakage is heavily dependent on knowing the vertical hydraulic conductivity (van der Kamp, 2001) and the head gradient between two formations. While the latter parameter can easily be determined provided that discreetly screened wells or piezometers are present, the former parameter has always been a challenge to estimate at appropriate scales (Hart et al., 2006; Mazurek et al., 2011). Traditional techniques of estimating inter-aquifer leakage usually involve measuring hydraulic

conductivity of aquitard material at the core scale. These value(s) are then applied to the entire formation. This approach generally causes an underestimation of leakage rates because formation scale features such as fractures or variations in lithology are not captured at the scale of core samples. Furthermore, these discreet estimates are generally applied to large data-poor (REM, 2006a) areas (Hart et al., 2006).

Hydrochemical analysis of aquitard pore water has been used to estimate fluid velocities at the scale of the formation thickness (Mazurek et al., 2011). This approach generally involves the measurement of one or more environmental tracers through a vertical profile, which is then used to constrain advection-dispersion models. Environmental tracers used for these purposes are usually helium (Gardner et al., 2012), stable isotopes of water ( $2\text{H}$ ,  $18\text{O}$ ) and chloride (Harrington et al., 2013). These tracers are generally chosen because they are completely or relatively conservative and may vary with different timescales, which may be used to constrain the history of fluid flow or the timing of geological events (Hendry et al., 2004; Hendry et al., 2005).

In this study, we aimed to quantify inter-aquifer leakage in the Adelaide Plains Sub-basin using environmental tracers. Due to the heavy demand on the T1 and T2 aquifers, the focus of this study is on the Munno Para Clay Member that separates these two aquifers. With abstraction rates of 8.1 and 14.3 GL/year in the T1 and T2 aquifers (REM, 2006b), causing increased vertical hydraulic gradients, the potential for inter-aquifer leakage is significant. To constrain rates of inter-aquifer leakage, helium, stable isotopes of water and chloride concentrations were measured within the aquitard and adjacent aquifers. These techniques have traditionally been used for thick aquitards, unlike the Munno Para Clay that has an average thickness of 10 m.



Apx Figure F.1 Coring locations and thickness and extent of the Munno Para Clay; thicknesses are from the WaterConnect database (DEWNR, 2015).

## F.2.1 STUDY AREA

## F.2.2 SITE DESCRIPTION

The Adelaide Plains Sub-basin and Golden Grove Embayment are comprised of a layered sequence of Quaternary and Tertiary aquifers and aquitards overlying much older fractured bedrock. The eastern boundary of the basin is juxtaposed against the Eden-Burnside Fault Zone that separates the sedimentary

basin and the fractured basement rock of the Mount Lofty Ranges. The groundwater flow system is expected to be gravity driven with recharge occurring in Mount Lofty Ranges and groundwater flows west towards the Gulf of St Vincent. The study area is divided into two Prescribed Well Areas (PWA): Northern Adelaide Plains (NAP) and Central Adelaide Plains (CAP).

### F.2.3 HYDROGEOLOGY

The hydrogeology, as extensively documented by Gerges (1999), consists of six Quaternary aquifers and four Tertiary aquifers. These are separated by 14 aquitards or confining beds (designated Cb1-14). Underlying the sedimentary basin is the complex lithology of the basement (see Appendix B). The CAP PWA is divided by the Para Fault, causing a significant offset of stratigraphic units. Aquifer and aquitard designation is based on the vertical order of occurrence as opposed to stratigraphic units. Primarily west of the Para Fault, the T1 and T2 aquifers are separated by the Munno Para Clay Member of the Port Willunga Formation (Cb9; hereafter referred to as the Munno Para Clay; Apx Figure F.1).

The Munno Para Clay Member is composed of calcareous marine clay interbedded with limestone (Gerges, 1999). The average thickness is 10 m and thins to a few meters in the NAP PWA. The spatial extent of the Munno Para Clay in the NAP PWA is questionable because only about 30 wells have stratigraphic logs containing this formation. A northern deposition limit has been shown in a previous study (REM, 2006a) and will be used here. Overall the member underlies 23 % of the CAP PWA and 75 % of the NAP PWA. This aquitard is thought to be relatively impermeable, but this is based on limited studies (Gerges, 1999).

### F.2.4 DRILL SITES

Coring occurred at two sites: NCGRT – Site 6 (Barrpowell Street, Welland) and NCGRT – Site 13 (Whicker Road, Gillman) – hereafter these sites will be referred to Site 6 and Site 13. Site 6 is located ~4 km northwest of the Adelaide CBD (Apx Figure F.1; for lithological logs and construction details see Appendix A. This site is located to the west of the Para Fault and the (hydro)stratigraphy includes Quaternary aquifers (Q1-Q6; Hindmarsh Clay) and aquitards (Cb1-Cb7; Hindmarsh Clay) underlain by Tertiary T1a aquifer (Dry Creek Sand), Croydon Facies aquitard (Cb8) and T1b aquifer (Upper Limestone of the Port Willunga Formation). Underlying the T1b is the Munno Para Clay (Cb9). The underlying T2 aquifer is the Lower Limestone of the Port Willunga Formation. The sequence of aquifers and aquitards is reasonably thick at ~226 m to the top of the Munno Para. Estimates of pre-pumping potentiometric surfaces show that the hydraulic gradient was upward (i.e. head is higher in the T2 aquifer as compared to the T1 aquifer) (Gerges, 1999).

Site 13 is located near Port Adelaide and is 13 km northwest of the Adelaide CBD (Apx Figure F.1). This site is also located west of the Para Fault but the sediment package is considerably thinner than Site 6 with the top of the Munno Para Formation found at ~165 m; the (hydro)stratigraphy is quite similar as well, barring a division of the T1 aquifer as the Croydon Facies were not present. Like Site 6, pre-pumping potentiometric surfaces show that the hydraulic gradient was upward (Gerges, 1999).

### F.2.5 PREVIOUS PERMEABILITY AND LEAKAGE ESTIMATES

The vertical hydraulic conductivity of the Munno Para Clay has previously been estimated by Gerges (1999) at  $2.1 \times 10^{-6}$  m/day. Several subsequent groundwater models have adopted values in the range  $2.6 \times 10^{-7}$  to  $1.7 \times 10^{-5}$  m/day (Zulfic et al., 2008).

#### Core-scale

The permeability of Adelaide Plains Quaternary and Tertiary aquitards was measured at the core-scale by Gerges (1999). Average hydraulic conductivities were calculated for individual confining beds and geological units, after assuming a log normal distribution of values. Mean hydraulic conductivities of Quaternary aquitards are compiled as individual confining beds (Cb1-Cb7 and TQCB; Apx Table F.1). Mean hydraulic

conductivities of Tertiary aquitards are compiled as individual hydrostratigraphic units (U5, U7, U9, U10 and U14; Apx Table F.2).

The arithmetic mean vertical hydraulic conductivity of the Munno Para Clay (Unit 7) was calculated as  $2.1 \times 10^{-6}$  m/day (Gerges 1999) whereas the geometric mean and standard deviation of the vertical hydraulic conductivity is  $4.0 \pm 7.0 \times 10^{-6}$  m/day. The cumulative probability function (not shown) indicates that there is a 90 % chance that the hydraulic conductivity is less than  $9.0 \times 10^{-6}$  m/day. However, this analysis is only based on 18 measurements and the higher permeability limestone layer of Unit 7 was omitted from the calculations here and those of Gerges (1999).

**Apx Table F.1 Summary of vertical hydraulic conductivities of Quaternary aquitards (Unit 1).**

VERTICAL HYDRAULIC CONDUCTIVITY ( $10^{-6}$ m/d)								
	CB1	CB2	CB3*	CB4	CB5	CB6	CB7	TQCB**
mean	487	316	2420	117	146	27.3	15.5	57.1
$\sigma$	647	6860	141000	618	440	114	44.9	163
n	6	12	6	6	3	5	3	7

\*includes 'very sandy' analysis removed from Gerges (1999) average

\*\*includes two analyses where core orientation was unknown

Source: Gerges (1999)

**Apx Table F.2 Summary of vertical hydraulic conductivities of Tertiary aquitards including the Munno Para Clay (Unit 7).**

VERTICAL HYDRAULIC CONDUCTIVITY ( $10^{-6}$ m/d)					
	U5	U7*	U9	U10	U14
mean	-	4.0	32.1	0.6	8.5
$\sigma$	-	7.0	96.4	0.3	3.6
n	-	18	2	2	2

\*excludes the higher permeability limestone layer ( $K=0.112$  m/day)

Source: Gerges (1999)

### Formation-scale (pumping test)

The Quaternary and Tertiary aquitards were also assessed by means of aquifer pump testing at five sites (Kidman Park, Marion, Largs Bay, Grange, and Blackwood; Gerges, 1999). The hydraulic conductivity of the aquitards have a very large uncertainty and are summarized in Apx Table F.3.

**Apx Table F.3 Summary of aquitard leakage coefficients for Quaternary and Tertiary confining beds.**

VERTICAL HYDRAULIC CONDUCTIVITY ( $10^{-6}$ m/d)			
	T1-Q (CB5-7)	T1A-T1B (CB8)	T1-T2 (CB9)
mean	464	246	72.5
$\sigma$	3160	658	212
n	9	10	11

Source: Gerges (1999)

### Leakage rate

Using the mean hydraulic conductivity of the Munno Para Clay and potentiometric surfaces for the Adelaide Plains in summer and winter, Gerges (1999) estimated the leakage rate across the Munno Para Clay. The weighted yearly leakage rate was estimated as 55.5 ML/year for hydrogeological zones 3C-E (as defined by Gerges (1999) and 144 ML/year for zones 3A-B. Gerges' (1999) assessment takes the area of

these zones to extend into the Spencer Gulf to an expected discharge area. This estimate is subject to significant uncertainty in the NAP PWA where the Munno Para Clay thickness and hydraulic gradient were not spatially mapped. The coring sites of this study are located in zone 3E (Welland) and zone 3B (Gillman).

## F.3 Methods

### F.3.1 FIELD METHODS

The project's drilling program aimed to create a transect of nested wells that spanned the Adelaide Plains Basin, east to west along the expected groundwater flow path (see Appendix A). Drilling commenced in February 2014 and continued through to September 2014. During this campaign, core samples were collected for hydrogeochemical analysis and vibrating wire pressure sensors were installed to monitor pressure propagation through the aquitards (see Appendix K).

At both sites, an initial well was drilled into the T2 aquifer using rotary mud methods. Afterwards, standard geophysical tools were run in order to determine the (hydro)stratigraphic formation depths. Adjacent to this well, a second well was drilled into the T1(b) aquifer. After well casing was set, wireline diamond HQ coring methods continued down through the Munno Para Clay and into the T2 aquifer. Coring was drilled and lifted in approximately 1 m long sections.

#### Helium-4

To assess vertical fluid velocities through the Munno Para Clay, a vertical profile of samples were collected for helium analysis using the general methods of Osenbrück et al. (1998). Immediately upon recovery, 1-2 sub-samples were separated using hand tools (mallet and cold chisel). The outer surface of the cores were cut or scraped off to remove sections that may be contaminated with drilling mud and thus would not be representative of the in situ helium. Each sub-sample of ~150 g was immediately placed in an all-metal canister. The gas in the canister was evacuated with a rotary vane vacuum pump for 45 seconds giving a dynamic vacuum pressure of approximately 0.5 kPa. The canister was then purged with Grade 5.0 (99.999 % purity) nitrogen, after Ali et al. (2011), to a pressure of approximately 150 kPa. This pump-purge process was repeated a second time before the canister was evacuated a final time while the canister was sealed using a stainless steel pinch-off clamp. Helium loss during drilling and handling is expected to be up to 20-30 % as was determined by a study using similar methods (Osenbrück et al., 1998).

Dissolved noble gas samples were collected from adjacent wells in the T1 and T2 aquifers to be used as boundary conditions. This was done using passive headspace diffusion samplers (Gardner and Solomon, 2009) that were suspended within the screened interval of the well and allowed to equilibrate for at least 48 hours.

#### Stable isotopes

Samples for stable isotope analysis of pore water were collected at ~1 m intervals and using a similar method to the helium samples. However these samples were not placed in an all-metal container, but instead double-sealed in plastic bags using a consumer vacuum sealer (Hendry et al., 2004). The drilling mud was spiked with 99 % deuterated water as a means of identifying contamination from the drilling mud. Duplicate filtered samples of the drilling mud were collected during the coring process – however, the drilling mud from Site 13 could not be analysed for technical reasons.

Groundwater for stable isotope analysis was also collected from adjacent T1 and T2 wells. These samples were collected using the same method used for the drilling mud.

#### Chloride

Samples for chloride analysis were collected at ~ 1m intervals. Approximately 35 g of clean chippettes from discreet depths were sealed in plastic containers to prevent the loss of water.

Groundwater for chloride, as well as other major ions, analysis was collected from adjacent wells. Drilling mud was also sampled as a means to identifying any possible contamination. Mains water was used to make the drilling mud and it was expected that the drilling mud would have a chloride concentration that differs from the formation water.

### F.3.2 ANALYTICAL METHODS

#### Helium-4

After collection, samples were allowed to equilibrate for at least 25 days to allow the dissolved gases in the cores to diffuse into the headspace within the canister. Samples were analysed by CSIRO at Waite Campus using a custom high-vacuum quadrupole system with cryogenic gas separation similar to that described by Poole et al. (1997) and the methods of Gardner et al. (2012). After the gases were extracted from the canisters, select canisters were resealed and allowed to equilibrate for an additional 4-15 weeks before being reanalysed, ensuring that all gases had been extracted and measured. Afterwards, the canisters were unsealed and heated to 105 °C to determine their water content, used to calculate noble gas concentrations. Heating continued for at least 12 hour and until the sample mass became constant. Helium-4 ( $^4\text{He}$ ) concentrations (expressed as volume of gas at standard temperature and pressure per unit of water; cc STP/g) and the enrichment factor  $F(\text{He})$  are presented here.  $F(\text{He})$  is defined as:

$$F(\text{He}) = \frac{{}^4\text{He}_s/{}^{20}\text{Ne}_s}{{}^4\text{He}_{sol}/{}^{20}\text{Ne}_{sol}}, \quad (\text{F.1})$$

where  ${}^4\text{He}_s$  and  ${}^{20}\text{Ne}_s$  are the helium and neon concentrations of the sample and  ${}^4\text{He}_{sol}$  and  ${}^{20}\text{Ne}_{sol}$  are the helium and neon concentrations in 15 °C water equilibrated with the atmosphere, respectively.

Sources of error in the resulting helium concentrations include (1) analytical uncertainty, (2) gas loss during core lifting and handling, and (3) incomplete pumping of air from the canisters. The last two points can be corrected using neon-20 concentrations as an independent parameter, because it has no terrigenous sources and the concentration should fall within a narrow range of values representing atmospheric recharge conditions. By assuming a recharge temperature of 15 °C, an elevation of 0 m, zero salinity and zero excess air (extra air trapped and dissolved during recharge (Heaton and Vogel, 1981), the pore water should have a  ${}^{20}\text{Ne}$  concentration of  $1.62 \times 10^{-7}$  cc STP/g. Because the recharge conditions cannot be constrained with the available data, this value is only assumed. By adding uncertainty to the recharge temperature, elevation, salinity and excess air concentration, we have an uncertainty of  $\sim 7\%$  ( $\pm 1.11 \times 10^{-8}$  cc STP/g).

If a sample has a neon concentration that exceeds solubility, we can assume that the headspace of the canister was not completely pumped and purged. Therefore, the ratio between helium and neon should be atmospheric, assuming fractionation while pumping is insignificant. This gives the correction equation:

$${}^4\text{He}_s = {}^4\text{He}_{meas} - ({}^{20}\text{Ne}_{meas} - {}^{20}\text{Ne}_{sol}) \frac{{}^4\text{He}_{atm}}{{}^{20}\text{Ne}_{atm}}, \quad (\text{F.2})$$

where  ${}^4\text{He}_s$  is the helium concentration in the sample,  ${}^4\text{He}_{meas}$  and  ${}^{20}\text{Ne}_{meas}$  are the measured helium and concentrations, respectively,  ${}^{20}\text{Ne}_{sol}$  is the neon concentration at recharge, and  ${}^4\text{He}_{atm}/{}^{20}\text{Ne}_{atm}$  is the atmospheric helium – neon ratio (0.318). Making this correction should decrease the helium concentration, but increase the helium/neon ratio.

For samples that have a deficit of neon, it can be assumed that helium and neon were lost from the sample during pumping. If fractionation did not occur during this gas loss, the He/Ne ratio should remain unchanged. To correct the helium concentration, a correction similar to Eq. F.2 can be used:

$${}^4\text{He}_s = {}^4\text{He}_{meas} - ({}^{20}\text{Ne}_{meas} - {}^{20}\text{Ne}_{sol}) \frac{{}^4\text{He}_{meas}}{{}^{20}\text{Ne}_{meas}}. \quad (\text{F.3})$$

This reduces to:

$${}^4\text{He}_s = {}^{20}\text{Ne}_{sol} \frac{{}^4\text{He}_{meas}}{{}^{20}\text{Ne}_{meas}}. \quad (\text{F.4})$$

Because a sample could have lost helium during lifting and pumping, and the canister could be only partially evacuated, there remains an uncertainty about how much gas loss could have occurred including processes that fractionate the gas composition. As such, at this point the best correction to take is the assumption that the sample could have lost 20-30 % of the original helium (Osenbrück et al., 1998) – these uncertainties are applied after the corrections in Eq. F.2 and F.4.

## Chloride

Gravimetric chloride content was measured by the CSIRO Analytical Services Unit at Waite Campus. Pore water chloride concentrations of sub-samples from the core were calculated using a 1:5 soil/water extract technique described by Rayment and Higginson (1992). Gravimetric water content was first measured on the samples at Flinders University by oven drying at 105°C for 24 hours. Soil pore water chloride analysis was completed on these same samples. The gravimetric water contents of the sample is required so that the chloride could be converted to a concentration per volume.

Chloride in drilling mud and groundwater samples were measured by the CSIRO Analytical Services Unit at Waite Campus by flow injection analysis.

## Stable isotope

Stable isotope ratios from core samples, groundwater and drilling mud were measured at School of Environment, Flinders University using a Picarro L2130-i  $\delta^{18}\text{O}/\delta^2\text{H}$  Ultra High Precision Isotopic Water Analyser. Results are reported relative to Vienna Standard Mean Ocean Water (VSMOW) in per mil (‰) using the delta ( $\delta$ ) notation. The analytical precision for  $\delta^{18}\text{O}$  and  $\delta^2\text{H}$  is  $\pm 0.025$  ‰ and  $\pm 0.1$  ‰, respectively. Core samples were measured using the direct pore water-equilibration method (Hendry et al., 2004).

### F.3.3 MODELLING METHODS

#### Solute Transport modelling

Because helium was the only tracer that produced results that could easily be interpreted, it was the only tracer that was modelled. Modelled was done using a one-dimensional analytical solution to the advection-dispersion-production equation:

$$\frac{\partial C}{\partial t} + V_z \frac{\partial C}{\partial z} = D_e \frac{\partial^2 C}{\partial z^2} + \frac{g^*}{n_e}, \quad (\text{F.5})$$

where  $C$  is the concentration of the tracer (cc STP/g) [ $\text{L}^3/\text{M}$ ],  $V_z$  is the vertical groundwater velocity (m/year) [ $\text{L}/\text{t}$ ],  $D_e$  is the effective diffusivity (defined below),  $g$  is the internal production rate of the tracer (cc STP/g/year) [ $\text{L}^3/\text{M}/\text{t}$ ], and  $n_e$  is the effective formation porosity. The porosity used was 0.45 – the average of previously measured values (Gerges, 1999). The effective diffusion coefficient was determined using:

$$D_e = D_0 n_e^m, \quad (\text{F.6})$$

where  $D_0$  is the free water diffusion coefficient of the tracer ( $\text{m}^2/\text{year}$ ) [ $\text{L}^2/\text{t}$ ] and  $m$  is a tracer dependent factor, which is taken as 2 for helium (Mazurek et al., 2011).

The internal helium production rate is a function of the U and Th concentration of the aquitard. Both of these elements decay to produce radiogenic alpha particles that become helium-4 atoms. It is assumed that this helium is being release into the pore water at the same rate it is being created. The production rate was estimated from U and Th concentrations found in pelagic clays (Earthref.org, 2015). The average concentrations of U and Th are 1.0 ppm and 10.2 ppm, respectively. This gives a production rate of  $1.3 \times 10^{-10}$

<sup>20</sup> cc STP/g/second – or 36 % less than the average rate of the upper crust (Ballentine and Burnard, 2002). The sensitivity of this factor is very low because helium diffusion rates are high enough to remove the vast majority of this helium, preventing it from accumulating in the thin aquitard. For example, at Site 6, increasing the production rate by a factor of 20 increased the helium concentration by a maximum of 1 %. Any decrease in production rate has a negligible affect.

## Leakage rate

To determine the potential leakage rate across the Munno Para Clay for the entire basin, we first calculated the vertical hydraulic conductivity ( $K_v$ ; m/year) [L/t] using the modelled fluid velocity ( $V_z$ ) and the historical (early-1900s; pre-pumping) gradient  $dh/dz$  (Gerges, 1999), as the tracer profile was established before modern pumping began – at Site 6 and 13 the historical gradient is upward with a higher head in the T2 and compared to the T1. The leakage rate was then calculated simply using Darcy’s Law:

$$K_v = -V_z n_e \frac{dz}{dh}. \quad (\text{F.7})$$

The current hydraulic gradient across the entire basin was calculated by taking the difference between recent potentiometric surfaces of the T1 and T2 aquifers provided by the Department of Environment, Water and Natural Resources (DEWNR). Hydraulic head differences were then used in combination with an isopach map of the Munno Para to determine the hydraulic gradient. Ultimately, this was used to estimate the vertical flux throughout the basin by rearranging Darcy’s Law:

$$Q = -K_v A \frac{dh}{dz}, \quad (\text{F.8})$$

where  $Q$  is the volumetric flux ( $\text{m}^3/\text{year}$ ) [ $\text{L}^3/\text{t}$ ] and  $A$  is the area of each grid cell exported from ArcGIS ( $\sim 114 \times 114 \text{ m}$ ) [ $\text{L}^2$ ].

## F.4 Results

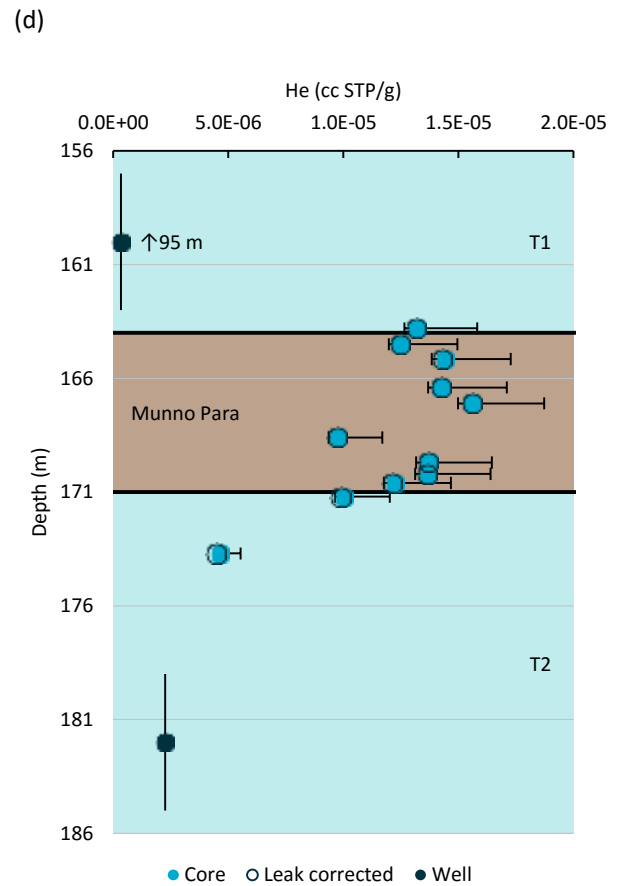
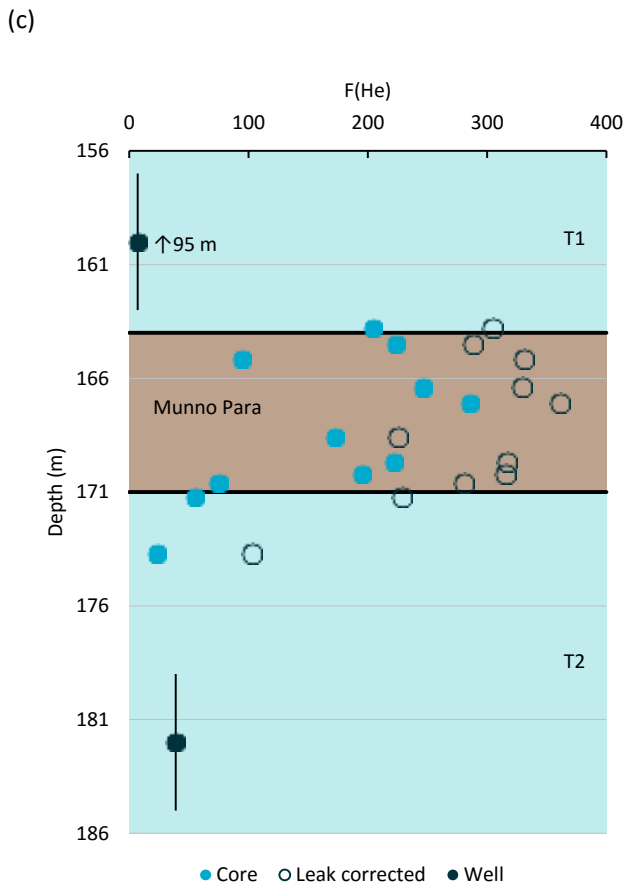
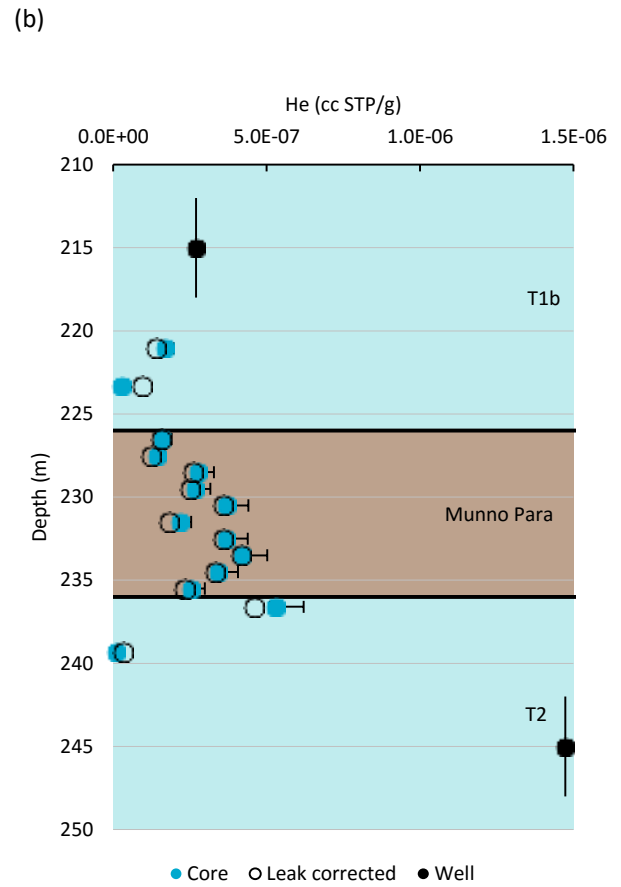
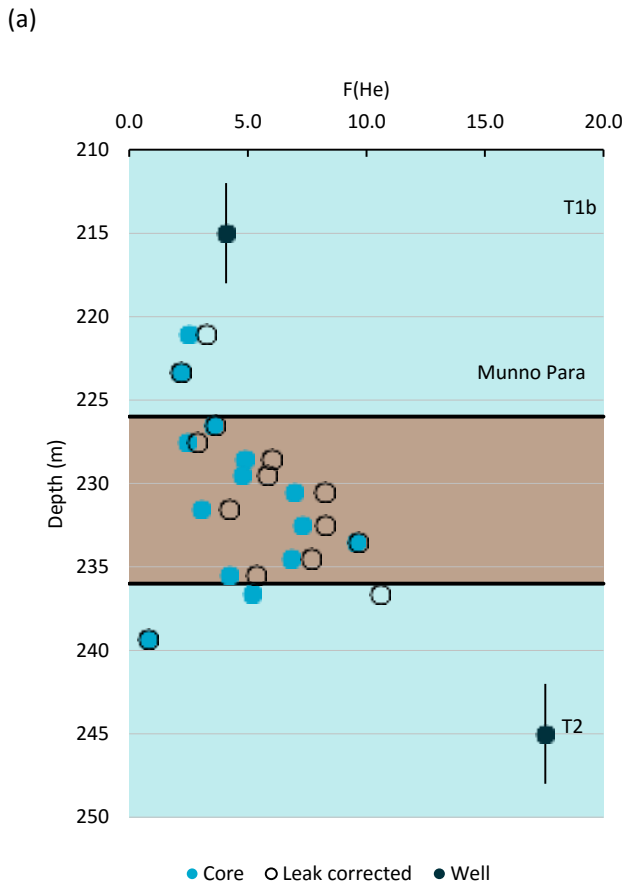
### F.4.1 ENVIRONMENTAL TRACER RESULTS

Environmental tracer results are summarised below and given in Apx Table F.4 (noble gases), Apx Table F.5 and Apx Table F.6 (chloride) and Apx Table F.8 and Apx Table F.9 (stable isotopes).

#### Helium

Noble gas analysis results are given in Apx Table F.4. At Site 6 there is a trend that helium increases with depth, before decreasing slightly as the bottom of the aquitard, and then increasing again in the T2 aquifer (Apx Figure F.2a, b). Corrected  $F(\text{He})$  factors increase from approximately 1 to 12. This data set has some scatter, which can be attributed to contamination or degassing of select samples. The most problematic samples appear to be those composed of limestone. Due to their higher permeability, it is likely that some of these samples are contaminated with drilling mud or lost a significant amount of gas during pumping – in either case these samples are not representative of the undisturbed formations. The theory of contamination is supported by contamination seen in stable isotope samples (see below). These high permeability samples include those in the T1b and T2 aquifer where the neon concentration was less than the expected solubility.

At Site 13, the helium concentrations are much higher with corrected  $F(\text{He})$  values between 100 and 350 (Apx Figure F.2c, d). The trend appears to show helium increasing downward, before decreasing in the lower section of the aquitard and into the T2 aquifer.



Apx Figure F.2 Noble gas results for Site 6: (a) F(He), (b) helium concentrations, and Site 13: (c) F(He), (d) helium concentrations.

Apx Table F.4 Noble gas concentrations and ratios in core samples and adjacent wells.

DEPTH (m)	SOURCE	UNIT	<sup>4</sup> He (cc STP/g)*	ΔHe CORRECTION (%)	F(He)**
<b>NCGRT Site 6 – Barrpowell St, Welland</b>					
212-218	NCGRT-6B	T1b	2.71E-07	-	4.08
221.05	core	T1b	1.40E-07	-17	3.25
223.3	core	T1b	9.31E-08	242	2.16
226.5	core	MP	1.57E-07	-2	3.64
227.5	core	MP	1.24E-07	-13	2.87
228.5	core	MP	2.60E-07	-6	6.03
229.5	core	MP	2.51E-07	-6	5.84
230.5	core	MP	3.57E-07	-3	8.30
231.5	core	MP	1.83E-07	-16	4.25
232.5	core	MP	3.58E-07	-2	8.32
233.5	core	MP	4.18E-07	0	9.70
234.5	core	MP	3.32E-07	-2	7.72
235.5	core	MP	2.32E-07	-8	5.39
236.6	core	T2	4.58E-07	-13	10.64
239.3	core	T2	3.33E-08	227	0.77
242-248	NCGRT-6A	T2	1.47E-06	-	17.54
<b>NCGRT Site 13 – Whicker Rd, Gillman</b>					
92-98	NCGRT-13B	T1	3.47E-07	-	7.19
163.8	core	T1	1.32E-05	0	304
164.5	core	MP	1.25E-05	0	288
165.15	core	MP	1.43E-05	-1	330
166.4	core	MP	1.42E-05	0	329
167.1	core	MP	1.56E-05	0	360
168.6	core	MP	9.74E-06	0	225
169.7	core	MP	1.37E-05	0	316
170.2	core	MP	1.36E-05	0	315
170.6	core	MP	1.21E-05	-1	280
171.2	core	T2	9.88E-06	-2	228
173.7	core	T2	4.46E-06	-4	103
179-185	NCGRT-13A	T2	2.27E-06	-	39.0

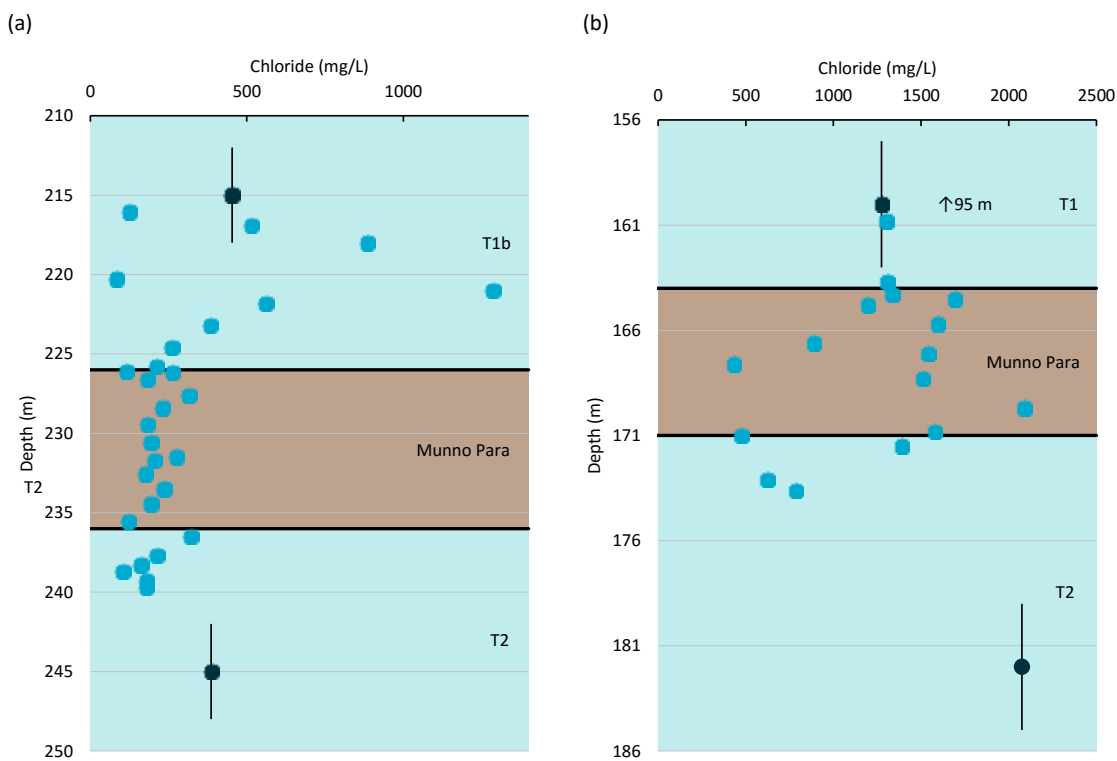
\*Corrected for excess (Eq. F.2) of deficit (Eq. F.4) in neon

\*\*Assuming 15 °C recharge temperature; <sup>4</sup>He/<sup>20</sup>Ne=0.267

## Chloride

Chloride concentrations at Site 6 are highly variable in the T1b aquifer (~100-1300 mg/L), consistent through the Munno Para Clay (~120-320 mg/L) and slightly more variable in the T2 aquifer (~100-320 mg/L; Apx Figure F.3). The high concentrations of chloride in the T1b (Apx Table F.5) appear to be valid as contamination from drilling mud would be much less saline at  $73 \pm 36$  mg/L Cl (Apx Table F.7). The water for the drilling mud was mains water and the salinity increased during drilling due to the addition of saline water from the formation and possibly mud additives. This data shows that the connate seawater has long been flushed from the clay.

Chloride concentrations at Site 13 (Apx. Table F.6) are much higher than Site 6 and are much more variable. Concentrations in the Munno Para Clay range from approximately 430-2090 mg/L. The lower concentrations are expected to be a drilling contamination issue as the drilling mud had a chloride concentration of  $263 \pm 69$  mg/L (Apx Table F.7; contamination is further discussed in the following section).



Apx Figure F.3 Depth profiles of chloride Site 6 and Site 13.

**Apx Table F.5 Chloride concentrations from core samples and adjacent wells – Site 6.**

DEPTH (m)	SOURCE	UNIT	Cl (g/g)	Cl (mg/L)
<b>NCGRT Site 6 – Barrpowell St, Welland</b>				
212-218	NCGRT-6B	T1b	-	453
216.05	core	T1b	0.25	125
216.89	core	T1b	0.21	514
218	core	T1b	0.17	885
220.3	core	T1b	0.24	83.8
221	core	T1b	0.26	1290
221.8	core	T1b	0.29	562
223.2	core	T1b	0.28	384
224.6	core	T1b	0.28	261
225.8	core	T1b	0.16	211
226.1	core	MP	0.20	116
226.16	core	MP	0.45	262
226.6	core	MP	0.47	182
227.6	core	MP	0.36	315
228.41	core	MP	0.42	231
229.45	core	MP	0.51	182
230.58	core	MP	0.48	193
231.5	core	MP	0.26	275
231.7	core	MP	0.18	205
232.55	core	MP	0.46	177
233.5	core	MP	0.40	236
234.45	core	MP	0.63	193
235.55	core	MP	0.28	122
236.5	core	T2	0.38	322
237.7	core	T2	0.28	214
238.3	core	T2	0.31	163
238.7	core	T2	0.76	104
239.3	core	T2	0.23	180
239.7	core	T2	0.29	180
242-248	NCGRT-6A	T2	-	386

**Apx Table F.6 Chloride concentrations from core samples and adjacent wells – Site 13.**

DEPTH (m)	SOURCE	UNIT	Cl (g/g)	Cl (mg/L)
<b>NCGRT Site 13 – Whicker Rd, Gillman</b>				
92-98	NCGRT-13B	T1	-	1275
160.8	core	T1	0.14	1300
163.7	core	T1	0.28	1310
164.3	core	MP	0.43	1340
164.5	core	MP	0.21	1690
164.8	core	MP	0.48	1190
165.7	core	MP	0.47	1590
166.6	core	MP	0.33	889
167.1	core	MP	0.52	1540
167.6	core	MP	0.27	432
168.3	core	MP	0.60	1510
169.7	core	MP	0.35	2090
170.8	core	MP	0.55	1580
171	core	MP	0.28	476
171.5	core	T2	0.33	1390
173.1	core	T2	0.29	621
173.6	core	T2	0.24	785
179-185	NCGRT-13A	T2	-	2075

\*

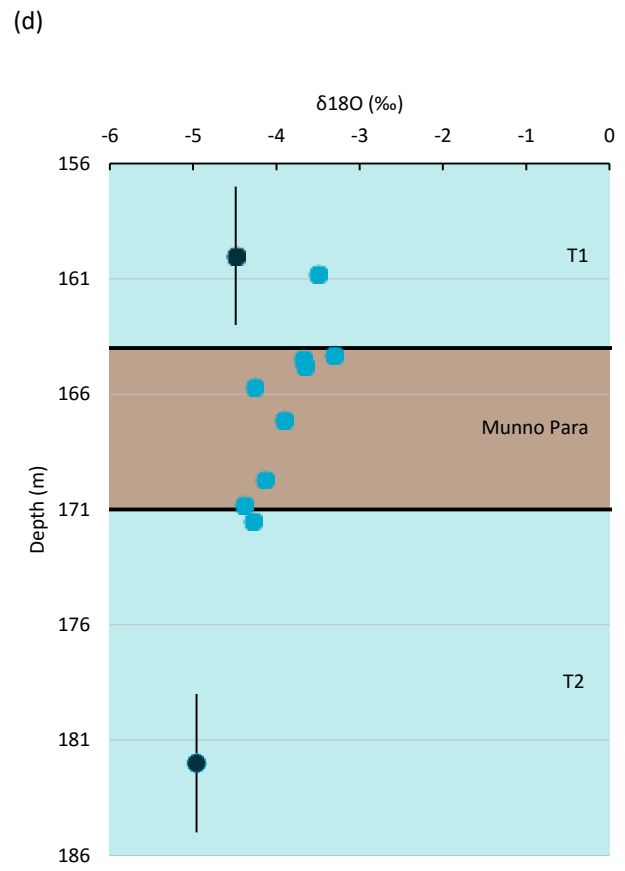
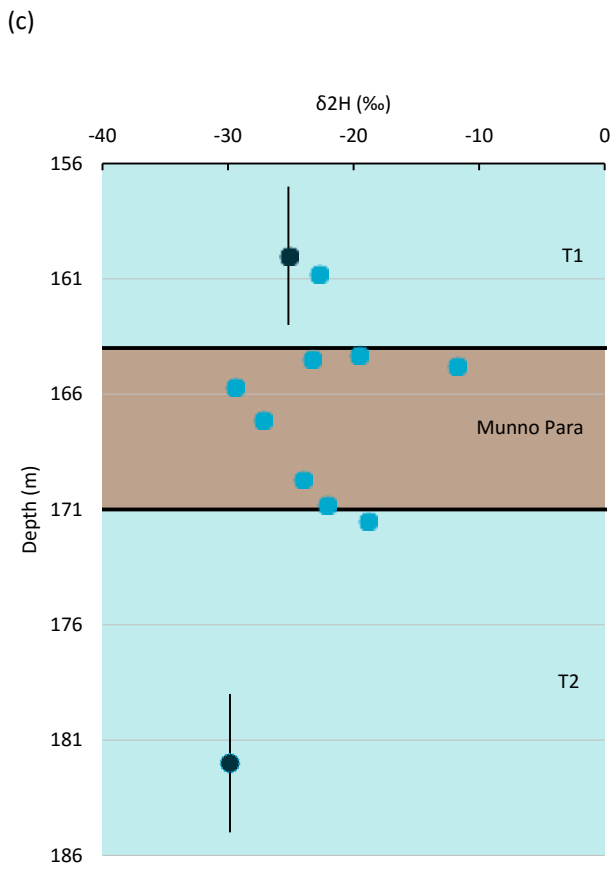
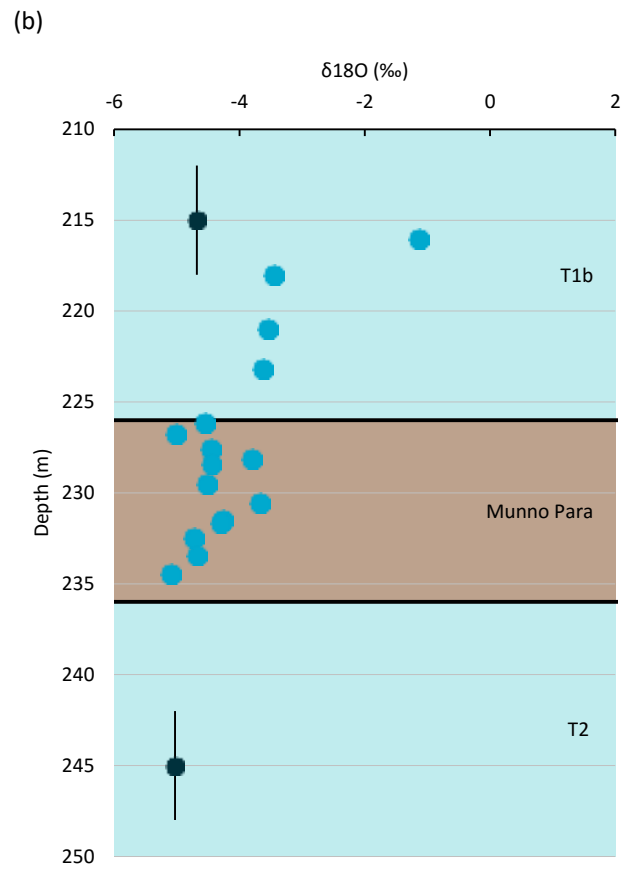
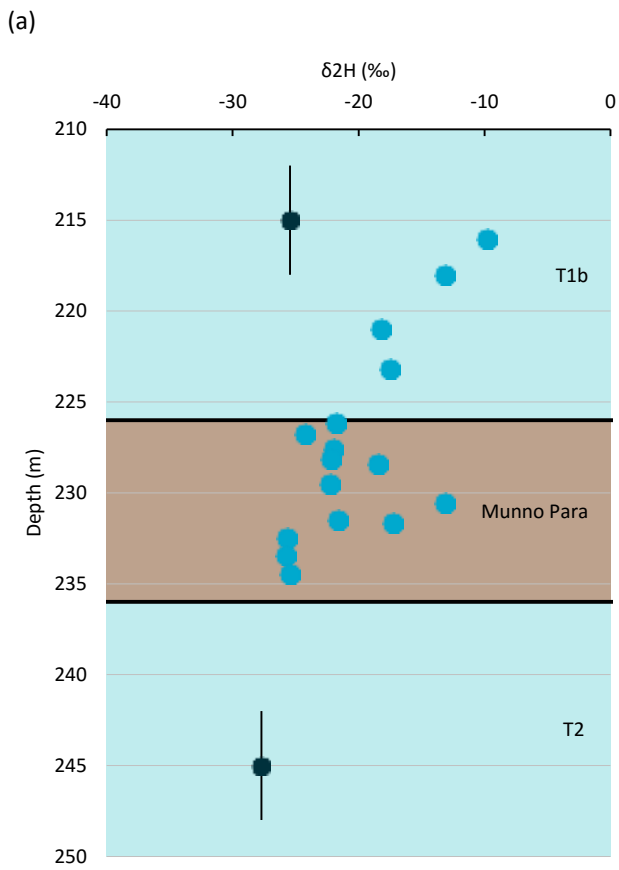
**Apx Table F.7 Chemistry of drilling mud.**

SAMPLE TIME	$\delta^2\text{H}$ (‰ VSMOW)	$\delta^{18}\text{O}$ (‰ VSMOW)	F (mg/L)-	Cl (mg/L)	Br (mg/L)	NO <sub>3</sub> (mg/L)	SO <sub>4</sub> (mg/L)
<b>NCGRT Site 6 – Barrpowell St, Welland</b>							
3/06/2014 10:12	1839.75	1.45	0.9	27	<0.05	<0.05	13
3/06/2014 15:00	98.29	1.03	0.57	40	0.1	<0.05	17
4/06/2014 11:00	62.53	0.13	0.59	101	0.28	0.22	38
5/06/2014 14:00	140.87	0.77	0.86	95	0.22	<0.05	73
6/06/2014 10:00	-	-	1.1	102	0.32	<0.05	117
<b>NCGRT Site 13 – Whicker Rd, Gillman</b>							
3/09/2014	-	-	0.72	325	0.92	0.72	106
4/09/2014	-	-	0.8	189	0.41	<0.05	82
5/09/2014	22.93	-2.44	0.97	274	0.51	0.11	119

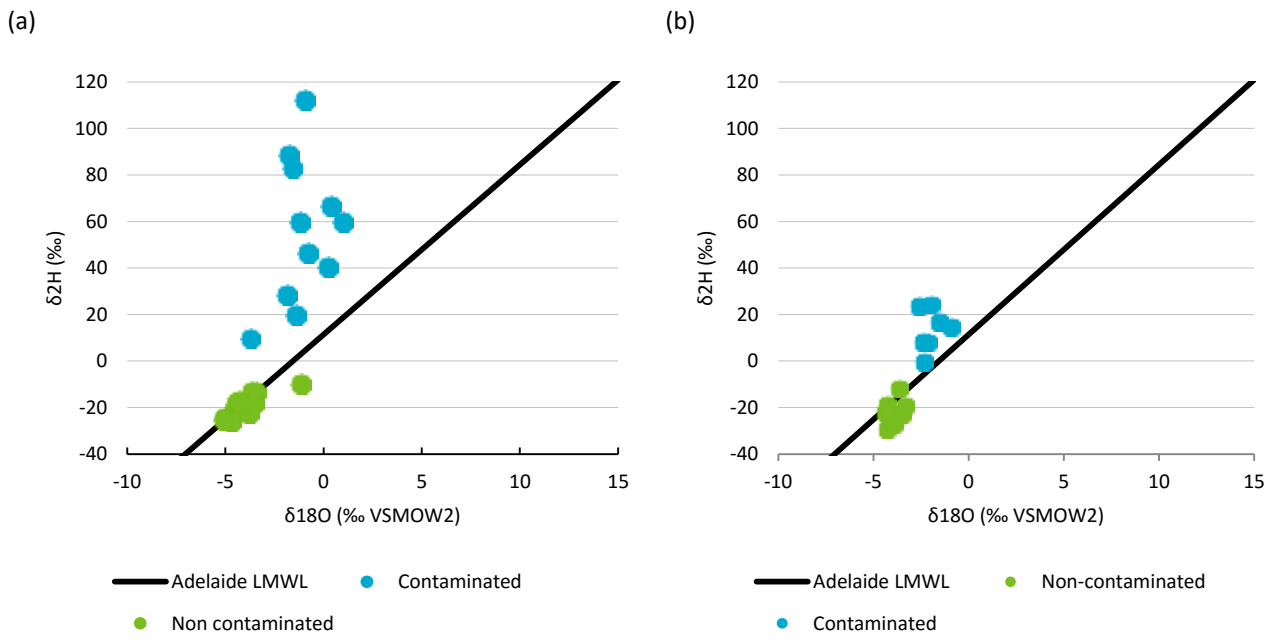
## Stable Isotopes

Stable isotope ratios, presented in relation to VSMOW, at Site 6 are between -25.7 and -9.8 for  $\delta^2\text{H}$  and between -5.1 and -1.1 for  $\delta^{18}\text{O}$  (Apx Figure F.4a,b and Apx Table F.8). Most values plot near or on the local meteoric water line (Apx Figure F.5a), the latter of which was recently updated by (Crosbie et al., 2012). This excludes several samples that were clearly contaminated by drilling mud, which had  $\delta^2\text{H}$  ratios of approximately 1800 ‰ (these values are not shown in Apx Figure F.4). Contamination strongly affected samples in the T1b and T2 aquifers and may have slightly affected samples within the Munno Para Clay. Furthermore, contaminated stable isotope samples appear to show chloride contamination at the same depth (Apx Figure F.6a). Groundwater analyses from adjacent wells show more representative ratios (Apx Figure F.4a,b). After excluding the obviously contaminated samples, moving downward through the Munno Para Clay, the  $\delta^2\text{H}$  values increase from approximately -21 to -12 ‰ before decreasing and remaining relatively constant at approximately -25 ‰. Values of  $\delta^{18}\text{O}$  follow a similar trend.

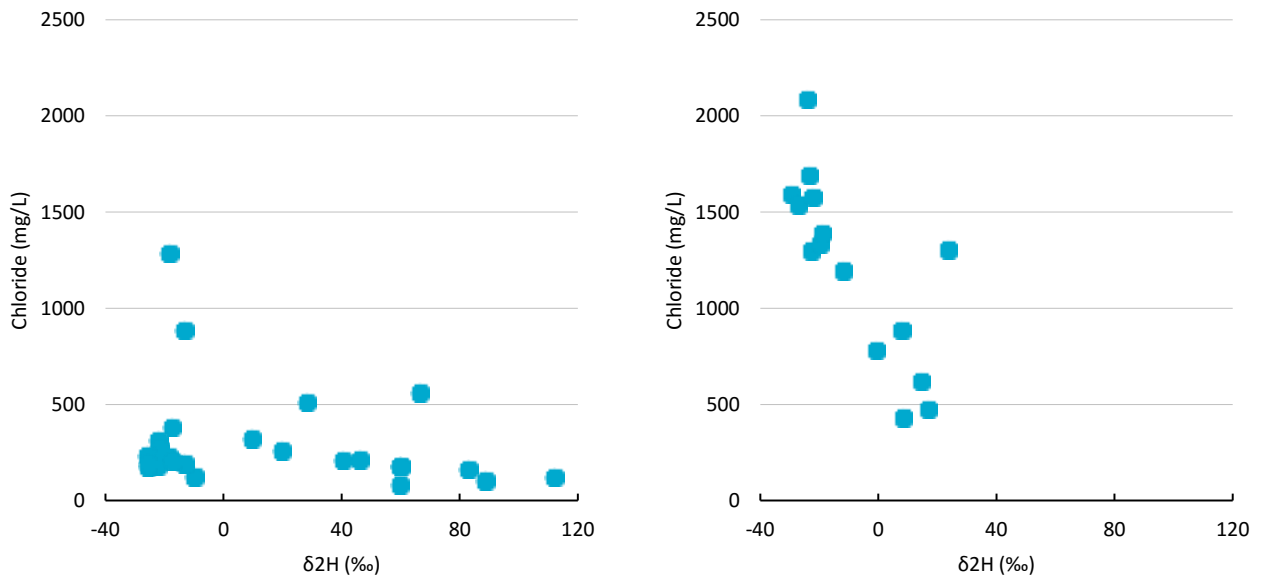
At Site 13,  $\delta^2\text{H}$  ratios are variable at the top of the Munno Para Clay and then increase linearly down to the T2;  $\delta^{18}\text{O}$  values decrease downward through the Munno Para clay (Apx Figure F.4c, d and Apx Table F.9). It is unclear why  $\delta^2\text{H}$  and  $\delta^{18}\text{O}$  ratios would have opposing trends as no physical process would cause this trend. Therefore it is suggested that contamination increases with depth, affecting the  $\delta^2\text{H}$ , but with little to no affect on the  $\delta^{18}\text{O}$  ratios. Similar to Site 6, high  $\delta^2\text{H}$  ratios in several samples suggest contamination from drilling mud – decreasing chloride concentration with increasing  $\delta^2\text{H}$  ratios (Apx Figure F.6b). Data collected from adjacent wells 13A and 13B, which respectively underlie and overlie the aquitard, have  $\delta^2\text{H}$  values similar to those measured in the aquitard and  $\delta^{18}\text{O}$  values that are slightly less than those measured in the aquitard.



Apx Figure F.4 Depth profiles of stable isotopes at Site 6: (a)  $\delta^{2}\text{H}$  and (b)  $\delta^{18}\text{O}$  and Site 13: (c)  $\delta^{2}\text{H}$  and (d)  $\delta^{18}\text{O}$ ; data from contaminated samples are not shown.



Apx Figure F.5  $\delta^{18}\text{O}$  vs.  $\delta^2\text{H}$  for (a) Site 6 and (b) Site 13.



Apx Figure F.6 Comparison of deuterium and chloride measurements in core samples; (a) Site 6 and (b) Site 13.

**Apx Table F.8 Stable isotope ratios from core samples and adjacent wells – Site 6.**

DEPTH (m)	SOURCE	UNIT	$\delta^2\text{H}$ (‰ VSMOW)	$\delta^{18}\text{O}$ (‰ VSMOW)
<b>Site 6 – Barrpowell St, Welland</b>				
212-218	NCGRT-6B	T1b	-25.44	-4.68
216.05	core	T1b	-9.82	-1.13
216.93*	core	T1b	28.37	-1.88
218.025	core	T1b	-13.15	-3.45
220.275*	core	T1b	59.73	0.99
221	core	T1b	-18.23	-3.54
221.875*	core	T1b	66.64	0.37
223.2	core	T1b	-17.48	-3.63
224.625*	core	T1b	19.94	-1.42
225.8*	core	T1b	40.47	0.23
226.175	core	MP	-21.82	-4.55
226.75	core	MP	-24.30	-5.01
227.6	core	MP	-22.00	-4.45
228.125	core	MP	-22.19	-3.81
228.42	core	MP	-18.45	-4.44
229.5	core	MP	-22.25	-4.51
230.58	core	MP	-13.14	-3.67
231.475	core	MP	-21.64	-4.26
231.675	core	MP	-17.26	-4.30
232.5	core	MP	-25.65	-4.72
233.45	core	MP	-25.73	-4.68
234.47	core	MP	-25.46	-5.09
235.55*	core	MP	112.17	-0.95
236.6*	core	T2	9.76	-3.72
237.675*	core	T2	46.35	-0.79
238.325*	core	T2	83.00	-1.59
238.725*	core	T2	88.70	-1.78
239.5*	core	T2	59.91	-1.21
242-248	NCGRT-6A	T2	-27.72	-5.03

\*Contaminated

Apx Table F.9 Stable isotope ratios from core samples and adjacent wells – Site 13.

DEPTH (M)	SOURCE	UNIT	$\delta^2\text{H}$ (‰ VSMOW)	$\delta^{18}\text{O}$ (‰ VSMOW)
<b>Site 13 – Whicker Rd, Gillman</b>				
92-98	NCGRT-13B	T1	-25.18	-4.49
160.80	core	T1	-22.7	-3.50
163.70*	core	T1	23.8	-2.59
164.30	core	MP	-19.5	-3.31
164.50	core	MP	-23.3	-3.69
164.80	core	MP	-11.8	-3.66
165.15*	core	MP	24.3	-1.98
165.70	core	MP	-29.4	-4.26
166.60*	core	MP	8.0	-2.12
167.10	core	MP	-27.2	-3.91
167.60*	core	MP	8.4	-2.37
169.70	core	MP	-24.1	-4.14
170.80	core	MP	-22.1	-4.39
171.00*	core	T2	16.9	-1.52
171.50	core	T2	-18.9	-4.28
173.10*	core	T2	14.5	-0.89
173.60*	core	T2	-0.6	-2.30
179-185	NCGRT-13A	T2	-29.84	-4.96

\*Contaminated

## F.4.2 MODELLING RESULTS

The modelling of helium concentrations is complicated by properly defining the boundary conditions. At Site 13, the upper boundary condition comes from a well (NCGRT-13B) that is 69 m from the top of the Munno Para Clay. This makes the data from core samples a better boundary concentration. The lower boundary at both sites is complicated by lower concentrations caused by apparent transient conditions, which will be discussed. Different scenarios have been produced for each site in an attempt to both constrain and demonstrate the range of uncertainty of the leakage rate.

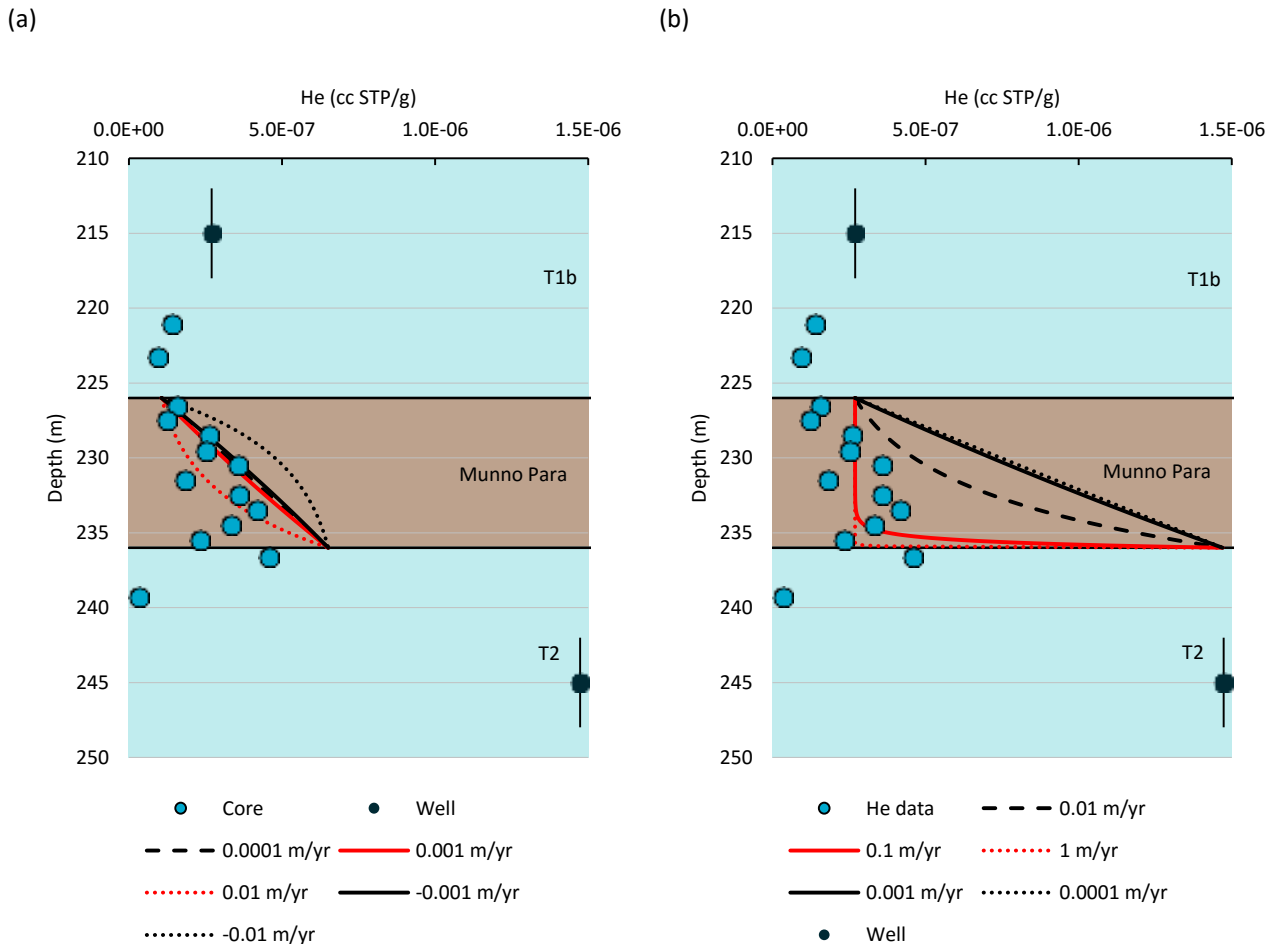
### Site 6

#### Scenario 1: steady-state, boundary conditions based on core sample concentrations

In this scenario, helium boundary concentrations were selected by taking a linear fit through the samples in the upper portion of the aquitard, as these samples do not appear to be affected by transient conditions. The majority of the linear data fits within a fluid velocity of  $<\pm 10$  mm/year, with several fitting with a fluid velocity of  $<\pm 1$  mm/year (where a positive velocity indicates downward advection and a negative velocity indicates upward advection), while the other data points would fit with a downward velocity exceeding 10 mm/year (Apx Figure F.7a). However, a downward vertical gradient seems unlikely based on current (Apx Figure F.11a) and historical head measurements (Section F.2.4).

#### Scenario 2: steady-state, boundaries fixed by well samples

Using the helium concentrations obtained from wells NCGRT 6A and 6B (part of a nested well set installed at the same site as the coring), the result is quite different to the first scenario. To fit the majority of the data, the fluid velocity would need to be downward at 10-1000 mm/year (Apx Figure F.7b). As mentioned in Scenario 1, this downward advection seems improbable based on historic and current hydraulic gradients (Section F.2.4; Apx Figure F.11a), however these estimates are still subject to uncertainty because early estimates of the potentiometric surface relied on sparse data.



Apx Figure F.7 Site 6 modelled helium profiles from (a) Scenario 1 and (b) Scenario 2.

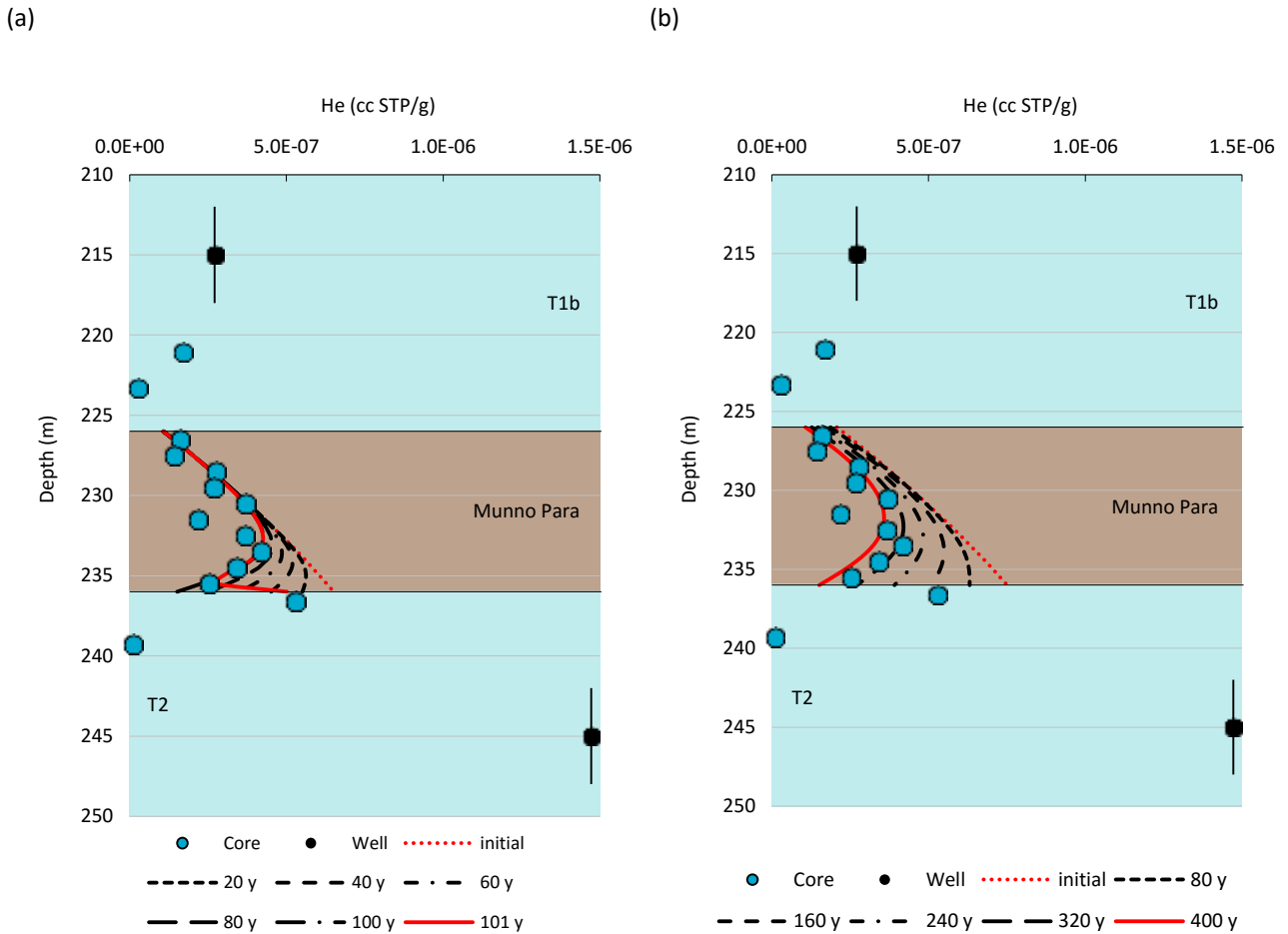
**Scenario 3: transient, instantaneous change, diffusion only**

This scenario assumes that vertical fluid velocities are below 1 mm/year. As an initial condition, a linear regression was fit through the upper four aquitard core samples where the data is relatively linear. At the beginning of the model run, the lower boundary was reduced in 10 equal steps to a concentration of  $2.0 \times 10^{-7}$  cc STP/g, which is a linear regression fit through the lower three aquitard samples. Also, an attempt was made to fit the data point directly below the Munno Para Clay, which trends with the concentrations measured in NCGRT-6A. The modelled profile fits the aquitard data relatively well using a time-step of 10 years, therefore a model run of 100 years (Apx Figure F.8a). To maintain the data fit in the bottom of the Munno Para Clay, the helium concentration in the T2 would need to change rapidly within the timeframe of one year. A rapid change in helium concentration like this could be caused by pumping, lacking any better explanation – however, a rapid change like this seems unlikely.

**Scenario 4: transient, stepped change, diffusion only**

This scenario looks at the possibility of historically higher helium concentrations in the T1b and T2 aquifers, resulting in higher helium concentrations in the Munno Para Clay. The upper and lower initial boundary helium concentrations were set at  $2.0 \times 10^{-7}$  and  $7.0 \times 10^{-5}$  cc STP/g, respectively, and in equal increments,

these were reduced to the present boundaries inferred from Scenario 3. This initial condition is somewhat arbitrary but assumes helium is greater in deeper aquifers, which is generally observed due to older groundwater at depth. After 320-400 years, the model fits the data moderately well (Apx Figure F.8b). This model provides a reasonable fit, however there is no known mechanism that would have caused helium concentrations in the aquifers to decrease a few hundreds of years ago.



**Apx Figure F.8 Site 6 modelled helium profiles for (a) Scenario 3 and (b) Scenario 4.**

Of the four scenarios, Scenario 3 does the best at fitting the data, however as mentioned above, the rapid change required to fit the data point in the top of the T2 aquifer seems unlikely. It is possible that this sample point is erroneous, however, it does trend with the analysis from well NCGRT 6A. Of the remaining scenarios, Scenario 1 reasonably fits the data and helps constrain the fluid velocity at 1 mm/year; Scenario 2 poorly fits the data and seems improbable; Scenario 4 fits the aquitard data reasonably well, but there are too many parameters left unconstrained and requires too much guesswork in determining an initial condition.

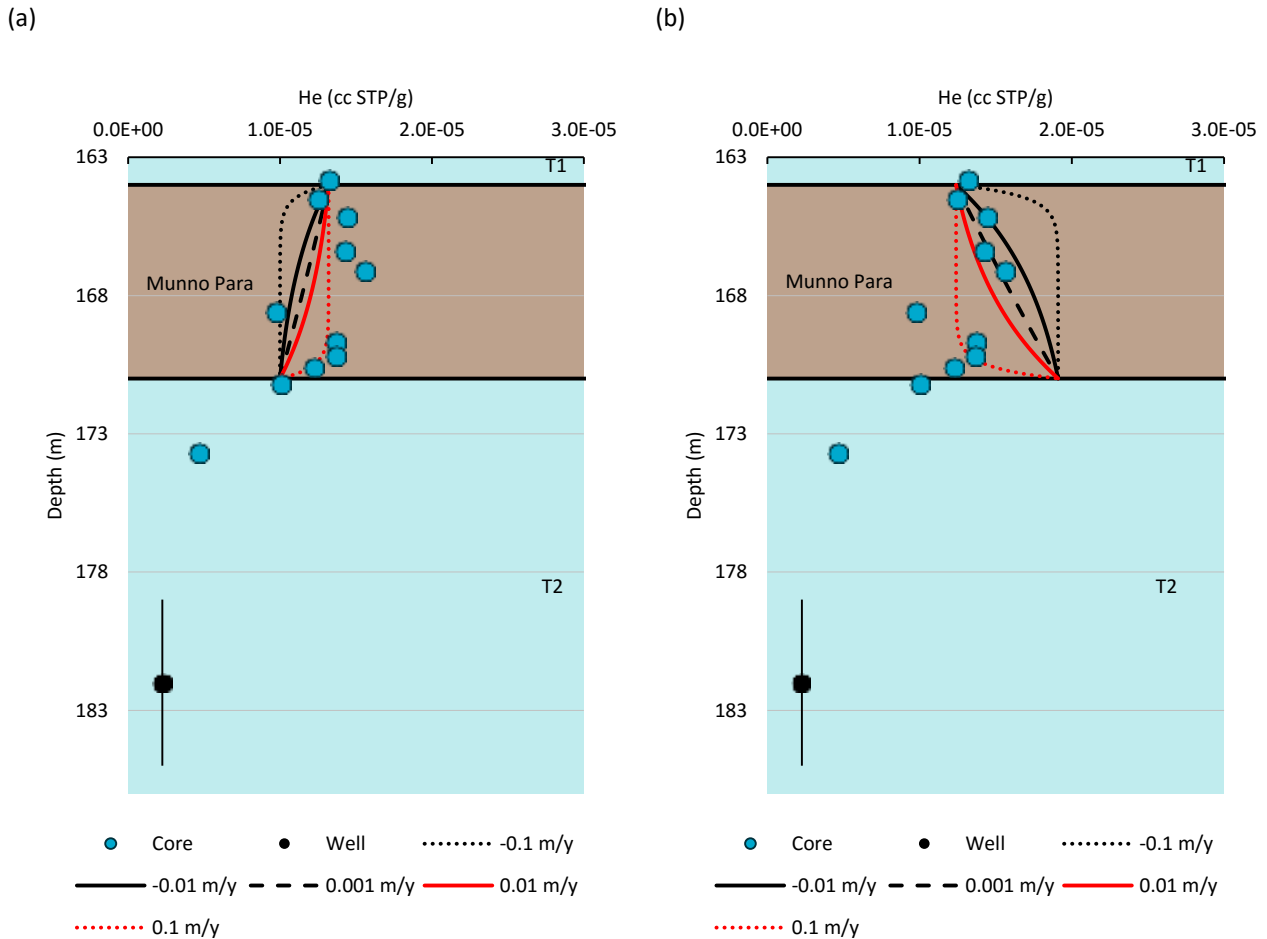
### Site 13

#### Scenario 1: steady-state, boundaries fixed by core samples

In this scenario, the concentration measured in the T1 and T2 aquifers adjacent to the Munno Para Clay are used as boundary conditions. The concentrations in the T1 exceeds that of the T2, therefore a downward advection rate of 0.1 m/year begins to fit the data in the lower portion of the aquitard, but the increase in concentration seen in the upper portion of the aquitard is not captured in this model (Apx Figure F.9a). Furthermore, a downward gradient is not expected for this part of the basin.

#### Scenario 2: steady-state, boundaries interpolated from linear data

Using the data in the upper portion of the aquitard, a linear trend was fit through the data to produce the boundary conditions. This assumes that the concentrations in the upper half of the aquitard have not been affected by transient conditions and can still be used to determine a steady state flux rate. Based on this choice of boundaries, an upward fluid velocity of approximately 0.001 to 0.01 m/year captures the data in the upper portion of the aquitard (Apx Figure F.9b). As expected, the trend of data in the lower portion of the aquitard is not captured.



Apx Figure F.9 Site 13 modelled helium concentrations for (a) Scenario 1 and (b) Scenario 2.

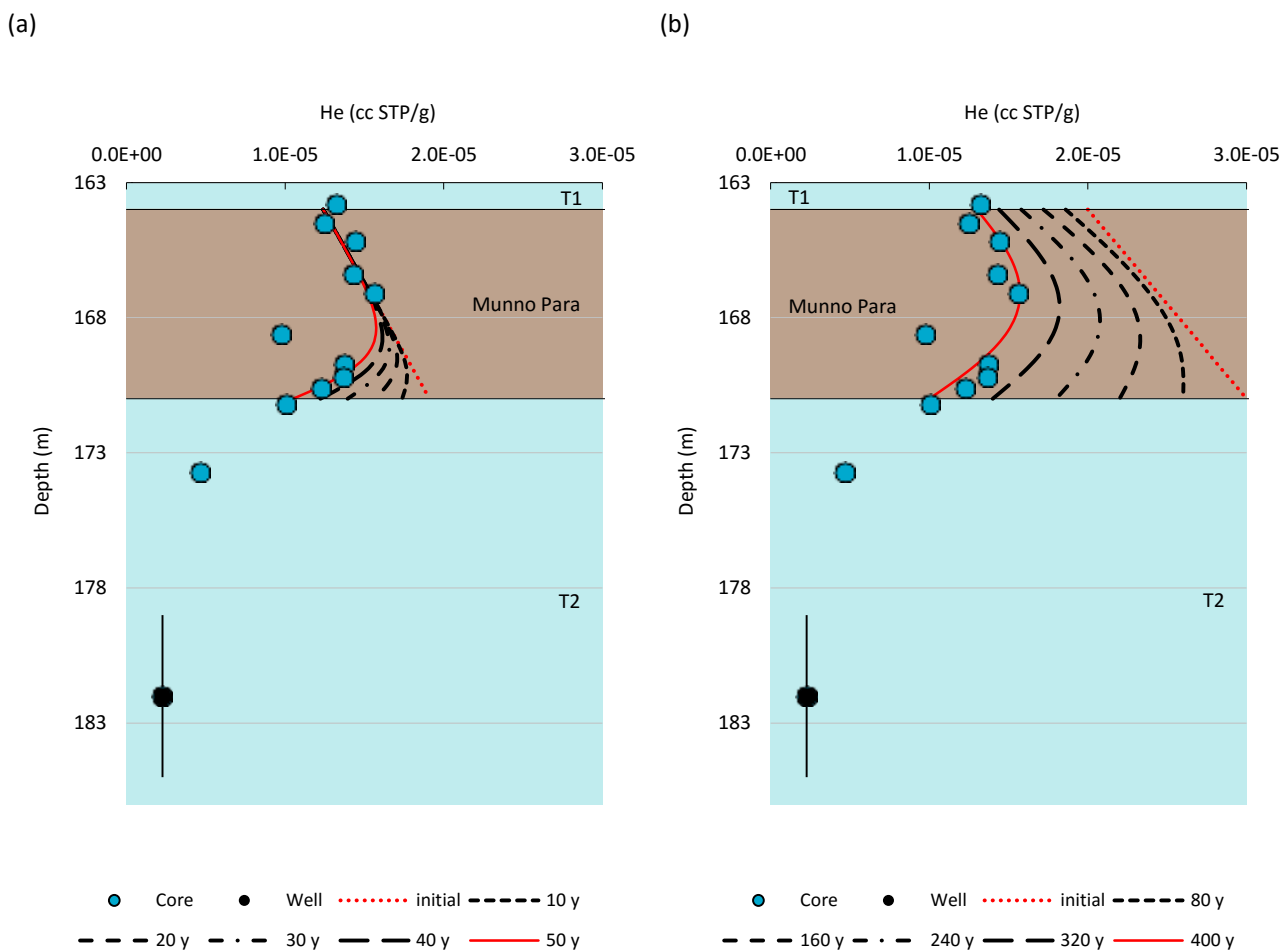
**Scenario 3: transient lower boundary, diffusion only**

This scenario looked at the possibility of transient conditions. The initial condition was that defined in Scenario 2 and fluid velocity below  $\pm 1$  mm/year. At the beginning of the scenario, the lower boundary concentration is reduced to  $1.0 \times 10^{-5}$  cc STP/g in 10 equal increments to match the observed boundary condition. After 50 years, the helium concentration in the upper portion of the aquitard is largely unchanged, while the helium profile in the lower portion matches the observed values (Apx Figure F.10a). Due to the change in boundary condition, helium is lost from the Munno Para Clay and into the T2 aquifer. The total amount of helium lost is 2.1 cc STP He per square metre of aquitard. This helium will get mixing into the T2 groundwater through advection, dispersion and diffusion and could be the source of high helium concentrations measured in the top of the T2 aquifer between 171 and 182 m depth. Further modelling would need to be performed to confirm the likelihood of this scenario.

**Scenario 4: transient upper and lower boundaries, diffusion only**

This scenario looks at the possibility of historically higher helium concentrations in the T1 and T2 aquifers. The initial boundary helium concentrations were set at  $2.0 \times 10^{-5}$  and  $3.0 \times 10^{-5}$  cc STP/g and reduced to the present boundaries in equal increments. This initial condition is somewhat arbitrary but assumes helium is

greater at depth, which is generally observed due to older groundwater at depth. After 360-400 years, the model fits the data moderately well (Apx Figure F.10b). However, as stated above, there is no known reason that helium concentrations would have begun to decrease a few hundred years ago.



**Apx Figure F.10 Site 13 modelled helium concentrations for (a) Scenario 3 and (b) Scenario 4.**

Of the four scenarios, Scenario 3 does the best at fitting the data. Furthermore, the interpretation is relatively consistent with Site 6. Of the remaining scenarios, Scenario 1 poorly fits the data and thus seems unlikely, Scenario 2 reasonably fits the data and helps constrain the fluid velocity at 1 mm/year, and Scenario 4 fits the aquitard data reasonably well, but there are too many parameters left unconstrained and requires too much guesswork in determining an initial condition.

### F.4.3 LEAKAGE RATE

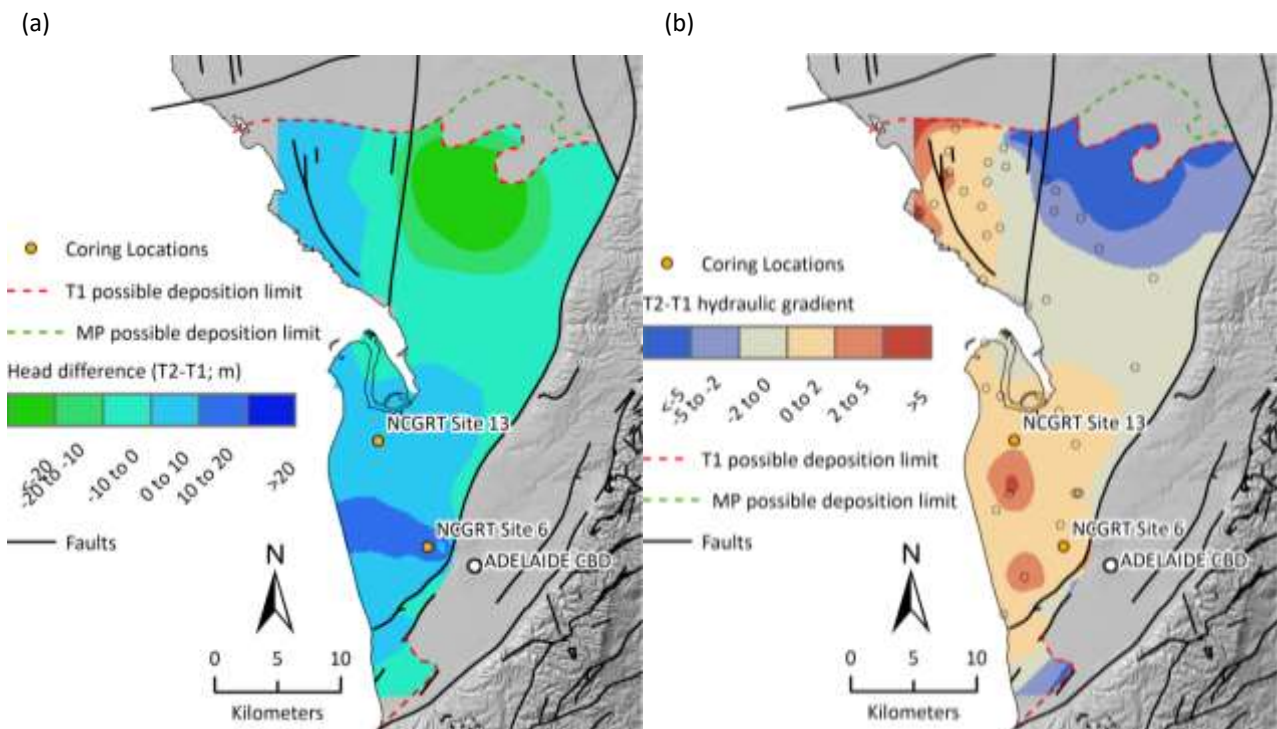
Based on the fluid velocities presented above, the best fit of the data is with low fluid velocities. From this analysis, it can be expected that at Site 6 and Site 13, groundwater is leaking vertically at a rate less than 1 mm/year. Based on historical (pre-pumping) hydraulic gradients of 0.35 and 0.43 (Site 6 and Site 13, respectively) (Gerges, 1999), the hydraulic conductivities of the Munno Para Clay are  $4.1 \times 10^{-11}$  at Site 6 and  $3.8 \times 10^{-11}$  at Site 13. By using the current potentiometric head difference and the isopach map of the Munno Para Clay (Apx Figure F.1), the mean and standard deviation of the vertical hydraulic gradient across the Munno Para Clay is  $0.71 \pm 0.56$ . The majority of the CAP has an upward gradient (lower pressure in the T1(b) aquifer). Downward gradients are present at select patches throughout the basin and near the boundary between Salisbury and Gepps Cross.

By applying the average  $K_v$  determined for the Munno Para Clay, the potential for leakage is 1190 ML/year from the T1 aquifer down into the T2 aquifer and 366 ML/year from the T2 aquifer up into the T1 aquifer.

These values are significantly larger than previous ‘present-day’ estimates (Gerges, 1999), while also considering a much smaller area. The mean leakage per area in this study is 3.5 ML/km<sup>2</sup>/year, whereas Gerges estimate was 0.41 ML/km<sup>2</sup>/year. The difference in these potential estimates is largely attributed to the area north of Virginia in the NAP where the Munno Para Clay is thin and the vertical head difference is large. This area was not previously assessed with much vigour as the gradient across the Munno Para Clay was estimated to be constant (Gerges, 1999). The higher potential leakage can also be attributed to higher conductivities (52 % larger).

Barring any spatial variations in permeability, the areas with the greatest potential for leakage are those with the largest vertical gradient. These locations are related to pumping centres in west of Adelaide CBD and near Virginia in the NAP PWA (Apx Figure F.11).

Both of these areas have high rates of extraction from either the T1 or T2 aquifer. Hydraulic gradients at the northern limit of the Munno Para Clay have extreme values, with absolute values exceeding 10 with a maximum of 24. It should be noted that this area is very data poor and there is little constraint in the formation thickness and the vertical head difference as there are few actively monitored observation wells in this area. Surprisingly, the potential for leakage from pumping the T2 aquifer near Osborne is not readily apparent from Apx Figure F.11a. This could be the result of drawdown in both the T1 and T2 aquifers, resulting in a subtle change in hydraulic gradient. Conversely, the lack of gradient at Osborne could be an indication of high leakage.



Apx Figure F.11 2014 map of T2 – T1 (a) head difference and (b) hydraulic gradient.

## F.5 Discussion

### F.5.1 PERMEABILITY ESTIMATES

The data and modelling above shows that helium is a suitable tracer to determine leakage rates across the Munno Para Clay Formation, though transient conditions complicate these estimates. This observation is based on the fact that there is an appreciable difference in concentration between the adjacent aquifer and the profile through the aquitard which can be interpreted with simple models. In contrast, much of the stable isotope and chloride data is highly scattered in the aquitard and aquifers, with many samples showing contamination from the drilling mud. However, that is not to say that the use of helium as a tracer

does not constrain all uncertainty in estimating  $K_v$ . Having a helium profile that indicates transient conditions in the aquifer adds a great level of complexity to modelling the fluid velocities. Also as previously stated, there is no way to independently verify an initial condition for the helium boundary concentration. However, because the Munno Para is very thin in comparison to most studied aquitards and the transient condition does not affect the entire profile, there is relative confidence that the fluid velocity is low.

## F.5.2 INTERPRETATION OF TRANSIENT CONDITIONS

A comparison between aquifer and aquitard helium concentrations shows that the aquitard helium concentrations are showing remnant palaeo-hydrological conditions when helium concentrations in the T2 aquifer (and possibly T1 aquifer) differed from what they are today. At Site 13 (where the aquifer concentrations are lower), the aquifer(s) must have had higher concentrations of helium because the aquitard itself cannot retain internally produced helium when the rate of diffusive loss exceeds the production rate. The remnant high helium concentrations in the aquitard coupled with high diffusion rates indicate that this change must have been relatively recent.

This abrupt change in helium concentration cannot be verified with the current information, but it may be the affect of industrial groundwater pumping centres including Osborne (T2 aquifer; Penrice Soda Products), Regency Park (Coopers Brewery) T2 aquifer; Penrice Soda Products T1). However, the change in helium concentrations is perplexing because even with high rates of pumping, the distance groundwater, and thus helium, has moved since pumping began is not expected to be great. However these concentration changes could be related to flow across faults where pumping has increased vertical gradients and induced vertical flow and mixing. With Site 6 adjacent to the Para Fault and Site 13 adjacent to the Redbank Fault, this scenario seems plausible.

Furthermore, helium concentrations are uncorrelated with carbon-14 activities presented in Appendix E. This suggests that helium is not uniformly being added to the groundwater, but instead helium is being released in more discreet areas. This could account for the large spatial variation in helium concentrations in the aquifers (see Appendix E) and account for the transient conditions seen the Munno Para Clay aquitard. Future noble gas sampling could verify the variability of these helium concentrations and see if there is a seasonality caused by varying pumping rates. If helium is an indicator of inter-aquifer leakage at fault zones, it would be valuable information in the management of the Adelaide Plains water resources.

## F.6 Conclusions

This study has modelled hydraulic conductivity through the Munno Para Clay and has found values that are similar, but higher than those previously determined by Gerges (1999). The leakage at the study areas appears to be on the order of 1 mm/y, leaking from the T2 aquifer, upward into the T1 aquifer. Whilst the previous measurements were valid, they were core-scale estimates that were then applied to the entire formation thickness and onto the entire basin. In this study environmental tracer measurements of the Munno Para Clay have been used to upscale to the formation-scale, which is more reliable as it integrates the small variations in permeability as they relate to lithology and structural features. It should be stressed that we now have two formation-scale estimates, but applying these values to the entire basin requires a great deal of extrapolation. The methods applied have limitations because of recent transient conditions that have altered the helium concentrations within the Munno Para Clay. However, the data still provides valuable insight into the permeability of the Munno Para Clay and the changes to the system that have likely occurred as a result of pumping. When applied to the entire Adelaide Plains sub-basin where the Munno Para Clay is present, the potential for vertical leakage as determined by the current hydraulic gradient shows that the net leakage is downward. This downward leakage is induced by pumping in the T2 in the Northern Adelaide Plains around Virginia.

## F.7 References

- Ali S, Stute M, Torgersen T and Winckler G (2011) Helium measurements of pore fluids obtained from the San Andreas Fault Observatory at Depth (SAFOD, USA) drill cores. *Hydrogeology Journal* 19, 317-332.
- Ballentine CJ and Burnard PG (2002) Production, release and transport of noble gases in the continental crust. In: Porcelli D, Ballentine CJ and Wieler R (eds) *Reviews in Mineralogy and Geochemistry*. Mineralogical Society of America, Geochemical Society, Washington, DC, 481-538.
- Crosbie RS, Morrow D, Cresswell RG, Leaney FW, Lamontagne S and Lefournour M (2012) New insights into the chemical and isotopic composition of rainfall across Australia. CSIRO Water for a Healthy Country Flagship, Australia.
- DEWNR (2015) WaterConnect. Viewed 6 February 2015, <<http://www.waterconnect.sa.gov.au/>>.
- Earthref.org (2015) Geochemical Earth Reference Model (GERM). Viewed February 12, 2015, <<http://earthref.org/GERM/>>.
- Gardner P and Solomon DK (2009) An advanced passive diffusion sampler for the determination of dissolved gas concentrations. *Water Resources Research* 45. DOI: Artn W06423 Doi 10.1029/2008wr007399.
- Gardner WP, Harrington GA and Smerdon BD (2012) Using excess (4)He to quantify variability in aquitard leakage. *Journal of Hydrology* 468, 63-75.
- Gerges NZ (1999) The geology and hydrogeology of the Adelaide Metropolitan Area. Flinders University.
- Harrington GA, Gardner WP, Smerdon BD and Hendry MJ (2013) Palaeohydrogeological insights from natural tracer profiles in aquitard porewater, Great Artesian Basin, Australia. *Water Resources Research* 49(7), 4054-4070. DOI: 10.1002/wrcr.20327.
- Hart DJ, Bradbury KR and Feinstein DT (2006) The vertical hydraulic conductivity of an aquitard at two spatial scales. *Ground Water* 44(2), 201-211. DOI: 10.1111/j.1745-6584.2005.00125.x.
- Heaton THE and Vogel JC (1981) Excess air in groundwater. *Journal of Hydrology* 50(1-3), 201-216. DOI: 10.1016/0022-1694(81)90070-6.
- Hendry MJ, Kelln CJ, Wassenaar LI and Shaw J (2004) Characterizing the hydrogeology of a complex clay-rich aquitard system using detailed vertical profiles of the stable isotopes of water. *Journal of Hydrology* 293(1-4), 47-56. DOI: 10.1016/j.jhydrol.2004.01.010.
- Hendry MJ, Kotzer TG and Solomon DK (2005) Sources of radiogenic helium in a clay till aquitard and its use to evaluate the timing of geologic events. *Geochimica et Cosmochimica Acta* 69(2), 475-483.
- Mazurek M, Alt-Epping P, Bath A, Gimmi T, Waber HN, Buschaert S, De Canniere P, De Craen M, Gautschi A, Savoye S, Vinsot A, Wemere I and Wouters L (2011) Natural tracer profiles across argillaceous formations. *Applied Geochemistry* 173(1-4), 219-240.
- Osenbrück K, Lippmann J and Sonntag C (1998) Dating very old pore waters in impermeable rocks by noble gas isotopes. *Geochimica et Cosmochimica Acta* 62(18), 3041-3045.
- Poole JC, McNeill GW, Langman SR and Dennis F (1997) Analysis of noble gases in water using a quadrupole mass spectrometer in static mode. *Applied Geochemistry* 12(6), 707-714. DOI: Doi 10.1016/S0883-2927(97)00043-7.
- Rayment GE and Higginson FR (1992) Australian laboratory handbook of soil and water chemical methods. Australian laboratory handbook of soil and water chemical methods., xvii + 330pp.-xvii + 330pp.
- REM (2006a) North Adelaide Plains – Water Balance.
- REM (2006b) Tertiary Aquifers of the Adelaide Coastal Plains Groundwater Model: Transient Model Set-up and Calibration Report - Working Draft.

- van der Kamp G (2001) Methods for determining the in situ hydraulic conductivity of shallow aquitards - an overview. *Hydrogeology Journal* 9(1), 5-16. DOI: 10.1007/s100400000118.
- Zulfic H, Osei-Bonsu K and Barnett S (2008) Adelaide Metropolitan Area Groundwater Modelling Project. Volume 1 - Review of Hydrogeology, and Volume 2 - Numerical model development and prediction run. Department of Water, Land and Biodiversity Conservation.

# Appendix G Seawater intrusion and sources of groundwater salinity

Author: *Post VEA and Banks EW*

## G.1 Executive Summary

Considerable uncertainty exists about the potential for seawater intrusion and the origin of dissolved salts in the groundwater system of the Adelaide Plains. However, an adequate monitoring infrastructure for detailed investigations along the coast is absent. Therefore, to increase the understanding of seawater intrusion, hydrochemical and isotope data were collected along a transect perpendicular to the coastline at Aldinga Beach. The objective was to establish the presence of intruded seawater, the geometry of the wedge and the age of the groundwater. The insights obtained were subsequently applied to the aquifer system of the Adelaide Plains.

The results show a consistent increase of the salinity with depth at all three sites along the 1 km long transect through the Port Willunga Formation (PWF, the equivalent of T1/T2 aquifers in the Adelaide Plains). The salinities in the lower part of the Port Willunga Formation are considerably higher than the salinity of seawater. Based on a combination of stable water isotopes and chloride, seawater could be discerned from the hypersaline water in the lower part of the aquifer, and the individual contributions of these two saline waters to mixtures with freshwater could be quantified. A unique finding is that seawater appears to have intruded over the top of the hypersaline groundwater instead of the bottom of the aquifer, which is normally observed.

The formation of hypersaline water is attributed to a combination of atmospheric deposition of solutes in combination with water removal by evapotranspiration under much drier climate conditions than today. While the exact age of the hypersaline water could not be established based on measured radiocarbon activities, it appears to be at least tens of thousands of years old. There exists a remarkable gap between this inferred age and that of the freshwater (age < 2000 years) in the uppermost part of the aquifer. Based on stable water isotope values  $^{87}\text{Sr}/^{86}\text{Sr}$  ratios two types of freshwater could be discerned: One originating from recharge further inland and one from local recharge through the Quaternary unit overlying the PWF.

Saline groundwater with the same stable water isotope characteristics as the hypersaline groundwater in Aldinga Beach was found in the newly-drilled wells at Strangways Tce/War Memorial Drive in North Adelaide. To test if it could also be identified elsewhere in the Adelaide Plains region, attempts were made to obtain samples from bores with a high salinity but these were unsuccessful. Instead, hydrochemical data were sourced from the WaterConnect database and a three-end member mixing model was developed based on ionic ratios. Based on this analysis it was found that the hypersaline groundwater, or mixtures thereof with other water types, appears to be pervasive across the greater Adelaide region and does not appear to be restricted to a particular aquifer or depth.

## G.2 Introduction

Seawater intrusion is a worldwide problem that causes salinization of abstraction wells in aquifers around the world (Werner et al 2012). Under natural conditions and with a stable coastline position, a wedge of seawater encroaches into the onshore portion of coastal aquifers. This wedge of dense seawater thus sits in the bottom portion of the aquifer, with fresh groundwater flowing seaward above it. The two water bodies are separated by a mixing zone in which the salinities change gradually.

A seminal case study that demonstrated the existence of a wedge of intruded seawater was published by Cooper et al. (1964), who used a detailed monitoring network of observation wells to investigate the salinity distribution in the Biscayne aquifer in Florida with a thickness of 40 m. They found that the wedge had a wide mixing zone and that the maximum inland distance of the toe varied along the coastline, ranging from 480 m to 3600 m. Another study from the eastern seaboard of the USA by Lusczynski and Swarzenski (1966) demonstrated the existence of a wedge of intruded seawater below Long Island (NY) and highlighted the controls of lithology.

Following these relatively early studies, the presence of a seawater wedge has been demonstrated in many coastal aquifers elsewhere (Reilly and Goodman, 1985). However, detailed hydrochemical studies of the wedge and the overlying mixing zone are rarer (Jones et al., 1999). Magaritz and Luzier (1985) published a detailed hydrochemical characterisation of the seawater intrusion wedge and the overlying fresh groundwater in Oregon (USA) based on samples taken from high resolution multi-level observation wells. They identified cation exchange and redox reactions as well as feldspar formation to produce observable changes in the groundwater composition. Stuyfzand (1998) provided a detailed characterisation of groundwater bodies below the coastal dunes of the Netherlands and discussed the chemical parameters that can be used to distinguish between different water types. He showed how a wedge of intruded seawater can be distinguished from relic seawater that infiltrated from a lagoon system that predates the formation of the coastal dunes.

Detailed insight into the chemical processes in a front of intruded seawater during a forced seawater intrusion experiment were presented by Andersen et al. (2005). Notably, they were able to identify cation exchange and changes in redox state triggered by flooding of the beach aquifer by seawater during a storm surge. Using data from the same research site Jørgensen et al. (2008) used a three-end member mixing model based on  $^{87}\text{Sr}/^{86}\text{Sr}$  ratios to distinguish between intruded seawater and two fresh groundwater sources.

A detailed chemical characterisation of the chemical processes within the mixing zone was performed by Sivan et al. (2005) who used a multi-level observation well with a vertical resolution of 10 cm. They identified three main water types and found that cation exchange mainly occurred in intruded seawater that is diluted by up to 20% freshwater. Sivan et al. (2005) further noted that  $^{14}\text{C}$  of  $^3\text{H}$ -bearing intruded seawater is depleted with respect to modern atmospheric carbon, which they attributed to anaerobic degradation of organic carbon with a low  $^{14}\text{C}$  activity. This hypothesis is consistent with negative  $\delta^{13}\text{C}$  values that were found. Voss and Wood (1994) reported comparable findings in a geochemical study of seawater intrusion on the island of Oahu in Hawaii.

Only a few previous studies have considered seawater intrusion in the Adelaide Plains. High salinities in the deep parts of the Q1 aquifer were attributed to seawater intrusion or saltwater upconing caused by overpumping (Lamontagne et al, 2005). Similarly, salinities ranging from 2,000 to 18,000 mg/L in the Q1 and Q2 aquifers in the North Adelaide Plains (NAP) were assumed to be due to seawater intrusion.

The most detailed characterisations of seawater intrusion have been made for the LeFevre Peninsula. Martin (1996) presented the results of a hydrogeological characterisation study, which showed the presence of a narrow transition zone in the Q1(a) aquifer along the western side of the peninsula. A wider transition zone was identified along the eastern side, which was attributed to the entrapment and release of connate saltwater. The groundwater salinity distribution is adjusting to the anthropogenic modifications to the hydrological system, which include containment of the Port Adelaide River, land reclamation and increased recharge due to urbanisation. Despite the increases in recharge, Martin (1996) found that evaporation and abstraction were resulting in a decline in freshwater volume and predicted that a landward shift of the fresh-saltwater interface would occur.

Ashenden (2008) used the time-domain electromagnetic method (TDEM) to delineate the position of the fresh-saltwater interface, validated with salinity measurements from boreholes, and inferred the presence of a freshwater lens in the Quaternary aquifer with a depth of up to 20 m below the ground surface. The lens is elongated in a north-south direction, and the deepest part of the freshwater lens appears to be a few hundred meters west of its central axis (Ashenden, 2008). Based on water balance calculations,

Ashenden (2008), like Martin (1996), concluded that the freshwater volume is presently declining and that active seawater intrusion must be occurring.

Salinity increases reported in near-coastal wells installed in the Port Willunga Formation and Maslin Sand aquifers in the Willunga embayment have been tentatively attributed to seawater intrusion (Martin et al, 1998; Lamontagne et al, 2005). To increase the understanding of seawater intrusion in the Willunga Embayment, three of multi-level observations wells were constructed along a transect perpendicular to the coastline at Aldinga Beach. The objective of the study was to establish the presence of intruded seawater, the geometry of the wedge and the age of the groundwater. The insights obtained from this study are believed to be transferable to the sedimentary aquifer system of the Adelaide Plains, with the provision that the thickness of the sedimentary units at Aldinga Beach, in particular the Quaternary cover, is less than across most parts of the Adelaide region.

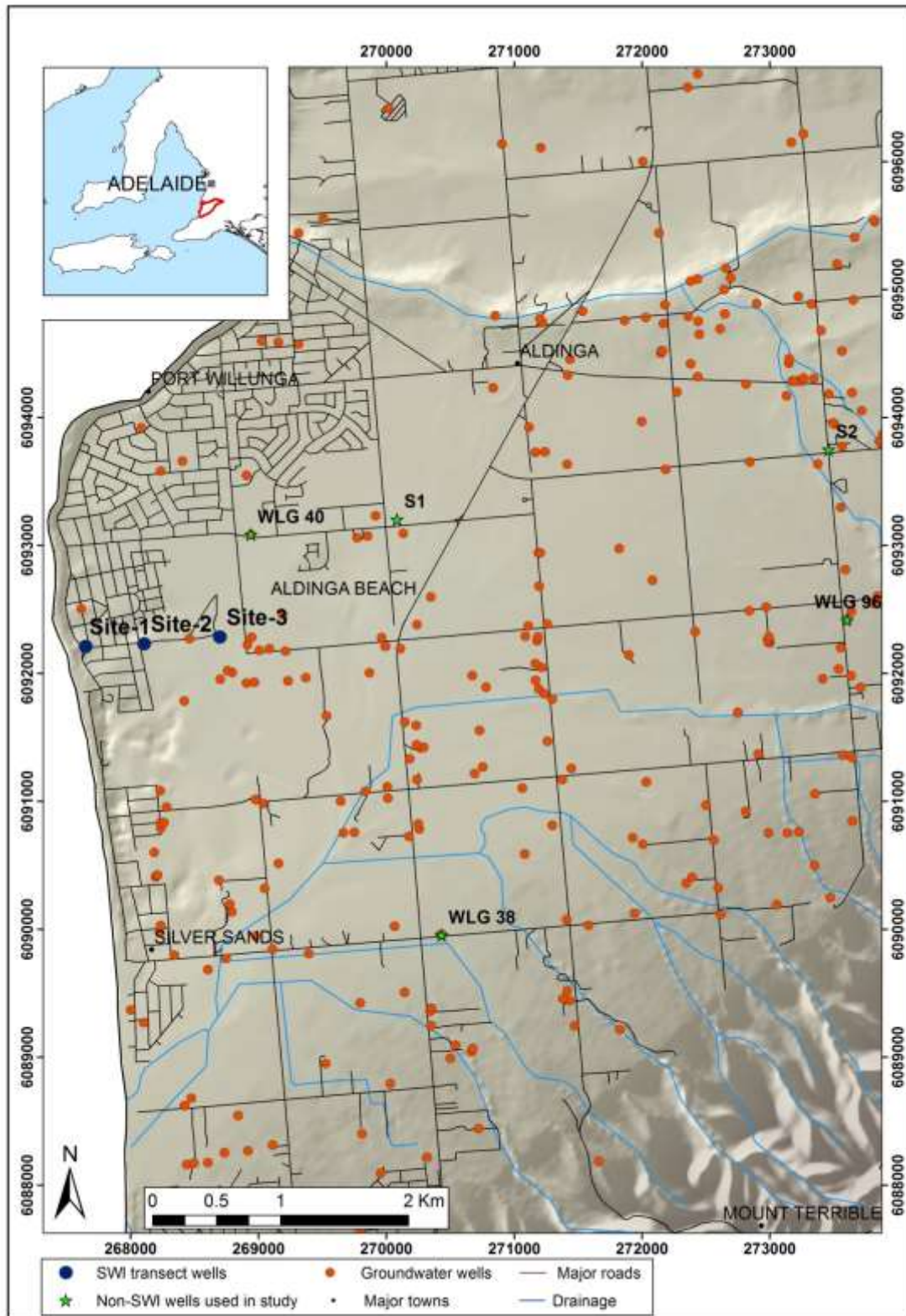
As will be shown below, the aquifers in the Willunga Embayment contain groundwater with a salinity much higher than seawater. This complicates the interpretation of groundwater salinities, as an elevated salinity in a sample might indicate seawater intrusion or mixing of freshwater and the hypersaline groundwater, or another process like strong evaporation. The final part of this document will discuss the implications for the interpretation of high salinities of groundwater in the Adelaide Plains region.

### G.3 Methods

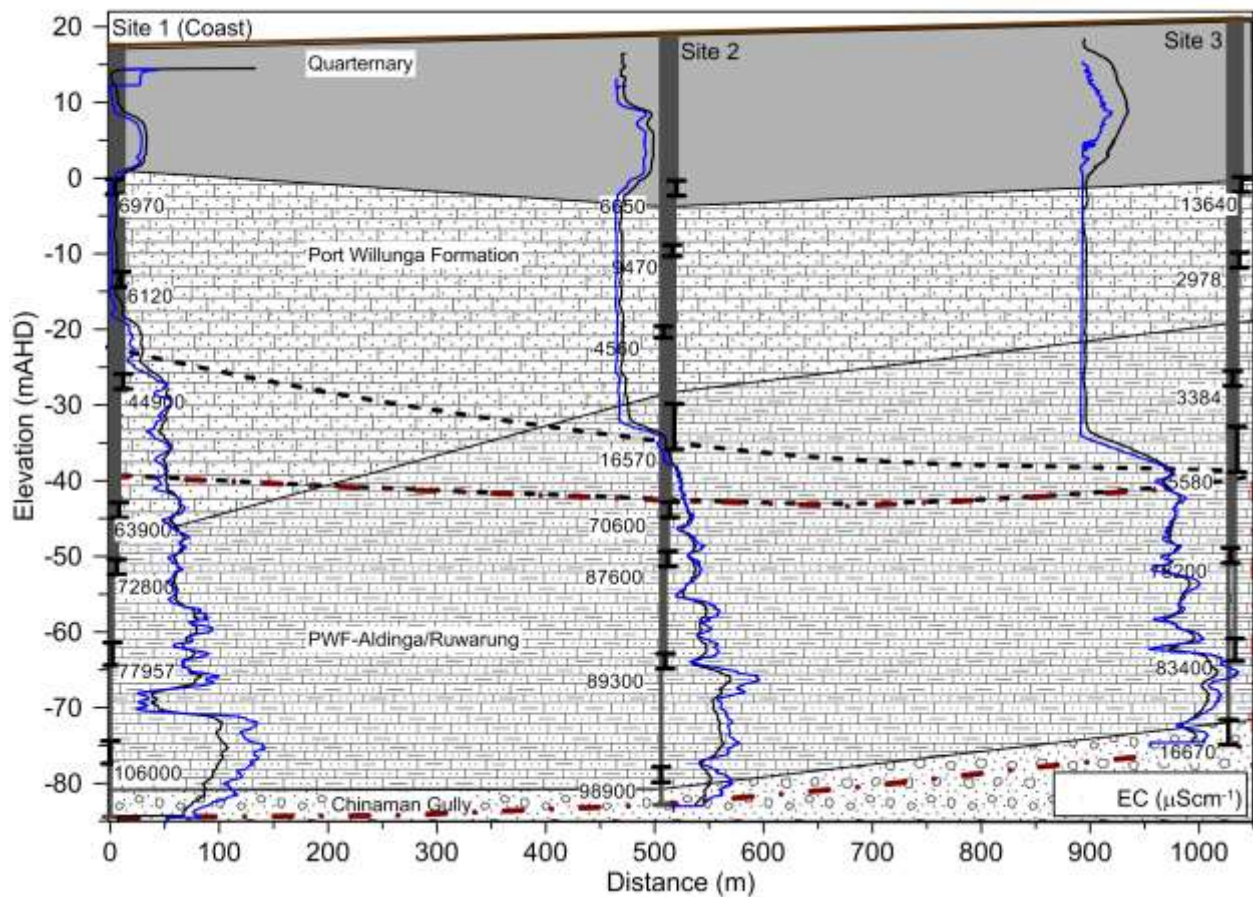
Drilling of the wells took place in November and December 2012. A total of 22 observation wells were installed at 3 sites along a transect at variable distances from the coastline (Apx Figure G.1). The wells at site 1, nearest to the shore, is about 150 m from the midpoint between the low- and high-tide marks and is located on the Esplanade in the town of Aldinga Beach. A total of seven observation wells have been installed at this location and at multiple depths with short screen intervals (Apx Figure G.2). At site 2, which is located 503 m inland from site 1, 8 wells have been completed, and at site 3, which is 1022 m inland from site 1, seven wells have been installed. Except the topmost well screen at site 2, which sits in the Quaternary sediments, and the deepest at site 3, which sits in the Chinaman Gully Formation, all screens are constructed in the Port Willunga Formation (PWF), which has been found along the transect roughly between 0 and -80 m AHD (Apx Figure G.2).

Sampling of the wells took place in January and February of 2013. Prior to sampling, wells were purged with either Grundfos MP1 pumps or Proactive 12V Monsoon pumps. As many of the wells are low-yielding, the purge volumes varied, but were never less than 1 well volume, more often close to or more than 3 well volumes. Flow rates were kept between 2L/min and 5L/min to prevent inter-well interference. A YSI or WTW multi-probe was used to monitor chemical parameters which were used as a guide for sampling. Alkalinity was measured in the field using a Hach digital titrator.

Samples were taken for major ions (50 ml each for anions and cations, HDPE), stable isotopes of water (2 ml glass vials), carbon isotope ( $^{13}\text{C}/^{12}\text{C}$  and  $^{14}\text{C}$ ) (250 ml HDPE), and  $^{87}\text{Sr}/^{86}\text{Sr}$  (500 ml HDPE). Field filtration was done for major ions and  $^{87}\text{Sr}/^{86}\text{Sr}$  using 45  $\mu\text{m}$  filters. The sample bottles for cations were also pre-acidified with a few drops of ultrapure  $\text{HNO}_3$  in the field to obtain a  $\text{pH} < 2$ . Samples for helium (He), neon (Ne), argon (Ar) and nitrogen ( $\text{N}_2$ ) analysis were collected using passive gas diffusion samplers (Gardner and Solomon, 2009) installed at screen depth for a minimum of 4 days. Some low yielding wells (SWI-1C, SWI-5D, SWI-7A, SWI-8D) were sampled using a bailer and only sampled for major ions and stable water isotopes. SWI-1C and SWI-1B were resampled in August 2013 due to insufficient purging.



Apx Figure G.1 Map showing the locations of the wells along the seawater intrusion transect, and other wells in the vicinity.



Apx Figure G.2 Cross-section along the seawater intrusion well transect in Aldinga Beach showing the geology, electrical conductivity distribution and the boundary between fresh, saline and hypersaline groundwater. Black and blue lines represent the measured bulk conductivity (mS/m) of the aquifer. Black dashed line shows the boundary between intruded seawater and fresh groundwater. Red dashed line shows the bounds of the hypersaline groundwater.

## G.4 Results

The data show a consistent increase of the salinity with depth at all three sites (Apx Figure G.2, Apx Table G.1 Apx Table G.2). The salinities in the lower part of the Port Willunga Formation are considerably higher than the salinity of seawater. Apx Figure G.3 shows a graph of  $\delta^{18}\text{O}$  and  $\delta^2\text{H}$  versus chloride ( $\text{Cl}^-$ ) for the three sites. For site 1, the data plots along two mixing lines; one mixing line represents mixing between fresh groundwater with the measured isotopic composition and salinity of seawater in the Gulf St Vincent and the other mixing line between fresh groundwater and hypersaline water. One data point (SWI-2B, screen elevation -44.0 m) has an almost identical  $\delta^{18}\text{O}-\text{Cl}^-$  and  $\delta^2\text{H}-\text{Cl}^-$  signature as seawater. The sample from the screen above (SWI-3A, screen elevation -27.0 m) plots near the mixing line between seawater and fresh groundwater, whilst the deeper wells at the site -63.0 m and -76.0 m plot near the hypersaline end member.

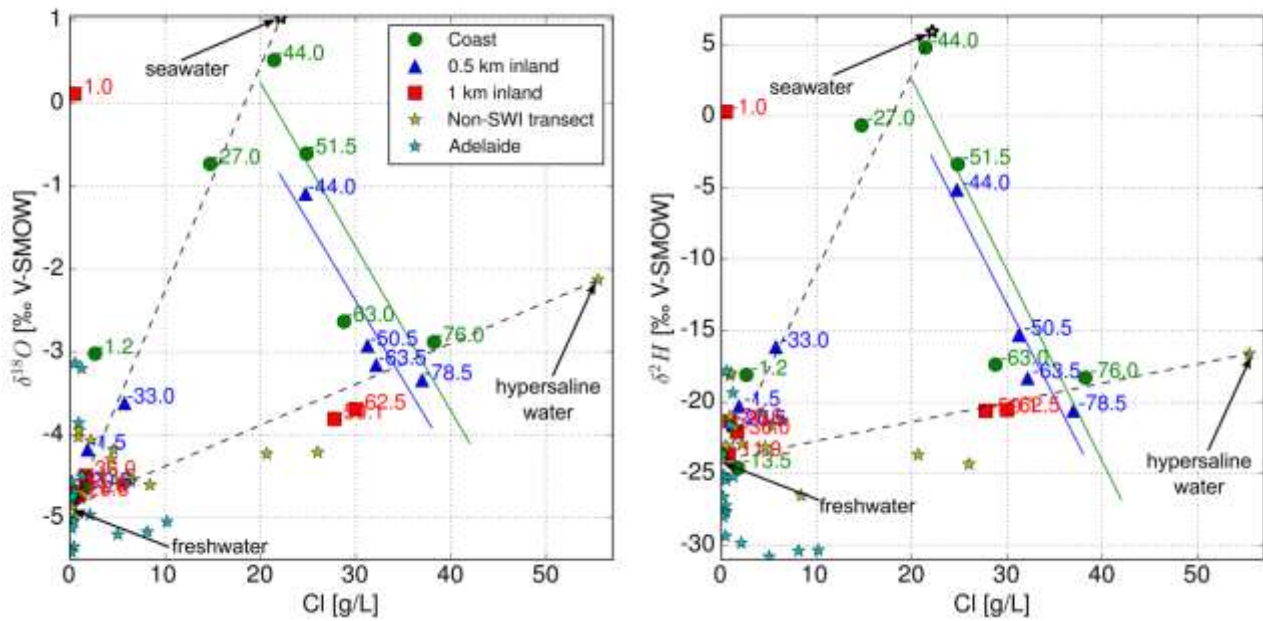
A similar pattern is visible for site 2, with the samples from the bottom part of the aquifer plotting near a mixing line between hypersaline water and seawater, and those from the upper part of the aquifer plotting near a mixing line between seawater and fresh groundwater. At site 3, however, there are no data points that suggest a presence of seawater at this location, and here, only fresh groundwater overlying hypersaline groundwater can be recognised.

**Apx Table G.1 Coordinates, well depths, pH, alkalinity and major ion concentrations of the wells along the seawater intrusion transect.**

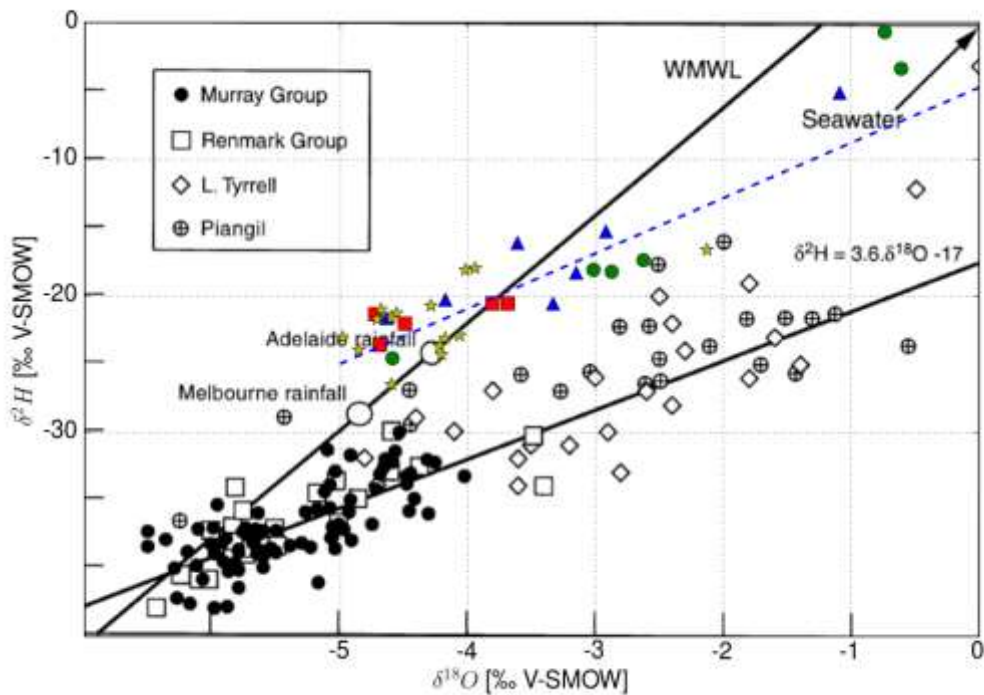
Sample ID	Easting	Northing	Screen top	Screen Bottom	Sampling Date	pH	Specific conductivity	Total Alkalinity	F	Cl	Br	NO3	SO4	Ca	K	Mg	Na	Si	Sr
			m AHD	m AHD			dS/m	meq/L	mg/L	mg/L	mg/L	mg/L	mg/L	mg/L	mg/L	mg/L	mg/L	mg/L	mg/L
SWI - 1A	267634.5	6092213	-74.5	-77.5	17/01/2013	6.9	106	5.9	<5	38226	120	4.1	2146	1650	506	1650	20700	<10	33.3
SWI - 1B	267634.5	6092213	-61.5	-64.5	15/08/2013	6.8		5.3	2.8	28800	86	1170.0	8470	1490	390	1050	15800		18
SWI - 1C	267634.4	6092213	-0.2	-2.2	7/02/2013	12.1	7.0	12.3	2.1	2619	7.9	nd	365	214	36		1722	1.41	1.7
SWI - 2A	267633.5	6092215	-50.5	-52.5	18/01/2013	7.1	73	3.5	<5	24831	77	5.5	2336	1200	398	1270	14600	<5	22.3
SWI - 2B	267633.5	6092215	-43.0	-45.0	18/01/2013	7.8	64	2.6	<5	21432	66	3.9	2867	639	437	1330	13100	<5	10.9
SWI - 2C	267633.5	6092215	-12.5	-14.5	17/01/2013	7.8	6.1	6.8	<0.5	1750	5.2	3.5	179	116	31.4	121	982	11.7	1.93
SWI - 3A	267632.5	6092217	-26.0	-28.0	18/01/2013	7.8	45	3.4	<2	14739	48	1.7	2166	470	309	941	8620	<2.5	7.38
SWI - 4A	268134.5	6092241	-77.0	-80.0	30/01/2013	6.7	99	6.5	<0.2	36973	114	4.2	2114	1430	440	1390	18400	<10	27.6
SWI - 4B	268134.5	6092241	-19.7	-21.2	29/01/2013	7.5	4.6	6.2	<0.2	1267	4.1	5.5	150	118	14.1	83.2	647	13.5	1.63
SWI - 5A	268136.8	6092241	-62.5	-64.5	29/01/2013	7.1	89	5.4	<5	32162	100	6.0	1855	1450	364	1310	16500	<10	29.4
SWI - 5B	268136.8	6092241	-49.5	-51.5	30/01/2013	6.9	88	5.4	<5	31252	96	5.5	1926	1450	354	1290	16000	<10	29.8
SWI - 5C	268136.7	6092241	-43.0	-45.0	6/02/2013	7.5	71	5.0	<5	24739	81	12	2499	1050	333	1300	12700	<10	22.2
SWI - 5D	268136.7	6092241	-9.0	-10.5	22/04/2013	12.4				344	1		28	480	302	0.05	462		
SWI - 6A	268138.9	6092241	-30.0	-36.0	30/01/2013	7.4	17	6.0	<1	5726	37	4.8	857	224	79	341	2790	11.8	3.49
SWI - 6B	268138.9	6092241	-0.5	-2.5	30/01/2013	7.6	6.7	7.0	0.8	1864	5.5	3.4	386	112	26.2	124	1060	9.52	2.4
SWI - 7A	268651.9	6092289	-71.6	-75.1	22/04/2013	12.0		12.3		4216	7.3		92	916	221	0.06	2400		
SWI - 7B	268652	6092289	-49.1	-51.1	7/06/2013	7.0	78	5.9	<5	27774	89	6.2	1533	1380	258	1160	14100	<10	27
SWI - 7C	268652	6092289	-25.6	-27.6	7/02/2013	8.0	3.4	6.5	0.4	899	2.8	9.8	100	120	11.8	74.1	418	13	1.47
SWI - 8A	268654.8	6092289	-61.0	-64.0	6/02/2013	6.8	83	6.3	<5	30009	92	4.9	1773	1370	308	1240	15200	<10	26.6
SWI - 8B	268654.9	6092289	-33.0	-39.0	6/02/2013	7.7	5.6	5.5	0.3	1652	5.0	7.5	139	179	23.3	92.1	786	12.6	2.7
SWI - 8C	268654.9	6092289	-10.0	-12.0	6/02/2013	7.9	3.0	6.4	0.4	758	2.2	5.4	86	117	14.5	70.1	373	13	1.65
SWI - 8D	268654.8	6092290	0.0	-2.0	8/02/2013	12.6				480	0.7		3.2	439	639	0.05	1080		

**Apx Table G.2 Isotope values of the wells along the seawater intrusion transect.**

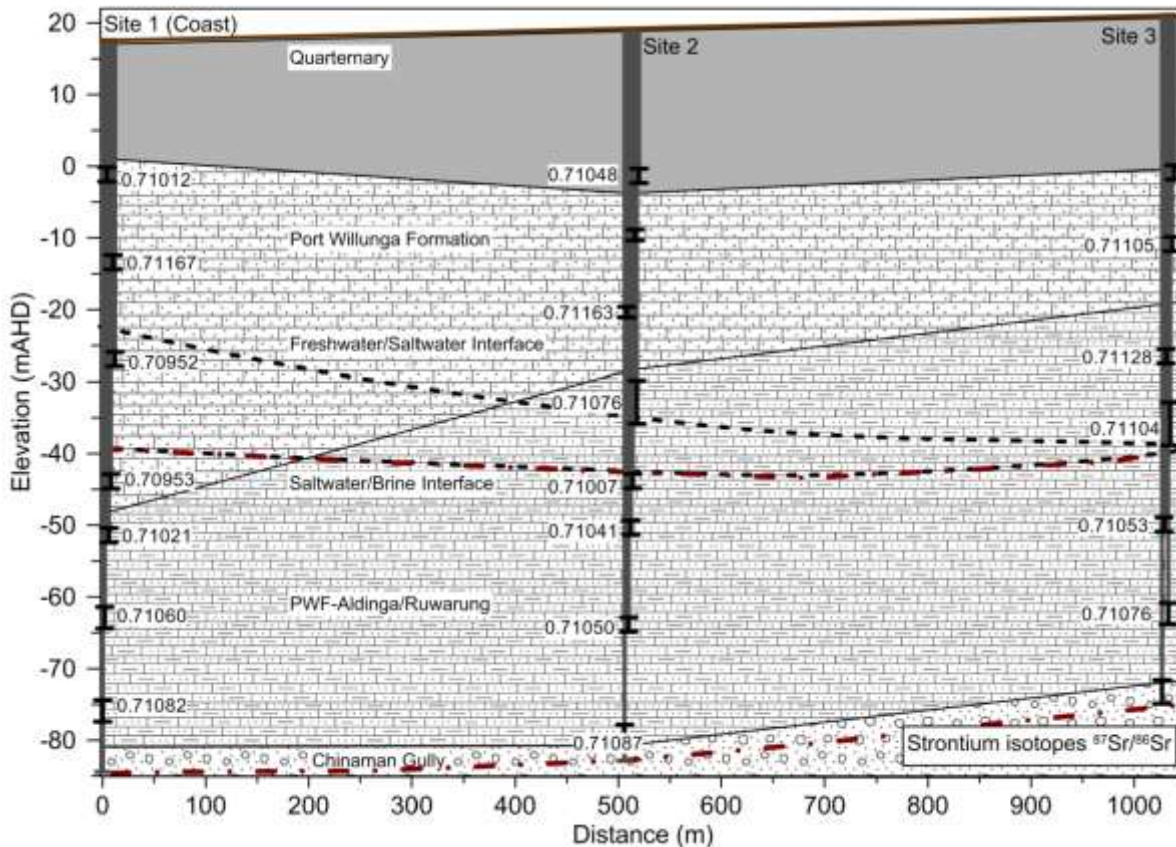
Sample Id	$\delta^2H$ ‰	$\delta^{18}O$ ‰	$\delta^{13}C$ ‰	$^{14}C$ pmC	$^{87}Sr/^{86}Sr$
SWI - 1A	-18.3	-2.88	-5.83	0.7	0.71082
SWI - 1B	-17.4	-2.63			0.7106
SWI - 1C	-18.1	-3.02			0.71012
SWI - 2A	-3.4	-0.61	-5.95	3.8	0.71021
SWI - 2B	4.8	0.52	-6.2	13.5	0.70953
SWI - 2C	-24.6	-4.59	-9.76	40.7	0.71167
SWI - 3A	-0.7	-0.73	-6.71	46.5	0.70952
SWI - 4A	-20.6	-3.34	-8.07	1.4	0.71087
SWI - 4B	-21.6	-4.63	-10.02	45.4	0.71163
SWI - 5A	-18.3	-3.15	-6.43	1.6	0.7105
SWI - 5B	-15.3	-2.92	-5.95	1.8	0.71041
SWI - 5C	-5.1	-1.09	-5.82	3.3	0.71007
SWI - 5D					
SWI - 6A	-16.1	-3.62	-9.55	42.1	0.71076
SWI - 6B	-20.3	-4.17	-11.12	59.0	0.71048
SWI - 7A					
SWI - 7B	-20.6	-3.81	-6.5	2.8	0.71053
SWI - 7C	-21.3	-4.73	-10.96	52.7	0.71128
SWI - 8A	-20.5	-3.69	-7.87	2.9	0.71076
SWI - 8B	-22.1	-4.49	-10.58	52.5	0.71104
SWI - 8C	-23.6	-4.69			0.71105
SWI - 8D	0.29	0.11			



Apx Figure G.3 Graphs showing (left)  $\delta^{18}\text{O}$  versus Cl- concentration (right)  $\delta^2\text{H}$  versus Cl concentration for the samples from the seawater intrusion well transect in Aldinga Beach. Sample labels show the mid-screen depth referenced to mAHD. Samples from nearby observation wells not part of the transect are also shown (star symbol). Green and blue lines represent line of best fit, which is included to emphasise the mixing behaviour between hypersaline groundwater and seawater. Black dashed lines represent mixing lines between fresh groundwater (sample WLG102) and seawater (based on Short, 2011, Corlis et al. 2001), as well as fresh groundwater and the selected hypersaline end member (WLG096). Blue stars represent data from the new wells drilled for this project in the Adelaide Plains.



Apx Figure G.4 Graph showing  $\delta^2\text{H}$  versus  $\delta^{18}\text{O}$  published by Herczeg et al. (2001) with data points from this study overlain. The dashed blue line shows the line of best fit through the data points of the samples from the SWI transect and nearby wells that were found to have a contribution of the seawater end member less than 5%.



Apx Figure G.5 Cross-section along the seawater intrusion well transect in Aldinga Beach showing  $^{87}\text{Sr}/^{86}\text{Sr}$  ratios.

The shallowest samples from sites 1, 2 and 3 appear to be more enriched in stable water isotopes than fresh groundwater (Apx Figure G.3). At site 3 enrichment is quite extreme ( $\delta^2\text{H} = 0.29\text{‰}$ ,  $\delta^{18}\text{O} = 0.11\text{‰}$ , sample SWI-8D). Similar water types have been found in nearby wells (Apx Figure G.3) from the Quaternary, PWF and Maslin Sands aquifers. These water samples that have experienced strong enrichment of the stable water isotopes with an only moderate increase of the  $\text{Cl}^-$  concentration, is indicative for direct evaporation of water. A graph of  $\delta^2\text{H}$  versus  $\delta^{18}\text{O}$  (Apx Figure G.4) appears to support this as the groundwater samples that have a negligible contribution of seawater (as detailed below) plot along a line with a slope of 4.05 (intercept  $-4.8\text{‰}$ ). It is worth noting here also that the slope is comparable to the slope of 3.6 reported by Herczeg et al (2001) for groundwater samples from the Murray-Darling Basin covering a comparable range of salinity.

The  $^{87}\text{Sr}/^{86}\text{Sr}$  ratios of the wells in the transect range between 0.70952 and 0.71167. Sample SWI-2B, which was identified as the closest resemblance to seawater (Apx Figure G.5) has a  $^{87}/^{86}\text{Sr}$  ratio of 0.70953, which is close to the marine ratio of 0.7092 (Jørgensen et al. 2008). Values in the hypersaline groundwater in the bottom half of the PWF are characterised by values of 0.710 to 0.711 or higher, whilst those in the fresher water above are larger than 0.711. The shallowest samples at sites 1 and 2, however, have slightly but significantly lower  $^{87}/^{86}\text{Sr}$  ratios (0.71012 and 0.71048, respectively) again.

Owing to the identification of three distinct water types (hypersaline groundwater, intruded seawater, fresh groundwater, Apx Figure G.3), a three-end member mixing model could be applied to quantify the contribution of each end member to each sample. Based on a mass balance for  $\text{Cl}$  and  $^{18}\text{O}$ , and noting that the proportions of each end member should add up to 1, the following system of equations defines the mixing model:

$$\begin{aligned}
m_{Cl, sample} &= f_{hypersaline} \times m_{Cl, hypersaline} + f_{sea} \times m_{Cl, sea} + f_{fresh} \times m_{Cl, fresh} \\
\delta^{18}O_{sample} &= f_{hypersaline} \times \delta^{18}O_{hypersaline} + f_{sea} \times \delta^{18}O_{sea} + f_{fresh} \times \delta^{18}O_{fresh} \quad (1) \\
f_{hypersaline} + f_{sea} + f_{fresh} &= 1
\end{aligned}$$

where  $m_{Cl}$  denotes the Cl<sup>-</sup> concentration (mol/kgw),  $\delta^{18}O$  the  $\delta$ -value for <sup>18</sup>O (‰ V-SMOW) and  $f$  represents the fraction of each end member that contributes to the sample. The subscripts refer to each of the end members defined previously. Sample WLG096 was selected as the hypersaline end member, sample WLG102 as the fresh end member and values for the seawater end member were based on values reported by Short (2011) and Corlis et al (2001). Chloride concentrations and  $\delta^{18}O$  values of the end members are listed in Apx Table G.3.

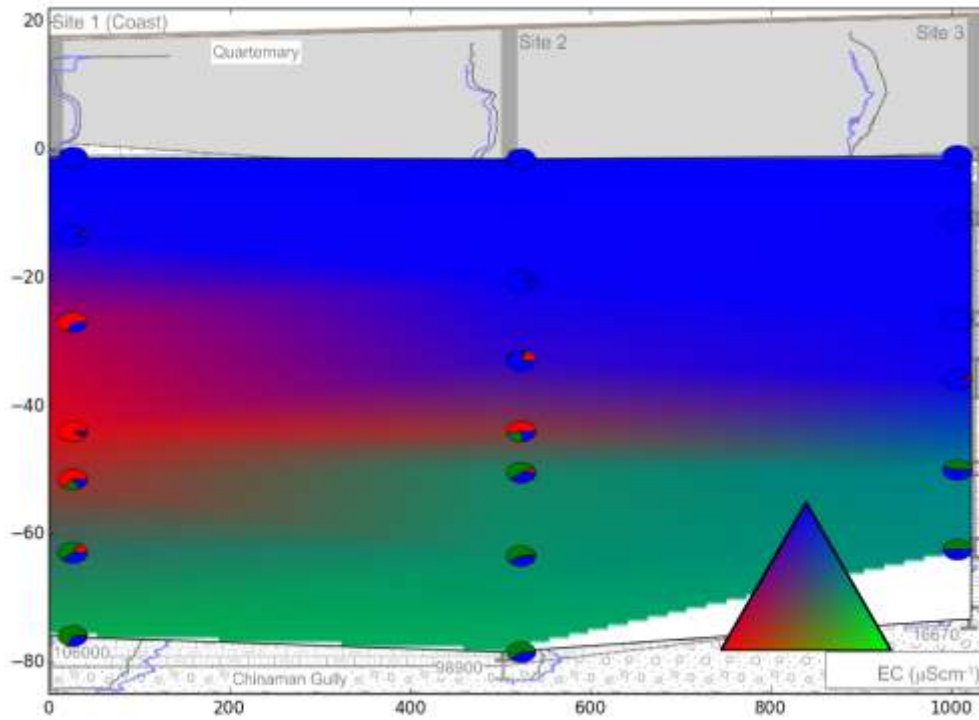
**Apx Table G.3 Chloride concentration, isotopic composition and ionic ratio of the end members used in the mixing calculations.**

End member	Obswell number	Cl mg/L	$\delta^{18}O$ ‰	$\delta^{13}C$ ‰	<sup>14</sup> C pmC	Cl / (TIC + SO <sub>4</sub> )	Na / (K + Ca + Mg)
Hypersaline (Willunga)	WLG096	55458	-2.13	-7.13	0	36.9	4.7
Hypersaline (Adelaide)	YAT087	82767	-0.8	-	0	42.4	5.2
Seawater	-	22160	1.03	1	30	9.1	3.4
Freshwater	WLG102	370	-4.85	-11.1	60	1.5	1.2
Sediment source	-	-	-	0.0	0.0	-	-

The system of equations can be written in matrix form

$$\begin{bmatrix} m_{Cl, hypersaline} & m_{Cl, sea} & m_{Cl, fresh} \\ \delta^{18}O_{hypersaline} & \delta^{18}O_{sea} & \delta^{18}O_{fresh} \\ 1 & 1 & 1 \end{bmatrix} \begin{bmatrix} f_{hypersaline} \\ f_{sea} \\ f_{fresh} \end{bmatrix} = \begin{bmatrix} m_{Cl, sample} \\ \delta^{18}O_{sample} \\ 1 \end{bmatrix} \quad (2)$$

which was solved using SciPy's least squares solver (Jones et al. 2001). For some samples, due to scatter in the data, small (< 0.05) negative fractions were sometimes calculated, in particular for the fraction of hypersaline end member. In those cases, the negative fraction was set to 0 and half of the absolute value of the negative fraction was added to each of the other two fractions. The shallowest wells from the transect were excluded from the analysis as, based on their stable isotope values and <sup>87/86</sup>Sr ratios, these are considered to constitute a fourth water type, influenced by fractionation due to evaporation so that the three-end member mixing model is not applicable. These samples are assumed to consist of 100% freshwater ( $f_{fresh} = 1$ ). The results of the calculations according to Equation 2 are shown graphically in Apx Figure G.6.



Apx Figure G.6 Cross-section along the seawater intrusion well transect in Aldinga Beach showing the fractions of the end members in each of the samples and the inferred three end member mixing based on a ternary contour plot. Inset triangle shows colour scheme with green indicating hypersaline water, red indicating seawater and blue freshwater.

Measured radiocarbon activities are shown in Apx Figure G.7 as a function of the calculated mixing fractions. Samples that are dominated by freshwater have  $^{14}\text{C}$  activities between 42 and 59 pmC. Samples that have a large proportion of the hypersaline end member have very low  $^{14}\text{C}$  activities, and the values decrease with increasing values of  $f_{\text{hypersaline}}$ . The values of samples that have a significant seawater contribution vary considerably between 3.3 and 46.5 pmC.

Because mixing clearly exerts a strong control on the measured water composition and isotope values, the radiocarbon data need to be corrected in order to obtain estimates of their apparent age. The approach that was followed here was to select end members values of total inorganic carbon (TIC) and the  $^{14}\text{C}$  activity (Apx Table G.3). TIC concentrations were calculated based on measured major ion chemistry and pH using PHREEQC version 2.18 (Parkhurst and Appelo, 1999). For these calculations, PHREEQC's Pitzer database was used, which provides the most accurate ion speciation model at the high ionic strength levels observed. The concentration of TIC ( $m_{\text{TIC}}$ ),  $\delta^{13}\text{C}$  value and  $^{14}\text{C}$  activity ( $^{14}A$ ) of the mixture of the end members was calculated as

$$m_{\text{TIC},\text{mix}} = f_{\text{hypersaline}} \times m_{\text{TIC},\text{hypersaline}} + f_{\text{sea}} \times m_{\text{TIC},\text{sea}} + f_{\text{fresh}} \times m_{\text{TIC},\text{fresh}} \quad (3)$$

$$\delta^{13}\text{C}_{\text{mix}} = \frac{f_{\text{hypersaline}} \times m_{\text{TIC},\text{hypersaline}} \times \delta^{13}\text{C}_{\text{hypersaline}} + f_{\text{sea}} \times m_{\text{TIC},\text{sea}} \times \delta^{13}\text{C}_{\text{sea}} + f_{\text{fresh}} \times m_{\text{TIC},\text{fresh}} \times \delta^{13}\text{C}_{\text{fresh}}}{m_{\text{TIC},\text{mix}}} \quad (4)$$

$$^{14}A_{\text{mix}} = \frac{f_{\text{hypersaline}} \times m_{\text{TIC},\text{hypersaline}} \times ^{14}A_{\text{hypersaline}} + f_{\text{sea}} \times m_{\text{TIC},\text{sea}} \times ^{14}A_{\text{sea}} + f_{\text{fresh}} \times m_{\text{TIC},\text{fresh}} \times ^{14}A_{\text{fresh}}}{m_{\text{TIC},\text{mix}}} \quad (5)$$

Additions of carbon by carbonate mineral dissolution or organic matter degradation were accounted for by comparing  $m_{TIC,mix}$  (mol/kgw) to the TIC concentration of the sample  $m_{TIC,sample}$  (mol/kgw)

$$m_{TIC,react} = m_{TIC,sample} - m_{TIC,mix} \quad (6)$$

where  $m_{TIC,react}$  is the concentration of TIC that was added to the sample by geochemical reactions. The  $\delta^{13}C$  value for  $^{13}C$  following from mixing and reactions ( $\delta^{13}C_{corr}$ ) was then calculated from

$$\delta^{13}C_{corr} = \frac{m_{TIC,mix} \times \delta^{13}C_{mix} + m_{TIC,react} \times \delta^{13}C_{sed}}{m_{TIC,sample}} \quad (7)$$

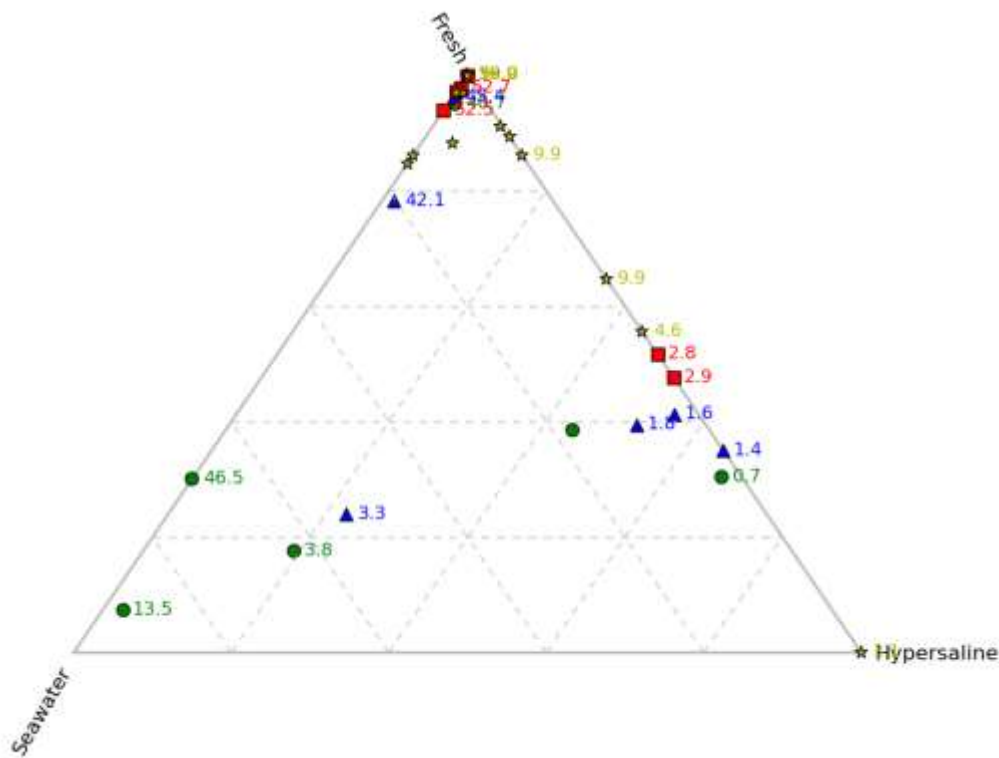
And, assuming the sediment contains negligible radiocarbon, the corresponding  $^{14}C$  activity ( $^{14}A_{corr}$ ) was calculated according to

$$^{14}A_{corr} = \frac{m_{TIC,mix} \times ^{14}A_{mix}}{m_{TIC,sample}} \quad (8)$$

And the corrected age was calculated from

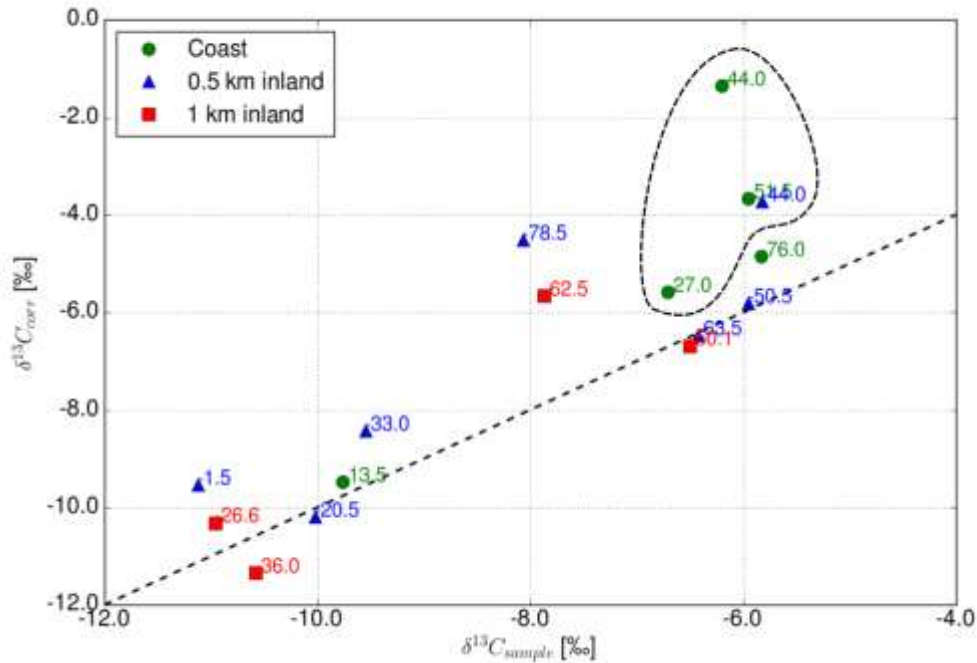
$$t = -\lambda \ln \left( \frac{^{14}A_{sample}}{^{14}A_{corr}} \right) \quad (9)$$

where  $\lambda$  is the decay constant for radiocarbon (0.000121 / year). The results of Equations 7 and 9 are shown graphically in Apx Figure G.8 and Apx Figure G.9 respectively.

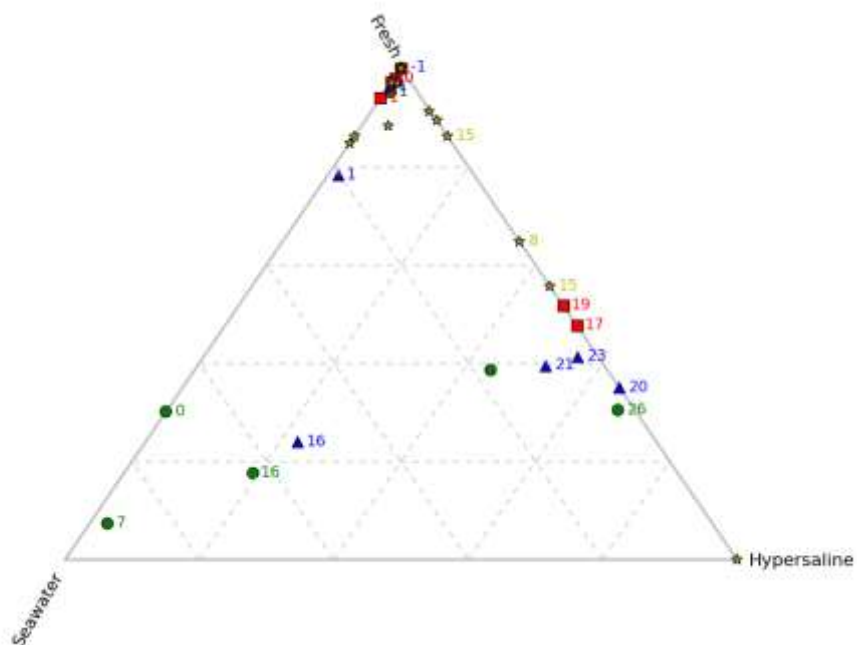


Apx Figure G.7 Ternary diagrams showing measured  $^{14}C$  activity (pmC) as a function of the fractions of the three end members in each sample.

The data points in the graph of  $\delta^{13}C_{corr}$  versus  $\delta^{13}C_{sample}$  show significant scatter but plot along a 1:1 relationship, except the samples which have a seawater contribution  $f_{sea} > 0.5$ . The  $\delta^{13}C_{corr}$  values of the deepest hypersaline samples are higher than the measured values by up to  $\sim 4$  ‰. The corrected radiocarbon ages range up to 26,000 years for the most saline sample in the transect.



Apx Figure G.8 Graph showing  $\delta^{13}C_{corr}$  versus  $\delta^{13}C_{sample}$  for the wells of the seawater intrusion transect. The dashed black line represents a 1:1 relationship. Samples with a fraction of seawater  $f_{sea} > 0.5$  have been encircled.



Apx Figure G.9 Ternary diagram showing the corrected age (in ka BP) estimates as a function of the fractions of the three end members in each sample.

## G.5 Discussion

The data show that a clear stratification of water types is present in the Port Willunga Formation in Aldinga Beach. Based on the stable water isotope values,  $\text{Cl}^-$  concentrations and  $^{87}\text{Sr}/^{86}\text{Sr}$  ratios, 4 different water types can be discerned. The deepest and most saline is a hypersaline (salinity larger than seawater) water type, which can be recognised in the water samples from the bottom half of the aquifer cross-section. At sites 1 and 2, the hypersaline groundwater is overlain by intruded seawater and based on the available data, a wedge shape can be inferred which resembles the shape of intruded seawater bodies described in studies elsewhere (Cooper, 1964; Reilly and Goodman, 1985). No significant seawater contribution could be established in the samples at site 3, suggesting that the toe of the wedge is located approximately between 0.5 and 1 km inland.

Within the fresher water sitting on top of the saline groundwater, two different types can be discerned. The shallowest, which has been found in the topmost wells of sites 1, 2 and 3 is characterised by relatively enriched stable water isotope values (Apx Figure G.3) and a  $^{87}\text{Sr}/^{86}\text{Sr}$  ratio  $< 0.711$  (Apx Figure G.5). The stable water isotope composition of the fresh groundwater below is more resemblant of that of rainwater and has  $^{87}\text{Sr}/^{86}\text{Sr}$  ratios  $> 0.711$ . This differentiation within the fresh groundwater is attributed to a difference in recharge area, with the shallowest groundwater having recharged locally through the Quaternary aquifer and the deeper water having an origin further inland. The stable isotope enrichment of the shallowest groundwater can be attributed to direct evaporation from surface water ponds which are a common occurrence along the transect and the Aldinga Scrub conservation area to the south of it. The origin from the Quaternary aquifer is corroborated by the  $^{87}\text{Sr}/^{86}\text{Sr}$  ratios, which are attributed to recent localised recharge and being close to the coast with a marine rainfall signature.

The seawater appears to have intruded over the top of the hypersaline groundwater instead of the bottom of the aquifer. This study is probably the first to provide a detailed characterisation of such a situation based on field data, albeit that Oz et al (2012) and Oz et al (2014) used numerical models and sand tank experiments to demonstrate that a comparable composite wedge can develop in aquifers that are in contact with a stratified saline surface water body, such as a meromictic lake. It is unlikely, however, that this is the cause for the observed stratification in the PWF as found here. The modern Gulf St Vincent has salinities that are much lower than the highest salinities found in the deepest wells. Salinities could have been higher during the past though, but the slope of the seafloor along the coast near Aldinga Beach is much less than the one considered by Oz et al (2012) and Oz et al (2014) so that even if a stratified water body existed in the Gulf St Vincent, the stratification present in the surface water would probably not have been easily transferred to the aquifer.

Moreover, the present coastline did not become established until 6.4 ka BP (Belperio et al. 2002) and open marine conditions have prevailed since then. The Gulf St Vincent did contain a salt lake at the end of the last glacial period (Cann et al. 1993), and the earliest marine incursions during the Holocene sea level rise may have given rise to stratified conditions, but at the time the coastline was  $\sim 15$  km west of the present location. Numerical modelling not shown here suggests that it is highly unlikely that the hypersaline groundwater formed under those conditions would have migrated across this distance to the point where it is found today. Therefore, at present, we reject the hypothesis that the hypersaline groundwater originated from a salt lake environment.

Based on the  $\text{Br}/\text{Cl}$  ratio (Jones et al. 1999) and the fact that halite has only been found in very low amounts in the PWF (Cooper, 1979), it can be ruled out that halite dissolution has led to the high salinities. The formation mechanism that is supported by the data is a combination of atmospheric deposition of solutes in combination with water removal by evapotranspiration, which has been put forward by Herczeg et al. (2001) as the cause for the widespread occurrence of hypersaline groundwater in the Murray Basin. Indeed, the data points of the seawater intrusion transect plot along a line of best fit that has the same slope as the one inferred by Herczeg et al. (2001), Apx Figure G.4.

The mixing-dissolution model appears to provide an adequate explanation of the measured  $\delta^{13}\text{C}$  values based on the fact that calculated  $\delta^{13}\text{C}$  values line up along 1:1 line when compared to measured values (Apx Figure G.8). Only the samples with significant seawater contribution deviate considerably, but the reason

for which is not clear. Only small values of  $m_{react,TIC}$  were calculated for these samples and therefore it would appear that the net contribution from geochemical reactions involving sedimentary carbon is limited. A mechanism that alters the carbon isotope values but not the carbon concentrations is required but this remains to be identified. The higher deviation of the most saline samples in the deepest part of the aquifer can be explained by assuming that these are not influenced by sedimentary carbon with  $\delta^{13}C = 0$ , but by a carbon source with more depleted values. Since lignite has been identified in the drill cuttings, it seems likely that these samples are influenced by the degradation of organic matter. This would not affect the interpretation of the  $^{14}C$  results as both carbonate minerals and organic matter would have a radiocarbon activity of zero.

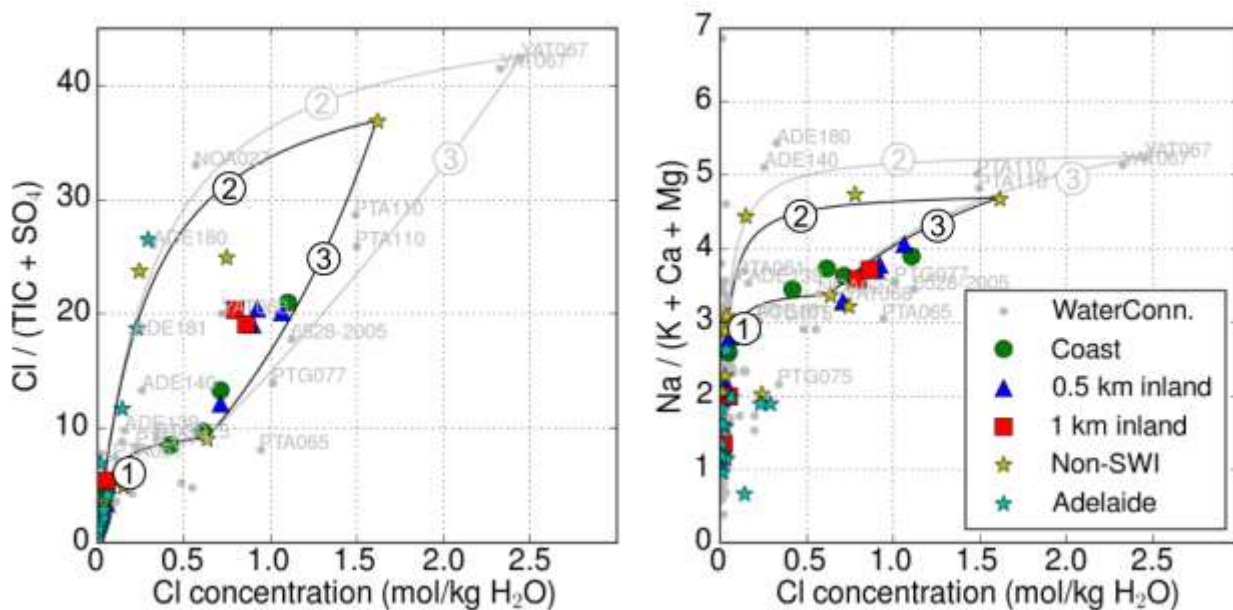
Considerable uncertainty exists about the composition of the hypersaline end member. If this end member were to be 1.5 times more saline, the values of  $f_{hypersaline}$  would be reduced and consequently, the corrected ages would increase. In this case the range would become 20 – 31 ka BP for the six most saline samples, versus 17 – 26 ka BP in Apx Figure G.9. Since the hypersaline end member has  $^{14}A = 0$  the radiocarbon age that is calculated based on Equation 9 is only for the TIC of the freshwater end member in the sample mixture. Despite the uncertainty in corrected ages, there exists a remarkable gap between the inferred age of the freshwater samples (< 2 ka) in the hypersaline samples (> 17 ka) and the ages of the freshwater samples.

## G.6 Comparison with the Adelaide Plains

The identification of two saline end members, i.e. the hypersaline groundwater and seawater, raises the question if these can also be found in the aquifer system beneath the Adelaide metropolitan area. Indeed, groundwater with salinities much higher than seawater has been discovered at a number of locations and the T3 and T4 aquifers in particular are known to contain groundwater with a high salinity (Gerges, 1999). In order to address the question if this groundwater has the same characteristics as the hypersaline groundwater in the PWF at Aldinga Beach, attempts were made to locate these bores in order to assess the feasibility of obtaining samples. Unfortunately, the majority of these bores either (i) could not be found, (ii) had been destroyed or backfilled, or (iii) access was not permitted. Of the bores where sampling appeared feasible, further inspection and/or pumping revealed poor bore condition and no satisfactory samples could be collected for analysis.

As an alternative, hydrochemistry data were therefore source from the WaterConnect database (<https://www.waterconnect.sa.gov.au/Systems/GD/Pages/default.aspx>). Only samples for which pH, alkalinity and the major ions Cl, HCO<sub>3</sub>, SO<sub>4</sub>, Na, Ca and Mg were reported were selected for further analysis. Total inorganic carbon concentrations (TIC) were calculated using PHREEQC-2 (Parkhurst and Appelo, 1999). Apx Figure G.20 shows the ratios of Cl / (TIC + SO<sub>4</sub>) and Na / (K + Ca + Mg) (i.e. the most dominant major ion over those remaining) versus the chloride concentration of the samples with an electrical balance better than 5%.

The samples from the seawater intrusion transect cluster along the lines that represent conservative mixing between the freshwater, seawater and hypersaline water end members, consistent with the model presented above. Deviations are due to uncertainty about the exact end-member composition and measurement inaccuracy, and particularly due to chemical reactions as the ratios are based on non-conservative ions. Sulphate reduction for example will reduce the SO<sub>4</sub> concentration, which will result in data points shifting vertically upward in the left panel of Apx Figure G.10. Dissolution of carbonate minerals would results in the data points moving vertically downward in the right panel of Apx Figure G.10.

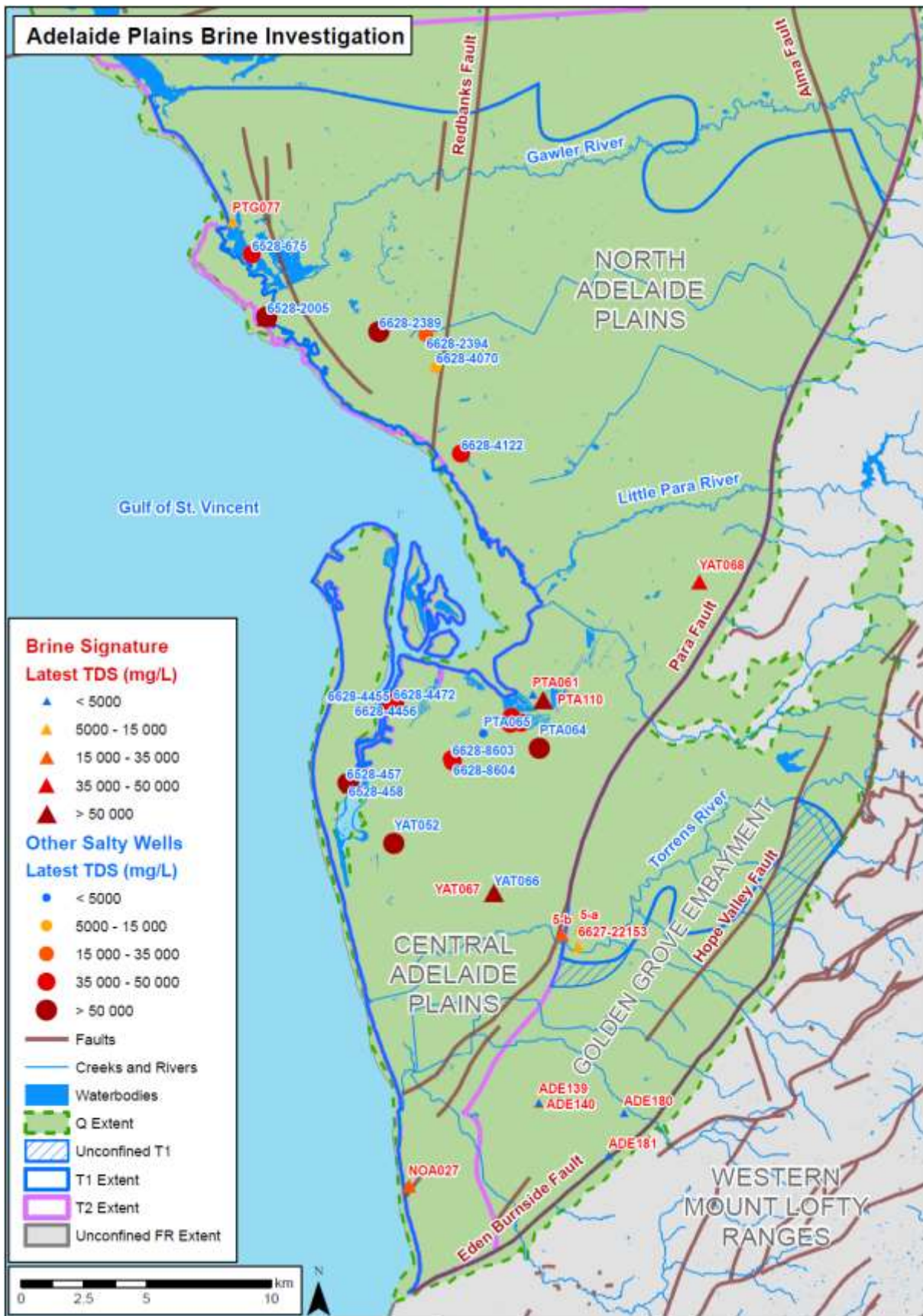


Apx Figure G.10 Graphs showing (left) the ratio of  $\text{Cl} / (\text{TIC} + \text{SO}_4)$  versus the chloride concentration and (right) the ratio of  $\text{Na} / (\text{K} + \text{Ca} + \text{Mg})$  versus the chloride concentration. Ratios are based on concentrations expressed in meq/L. Numbered lines represent the relationships resulting from mixing between freshwater and seawater (1), freshwater and hypersaline water (2) and seawater and hypersaline water (3). Black lines are based on the most saline sample from the Wilunga area (WLG096), grey lines are based on the most saline sample from the Adelaide Plains area (YAT067). See Figure G.3 for legend of the coloured symbols, grey symbols are data points for the Adelaide Plains area from the WaterConnect database, blue stars represent data from the new wells drilled for this project.

Despite the scatter thus introduced, it can be seen that several of the data points of saline groundwater from the Adelaide Plains aquifers (NOA027, ADE180, ADE181, ADE139, ADE140, PTA061) plot along the conservative mixing line between fresh groundwater and the most saline groundwater sample (YAT067). This includes samples from the newly-installed well screens at site 5 (blue stars in Apx Figure G.10) on Strangways Tce/War Memorial Drive in North Adelaide. Some data points (PTA065, PTA110, PTG077, 6528-2005) cluster around the mixing line between this hypersaline end member and seawater. Therefore, it would seem that the same three-end-member mixing model that was identified for the seawater intrusion transect in Aldinga Beach applies to the Adelaide Plains groundwater system. This needs to be verified independently by the measurement of stable isotopes of water which can be expected to behave more conservative than the ionic ratios used here. It can be seen that the samples from the wells at site 5 follow a similar trend as the samples that represent a mixture between freshwater and hypersaline groundwater in the seawater intrusion transect in Aldinga Beach in the graphs of  $\delta^{18}\text{O}$  versus  $\text{Cl}^-$  and  $\delta^2\text{H}$  versus  $\text{Cl}^-$  (Apx Figure G.3).

It is interesting to note that some groundwater samples south of the Adelaide CBD have high salinities and appear to have a signature that suggest a contribution from the hypersaline end member. This includes observations wells ADE139, ADE140, ADE180 and ADE181. In ADE180, the most saline sample was sourced from the basement (fractured rock) aquifer, whereas in the other wells the samples were from the T1 (ADE181), T2 (ADE139) and T3 (ADE140) aquifers. This seems to be analogous to the Willunga Embayment where the hypersaline end member can be recognized in the equivalents of these aquifers.

The hypersaline groundwater, or mixtures thereof with other water types, thus appears to be pervasive across the greater Adelaide region and does not appear to be restricted to a particular aquifer or depth (Apx Figure G.11).



Apx Figure G.11 Map showing location of selected wells with high groundwater salinity (circles) and/or that appear to have a brine signature (triangles).

## G.7 References

- Andersen, M.S., V. Nyvang, R. Jakobsen, D. Postma (2005) "Geochemical Processes and Solute Transport at the Seawater/freshwater Interface of a Sandy Aquifer." *Geochimica et Cosmochimica Acta* 69 (16): 3979–94. doi:10.1016/j.gca.2005.03.017.
- Ashenden JP (2008) Application of the Time Domain Electromagnetic method for the delineation of the position of the freshwater-saltwater interface in an urbanised coastal environment: A case study of the LeFevre Peninsula, South Australia. Honours thesis, Department of Geology & Geophysics, University of Adelaide.
- Belperio, a.P., N. Harvey, and R.P. Bourman (2002) "Spatial and Temporal Variability in the Holocene Sea-Level Record of the South Australian Coastline." *Sedimentary Geology* 150 (1-2): 153–69. doi:10.1016/S0037-0738(01)00273-1.
- Cann, J. H., a. P. Belperio, V. a. Gostin, and R. L. Rice. 1993. "Contemporary Benthic Foraminifera in Gulf St Vincent, South Australia, and a Refined Late Pleistocene Sea-level History." *Australian Journal of Earth Sciences* 40 (2): 197–211. doi:10.1080/08120099308728074.
- Cooper, H.H. Jr., Kohout, F.A., Henry, H.R. and Glover, R.E. 1964. *Sea Water in Coastal Aquifers*, U.S. Geol. Survey Water-Supply Paper 1613-C.
- Corlis, Nicholas J., H. Herbert Veeh, John C. Dighton, and Andrew L. Herczeg. 2003. "Mixing and Evaporation Processes in an Inverse Estuary Inferred from  $\delta^2\text{H}$  and  $\delta^{18}\text{O}$ ." *Continental Shelf Research* 23 (8): 835–46. doi:10.1016/S0278-4343(03)00029-3.
- Gardner, P., and D. K. Solomon. 2009. "An Advanced Passive Diffusion Sampler for the Determination of Dissolved Gas Concentrations." *Water Resources Research* 45 (6): n/a – n/a. doi:10.1029/2008WR007399.
- Gerges N (1999) The geology & hydrogeology of the Adelaide metropolitan area. PhD, Earth Sciences, Flinders University of South Australia, Adelaide.
- Herczeg AL, Dogramaci SS, Leany FWJ. 2001. Origin of dissolved salts in a large, semi-arid groundwater system: Murray Basin, Australia. *Marine and Freshwater Research* 52, 41–52
- Jones BF, Vengosh A, Rosenthal E, Yechieli Y (1999) Geochemical investigations. In: Bear et al., editors. *Seawater intrusion in coastal aquifers – concepts, methods and practices*. p 51–72.
- Jones E, Oliphant E, Peterson P, et al. (2001) SciPy: Open Source Scientific Tools for Python, <http://www.scipy.org/> [Online; accessed 2015-04-09].
- Jørgensen, N.O., M.S. Andersen, and P. Engesgaard. 2008. "Investigation of a Dynamic Seawater Intrusion Event Using Strontium Isotopes ( $^{87}\text{Sr}/^{86}\text{Sr}$ )." *Journal of Hydrology* 348 (3-4): 257–69. doi:10.1016/j.jhydrol.2007.10.001.
- Lamontagne S, Le Gal La Salle C, Simmons C, James-Smith J, Harrington N, Love A, Hancock G and Fallowfield H (2005) Estimation of Groundwater and Groundwater N Discharge to the Adelaide Coastal Waters Study Areas. ACWS Technical Report No.4 prepared for the Adelaide Coastal Waters Study Steering Committee by the Flinders Centre for Coastal and Catchment Environments: In Department for Environment & Heritage (2007b) *Adelaide and Mount Lofty Ranges Natural Resources Management Region Estuaries Information Package*, Department for Environment and Heritage, Adelaide, SA.
- Luszczynski NJ, Swarzenski WV (1966) *Salt-Water Encroachment in Southern Nassau and Southeastern Queens Counties Long Island, New York*. Geological Survey Water-Supply Paper 1613-F. United States Government Printing Office, Washington.
- Magaritz, Mordeckai, and James E. Luzier. 1985. "Water-Rock Interactions and Seawater-Freshwater Mixing Effects in the Coastal Dunes Aquifer, Coos Bay, Oregon." *Geochimica et Cosmochimica Acta* 49 (12): 2515–25. doi:10.1016/0016-7037(85)90119-X.

- Oz, I., E. Shalev, H. Gvirtzman, Y. Yechieli, and I. Gavrieli. 2011. "Groundwater Flow Patterns Adjacent to a Long-Term Stratified (meromictic) Lake." *Water Resources Research* 47 (8): n/a – n/a. doi:10.1029/2010WR010146.
- Oz, Imri, Eyal Shalev, Yoseph Yechieli, Ittai Gavrieli, and Haim Gvirtzman. 2014. "Flow Dynamics and Salt Transport in a Coastal Aquifer Driven by a Stratified Saltwater Body: Lab Experiment and Numerical Modeling." *Journal of Hydrology* 511 (April). Elsevier B.V.: 665–74. doi:10.1016/j.jhydrol.2014.02.020.
- Reilly, TE and Goodman, AS (1985) Quantitative analysis of saltwater-freshwater relationships in groundwater systems- a historical perspective, *J. Hydrol.*, 80, 125-160.
- Short, MA (2011) Submarine groundwater discharge from the Willunga Basin, South Australia. Honours Thesis, Flinders University, 56 pp.
- Sivan, Orit, Yoseph Yechieli, Barak Herut, and Boaz Lazar. 2005. "Geochemical Evolution and Timescale of Seawater Intrusion into the Coastal Aquifer of Israel." *Geochimica et Cosmochimica Acta* 69 (3): 579–92. doi:10.1016/j.gca.2004.07.023.
- Stuyfzand, Pieter J. 1999. "Patterns in Groundwater Chemistry Resulting from Groundwater Flow," no. October 1998: 15–27.
- Voss CI, Wood WW (1994) Synthesis of geochemical, isotopic and groundwater modeling analysis to explain regional flow in a coastal aquifer of southern Oahu, Hawaii. In: *Mathematical models and their applications to isotope studies in groundwater hydrology*, IEAE-TECDOC-777, international atomic energy agency (IAEA), Vienna, Austria, p. 147–78.
- Werner, AD, M Bakker, VEA Post, A Vandenbohede, C Lu, B Ataie-Ashtiani, CT Simmons, DA Barry (2012) Seawater intrusion processes, investigation and management: Recent advances and future challenges. *Advances in Water Resources*. <http://dx.doi.org/10.1016/j.advwatres.2012.03.004>

# Appendix H Coastal aquifer hydraulic parameter estimation based on tidal responses

Authors: *Pool M and Post VEA*

## H.1 Executive summary

Groundwater response to sea level fluctuations provides information about hydraulic parameters of coastal aquifers. The tidal method is a technique of analyzing the aquifer response to tidal fluctuations in order to determine aquifer hydraulic diffusivity (ratio of transmissivity to storage coefficient). The objective of this study is to apply the tidal method considering different aquifer configurations to the tidally influenced head responses at seven wells located in the Adelaide Metropolitan Area for the characterization of the T1 and T2 Tertiary aquifers. Head data collection was recorded for a period of 1 month at a 2 minute sampling interval. Spectral harmonic analysis was applied to the groundwater responses to determine the principal harmonic components, their amplitude and frequency. Different analytical solutions have been used to calculate transmissivity estimates. The results obtained from this analysis converge to a narrow range of transmissivity values, which is consistent with values obtained previously from pumping test.

## H.2 Introduction

Sustainable management of groundwater resources in coastal aquifers requires a detailed knowledge of the variability of their hydrogeological parameters. Much effort has been dedicated for many decades to the estimation of the hydraulic properties of groundwater systems, specifically transmissivity (see, e.g., Theis, 1935; Cooper and Jacob, 1946). There are several methods for determining the aquifer transmissivity, but in most practical applications it is generally obtained from pumping tests. However, in coastal aquifers pumping tests difficult to conduct because they can promote the contamination of groundwater resources by seawater intrusion, and their interpretation is complicated by tides. For this reason, alternative techniques based on the analysis of groundwater response to tidal fluctuations have been developed for the hydraulic characterization of coastal aquifers.

The first analytical solution to describe the propagation of tidal water level fluctuations in a confined coastal aquifer was derived independently both by Jacob (1950) and Ferris (1951), and its application for the estimation of aquifer properties was referred to in the literature as 'the tidal method'. They observed that the amplitude of the tide-induced groundwater head fluctuation declines exponentially with distance from the coastline whereas the phase lag increases linearly, and that the response to tidal perturbations depends on the hydraulic diffusivity of the aquifer. Subsequent to these studies, more sophisticated analytical solutions have been developed for confined aquifers connected to the sea (Van Der Kamp, 1972), semi-confined aquifers (Li and Jiao, 2001a) and semi-confined aquifers considering the effect of the elastic storage of the aquitard (Li and Jiao, 2001b, 2002a; Guarracino et al., 2012).

In the present study we present and apply the tidal method to a series of field observations obtained from wells located in the Adelaide Metropolitan Area in order to estimate the hydraulic properties of the sedimentary aquifers and then to improve the understanding of the groundwater systems, including the connectivity of the Tertiary aquifers to the Gulf St Vincent.

## H.3 Study Area

The Adelaide Metropolitan Area occupies about 560 km<sup>2</sup> of coastal plain and forms part of the sedimentary St Vincent Basin. The area is bounded by the Gulf St. Vincent to the east and the Mount Lofty Ranges to the west.

### H.3.1 HYDROGEOLOGY

This study focuses on the quantification of the hydraulic properties of the T1 and T2 Tertiary aquifers underlying the Adelaide Metropolitan Area. These Tertiary aquifers represent the main source of groundwater supply in the study area. The T1 aquifer comprises the Carisbrooke Sand, Hallett Cove Sandstone, Dry Creek Sand, Croydon Facies and the upper Port Willunga Formation and consists of limestone and sand. The T1 aquifer is predominantly confined by Quaternary layers and has a maximum thickness of 130 m separated from the T2 aquifer by the Munno Para Clay aquitard, which consists of grey clay 8-11 m thick (Gerges, 1999). The T2 aquifer is confined and is made up by the well-cemented limestone of the Lower Port Willunga Formation. The thickness of the T2 formation ranges between 80 and 110 m. The aquifer system of the Adelaide Plains extends beneath the Gulf St Vincent, but hardly any information exists about the offshore part of the system.

**Apx Table H.1 Observation well number, unit number, aquifer, coordinates and screen depths of the monitoring wells used in this study.**

OBS_NO	UNIT_NUMBER	AQUIFER	LATITUDE	LONGITUDE	SCREEN TOP	SCREEN BOTTOM
ADE005	6628-29725	T1	138.5003	34.9342	116.03	137.16
					118	122
YAT043	6628-07417	T1	138.5062	34.9252	92.96	147.83
					123	126
YAT037	6281-9722	T1	138.5003	34.9049	185.04	201.17
					189.9	198
ADE037	6662-807625	T1	138.5092	34.9372	109.73	128.02
					48.3	128
YAT037	6281-9722	T1	138.5003	34.9049	185.04	201.17
					189.9	198
YAT099	6628-7385	T2	138.5015	34.9163	194	205.7
					222.27	250
YAT132	6628-11153	T2	138.5210	34.9122	186	220
					232	244
YAT066	6628-11385	T2	138.5540	34.8971	540	553
					234	248
BAROMETER			138.5062	34.9252		

[<https://www.waterconnect.sa.gov.au/Systems/RTWD/SitePages/Home.aspx>]

For this study, tidally influenced hydraulic head data were recorded for a period of 1 month (period of record October-November 2014) at a 2 minute sampling interval at seven wells equipped with data loggers. A data logger was also deployed at the Henley Beach jetty in order to collect the tidal fluctuations in the Gulf St Vincent. The observation well numbers, their coordinates as well as the depth intervals of the screens are provided in Apx Table H.1. The monitoring well locations are shown in Apx Figure H.1.



**Apx Figure H.1 Monitoring wells locations.** Red and blue colours represent the wells screened in T1 and T2 aquifers, respectively. A separate logger was attached to the Henley Beach Jetty to record the tide in the Gulf St Vincent.

### H.3.2 TIDAL FORCING

The tides of the South Australian Sea have been extensively studied (see e.g., Vincent et al., 1988; Middleton and Bye, 2007). The principal feature of the Gulf St Vincent in Adelaide are that the semi-diurnal  $M_2$  and  $S_2$  constituents are dominant, with approximately equal amplitudes of about 0.5 m. The two most important diurnal constituents,  $O_1$  and  $K_1$ , also make a significant contribution to the tidal signal. The amplitudes reach their maximum values in autumn (March-April) and spring (September-October). The principal diurnal and semi-diurnal harmonic components and their frequencies are shown in Apx Table H.2.

**Apx Table H.2 Tidal harmonics at Port Adelaide.**

CONSTITUENTS NOTATION	TYPE	PERIOD (H)	AMPLITUDE (M)
<b>O1 (basic lunar)</b>	Diurnal	25.819	0.158
<b>P1 (basic solar)</b>	Diurnal	24.066	0.067
<b>K1 (declinational P1)</b>	Diurnal	23.934	0.252
<b>N2 (elliptical M2)</b>	Semi-diurnal	12.568	0.027
<b>M2 (basic lunar)</b>	Semi-diurnal	12.421	0.518
<b>S2 (basic solar)</b>	Semi-diurnal	12.000	0.512
<b>K2 (declinational M2)</b>	Semi-diurnal	11.967	0.140

[R.W. Chapman and Captain Inglis, A.A.A.S. Reports, Vol. 7, 1898]

## H.4 Methods

### H.4.1 TIDAL HARMONIC ANALYSIS

Harmonic analysis was used to predict the water-level elevations as a function of time and to determine the change in water level caused directly by the tidal influence. The phase and amplitude of the main tidal constituents in the time series were computed using the program T\_TIDE (Pawlowicz et al., 2002). This harmonic analysis uses a least squares fit with a confidence interval estimation method to estimate tidal

constituents and their uncertainties in scalar and vector time series. A linearized analysis is used for the conversion from errors in the harmonic amplitudes to errors in standard parameters (amplitude and phase), i.e., for estimating noise levels in spectra. Diagnostics to assess constituent independence are: (1) the Rayleigh criterion, which is related to the frequency separation between neighboring constituents and the length of time series and is assumed to be 1 for tidal analysis; and (2) the signal-to-noise ratio (SNR), that is a signal-to-noise power ratio defined as the squared ratio of amplitude to the error in amplitude.

## H.4.2 TIDAL METHOD

The tidal method is a technique of analyzing the groundwater head fluctuations in a well or piezometer in response to tidal oscillations to determine aquifer diffusivity (ratio of transmissivity to storage coefficient). With the method, the hydraulic diffusivity can be estimated from the amplitude attenuation and from the phase lag ( $t_l$ ), the time required for a particular peak to travel a specific distance inland. Here, we first review the analytical solutions used in this study to analyze the measured water level fluctuations.

The simplest analytical solution was presented by Jacob (1950) and Ferris (1951), for the aquifer system shown in Apx Figure H.2a. They considered one-dimensional flow in a confined aquifer with a vertical seaside boundary and straight coastline. In this case, the partial differential equation governing flow in the absence of sources and sinks is given by,

$$\frac{\partial h(x,t)}{\partial t} = D_h \frac{\partial^2 h(x,t)}{\partial^2 x} \quad (1)$$

where  $D_h = T/S$  is the hydraulic diffusivity [ $L T^{-1}$ ], with  $S$  the storage coefficient [-] and  $T$  the transmissivity [ $L^2 T^{-1}$ ]. The solution to equation (1) is subject to a simple harmonic oscillation at the seaside boundary,  $h(0,t) = A_0 \sin(2\pi t/\tau)$  with  $A_0$  [L] the ocean-tide amplitude and  $\tau$  the period [T]. Considering  $h(\infty,t) = 0$ , yields the solution to equation (1)

$$h(x,t) = A_0 e^{-x\mu} \sin\left(\frac{2\pi t}{\tau} - x\mu\right) \quad (2)$$

where  $\mu$  [ $L^{-1}$ ] is the confined aquifer's tidal propagation defined as  $\mu = \sqrt{\pi/D_h\tau}$ .

It may be seen from equation (2) that the amplitude of the tide-induced groundwater head fluctuation decays exponentially with distance from the coastline by a factor of  $e^{-x\mu}$ , and that the phase lag increases linearly by  $x\mu$ . From equation (2), two independent solutions for the hydraulic diffusivity can thus be obtained in a well at a distance  $x$  inland from the coast, either based on the amplitude attenuation ( $D_h^A$ ) or the phase lag ( $D_h^t$ ), which are given, respectively, by

$$D_h^A(x) = \frac{\pi x^2}{\tau \left[ \ln\left(\frac{A}{A_0}\right) \right]^2}, \quad (3a)$$

$$D_h^t(x) = \frac{\tau x^2}{4\pi t_l^2} \quad (3b)$$

Van der Kamp (1972) extended the tidal method to the case of a confined aquifer separated from the overlying water body by a confining layer below the seafloor of infinite length, Apx Figure H.1.2b. In this case, the boundary condition for the subsea region ( $x < 0$ ) is defined as,

$$h(-\infty, t) = L_e A_0 \sin(2\pi t / \tau), \quad (4)$$

with  $L_e$  the loading efficiency defined as  $L_e = \alpha / (\alpha + \phi\beta)$ , in terms of the porosity,  $\phi$  [ $L^3L^{-3}$ ], the water compressibility,  $\beta$  [ $LT^2M^{-1}$ ],  $4.47 \times 10^{-10} \text{ ms}^2\text{kg}^{-1}$  for pure water at 20°C, and the bulk porous matrix compressibility,  $\alpha$  [ $LT^2M^{-1}$ ]. Using the above boundary condition, the solution for the head fluctuation in the inland and subsea regions is given by,

$$h(x, t) = \frac{1}{2} L_e A_0 e^{-x\mu} \sin\left(\frac{2\pi t}{\tau} - x\mu\right), \text{ for } x > 0 \text{ (onshore)} \quad (5a)$$

$$h(x, t) = L_e A_0 \sin\left(\frac{2\pi t}{\tau}\right) + \frac{1}{2} L_e A_0 e^{-x\mu} \sin\left(\frac{2\pi t}{\tau} + x\mu + \pi\right), \text{ for } x < 0 \text{ (offshore)} \quad (5b)$$

The solutions for the hydraulic diffusivity obtained in a well at a distance  $x$  inland from the coast are given by,

$$D_h^A(x) = \frac{\pi x^2}{\tau \left[ \ln\left(\frac{2}{L_e} \frac{A}{A_0}\right) \right]^2}, \quad (6a)$$

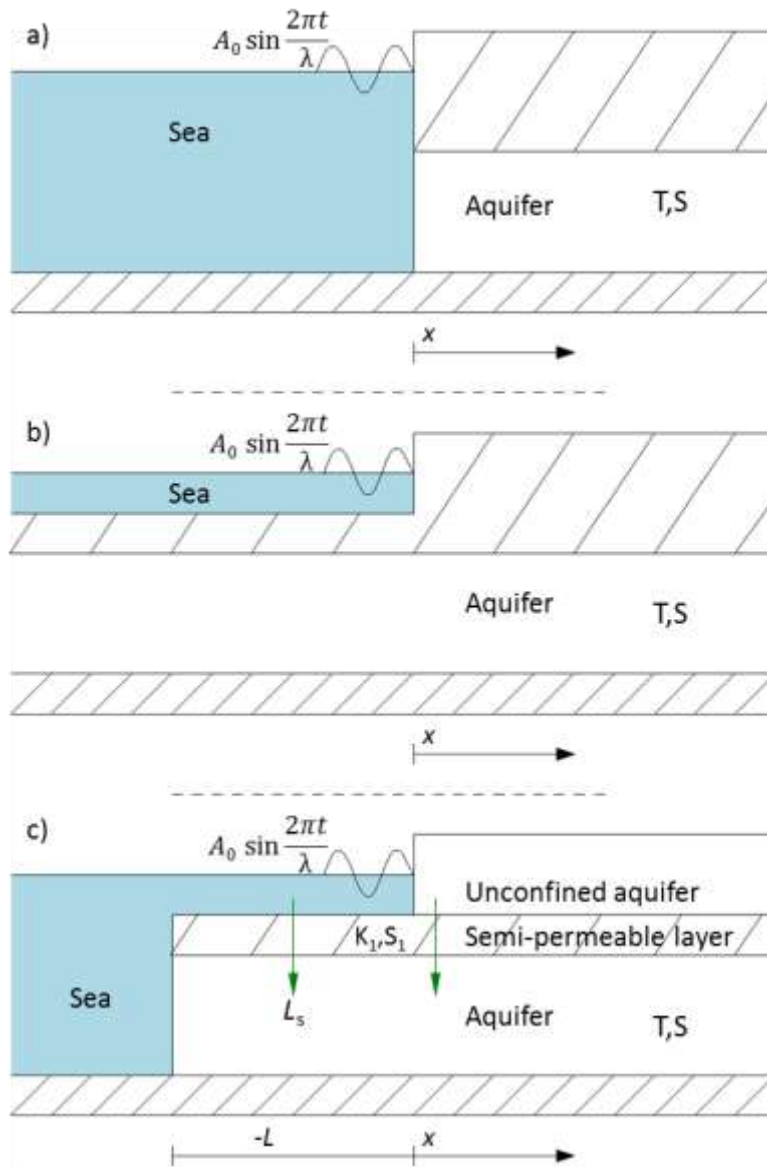
$$D_h^I(x) = \frac{\tau x^2}{4\pi t_1^2} \quad (6b)$$

Note that the solution for  $D_h^I$  is exactly the same equation as the one obtained by Jacob (1950) and Ferris (1951), and is thus independent of the extent of the aquifer and the confining layer under the sea.

Finally, a generalization of the above solutions was presented by Li and Jiao (2001a). They derived an exact analytical solution to describe groundwater level fluctuation in a coastal aquifer system consisting of an unconfined aquifer and a semi-confined aquifer separated by a leaky semipermeable layer. The unconfined aquifer ends at the coastline and both the leaky confined aquifer and the semi-permeable layer extend over a finite distance  $L$  under the sea, Apx Figure H.2c. The flow equation is given by,

$$S_s \frac{\partial h(x, t)}{\partial t} = k \frac{\partial^2 h(x, t)}{\partial^2 x} - L_s h(x, t), \quad (7)$$

where  $L_s$  is specific leakage [ $T^{-1}$ ] defined  $L_s = k_1 / b_1$  with  $k_1$  and  $b_1$  being the vertical conductivity ( $L T^{-1}$ ) and thickness [ $L$ ] of the semipermeable layer, respectively. Equation (7) is subject to the following boundary conditions:  $h(-L, t) = A_0 \cos(2\pi t / \tau)$  at the seaside boundary and  $h(\infty, t) = 0$  inland.



**Apx Figure H.2 Schematic of: (a) an idealized aquifer with an overlying confining layer crop out at or near coastline, (b) an infinite confined aquifer extending under the sea, and (c) a leaky confined aquifer with a finite semi-permeable layer under the sea.**

Li and Jiao (2001a) presented the solutions for the head in the inland and subsea regions in terms of two dimensionless numbers: the confined aquifer's tidal propagation  $\mu$  [ $L^{-1}$ ], previously defined, and the dimensionless leakage  $u$ , defined as  $u = \tau L_s / 2\pi S$ .

In this study, only the solutions for the hydraulic diffusivity are presented, and are given by,

$$D_h^A(x) = \frac{\pi p x^2}{\tau \left[ \ln \left( \frac{1}{C_e} \frac{A}{A_0} \right) \right]^2}, \quad (8a)$$

$$D_h^t(x) = \frac{\pi q^2 x^2}{\tau (\Phi - \phi)^2}, \quad (8b)$$

where  $\Phi = (2\pi t_i / \tau)$ , and  $p$  and  $q$  are determined by the dimensionless leakage ( $u$ ), and are given, respectively, by

$$p = \sqrt{\sqrt{1+u^2} + u} \text{ and } q = \sqrt{\sqrt{1+u^2} - u}, \quad (9)$$

$\varphi$  is the fixed phase shift, defined by

$$\varphi = \arctan \frac{2I_1 - \gamma}{2R_1 - \lambda}, \quad (10)$$

with

$$\lambda = \frac{u^2 + L_e}{u^2 + 1} \text{ and } \gamma = \frac{(1 - L_e)u}{u^2 + 1}, \quad (11)$$

$$R_1 = e^{-p\mu L} [(1 - \lambda)\cos(q\mu L) - \gamma \sin(q\mu L)] + \frac{1}{2} e^{-p\mu L} [\lambda \cos(q\mu L) + \gamma \sin(q\mu L)], \quad (12)$$

$$I_1 = e^{-p\mu L} [(1 - \lambda)\sin(q\mu L) - \gamma \cos(q\mu L)] + \frac{1}{2} e^{-p\mu L} [\lambda \sin(q\mu L) + \gamma \cos(q\mu L)], \quad (13)$$

and  $C_e$  is the comprehensive tidal efficiency of the leaky confined aquifer system, and is defined as

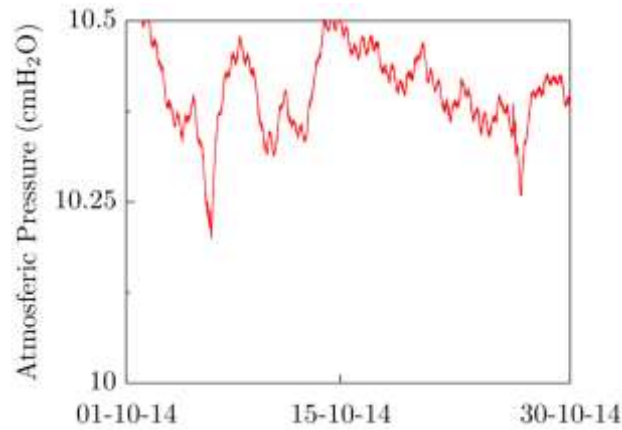
$$0 < C_e = \sqrt{(R_1 + \lambda/2)^2 + (I_1 - \gamma/2)^2} \leq 1, \quad (14)$$

## H.5 Results

### H.5.1 DATA ANALYSIS

In order to filter low-frequency fluctuations due to barometric effects, barometric pressure measurements were recorded for a one-month period (2-minutes sampling) with on-site barometer deployed at the top of the well YAT043. Barometric pressure fluctuations average approximately 25cm for the period evaluated. The data collected for the barometric pressure are shown Apx Figure H.3.

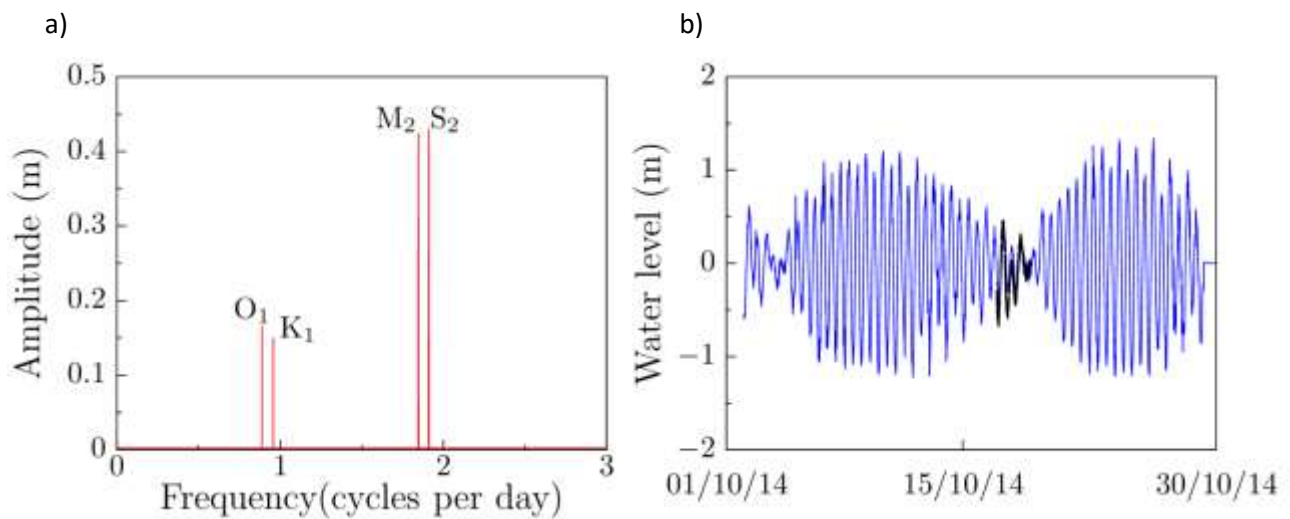
Assuming no areal variation of atmospheric pressure fluctuations (Post and von Asmuth, 2013), the barometric pressure was subtracted from the records prior to the harmonic analysis.



**Apx Figure H.3 Atmospheric pressure recorded for a period of one month at the top of the well YAT043.**

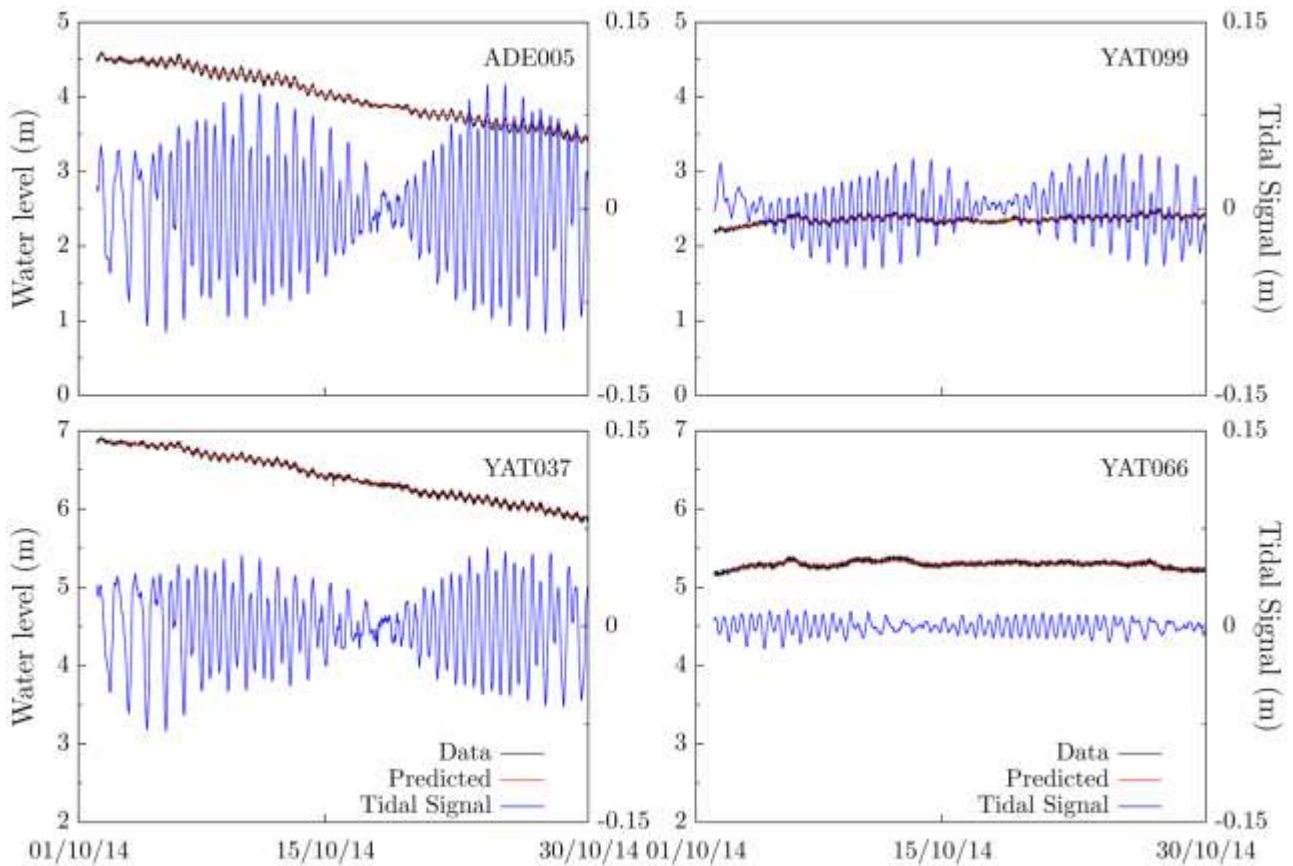
The harmonic analysis was applied over a one-month period to the Gulf St Vincent tide data measured at the Henley Beach jetty and to the head data in each monitoring well. In order to accurately determine the presence of harmonics, in addition to the aforementioned constituents in section 2.2 ( $O_1$ ,  $P_1$ ,  $K_1$ ,  $N_2$ ,  $M_2$ ,  $S_2$ , and  $K_2$ ), shallow water constituents, which result from the sum or difference of frequencies of the major constituents, were also included in the analysis. Apx Figure H.4 illustrates the spectrum obtained from the analysis, showing the amplitude and frequency of the four constituents judged to be significant ( $SNR > 10$ ), as well as the predicted tidal heights at Henley Beach over a one month period.

The analysis finds that over 96% of the variance of the horizontal displacements occurs at diurnal ( $O_1$ ,  $K_1$ ) and semidiurnal ( $M_2$  and  $S_2$ ) tidal frequencies, and therefore the predicted harmonic components are mainly at frequencies of one and two cycles per day. Note that the fortnightly tidal cycle is well represented in the prediction, with a good reproduction of amplitude and phase.



**Apx Figure H.4 Periodogram of harmonic frequencies present in ocean-tide data collected (a) and the predicted ocean tide at the Henley beach (b), October 2014.**

In order to eliminate any non-tidal influence, the groundwater head records at the wells were harmonically analysed in an identical manner to the reference open water tidal. Apx Figure H.5 shows results for the head data, residual noise and the predicted tidal response in four wells located at different distances from the coast. Note that, although the damping effect (amplitude attenuation) on groundwater levels in the observation well YAT066, located at a distance of 6km from the coast, is significant, tidally effects on the groundwater head are still evident.

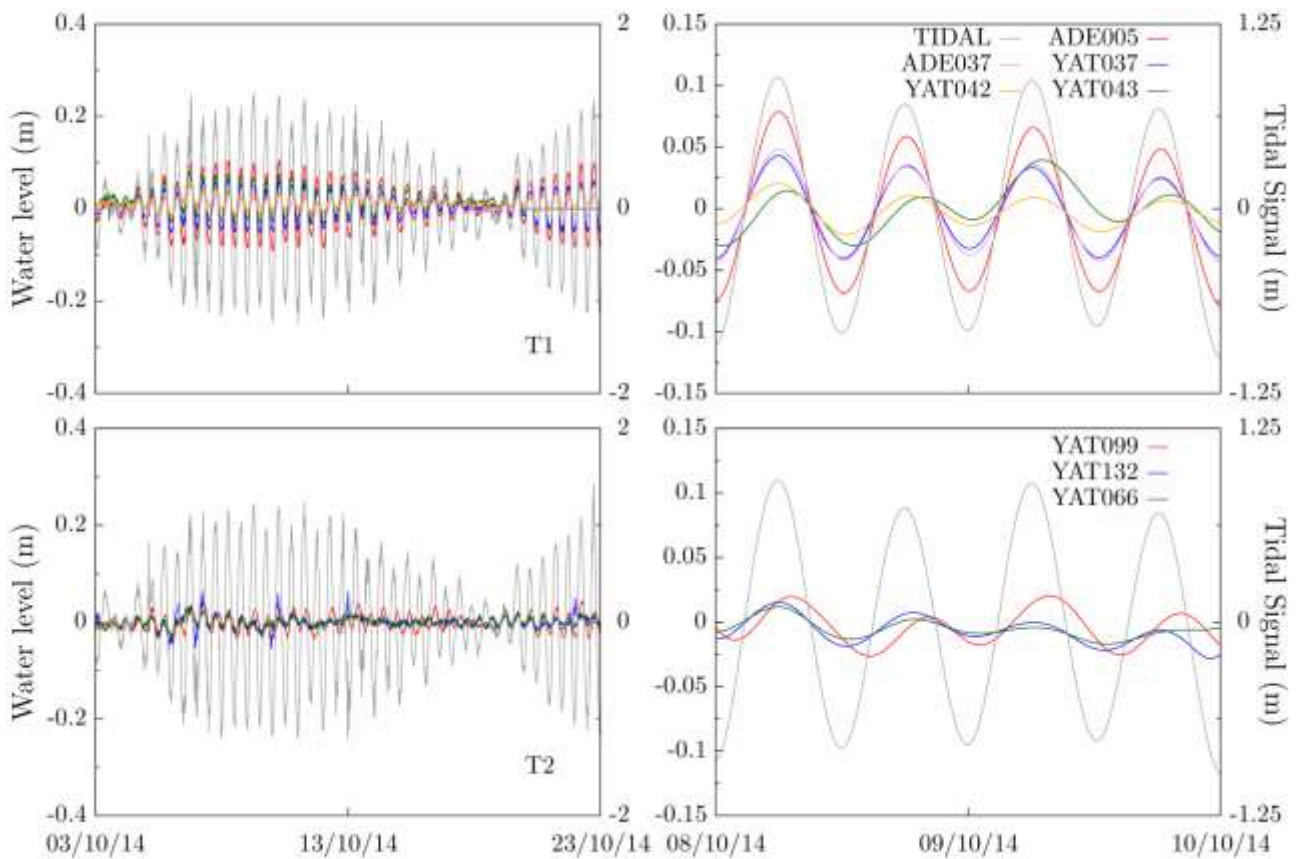


Apx Figure H.5 Results from the harmonic analysis at four different wells: ADE005 and YAT037, screened in the T1 aquifer; YAT099 and YAT066, screened in the T2 aquifer. Black lines represent the head data, red lines the nontidal residual noise (right y-axis) and blue lines the tidal response (left y-axis).

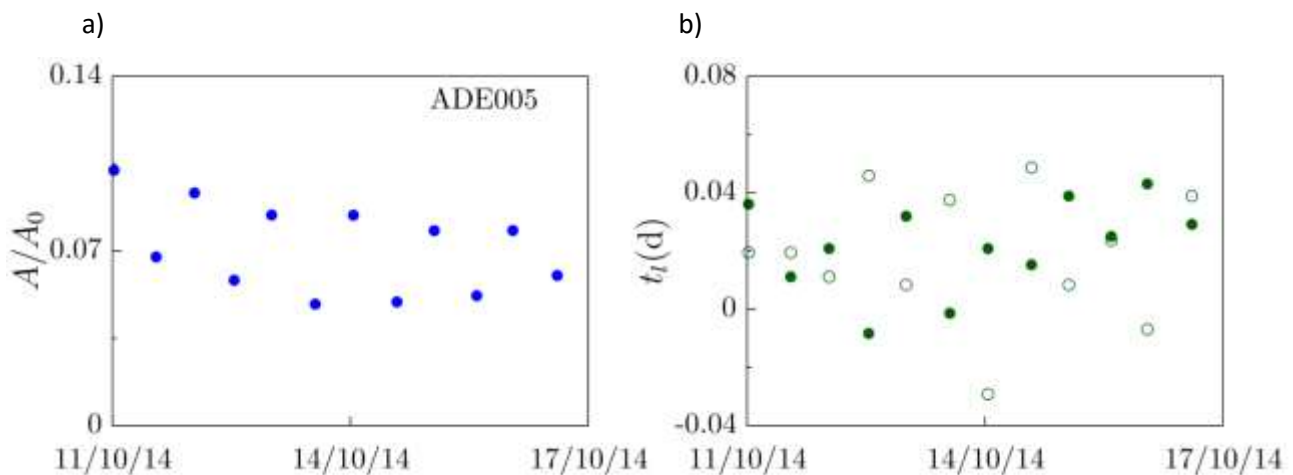
## H.5.2 ESTIMATES OF TRANSMISSIVITY

Time series of head oscillations used to apply the tidal method and evaluate the transmissivity for the T1 and T2 aquifers are shown in Apx Figure H.6.

The tidal amplitude at the monitoring wells and the sea was computed from the half distance between the maximum and minimum water level over each tidal cycle. The time lag was determined by measuring the time difference between the occurrence of a maximum water level in the well and the occurrence of the corresponding maximum in the sea level. Results show that amplitude and phase lag measured in the wells vary considerably over the tidal cycles. This temporal variation may be attributed to both the interference between the different harmonic components and heterogeneity effects (Trefry, 1999). Apx Figure H.7 illustrates the results for the lag and tidal efficiency evaluated in the well ADE005 for 9 days. Note that the lag is different considering the maximum water level (green solid dots) compared to the one obtained considering the minimum water level (green empty dots), and also note that even negative lag values are obtained.



Apx Figure H.6 Time series head data in the monitoring wells (left y-axis) and tidal signal (right y-axis) for the entire period of record (left) and detail over two tidal cycles.



Apx Figure H.7 Temporal variation of the tidal efficiency (a) and phase lag (b) calculated in the well ADE005.

It has been found that transmissivity estimates derived from amplitude attenuation may be significantly different to those derived from phase shift. Zhou (2008) evaluated the aquifer properties of a coastal aquifer in the Beihai area, China, and obtained hydraulic diffusivity estimates one order the magnitude lower from the amplitude damping than those obtained from the time lag. This difference may be related to zonation of hydraulic properties or connectivity effects between the monitoring wells and the sea.

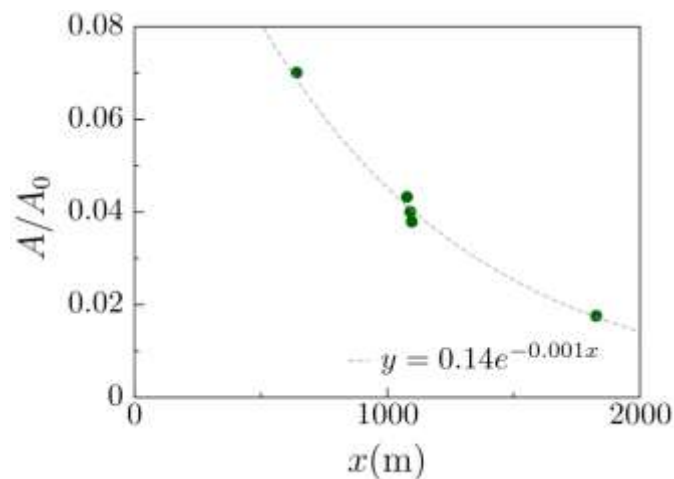
In addition to that, for interpretation of pumping tests in heterogenous media using the Jacob's straight line method, it has been demonstrated that transmissivity estimates based on the magnitude of the drawdown are close to the geometric mean of the transmissivity fields, whereas the storage coefficient estimates, evaluated from the time drawdown response, show a strong dependence on the connection

between the well and the observation points (see, e.g., Meier et al, 2001). Based on these findings, and also on our resulting lag values, we therefore contend that transmissivity estimates inferred from the time behavior of the tidal response may contain some information about the degree of heterogeneity and connectivity and therefore cannot be considered as representative values by themselves. Therefore, only averaged values for the tidal efficiency (ratio of the amplitude of harmonic components measured in the well to the ocean-tide amplitude) in the monitoring wells evaluated over the entire period of record are considered in order to apply the methods previously described.

The results for the averaged values for the tidal efficiency are summarized in Apx Table H.3. Figures 8 displays the results obtained for the averaged tidal efficiency at the wells screened in the T1 aquifer with respect to the distance of the wells from the coast. As expected, an exponential decrease of the tidal efficiency with distance from the coast is observed.

**Apx Table H.3 Tidal efficiency and phase lag measured in the monitoring wells.**

OBS-WELL	DISTANCE FROM THE COAST (M)	AQUIFER	TIDAL EFFICIENCY
ADE005	641	T1	7.01E-2
YAT037	1078	T1	4.33E-2
YAT043	1091	T1	4.01E-2
ADE037	1097	T1	3.79E -2
YAT042	1827	T1	1.76 -2
YAT099	906	T2	2.92E-2
YAT066	6060	T2	1.48E-2
YAT132	2773	T2	2.31E-2



**Apx Figure H.8 Results for the tidal efficiency and with respect to the distance from the coast for measurements at the monitoring wells screened in the T1 aquifer.**

Application of the Van der Kamp method requires specification of a value for loading efficiency. We consider a constant aquifer thickness of 130m for the T1 and 110m for the T2 aquifers. Because the spatial variability of storativity tends to be much smaller than the variability of transmissivity, the storage coefficient is also assumed to be constant and equal to  $2.5 \cdot 10^{-4}$  and  $1.4 \cdot 10^{-4}$  for the T1 and T2 aquifers,

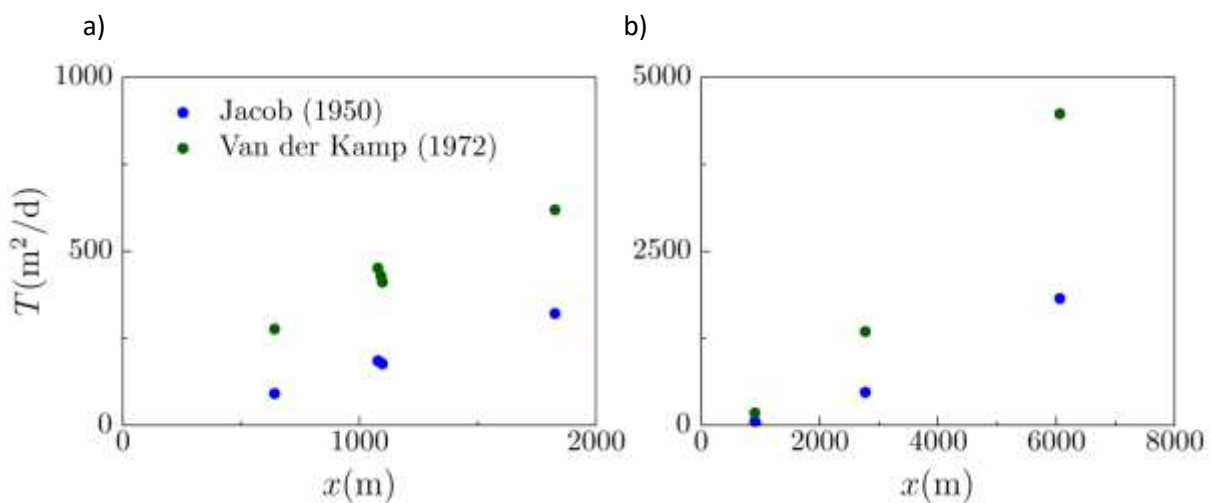
respectively (Gerges, 1999). The bulk porous matrix compressibility is calculated from the specific storage coefficient  $S_s$  [ $L^{-1}$ ], defined as  $S_s = \rho g [(1 - \phi)\alpha + \phi\beta]$ , in terms of the gravitational acceleration,  $g$  [ $LT^{-2}$ ], the porosity,  $\phi$  [ $L^3L^{-3}$ ] and fluid density,  $\rho$  [ $ML^{-3}$ ].

Using these values, and assuming a range for porosity from 10 to 25 percent, the matrix compressibility would range from  $1.6 \cdot 10^{-10}$  to  $1.1 \cdot 10^{-10} \text{ ms}^2\text{kg}^{-1}$  for the T1 aquifer and from  $9.4 \cdot 10^{-11}$  to  $2.4 \cdot 10^{-11} \text{ ms}^2\text{kg}^{-1}$  for the T2 aquifer. Then, the resulting averaged loading efficiency estimates considered for the T1 and T2 aquifers are 0.64 and 0.43, respectively. Results for the transmissivity estimates obtained by applying the methods of Jacob (1950) and Van der Kamp (1972) are shown in Apx Table H.4.

Transmissivity estimates obtained by applying the Jacob’s method, that is, considering a direct connection between the aquifer and the sea at the coast, are substantially lower than those from the Van der Kamp method. A remarkable feature that becomes apparent from the results is that transmissivities calculated from the amplitude attenuation increase linearly with distance from the coast, see Apx Figure H.9. A similar scale effect has been previously found in in long-term pumping tests, i.e., pumping tests with a large radius of influence tends to yield larger transmissivity estimates than local tests (Bredehoeft et al., 1983; Martinez-Landa and Carrera, 2005). At large observation distances, the head response to the tidal hydraulic perturbation samples a larger area.

**Apx Table H.4 Summary of transmissivities computed for the monitoring wells using the amplitude attenuation calculation methods of Jacob (1950) and Van der Kamp (1972).**

OBS-WELL	TRANSMISSIVITY ESTIMATES ( $M^2D^{-1}$ )	
	FROM AMPLITUDE ATTENUATION	
	Jacob Method (Eq. 3a)	Van der Kamp Method (Eq. 6a)
ADE005	91	277
YAT037	185	452
YAT043	180	429
ADE037	176	411
YAT042	321	619
YAT099	58	179
YAT132	477	1347
YAT066	1821	4476



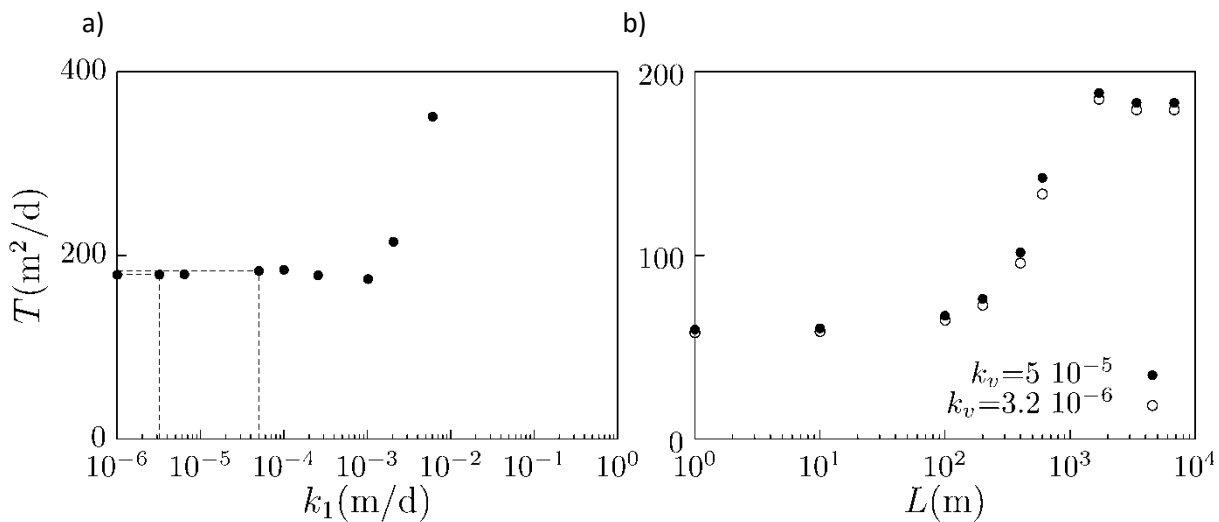
**Apx Figure H.9 Transmissivity estimates obtained from the methods of Jacob (1950) and Van der Kamp (1972) at the monitoring wells in the T1 (a) and T2 aquifer (b) as a function of the distance from the coast.**

In order to evaluate the effects of the length and leakage of the aquitard between the T1 and T2 aquifers (the Munno Para Clay formation), the method of Li and Jiao (2001a) was applied to monitoring well YAT099, located at a distance of about 1km from the coast. We first consider that the sub-sea extent of the T2 aquifer and the leaky semipermeable layer are infinite. That implies that  $R_1$  and  $I_1$ , equations (12) and (13), are equal to zero. The transmissivity of the T2 aquifer is evaluated from the amplitude attenuation, equation (8a), considering a value for the storage coefficient for the T2 aquifer of  $1.4 \cdot 10^{-4}$  and a thickness of the aquitard ( $b_1$ ) of 10m. In order to evaluate the effect of the vertical permeability of the aquitard, we consider a wide range for the specific leakage ( $L_s$ ) with values ranging from  $10^{-7}$  to  $6 \cdot 10^{-4} \text{ d}^{-1}$ , that is, considering values for the vertical conductivity ( $k_1$ ) from  $10^{-6}$  to  $6 \cdot 10^{-3} \text{ md}^{-1}$ .

**Apx Table H.5 Summary of the variables and transmissivities computed for the monitoring well YAT099 using the amplitude attenuation calculation method of Ji and Jiao (2001a).**

$L_s$	$u$	$\lambda$	$\gamma$	$p$	$q$	$C_e$	$T \text{ (M}^2\text{D}^{-1}\text{)}$
1.00E-07	1.26E-03	4.35E-01	7.10E-04	1.00E+00	9.99E-01	2.17E-01	179
3.20E-07	4.02E-03	4.35E-01	2.27E-03	1.00E+00	9.98E-01	2.18E-01	179
6.40E-07	8.04E-03	4.35E-01	4.54E-03	1.00E+00	9.96E-01	2.18E-01	179
5.00E-06	6.28E-02	4.37E-01	3.54E-02	1.03E+00	9.69E-01	2.19E-01	183
1.00E-05	1.26E-01	4.44E-01	6.99E-02	1.06E+00	9.39E-01	2.25E-01	184
2.56E-05	3.22E-01	4.88E-01	1.65E-01	1.17E+00	8.54E-01	2.58E-01	178
1.02E-04	1.29E+00	7.87E-01	2.74E-01	1.71E+00	5.86E-01	4.17E-01	174
2.05E-04	2.57E+00	9.26E-01	1.91E-01	2.31E+00	4.33E-01	4.73E-01	215
6.05E-04	7.60E+00	9.90E-01	7.31E-02	3.91E+00	2.56E-01	4.97E-01	351

Typical values of the vertical conductivity for the Munno Para measured from laboratory tests ranges between  $8.6 \cdot 10^{-7}$  to  $6.6 \cdot 10^{-5} \text{ md}^{-1}$  (Gerges, 1999). In order to evaluate the impact of the length of the semipermeable layer ( $L$ ), two different values for the vertical permeability are considered,  $3.2 \cdot 10^{-6}$  and  $5 \cdot 10^{-5} \text{ md}^{-1}$ . Using these values for an aquifer of infinite extent, the transmissivities obtained equal 179 and  $183 \text{ m}^2\text{d}^{-1}$ , respectively (dashed lines in Apx Figure H.10a). Then, the transmissivity estimates obtained by applying the method of Li and Jiao (2001a) for the case of finite extent for the aquifer and the leaky semipermeable layer are displayed in Apx Figure H.10b as a function of  $L$ . Results show that, as expected, as the length of the leaky confining layer decreases the transmissivity estimates tends to the values obtained from the method of Jacob (1950). The calculated transmissivity increases asymptotically with the extent of the aquitard beneath the seafloor, and reaches a constant value for extents larger than 2km, Apx Figure H.10b. That is, the transmissivity estimates are no longer sensitive to the extent of the leaky confining layer for lengths of larger than 2km.



**Apx Figure H.10** Transmissivity estimates obtained from the methods of Li and Jiao (2001a) as a function of the (a) vertical conductivity of the leaky semipermeable layer, and (b) length of the aquitard.

## H.6 Conclusions

The tidal method considering different aquifer configurations was applied to the tidally influenced head responses at seven wells located in the Adelaide Metropolitan Area to estimate hydraulic properties for the T1 and T2 Tertiary aquifers. The procedure presented in this study consists of four different steps: (1) Head data collection from seven monitoring wells for a one-month period, (2) correction of the barometric pressure effects to the head data, (3) application of spectral harmonic analysis to determine the principal harmonic components, their amplitude and frequency, and (4) application of different analytical solutions to calculate transmissivity estimates. Although theoretical solutions assuming a confining zone of infinite extent (Van der Kamp, 1972; Li and Jiao, 2001a) are more appropriate for the analysis of tidally influenced head data in the T1 and T2 aquifers, the classical method of Jacob (1950), which consider direct connection between the aquifer and the sea at the coastline, has been included for the purpose of comparison.

Spatial variations in the transmissivity estimates are observed showing a specific trend as a function of the distance of the monitoring well from the coast. This effect may be caused by a possible source of error in the filtering procedure. Due to the interference between different harmonic components and the inherent degree of noise in the head records, accuracy of determining the tidal efficiency and time lag may decrease with distance from the coast. However, the spatial variations in the transmissivity estimates (scale effect) may also be due to the spatial heterogeneity within the formations. It is well-known that groundwater head responses depend strongly on the details of aquifer properties. Therefore, one possible limitation to the applicability of the tidal method to real-world systems is that the solutions assume that the aquifer is homogeneous and of uniform thickness. Therefore, additional research to determine the impact of irregular patterns of spatial variability on the groundwater head responses to tidal fluctuations would be useful in investigating the error introduced by adopting the one-dimensional and homogeneous composite assumptions in the application of the tidal method.

However, in spite of the spatial variability observed in the transmissivity estimates, the results obtained from the tidal method considering the different aquifer configurations converge to a narrow range of values, except for the phase lag which is out by an order of magnitude near the coast, which are consistent with values obtained from pumping test. Therefore, whilst the tidal method has certain limitations, this method provides a simple and low-cost way to characterize coastal aquifers and reduces the need for pumping tests. A summary of the transmissivity estimates for the T1 and T2 aquifers obtained from the wells ADE005 and YAT099 located near the coastline is shown in Apx Table H.6.

**Apx Table H.6 Summary of transmissivities computed for the T1 and T2 aquifers from the wells ADE005 and YAT 099, using the amplitude attenuation calculation methods of Jacob (1950), Van der Kamp (1972) and Li and Jiao (2001a).**

AQUIFERS	TRANSMISSIVITY ESTIMATES (M <sup>2</sup> /D)			
	JACOB (1959)	VAN DER KAMP (1972)	LI AND JIAO (2001A) (INFINITE LEAKY AQUITARD)	LI AND JIAO (2001A) (FINITE LEAKY AQUITARD)
T1	91	241		
T2	58	179	179 - 351	58 – 179

## H.7 References

- Bredehoeft, J.D., Neuzil, C.E. and Milly, P.C.D. (1983). Regional flow in the Dakota aquifer: A study of the role of confining layers. U.S. Geol. Surv., Water-Supply Pap., 2237: I-45.
- Chapman, R.W. and Inglis C. (1898), Aust. Assoc. Adv. Science, Reports, Vol. 7. 241.244.
- Cooper, H. H., Jr., and C. E. Jacob (1946), A generalized graphical method for evaluating formation constants and summarizing well-field history, Eos Trans. AGU, 27(4), 526–534.
- Domenico, P.A., and Schwartz, Frank (1997). Physical and chemical hydrology, 2nd Edition: New York, John Wiley and Sons, 528 p.
- Ferris, J. G. (1951), Cyclic fluctuations of water level as a basis for determining aquifer transmissibility, Int. Assoc. Sci. Hydrol., 33, 148–155.
- Freeze, R. A., and J. A. Cherry (1979), Groundwater, 604 pp., Prentice-Hall, Englewood Cliffs, N. J.
- Gerges, N., 1999, 'The Geology and Hydrogeology of the Adelaide Metropolitan Area Volume 1 and Volume 2', PhD Thesis, Flinders University, Adelaide
- Guarracino, L., J. Carrera, and E. Vázquez-Suñe (2012), Analytical study of hydraulic and mechanical effects on tide-induced head fluctuation in a coastal aquifer system that extends under the sea, J. Hydrol., 450–451, 150–158.
- Jacob, C. E. (1950), Flow of groundwater, in Engineering Hydraulics, edited by H. Rouse, p. 321–386, John Wiley, N. Y.
- Li, H., and J. Jiao (2001a), Tide-induced groundwater fluctuation in a coastal leaky confined aquifer system extending under the sea, Water. Resour. Res., 37, 1165–1171.
- Li, H., and J. J. Jiao (2001b), Analytical studies of groundwater-head fluctuation in a coastal confined aquifer overlain by a leaky layer with storage, Adv. Water Resour., 24(5), 565–573.
- Martinez-Landa L, Carrera J (2005). An analysis of hydraulic conductivity scale effects in granite (full-scale engineered barrier experiment (febex), grimsel, switzerland). Water Resour Res 41(3). doi:10.1029/2004WR003458.
- Meier P, Medina A, Carrera J (2001). Geostatistical inversion of cross-hole pumping tests for identifying preferential flow channels within a shear zone. Ground Water 39(1), 10–7.
- Middleton, J.F., Bye, J.A.T. (2007). A review of the shelf-slope circulation along Australia's southern shelves; Cape Leeuwin to Portland. Progress in Oceanography, 75, 1–14.
- Post, V.E.A. and Von Asmuth, J. (2013), 'Hydraulic head measurements - New technologies, classic pitfalls', *Hydrogeology Journal*, Vol. 21 (4), 737-750.

- R. Pawlowicz, R., Beardsley, B. and Lentz S. (2002). "Classical tidal harmonic analysis including error estimates in MATLAB using T\_TIDE", *Computers and Geosciences* 28, 929-937
- Trefry, M.G. (1999), Periodic forcing in composite aquifers, *Advances in Water Resources*, Volume 22, Issue 6, Pages 645-656, ISSN 0309-1708.
- Theis, C. V. (1935), The relation between the lowering of the piezometric surface and the rate and duration of discharge of a well using ground-water storage, *Eos Trans. AGU*, 16, 519–524.
- Van Der Kamp, G. S. (1972). Tidal fluctuations in a confined aquifer extending under the sea, *Proc. Int. Geol. Congr.*, 24th, 101–106.
- Vincent, R. A., T. Tsuda, and S. Kato (1988). A comparative study of mesospheric solar tides observed at Adelaide and Kyoto, *J. Geophys. Res.*, 93(D1), 699–708.
- Zhou, X., (2008). Determination of aquifer parameters based on measurements of tidal effects on a coastal aquifer near Beihai, China. *Hydrol. Proc.* 22 (16), 3176–3180.

# Appendix I Vibrating wire piezometers – determination of other aquitard properties through pressure response

Authors: *Smith SD, Turnadge C and Cook PG*

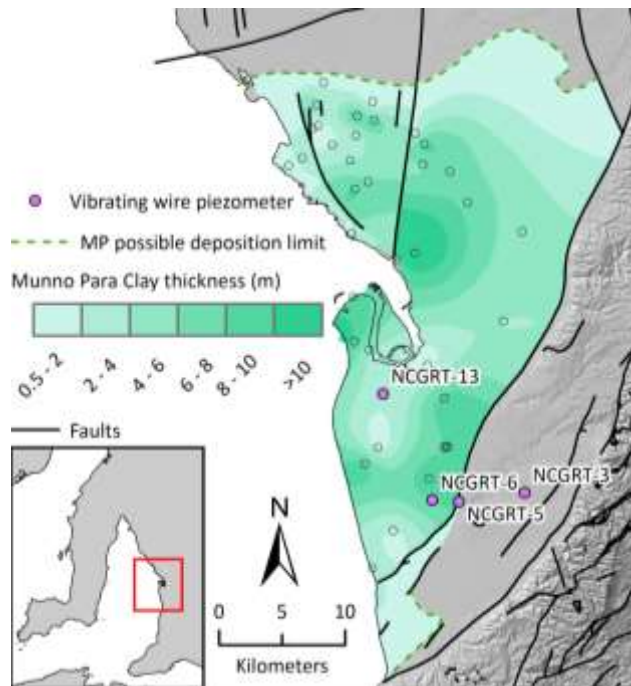
## I.1 Executive summary

In this study, vibrating wire piezometers were installed in several aquitards within the Central Adelaide Prescribed Wells Area (CA PWA). The vibrating wire piezometer is a pressure measurement device that can be attached to the outside of a well casing then gets fully encased in grout. Initial pressure data from these piezometers have been used to determine the aquitards' hydraulic properties including loading efficiency, formation compressibility and specific storage. All three of these parameters decrease with depth. Loading efficiencies are 0.74-0.97, formation compressibilities are  $6.1-59.6 \times 10^{-10} \text{ m}^2/\text{N}$  and specific storages are  $8.1-60.4 \times 10^{-6} \text{ 1/m}$ . The continuous data collection from this infrastructure makes it possible to use them for future studies looking at the inter-aquifer pressure responses to pumping, which may lead to better estimates of aquitard vertical hydraulic conductivity.

## I.2 Introduction

The management of stacked aquifer systems relies on determining rates of inter-aquifer leakage. Properly constraining this rate is highly dependent on an accurate characterisation of the aquitards that separate the aquifers of interest. Underlying the Adelaide metropolitan area is the Adelaide Plains basin, which contains up to nine distinct aquifers, separated by up to 14 confining beds. The water resources with these aquifers have been found to be of variable quality both between aquifers and spatially within given aquifers. With increasing levels of domestic and industrial usage, the proper management of these water resources is critical. Recent studies have used pressure responses within the aquitard as a means to determine hydraulic properties including loading efficiency, specific storage, and even hydraulic diffusivity (Smerdon et al., 2014; Smith et al., 2013). Conventional methods to study pressure propagation within aquitards are problematic due to the low permeabilities and thus low yields of these units. More recently, such studies have relied on the usage of vibrating wire piezometers, which get installed fully-grouted into the bore hole.

In this study, we installed vibrating wire piezometers in the confining beds at four sites as part of a program to add wells to the existing monitoring network (Apx Figure I.1; for additional information on the drilling program, see Appendix A). These vibrating wires were installed to determine hydraulic properties in the short-term (this study) and provide future use for monitoring pressure propagation during future studies, such as pumping tests.



**Apx Figure I.1** Locations of vibrating wire piezometer installation and thickness and extent of the Munno Para Clay; thicknesses are from the WaterConnect database (DEWNR, 2015).

## I.3 Study area

### I.3.1 SITE DESCRIPTION

The Adelaide Plains Sub-basin and Golden Grove Embayment are comprised of a layered sequence of Quaternary and Tertiary aquifers and aquitards overlying much older fractured bedrock. The eastern boundary of the basin is juxtaposed against the Eden-Burnside Fault Zone that separates the sedimentary basin and the fractured basement rock of the Mount Lofty Ranges. The groundwater flow system is expected to be gravity driven with recharge occurring in Mount Lofty Ranges and groundwater flows west towards the Gulf of St Vincent. This study is within the Central Adelaide Prescribed Well Areas (CA PWA).

### I.3.2 HYDROGEOLOGY

The hydrogeology, as extensively documented by Gerges (1999), consists of six Quaternary aquifers and four Tertiary aquifers. These are separated by 14 aquitards or confining beds (designated Cb1-14). Underlying the sedimentary basin is the complex lithology of the basement (see Appendix B). The CAP PWA is divided by the Para Fault, causing a significant offset of stratigraphic units. Aquifer and aquitard designation is based on the vertical order of occurrence as opposed to stratigraphic units. Within the Tertiary sediments, the T1 and T2 aquifers are primarily separated by the Munno Para Clay Member of the Port Willunga Formation, but are also separated by the Ruwarung Member, and the clay Aldinga Member. The T1 aquifer is locally divided by the Croydon facies, giving rise to the T1a and T1b aquifers.

## I.4 Methods

### I.4.1 INSTALLATION

Vibrating wire piezometers operate by using a magnet to vibrate a wire attached to a diaphragm. The frequency of vibration is measured and is a function of the tension on the wire and the pressure in the

formation. The sensors installed (Slope Indicator Standard Borehole Piezometer) also measures temperature, which is used as a correction factor. The advantage of this type of sensor is that they have a rapid response and can be completely encased in grout, removing the need to create a sand-pack during installation. The piezometers were installed on the outside of the casing in low permeability zones as determined by standard wireline geophysical logs and the visual inspection of cuttings. These piezometers were then fully grouted with a high-bentonite cement mixture. Data logging of pressure began several weeks after installation – this delay was to allow surface completion of the well, thus allowing the secure placement of the data loggers. Only one vibrating wire was available for Site 6 (Barrpowell St) because of a casing failure that resulting in the vibrating wire cables being severed. A list of installed piezometers is given in Apx Table I.1.

**Apx Table I.1 Vibrating wire installation sites and depths; formations estimated from Appendix A.**

SITE	FORMATION	DEPTH (m)
3 – Trinity Gardens	Q	23
	Blanche Point Fm	97
5 – North Adelaide	Q	16
	Weathered Bedrock	53
6 – Welland	T1a clay unit	126.7
13 - Gillman	Q	77
	Munno Para Clay	168

## I.4.2 DATA REDUCTION

Data from the vibrating wire piezometers must be processed to first achieve a pressure before correcting for the effects of barometric pressure and the loading efficiency of the formation. Measured frequencies were converted to pressures using temperature dependent (temperature integrated; TI) calibration factors:

$$p_{meas} = c_0 + (c_1\lambda) + (c_2T) + (c_3\lambda^2) + (c_4\lambda T) + (c_5T^2), \quad (K.1)$$

where  $p_{meas}$  is the measured formation pressure (kPa gauge),  $c_n$  are the calibration factors,  $\lambda$  is the measured frequency (1/second) and  $T$  is the formation temperature ( C).

Barometric pressures for correction were taken from the Adelaide (Kent Town) Bureau of Meteorology (BOM) station. While there are multiple weather stations recording barometric pressure within the study area, pressure readings are quite consistent between these stations, so it was deemed unnecessary to use multiple stations or interpolate pressures between these stations. The barometric pressure correction is defined as:

$$p^* = p_{meas} - \gamma(B - B_{ave}), \quad (K.2)$$

where  $p^*$  is the corrected pore water pressure (kPa gauge),  $\gamma$  is the loading efficiency (0–1),  $B$  is the measured barometric pressure (kPa absolute) and  $B_{ave}$  is the average barometric pressure corrected to the site elevation – however, this elevation correction is minimal as the highest site (Trinity Gardens) is only ~60 m above sea level (99.2 % of sea level pressure). The loading efficiency was determined by choosing the value between 0 and 1 that produced the smoothest trace of groundwater pressure. This was done using a least-squares polynomial regression through relatively clean sections of data that also included several barometric events.

Pressures were then converted to hydraulic heads after assuming zero salinity and a constant density of pore fluids ( $\rho_w = 1000 \text{ kg/m}^3$ ). The loading efficiency is related to porosity ( $n$ ) and the compressibility ( $\text{m}^2/\text{N}$ ) [ $\text{L}t^2/\text{M}$ ] of water ( $\beta$ ) and the formation ( $\alpha$ ):

$$\gamma = \frac{\alpha}{n\beta + \alpha}. \quad (\text{K.3})$$

The compressibility of water is constant at  $4.8 \times 10^{-10} \text{ m}^2/\text{N}$  for the temperatures of interest. Equation K.3 is rearranged to solve for  $\alpha$ :

$$\alpha = \frac{\gamma n \beta}{1 - \gamma}. \quad (\text{K.4})$$

Specific storage ( $S_s$ ;  $1/\text{m}$ ) was then calculated using

$$S_s = \rho_w g (\alpha + n\beta). \quad (\text{K.5})$$

Because porosity was not directly measured, it can be estimated from geophysical logs, specifically density logs derived from neutron density. The logs can be used provided that the matrix density of the formation is known. Because low permeability formations tend to have a wide range of mineral phases, the matrix density cannot be assumed. To avoid over interpreting the density logs, porosities were assumed to be constant at 0.45. The consequences of this assumption will be discussed below.

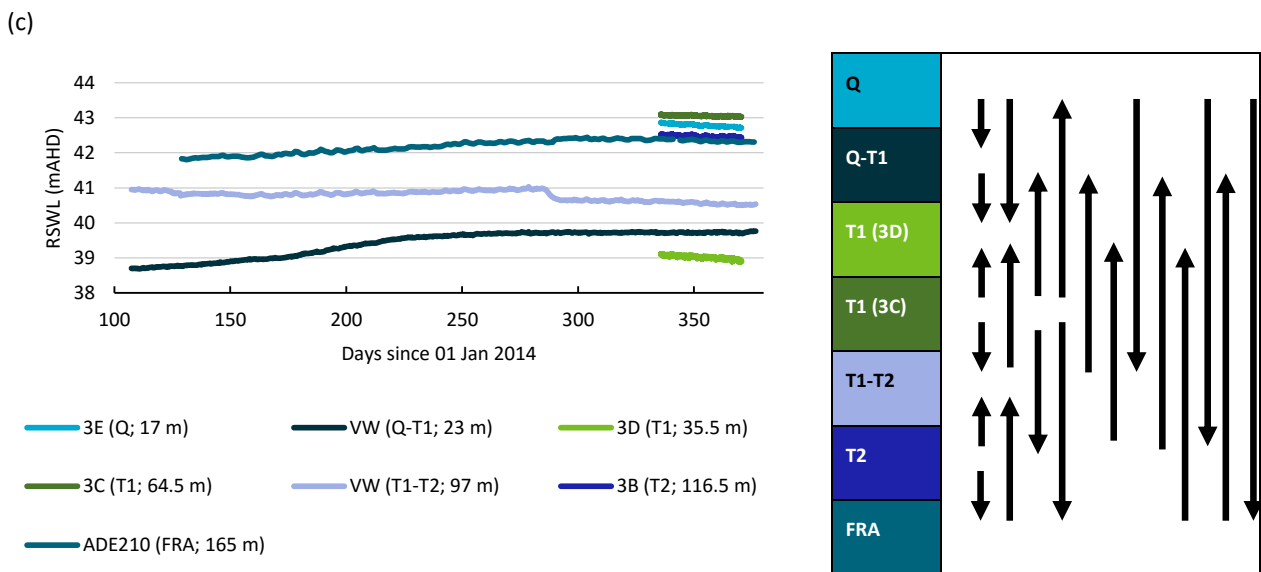
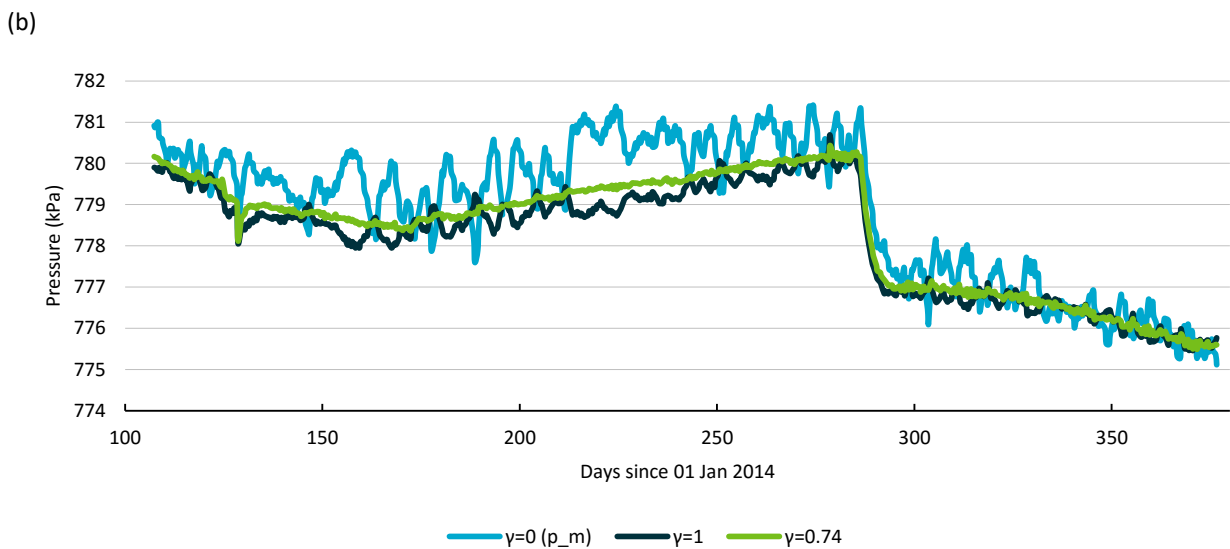
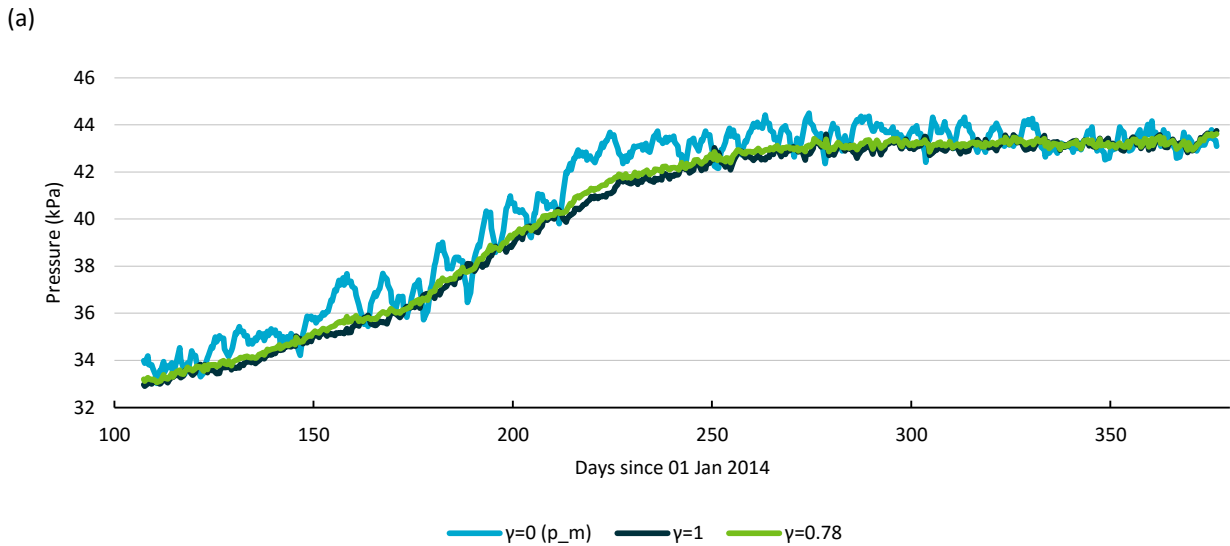
## 1.5 Results

The calculated loading efficiencies, aquitard compressibilities, and specific storage for each piezometer are given in Apx Table I.2. The raw and corrected pressure responses, plus head data for nearby wells, for each site are given in Apx Figure I.2 through Apx Figure I.5. At all sites with multiple vibrating wires, loading efficiency and thus compressibility and specific storage decrease with depth. Compressibility values are significantly lower than textbook values for clay ( $7\text{-}200 \times 10^{-8} \text{ m}^2/\text{N}$ ) (Schwartz and Zhang, 2003) suggesting a significant amount of compaction. Specific storage values range from  $8\text{-}60 \times 10^{-6} \text{ 1/m}$ . The pressure responses at the four different sites show considerably variable trends. Both Site 3 (Apx Figure I.2b) and Site 5 (Apx Figure I.3b) show sudden changes in pressure, which could be related to pumping activities. The piezometer at Site 6 was installed within a clay unit (inferred from high gamma counts) within the T1 aquifer, however this piezometer shows no isolation from pressure changes resulting from industrial pumping (Apx Figure I.4a). Because the magnitude of pumping induced pressure changes greatly exceed the magnitude of barometric pressure changes, the loading efficiency could not be calculated.

**Apx Table I.2 Formation parameters determined by vibrating wire data analysis.**

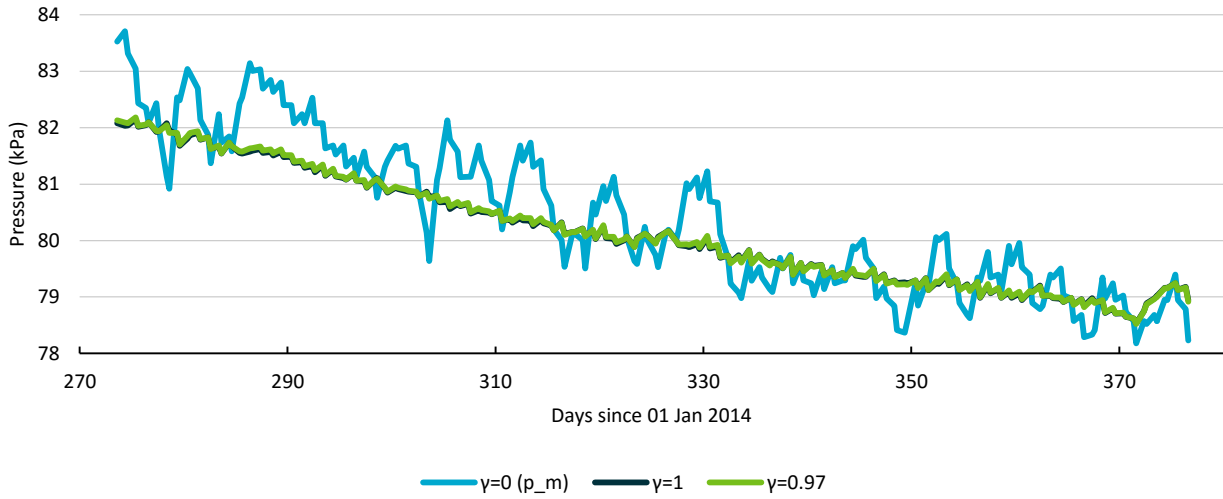
SITE	FORMATION	$\gamma$ (-)	$\alpha$ ( $\text{m}^2/\text{N}$ )	$S_s$ ( $1/\text{m}$ )
3 – Trinity Gardens	Q	0.784	7.82E-10	9.77E-06
	Blanche Point Fm	0.738	6.09E-10	8.08E-06
5 – North Adelaide	Q	0.965	5.96E-09	6.04E-05
	Q	0.810	9.21E-10	1.11E-05
6 – Welland*	Weathered Bedrock	-	-	-
13 - Gillman	T1a Clay Unit	0.900	1.94E-09	2.12E-05
	Munno Para Clay	0.840	1.13E-09	1.32E-05

All calculations assume  $n = 0.45$ ,  $\rho_w = 998.2 \text{ kg/m}^3$  and  $\beta_w = 4.80 \times 10^{-10} \text{ Pa}^{-1}$

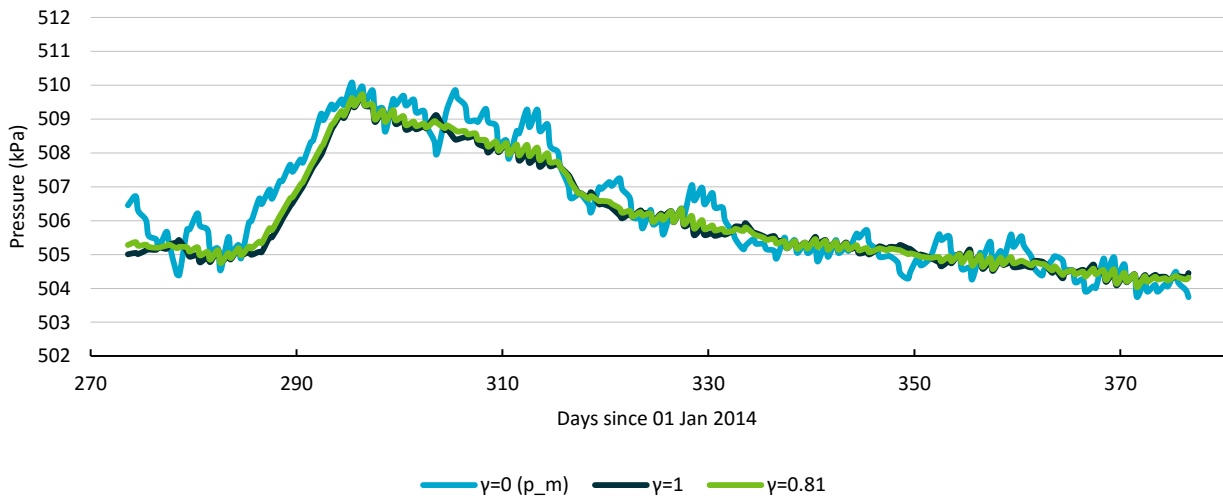


Apx Figure I.2 Site 3 – Trinity Gardens: (a) 23 m (b) 97 m and (c) RSWL with water levels from nested or adjacent wells and relative head differences between measurements.

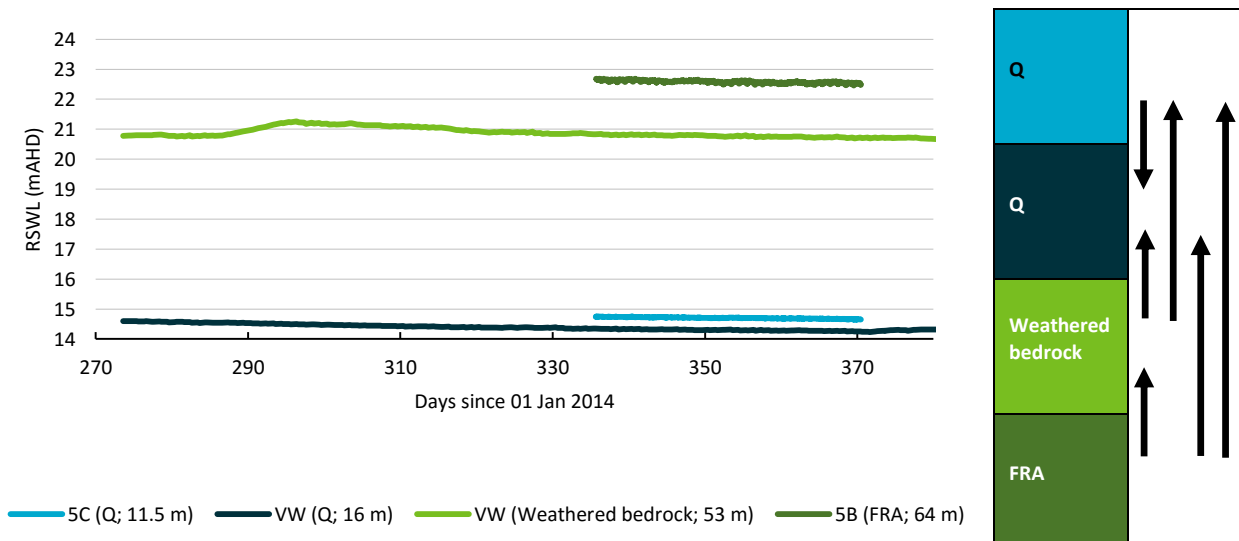
(a)



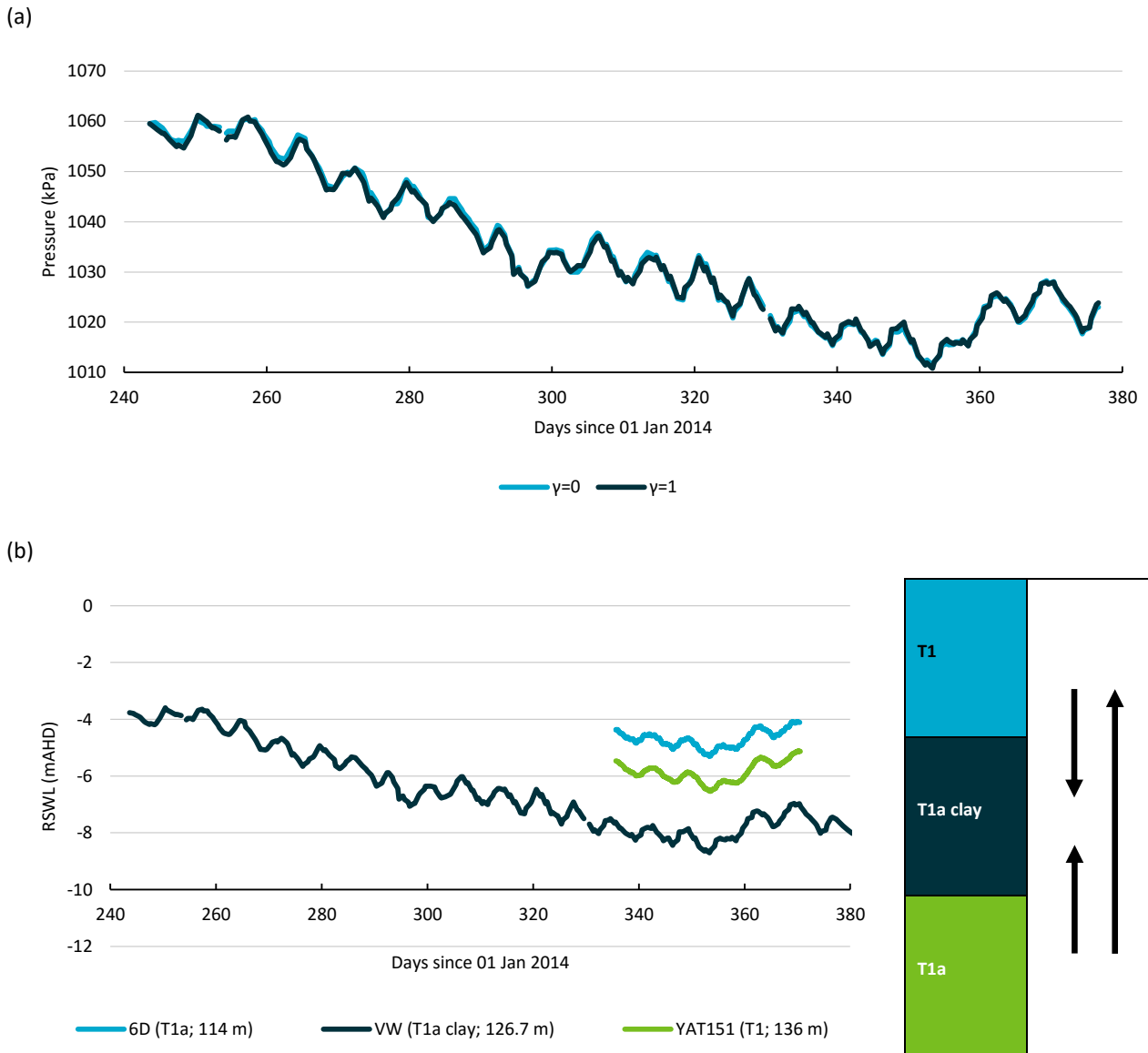
(b)



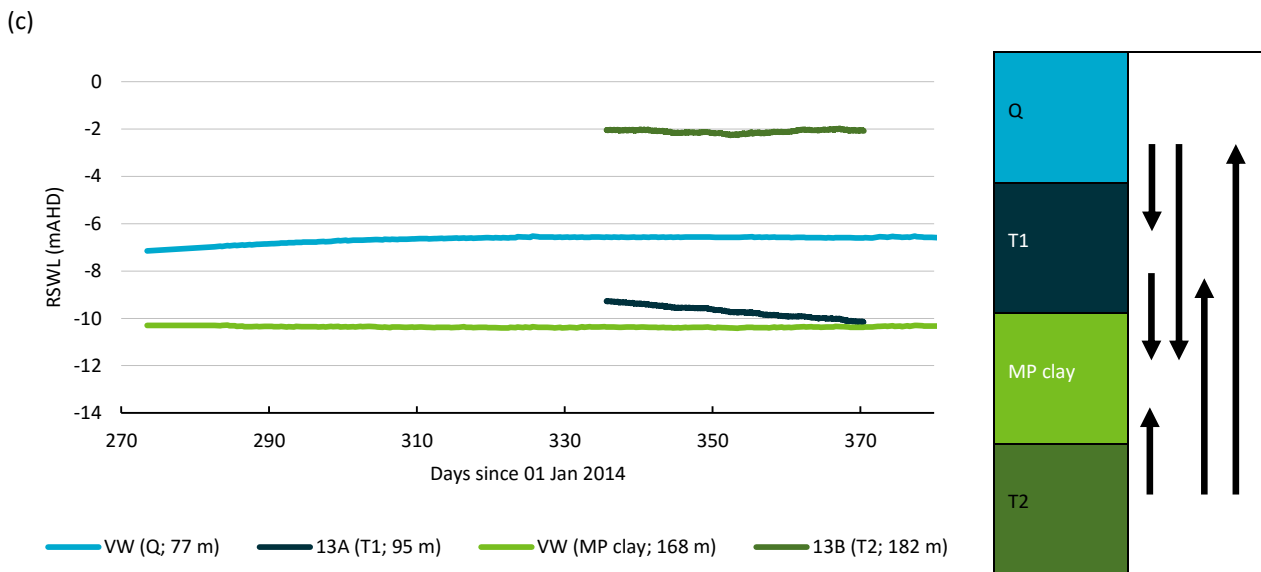
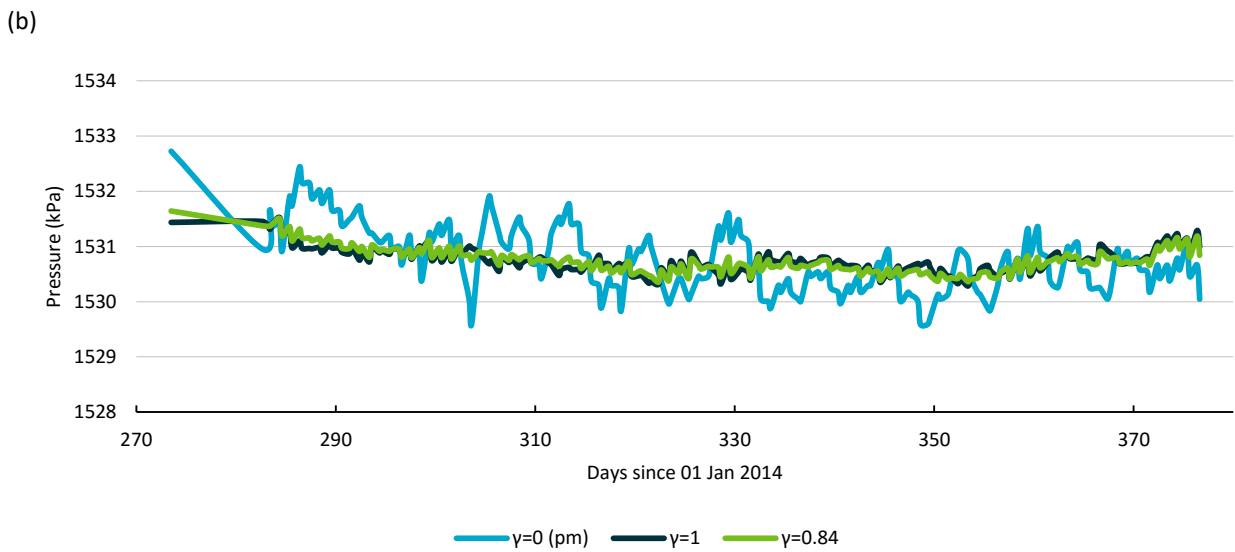
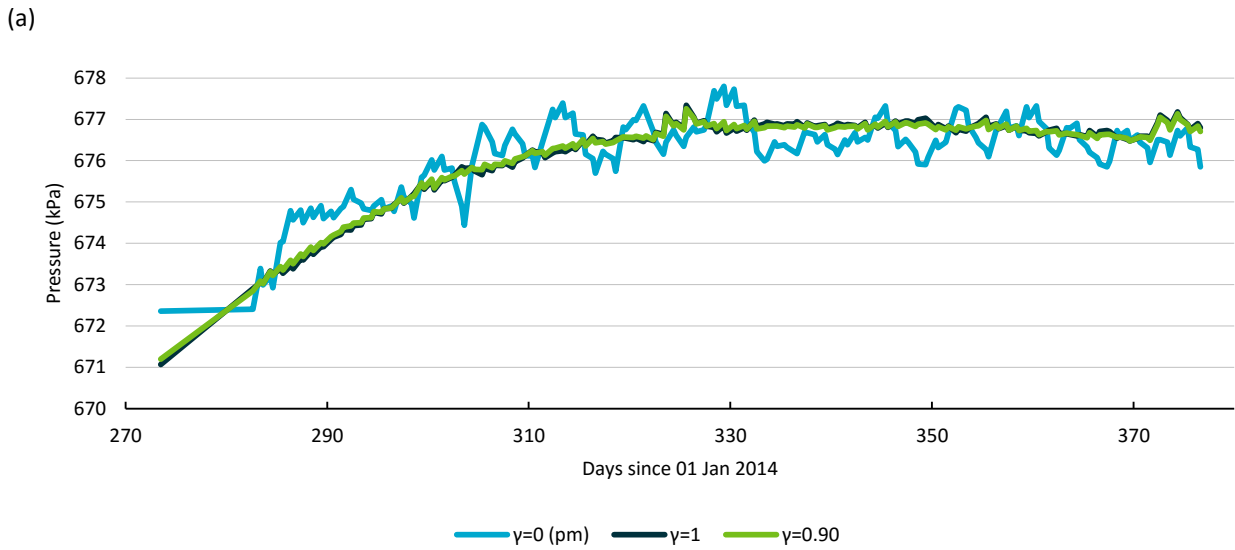
(c)



Apx Figure I.3 Site 5 – North Adelaide: (a) 16 m (b) 53 m and (c) RSWL with water levels from nested or adjacent wells and relative head differences between measurements.



Apx Figure I.4 Site 6 – Welland: (a) 126.7 m and (b) RSWL with water levels from nested or adjacent wells and relative head differences between measurements.



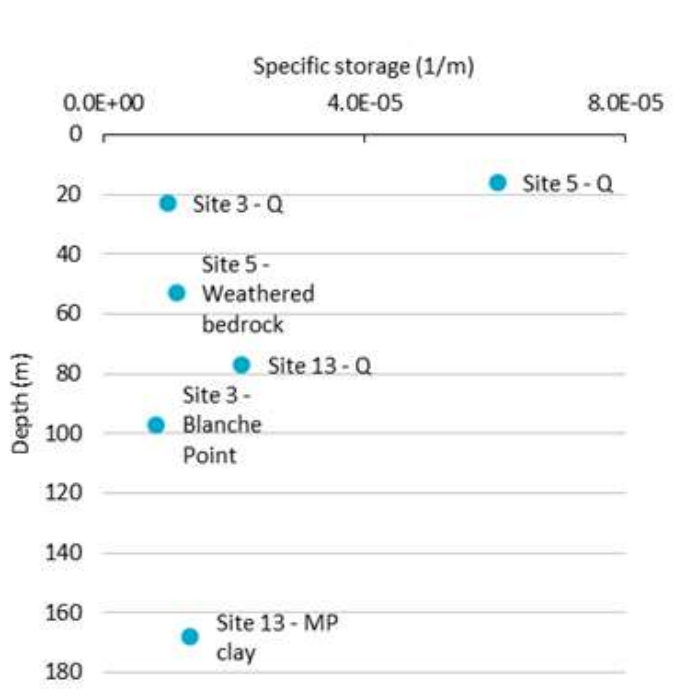
Apx Figure I.5 Site 13 – Gillman: (a) 77 m (b) 168 m and (c) RSWL with water levels from nested or adjacent wells and relative head differences between measurements.

## 1.6 Discussion and Summary

The specific storage values presented above are subject to uncertainty in the loading efficiency and the formation porosity. To assess the uncertainty associated with each calculation, a Monte Carlo analysis was performed for each vibrating wire piezometer. The fitting procedure used to find loading efficiency seems robust with a maximum uncertainty of 2% (standard deviation). The estimate of porosity is relatively weak and the porosity may be as variable as 5%. Given these uncertainties and assuming normal distributions of values, the average uncertainty in specific storage ranges between 16 and 367%. The outlier with high uncertainty is the shallow piezometer at Site 5 that has a high loading efficiency (0.965). Analysis of Eq. K.4 shows that as loading efficiency approaches unity, formation compressibility approaches infinity. Therefore the uncertainty increases as loading efficiency increases. This suggests that vibrating wire piezometers may give unreliable specific storage values for shallow, unconsolidated formations – in the Adelaide Plains, the minimum depth is approximately 20 m based on the data collected here (Apx Figure I.6).

The vertical head distributions presented below seem questionable when compared to monitoring well head data. For example at Site 6, the vibrating wire piezometer is located below NCGRT 6D and above YAT151, but the RSWL from the piezometer is approximately 2.5 m lower than both of these two wells, whereas it should be between these two wells (Apx Figure I.4b). There is likely to be some uncertainty in the installation depth of the vibrating wire piezometer, however, this uncertainty is likely to be on the order of up to 10 cm, not metres. Though unlikely, the piezometers could have been dragged to a shallower depth as the casing was inserted into the drill hole. This would explain the apparent offsets at Site 6 and 13. It is possible that the depth of these piezometers could be verified using downhole geophysical methods.

The ongoing collection of data from these vibrating wire piezometers can provide valuable information for future studies looking at inter-aquifer pressure response during pumping. If significant pressure changes can be made inside of the aquitard, it may be possible to calculate  $K_v$  based on these pressure responses. A study like this could provide greater insight into the aquitard properties of the Adelaide Plains sub-basin.



Apx Figure I.6 Specific storage versus piezometer depth.

## I.7 References

- DEWNR (2015) WaterConnect. Viewed 6 February 2015, <<http://www.waterconnect.sa.gov.au/>>.
- Gerges NZ (1999) The geology and hydrogeology of the Adelaide Metropolitan Area. Flinders University.
- Schwartz FW and Zhang H (2003) Fundamentals of Ground Water. John Wiley & Sons, Inc, New York, NY.
- Smerdon BD, Smith LA, Harrington GA, Gardner WP, Delle Piane C and Sarout J (2014) Estimating the hydraulic properties of an aquitard from in situ pore pressure measurements. *Hydrogeology Journal* 22(8), 1875-1887. DOI: 10.1007/s10040-014-1161-x.
- Smith LA, van der Kamp G and Hendry MJ (2013) A new technique for obtaining high-resolution pore pressure records in thick claystone aquitards and its use to determine in situ compressibility. *Water Resources Research* 49(2), 732-743. DOI: 10.1002/wrcr.20084.

# Appendix J Groundwater flow processes across fault zones

Authors: *Banks EW and Cook PG*

## J.1 Introduction

### J.1.1 BACKGROUND

An important source of groundwater recharge to sedimentary basin aquifers is from mountain front recharge (also known as Mountain Block Recharge) and in many instances the rate and direction of groundwater flow is controlled by regional scale fault systems (Ball, Ge *et al.* 2010; Bense, Van Balen *et al.* 2003). Vertical faults may act as either barriers to horizontal groundwater flow perpendicular to the fault, conduits to horizontal flow along the fault or a combination of both (Folch and Mas-Pla 2008; Marler and Ge 2003). Faults can also provide preferential pathways for vertical flow (Anderson and Bakker 2008; Haneberg 1995; Roques, Bour *et al.* 2014).

In many instances, fault zones influence the hydraulic head distribution between aquifer systems either side of the fault due to a change in the permeability structure; however, it is not straight forward what impact the fault zone has on the groundwater flux between aquifers. A number of studies have observed large hydraulic head discontinuities across fault systems due to significant groundwater extraction in mining operations (Baghbanan and Jing 2007; Bense and Person 2006; Gleeson, Novakowski *et al.* 2009a; Gleeson, Novakowski *et al.* 2009b; Haneberg 1995). There are very few field sites with groundwater monitoring wells closely spaced either side of a fault zone to evaluate the impact of fault zones on groundwater flow. A recent review paper by Bense *et al.* (2013) recommended that a stronger synergy between hydrogeology and structural geology disciplines is required in order to gain a more integrated understanding of fault zone hydrogeology. The various approaches that are used include outcrop mapping and structural geology, drilling and borehole geophysics, electrical resistivity tomography, hydraulics and Darcy's Law approximations, numerical modelling, flowmeter and pump testing, fault rock mineralogy and geochemistry, hydrochemistry and environmental tracers. In this study a multi-discipline approach is used to investigate the impacts of fault zones on regional scale groundwater flow processes.

### J.1.2 ADELAIDE PLAINS AND WILLUNGA EMBAYMENT

The extensive study of the hydrogeology of the Adelaide metropolitan area by Gerges (1999; 2006) identified that groundwater flow across the fault is one of the major recharge mechanisms to the sedimentary aquifer systems on the Adelaide Plains. The hydrogeological system of the Adelaide Plains includes three major fault systems (1) the Eden Burnside Fault, (2) The Para Fault, and (3) the Hope Valley Fault. The Eden-Burnside (E-B) Fault separates the Precambrian fractured rock aquifers to the east of the Golden Grove- Adelaide Embayment and the Tertiary and Quaternary sedimentary deposits on the plains. The Para Fault is a significant geological boundary that exists within the central part of the embayment and delineates the Quaternary and Tertiary sedimentary deposits into two main sub basins (Adelaide Plains sub-basin and the Golden Grove- Adelaide embayment) with much greater displacement and thickness of the sediments to the west of the fault (up to ~600m thickness) compared to ~150 metres east of fault. Groundwater extraction is far more prevalent from the Quaternary and Tertiary aquifers to the west of the Para Fault. The Hope Valley Fault is a less continuous fault and lies to the west of the Eden-Burnside Fault. Several geophysical studies (Leaf, Hart *et al.* 2012; Manning, Clark *et al.* 2012) have been done across the Adelaide Plains to describe the structure, orientation and displacement of the major fault systems.

Groundwater models that have since been developed by the work of Gerges (1999; 2006) have attempted to capture the mechanisms of groundwater flow across the E-B Fault, however, there is still a large amount of uncertainty around the boundary conditions to the model domain and difficulty in model calibration across the fault zone with hydraulic heads and flux. A field investigation by Green et al. (2010) was conducted to investigate mechanisms by which groundwater might flow across the E-B Fault and identify the location and areal extent of recharge zones around the fault zone. Despite the hydrochemical tracers providing no clear evidence of groundwater following preferential flowpaths across the fault zone, the structural geological observations suggested that groundwater may also flow directly across and along the fault from the fractured rock aquifer across into the sedimentary aquifers on the downthrown side of the fault where there are “zones of breakage”. Green et al. (2010) also hypothesised that an indirect pathway for groundwater from the fractured rock aquifer to the sedimentary aquifers is via the surface water features that traverse the fault zone and contribute to streambed recharge to the shallow sedimentary aquifers.

The Willunga Embayment has very similar geological and hydrogeological characteristics to the Adelaide Plains (this includes both the Golden Grove-Adelaide Embayment and the Adelaide Plains Sub-basin). A recent drilling project in 2012 (as part of the NCGRT Willunga Super Science program) to investigate groundwater flow processes across fault zones in the Willunga Embayment provides an invaluable analogue to the likely recharge mechanisms and groundwater flow processes across major fault systems within the Adelaide environment. For this reason, this body of work focuses on the Willunga Embayment.

The groundwater flow models that have been developed for both the Adelaide Plains and the Willunga Embayment have considered a hydrogeological conceptual model whereby some proportion of groundwater input to the sedimentary aquifers is from the fractured rock aquifer system above the major fault zones. In many instances and model iterations, the challenge has been on what boundary conditions to assign to the model domain, the choice of physical parameters to apply to the fault zone and what kind of approach and uncertainty is acceptable in hydraulic head observations either side of the fault.

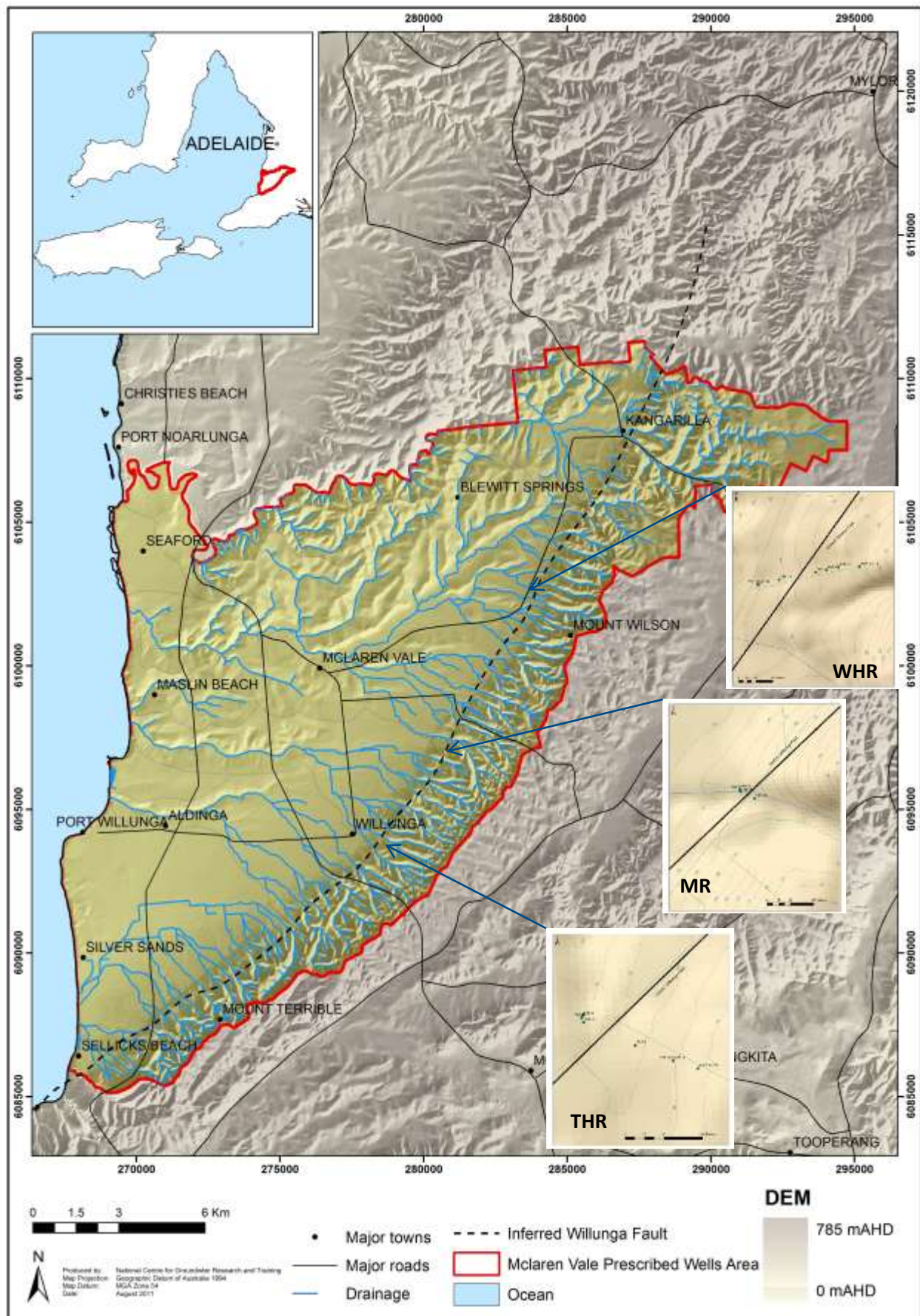
The aim of this study was to improve our understanding and knowledge of the mechanisms of regional groundwater flow processes across major fault zones at different spatial scales and resolve the hydrogeological conceptual model of the Willunga Embayment. Given the similar geological context of the Adelaide Plains, the outcomes of this study are seen to be transferable, and will contribute to the conceptual and numerical model for the Adelaide Plains. More specifically, this study: (1) applied both field and numerical modelling approaches to describe the permeability of a fault zone, (2) investigate the impact of the fault on regional groundwater flow and (3) determine whether the fault zone acts as a barrier or conduit to groundwater flow or a combination of both.

## J.2 Study Area

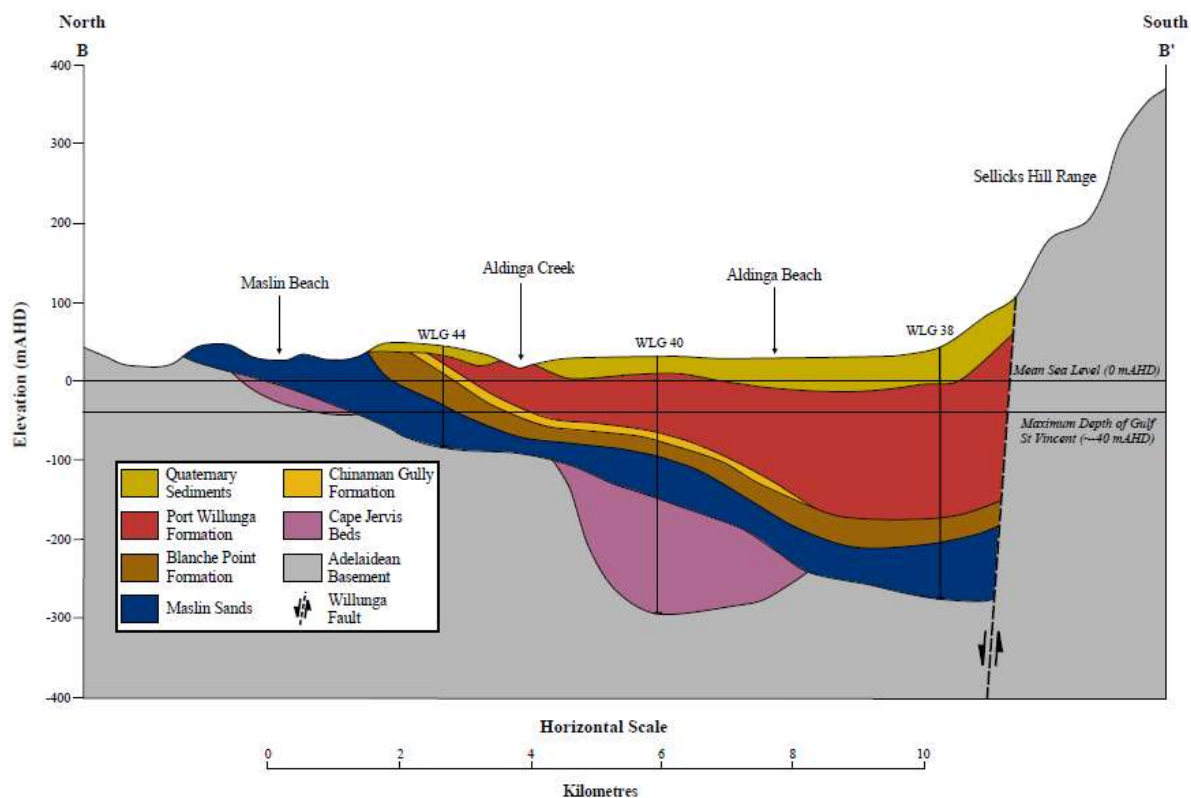
Field investigations were conducted in the Willunga Embayment, which is approximately 30 km south of Adelaide, South Australia. The embayment structure is a gently-dipping trough comprised of a thick sequence of Cainozoic sediments bounded to the north, east and south by bedrock of Cambrian Age and St Vincent’s Gulf to the west (Apx Figure J.1). The notable topographic feature is the Sellicks Hill Range that falls along the eastern boundary and it is at the base of the range where the Cainozoic sediments and Cambrian hard rock are separated by the Willunga Fault Zone with a north-east to south-west strike direction. The position of the Willunga fault has been determined primarily using geological data from a coastal cross section, distinct changes in topographic relief and a number of geophysical surveys (Reed 1982). The total throw of this fault system is estimated between 320 and 375 metres below sea level and it is close to sub-vertical, which can be observed in Cactus canyon just south of Sellicks Beach. The sedimentary sequences within the embayment increase in thickness eastwards towards the fault and become thinner further inland where they pinch out.

The climate of the region is characterised by hot dry summers and cool wet winters with the majority of rainfall and groundwater recharge occurring between May and August. There is a strong precipitation

gradient from the coast to the top of the embayment and the range; average rainfall at the township of Noarlunga is 450 mm per year whilst at Willunga, towards the range, it is about 650 mm per year. Elevation ranges from 200 metres above sea level in the northeastern corner of the embayment to 0 metres down at the coast on the western boundary. A water allocation plan has been in place for the region since 2000 due to the concern on the long-term sustainability of the water resources to support the viticultural and horticultural industry and community. This has resulted in a number of studies (Aldam 1989, 1990, Watkins and Telfer 1995, Sereda & Martin 2000, OCWMB 2000, Herczeg&Leaney 2002, James-Smith 2002, Harrington 2002, Brown 2004, Martin et al. 2006, Ecological Associates, 2003, 2006, SKM, 2008) to investigate groundwater flow processes, recharge mechanisms, groundwater dependent ecosystems, managed aquifer recharge, and a water balance to contribute to a groundwater numerical model for the water allocation plan.



Apx Figure J.1 Location map of the Willunga Embayment and the three field sites THR, MR and WHR



Apx Figure J.2 Geological cross section of the Willunga embayment along transect north to south near coastline (modified from Watkins, 1995)

### J.3 Methods

This investigation used a multidisciplinary field based and numerical modelling approach to constrain the physical mechanisms of fault zones on regional groundwater flow. Field work focused on three sites which were established during the Willunga Super Science program (2011-2015). At each of these sites (named Taylors Hill Rd (THR), Marshall Rd (MR) and Wickams Hill Road (WHR)) groundwater wells were designed and constructed to monitor the aquifer systems at different depths (up to 300 metres below ground level) as closely as possible to either side of the Willunga Fault. Near surface geophysical surveys were undertaken prior to drilling to finalise site locations and detailed analysis of the drillhole logs during the well construction process was advantageous in the overall outcome of the drilling program (Banks, Shanfield *et al.* 2014).

#### J.3.1 HYDRAULICS

The construction details of each of the nested observation wells either side of the Willunga fault are shown in Apx Table J.1. The well screen intervals at each of these sites are located in the sedimentary and fractured rock aquifer systems. The ground elevation and observation wells were surveyed and the water table elevations were corrected to a reduced standing water level (RSWL) relative to the Australian Height Datum (mAHD; i.e. the mean sea level). Manual water level measurements were made and In-situ data loggers were used to monitor the temporal variability in each of the aquifer systems on a regular basis between 2013 and 2015 to examine the vertical and horizontal gradients across the fault zone.

**Apx Table J.1 Construction details of the observation wells either side of the Willunga Fault at the three study sites**

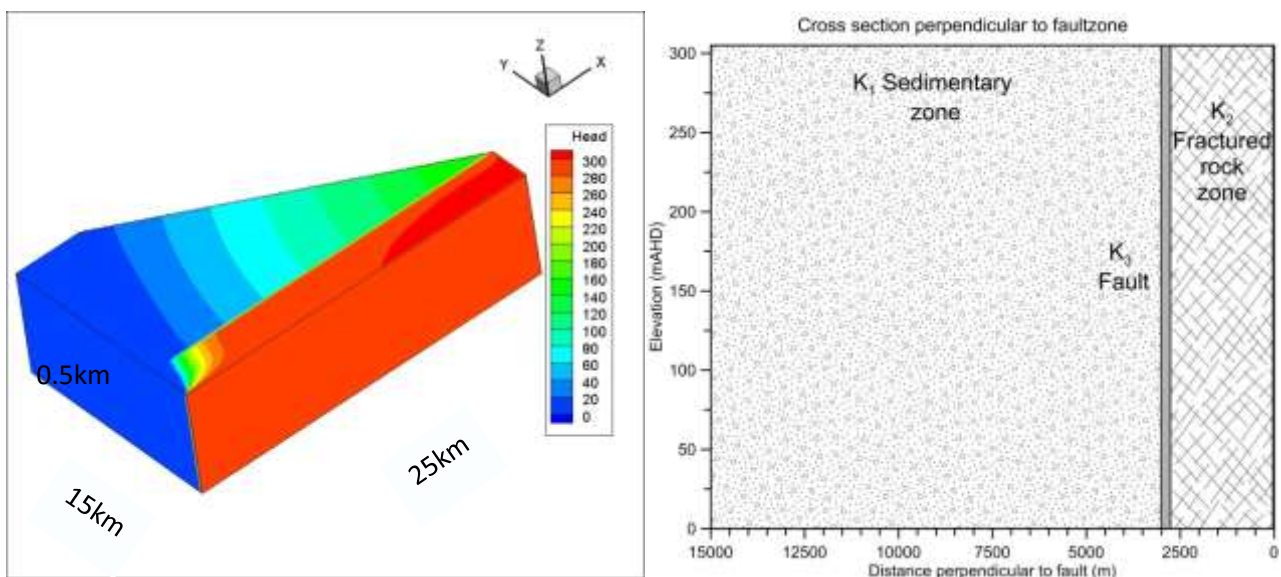
Unit number	Site ID	Aquifer	Well completion depth	Mid piezo depth	1/2 screen length	Mid piezo depth	TOC	Natural ground	Eastings	Northings	Date/Time	SWL	RSWL
			mbg	mbg	m	mAHD	mAHD	mAHD				mbTOC	mAHD
6627-14730	FAF-1A	FRA	53.05	52.55	0.50	86.15	138.59	138.70	278283	6094374	15/05/2013	12.91	125.68
6627-14731	FAF-1B	FRA	45.75	45.25	0.50	93.45	138.62	138.70	278283	6094374	15/05/2013	12.93	125.70
6627-14732	FAF-1C	FRA	28.65	28.15	0.50	110.55	138.60	138.70	278283	6094374	14/05/2013	12.42	126.18
6627-14686	FAF-2	PWF	114.00	112.50	1.50	19.79	132.24	132.29	278217	6094414	7/05/2013	86.13	46.11
6627-14733	FAF-3A	FRA	52.10	51.60	0.50	92.66	144.26	144.26	278333	6094355	15/05/2013	17.49	126.77
6627-14734	FAF-3B	FRA	41.50	41.00	0.50	103.26	144.25	144.26	278333	6094355	15/05/2013	17.47	126.78
6627-14736	FAF-3C	FRA	30.65	30.15	0.50	114.11	144.24	144.26	278333	6094355	15/05/2013	17.34	126.90
6627-14735	FAF-3D	FRA	35.00	34.50	0.50	109.76	144.14	144.26	278332	6094356	17/05/2013	26.36	117.78
6627-14737	FAF-3E	FRA	24.40	23.90	0.50	120.36	144.08	144.26	278332	6094356	15/05/2013	18.07	126.01
6627-14687	FAF-4	PWF	196.00	194.50	1.50	-61.51	132.86	132.99	278217	6094404	6/05/2013	85.72	47.14
6627-14685	FAF-5	PWF	168.90	167.40	1.50	-34.71	132.55	132.69	278214	6094410	6/05/2013	85.51	47.04
6627-14684	FAF-6	PWF	140.00	138.50	1.50	-6.01	132.32	132.49	278216	6094412	6/05/2013	85.21	47.11
6627-10777	10777	FRA	34.45	33.95	0.50	113.63	147.78	147.58	278364	6094345	13/08/2013	18.50	129.28
6627-14701	FAF-7	MS	282.00	279.00	3.00	-132.51	146.36	146.49	280113	6096873	15/05/2013	66.73	79.63
6627-14702	FAF-8	PWF	149.00	147.50	1.50	-1.01	146.35	146.49	280111	6096875	7/05/2013	91.91	54.45
6627-14699	FAF-9A	PWF	121.70	120.20	1.50	26.18	146.31	146.38	280110	6096878	8/05/2013	91.99	54.32
6627-14700	FAF-9B	PWF	95.70	94.20	1.50	52.18	146.30	146.38	280110	6096878	8/05/2013	70.10	76.20
6627-14738	FAF-10A	FRA	55.36	54.86	0.50	91.77	146.78	146.63	280142	6096859	17/05/2013	4.46	142.32
6627-14739	FAF-10B	FRA	39.15	38.65	0.50	107.98	146.78	146.63	280142	6096858	17/05/2013	3.66	143.12
6627-14740	FAF-10C	FRA	16.07	15.57	0.50	131.06	146.78	146.63	280142	6096858	17/05/2013	4.40	142.38
6627-10776	10776	FRA	95.55	53.78	41.78	100.97	154.88	154.75	280090	6096735	5/02/2015	12.15	142.73
6627-14741	FAF-11A	FRA	63.79	63.29	0.50	142.11	206.24	205.39	284103	6102534	29/04/2013	33.03	173.21
6627-14742	FAF-11B	FRA	57.74	57.24	0.50	148.15	206.32	205.39	284103	6102534	8/05/2013	33.40	172.92
6627-14743	FAF-11C	FRA	41.67	41.17	0.50	164.22	206.32	205.39	284103	6102534	17/05/2013	33.46	172.86
6627-14744	FAF-11D	FRA	38.57	38.07	0.50	167.32	206.32	205.39	284103	6102534	16/05/2013	33.57	172.75
6627-14745	FAF-12A	FRA	89.96	89.46	0.50	119.15	209.27	208.61	284135	6102541	20/05/2013	31.97	177.31
6627-14746	FAF-12B	FRA	69.63	69.13	0.50	139.48	209.27	208.61	284135	6102541	20/05/2013	29.08	180.19
6627-14747	FAF-12C	FRA	50.82	50.32	0.50	158.29	209.27	208.61	284135	6102541	17/05/2013	28.49	180.78
6627-14748	FAF-12D	FRA	35.46	34.96	0.50	173.65	209.27	208.61	284135	6102541	17/05/2013	26.99	182.28
6627-14749	FAF-13A	MS	150.00	148.50	1.50	42.59	191.78	191.09	283936	6102499	16/05/2013	90.29	101.49

6627-14750	FAF-13B		36.93	35.43	1.50	155.66	191.68	191.09	283936	6102499		DRY		
6627-14753	FAF-14A	FRA	39.37	38.87	0.50	173.06	212.61	211.93	284170	6102549	05/11/2013	23.72	188.89	
6627-14754	FAF-14B	FRA	30.49	29.99	0.50	181.94	212.54	211.93	284170	6102549	05/11/2013	23.86	188.68	
6627-14728	FAF-15		79.85	78.35	1.50	112.63	190.95	190.98	283933	6102499		DRY		
6627-14751	FAF-16A	MS	149.00	147.50	1.50	48.02	196.33	195.52	283997	6102512	17/05/2013	87.65	108.68	
6627-14752	FAF-16B		96.00	93.00	3.00	102.52	196.36	195.52	283997	6102513		DRY		
6627-10778	10778	FRA	74.68	73.68	1.00	144.28	218.28	217.96	284230	6102552	3/02/2015	53.94	164.33	
6627-10201	10201	FRA	79.00	66.50	12.50	103.50	170.00	170.00	280643	6096705		19.40	150.60	
6627-14803	14803	FRA	276.00	239.00	37.00	-79.00	160.00	160.00	283263	6102519	4/03/2014	70.08	89.92	

### J.3.2 HYDRAULIC MODELLING

A 3D numerical model was developed using HydroGeoSphere (HGS) (Therrien, McLarren *et al.* 2010) to investigate the hydraulic properties of the fault zone based on the observed hydraulic head profiles across the fault at the three study sites. The model domain is wedge-shaped to represent the Willunga embayment; 25 km in length, 15 km wide and 500 m thick, with 50 layers (Apx Figure J.3a). Cell size in the x-y direction is 100 m x 100 m except for near the fault zone where the cells are 100 m x 1 m width to capture the hydraulic dynamics of the fault zone layers (Apx Figure J.3b). The three study sites were included in the model domain at similar distances along the length of the fault as to what is observed (from the coast; THR 12km, MR 15 km and WHR 20 km). No flow boundaries were used along the base and two long sides of the model domain and a constant head of zero metres was specified on the western boundary to represent the coastline. The physical characteristics of the model were differentiated by three main zones of different hydraulic conductivities (Apx Table J.2). Zone 1 represents the area down gradient of the fault, zone 2 represents the area up gradient of the fault and zone 3 represents the fault, which is 20 m thick and penetrates the entire thickness of the model domain from the top of the embayment to the coast. Each of the three zones was considered isotropic and homogeneous (porosity was set to 0.25) and the only physical parameter that was varied between zones was the hydraulic conductivity. The top of the model had a constant flux applied to represent diffuse recharge across the basin and was based upon 10% of the annual rainfall (500 mm/year) for the area.

1000 steady state simulations were run using different combinations of the hydraulic conductivity in each of the three zones (Apx Table J.2) to match the observed hydraulic heads either side of the fault zone and the gradient across the fault at the three study sites. Comparing different ratios of hydraulic conductivity between the aquifer system below and above the fault to the hydraulic conductivity of the fault zone, a groundwater flux could be quantified.



Apx Figure J.3 (a) 3D numerical model domain and (b) 2D conceptual model of the groundwater system showing the three different hydraulic conductivity zones across the fault as defined in the numerical model.

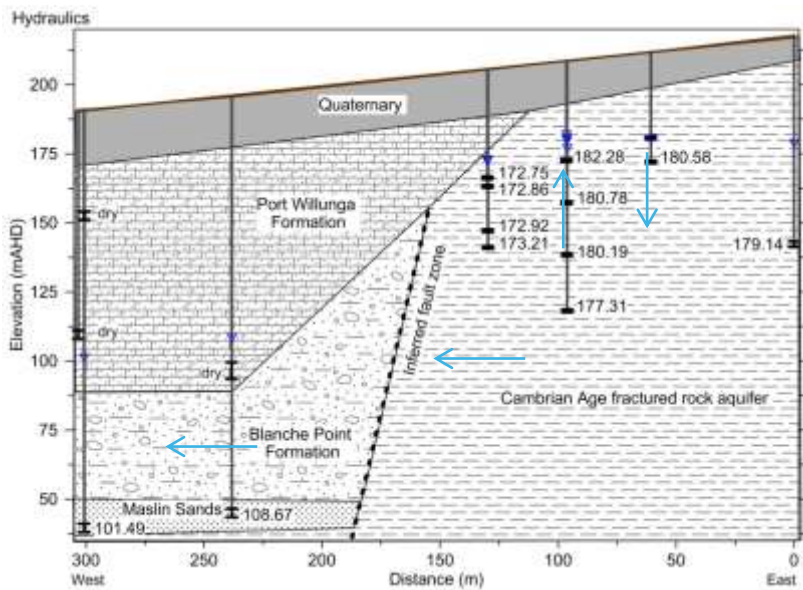
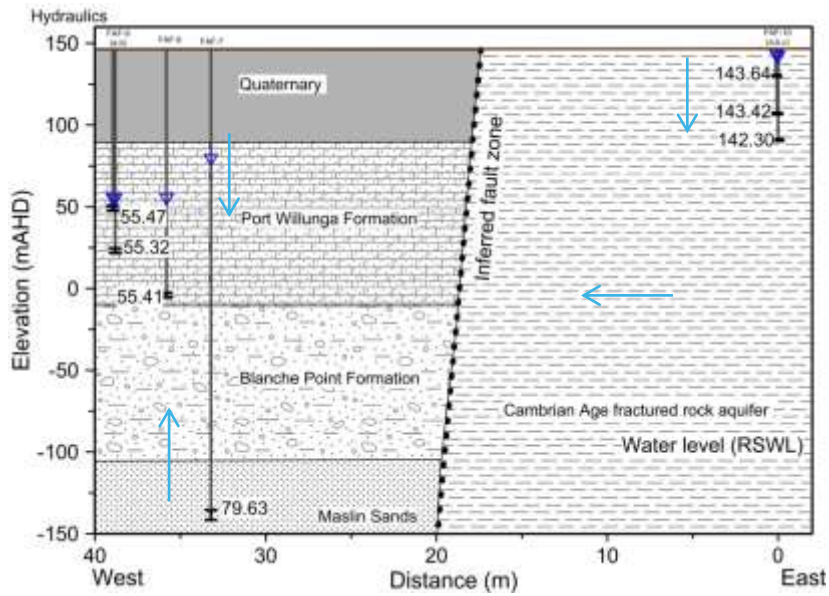
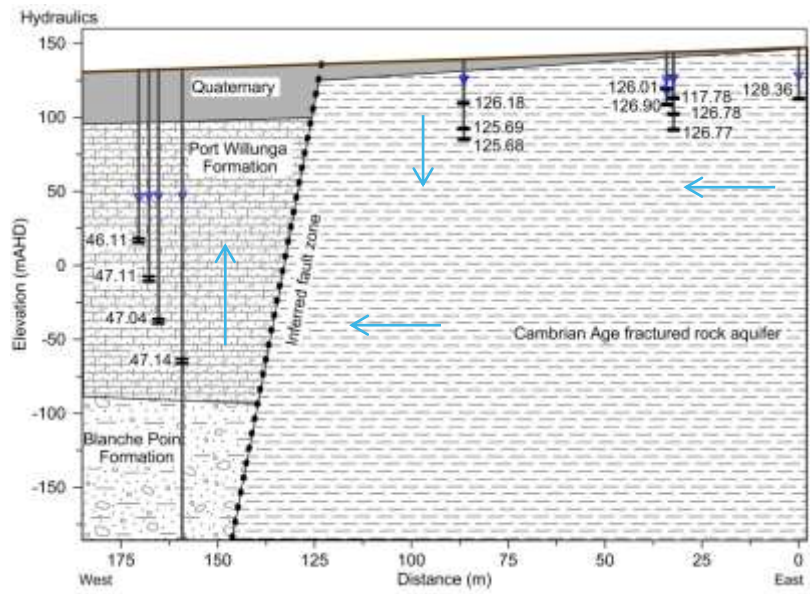
**Apx Table J.2 Range of hydraulic conductivity values for each of the model zones.**

Zone	Hydraulic conductivity (m/d)
K <sub>1</sub>	0.010- 10
K <sub>2</sub>	1x10 <sup>-8</sup> - 1
K <sub>3</sub>	0.010- 10

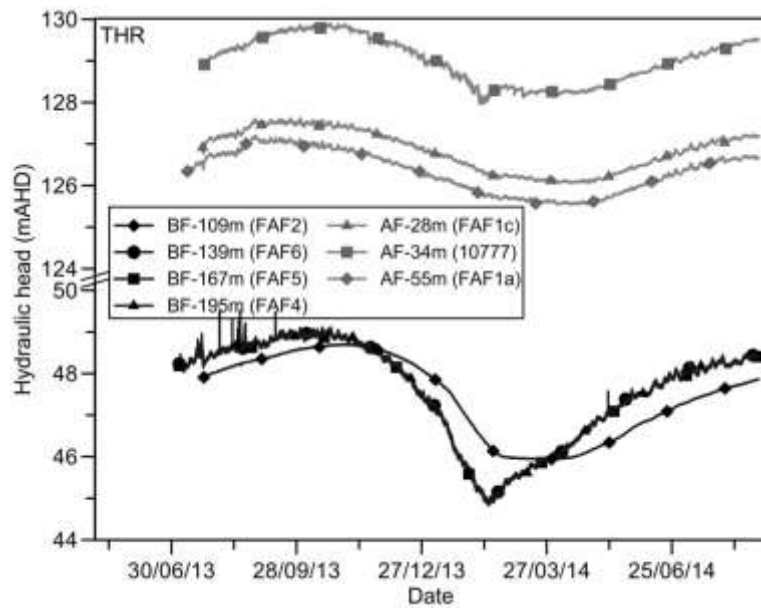
## J.4 Results

### J.4.1 HYDRAULICS

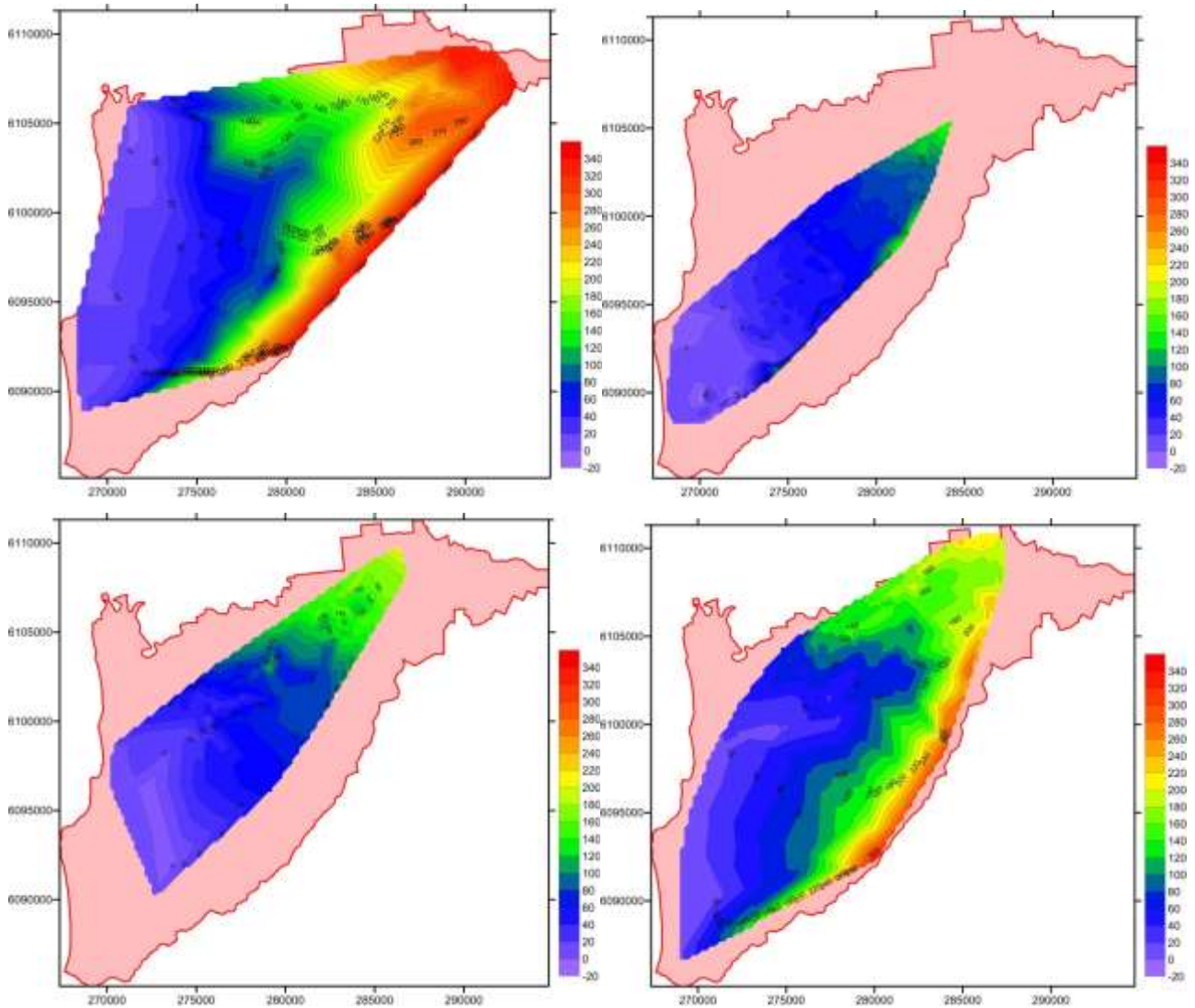
The hydraulic head measurements in the multi-completion observation wells either side of the fault zone at each of the three sites show large hydraulic gradients across the fault (Apx Figure J.4). The gradient ranged from 0.65 at the WHR site to 2.51 at the MR site with up to an 80 metre hydraulic head difference over a horizontal distance of less than 30 metres (Apx Figure J.4b). In comparison, the regional groundwater gradient within the Willunga Embayment is far less and in the order of 0.001. A large hydraulic gradient across the fault suggests that the groundwater flow rate and direction from the fractured rock aquifer system to the sedimentary aquifer systems is restricted by a low conductance barrier and that the flowpaths are likely to be diverted laterally along the fault zone and/or towards the ground surface as springs. There is also a relatively deep unsaturated zone (at least 80m) on the down thrown side of the fault (Apx Figure J.4) and the seasonal groundwater level fluctuations are about 5 metres in these aquifers between winter and summer, whilst above the fault they are more dampened and only fluctuate by about 2 metres (Apx Figure J.5). Regional potentiometric surface maps of the four major aquifer systems (Quaternary, Port Willunga Formation, Maslin Sands and Fractured rock) show sections along the fault where there are localised changes to the potentiometric surface gradient between the different aquifers and may represent movement of groundwater from the fractured rock into the Port Willunga and Maslin Sands aquifers (Apx Figure J.6).



Apx Figure J.4 Hydraulic heads corrected to mAHD (2013) at the study sites (top) THR, (middle) MR and (bottom) WHR. Also shown are the inferred groundwater flow directions.



Apx Figure J.5 Waterlevel time series data from study site THR showing the seasonal aquifer responses in the wells completed above and below the fault. Labels for each time series are: Above fault (AF), below fault (BF).

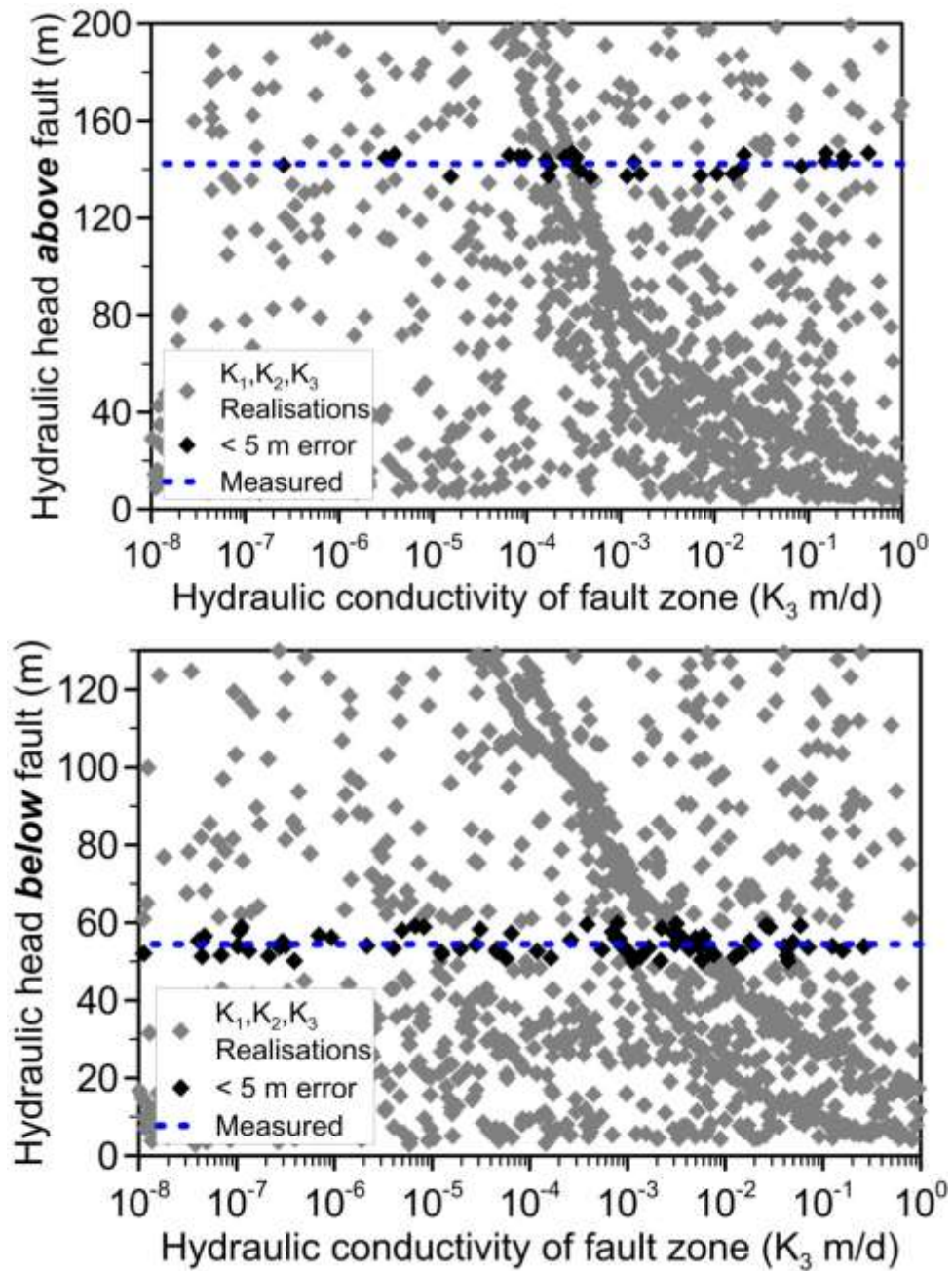


Apx Figure J.6 Potentiometric surfaces generated from all available well data from the SAGeodata base within the Willunga Embayment for the four major aquifer systems; (top left) Quaternary, (top right) Port Willunga Formation, (bottom left) Maslin Sands and (bottom right) Fractured rock.

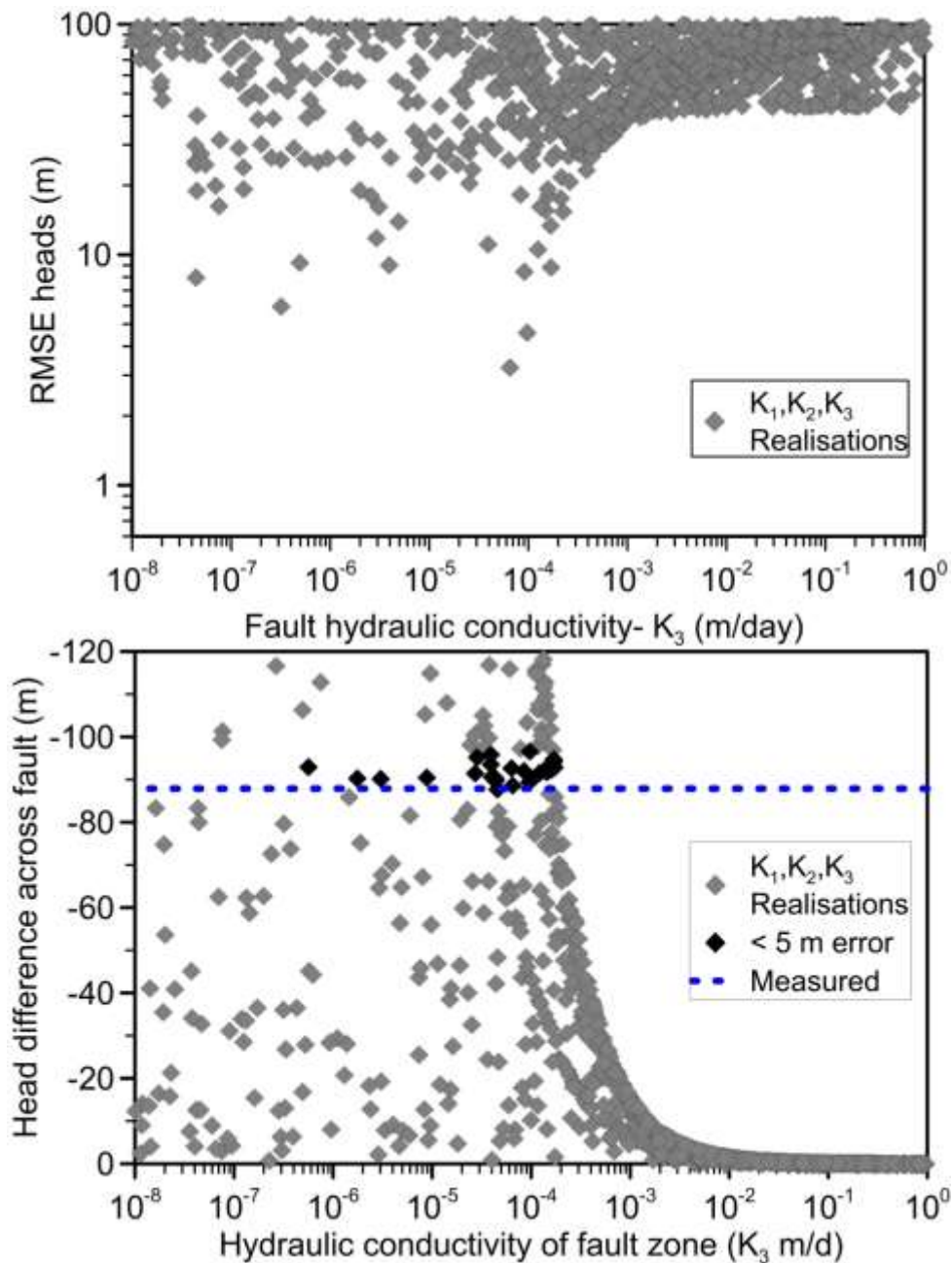
## J.4.2 HYDRAULIC MODELLING

The 3D modelling showed that by comparing different ratios of hydraulic conductivity between the aquifer system below and above the fault to hydraulic conductivity values of the fault zone, an estimate of the hydraulic properties of the fault zone can be determined. The results from each of the three study sites showed similar responses to changing the hydraulic conductivity ratios between the aquifers above and below the fault and the conductivity of the fault zone and therefore only selected figures will be shown.

The model, using 1000 realisations, showed that matching the heads above the fault could be achieved by increasing the hydraulic conductivity of the fault zone; however, this was often to the detriment of matching the heads below the fault zone (Apx Figure J.7). It is evident that there is any number of combinations in hydraulic conductivity for each of the zones to provide plausible matches to the heads observed above and below the fault. Changing the values of  $K_1$  and  $K_2$  and keeping the ratios the same showed similar trends in the modelled heads, however, the results were significantly different to what was observed at each of the study sites and therefore these realisations could be ignored. Analysing the head gradient across the fault (this can also be shown as head difference across the fault), shows that the modelled fits are improved and more tightly constrain the conductivity of the fault zone (Apx Figure J.8). It is a considerable improvement to what is achieved by only matching heads above or below the fault or the lowest RMSE of the heads.



Apx Figure J.7 Realisations of different hydraulic conductivity combinations to match observed hydraulic head (top) above and (bottom) below the fault at site MR. Blue dashed lines are the measured heads above and below the fault zone at the site. Selected data points (black) are within 5 metres of the measured head and show a very broad range of values for the fault.



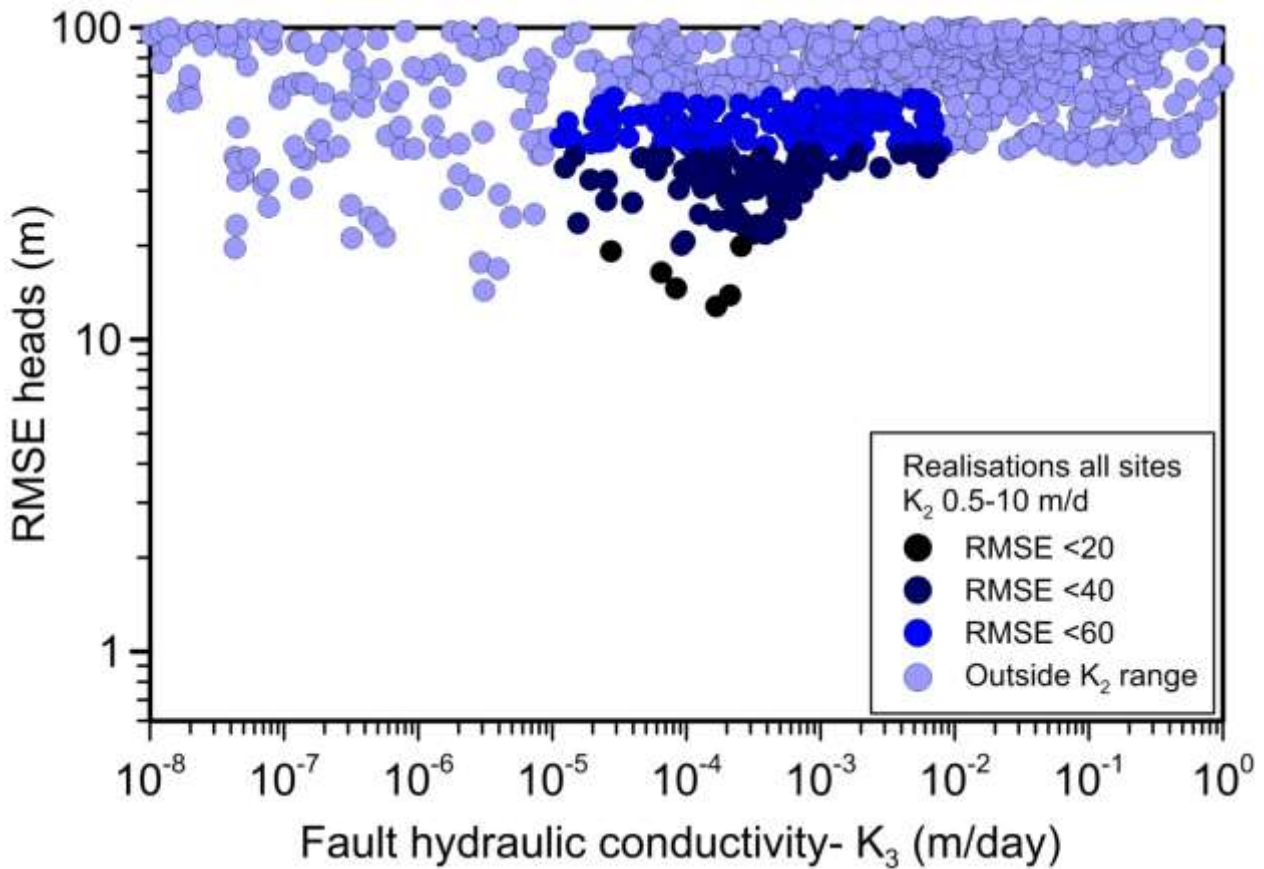
Apx Figure J.8 Realisations of different hydraulic conductivity combinations showing (top) the RMSE of heads and (bottom) the observed head difference above and below the fault at site MR. Blue dashed line is the measured head difference across the fault zone at the site. Selected data points (black) are within 5 metres of the measured head difference.

## J.5 Discussion

The numerical model constrained the range of likely hydraulic conductivity values of the fault zone at each of the study sites to several orders of magnitude based on an assessment of the gradient or difference in head across the fault. Observations of the head gradient provided much tighter control on these values when compared to only having information on the observed heads above or below the fault (Apx Figure J.7 and Apx Figure J.8) as is often the case with many data sets.

Expert knowledge on the range of hydraulic conductivities of the main aquifers within the embayment can provide some further constraint to minimising the uncertainty in the fault zone hydraulic conductivity by excluding some of the realisations which have very low values and unrealistic values in the aquifer below. The hydraulic conductivity of the sedimentary aquifer system below the fault is typically between 0.5-10

m/d (Martin, 2006), which reduces the range of plausible hydraulic conductivities of the fault zone to  $1.7 \times 10^{-4}$  to  $2.7 \times 10^{-5}$  m/d, with an RMSE in heads of less than 20 metres when considering data from all three sites (Apx Figure J.9). There is significantly more variability and range of hydraulic conductivity values of the fault when a much higher RMSE (>20 m) is considered.



Apx Figure J.9 Realisations of different hydraulic conductivity combinations showing the combined RMSE of heads at the three sites. Data points highlighted in black have a  $K_2$  value of 0.5-10 m/d and an RMSE less than 20 m (below the fault).

An estimate of the average groundwater flux across the fault was calculated using the modelling results along with the observed hydraulic gradient across the fault at each of the study sites. Using the dimensions in the model, the length of the fault is 25 km and has a saturated thickness of about 400 metres and a catchment area above the fault of  $74.5 \text{ km}^2$  (total catchment is  $190.5 \text{ km}^2$ ). Using the range in measured head gradients across the fault (0.65 to 2.51) and the range of fault zone hydraulic conductivities as determined by the modelling ( $1.7 \times 10^{-4}$  to  $2.7 \times 10^{-5}$  of m/day), the calculated flux across the fault is 176 to  $4267 \text{ m}^3/\text{day}$ . Calculating the annual flux along the length of fault is in the range of 2.6 to  $62 \text{ m}^3/\text{year}$  per metre length of fault. This equates to about 1.7 to 42 % of the groundwater recharge to the aquifer above the fault moving across the fault zone and the remainder moves parallel to the fault and discharges at the coast near Sellicks Beach.

## J.6 Conclusion

This study investigated groundwater flow characteristics across a fault zone between a fractured rock and sedimentary aquifer system. From the three study sites, the hydraulic results indicated that the groundwater flow rate and direction from the fractured rock aquifer system to the sedimentary aquifer systems is restricted by a low conductance barrier. The groundwater flowpaths are likely to be diverted laterally along the fault zone and/or towards the ground surface as springs, which make their way across

the fault as surface water features. The hydraulic gradients across the fault zone between the fractured rock and sedimentary aquifer systems were very significant (2.5), with up to an 80 metre hydraulic head drop over a horizontal distance of less than 30 metres. Despite the high hydraulic gradient, calculating the groundwater flux across the fault was more complicated. The 3D numerical model showed that, despite the fault zone acting as a dominantly barrier-type system, approximately 1.7 to 42 % of the groundwater recharge occurring above the fault zone is likely to make its way across the fault and the remainder moves parallel to the fault and discharges at the coast near Sellicks Beach. Using the range in measured head gradients across the fault (0.65 to 2.51) and the range of fault zone hydraulic conductivities as determined by the modelling ( $1.7 \times 10^{-4}$  to  $2.7 \times 10^{-5}$  of m/day), the annual flux along the length of fault is in the range of 2.6 to 62 m<sup>2</sup>/year/m length of fault.

One of the interesting findings of this study was how the uncertainty in the modelling was greatly reduced by knowing the gradient or head difference in close proximity, directly across the fault. Relying on only hydraulic head observations above or below the fault resulted in a broad range of fault zone hydraulic conductivities and significant uncertainty in whether there was movement of groundwater across the fault and if the fault acted as a conduit, barrier or a combination of both.

The findings from the Willunga Embayment study provides some valuable insight into groundwater flow processes and mechanisms that are likely to be taking place in the Adelaide Plains along the major fault zones. The annual groundwater flux along the length of the fault from the fractured rock aquifer to the sedimentary aquifers below is comparable to what was determined by examining the groundwater age tracer transects and profiles in the Adelaide area which estimated volumes of flow from the Mount Lofty Ranges to the plains range between 33 and 65 m<sup>2</sup>/year.

## J.7 References

- Aldam 1989, 1990, Watkins and Telfer 1995, Sereda & Martin 2000, OCWMB 2000, Herczeg&Leaney 2002, James-Smith 2002, Harrington 2002, Brown 2004, Martin et al. 2006, Ecological Associates, 2003, 2006, SKM, 2008, Short 2011.
- Anderson EI, Bakker M (2008) Groundwater flow through anisotropic fault zones in multiaquifer systems. *Water Resources Research* 44, W11433.
- Baghbanan A, Jing L (2007) Hydraulic properties of fractured rock masses with correlated fracture length and aperture. *International Journal of Rock Mechanics and Mining Sciences* 44, 704-719.
- Ball L, Ge S, Caine J, Revil A, Jardani A (2010) Constraining fault-zone hydrogeology through integrated hydrological and geoelectrical analysis. *Hydrogeology Journal* 18, 1057-1067.
- Banks EW, Shanafield MA, Cook PG (2014) Induced Temperature Gradients to Examine Groundwater Flowpaths in Open Boreholes. *Groundwater*, n/a-n/a.
- Bense VF, Gleeson T, Loveless SE, Bour O, Scibek J (2013) Fault zone hydrogeology. *Earth-Science Reviews* 127, 171-192.
- Bense VF, Person MA (2006) Faults as conduit-barrier systems to fluid flow in siliciclastic sedimentary aquifers. *Water Resources Research* 42, W05421.
- Bense VF, Van Balen R, De Vries JJ (2003) The impact of faults on the hydrogeological conditions in the Roer Valley Rift System: an overview. *Netherlands Journal of Geosciences/Geologie en Nijnbouw* 82, 41-54.
- Folch A, Mas-Pla J (2008) Hydrogeological interactions between fault zones and alluvial aquifers in regional flow systems. *Hydrological Processes* 22, 3476-3487.
- Gerges N (1999) The geology & hydrogeology of the Adelaide metropolitan area. PhD thesis, Flinders University of South Australia.
- Gerges N (2006) 'Overview of the hydrogeology of the Adelaide metropolitan area, South Australia.' Government of South Australia, through Department of Water, Land and Biodiversity Conservation, DWLBC Report 2006/10, Adelaide.
- Gleeson T, Novakowski K, Cook PG, Kyser TK (2009a) Constraining groundwater discharge in a large watershed: Integrated isotopic, hydraulic, and thermal data from the Canadian shield. *Water Resources Research* 45, W08402.
- Gleeson T, Novakowski K, Kurt Kyser T (2009b) Extremely rapid and localized recharge to a fractured rock aquifer. *Journal of Hydrology* 376, 496-509.
- Green G, Watt E, Alcoe D, Costar A, Mortimer L (2010) 'Groundwater flow across regional scale faults.' Government of South Australia, Department for Water, Technical Report 2010/15, Adelaide.
- Haneberg WC (1995) Steady State Groundwater Flow Across Idealized Faults. *Water Resources Research* 31, 1815-1820.
- Leaf AT, Hart DJ, Bahr JM (2012) Active Thermal Tracer Tests for Improved Hydrostratigraphic Characterization. *Ground Water* 50, 726-735.
- Manning AH, Clark JF, Diaz SH, Rademacher LK, Earman S, Niel Plummer L (2012) Evolution of groundwater age in a mountain watershed over a period of thirteen years. *Journal of Hydrology* 460–461, 13-28.
- Martin, R. (2006) Hydrogeology and numerical groundwater flow model for the McLaren Vale Prescribed Wells Area- Summary Report. Prepared for Adelaide and Mount Lofty Ranges Natural Resources Management Board.
- Marler J, Ge S (2003) The Permeability of the Elkhorn Fault Zone, South Park, Colorado. *Ground Water* 41, 321-332.

Reed GD (1982) 'Geophysical investigation of the willuna fault zone.' Department of Mines and Energy, South Australia, Report Book No: 82/15, South Australia.

Roques C, Bour O, et al. (2014) Hydrological behavior of a deep sub-vertical fault in crystalline basement and relationships with surrounding reservoirs. *Journal of Hydrology* 509, 42-54.

Therrien R, McLarren RG, Sudicky EA, Panday SM (2010) 'HydroGeoSphere: A Three-dimensional Numerical Model Describing Fully-integrated Subsurface and Surface Flow and Solute Transport. Code documentation and user's guide.' (Groundwater Simulations Group, University of Waterloo.)





Government of South Australia

Department of Environment, Water and Natural Resources



THE UNIVERSITY of ADELAIDE



University of South Australia



Flinders UNIVERSITY ADELAIDE • AUSTRALIA

The Goyder Institute for Water Research is a partnership between the South Australian Government through the Department of Environment, Water and Natural Resources, CSIRO, Flinders University, the University of Adelaide and the University of South Australia.